DTU Mathematics
Department of Mathematics

Technical University
of Denmark

Efficient Reanalysis Procedures in Structural Topology Optimization

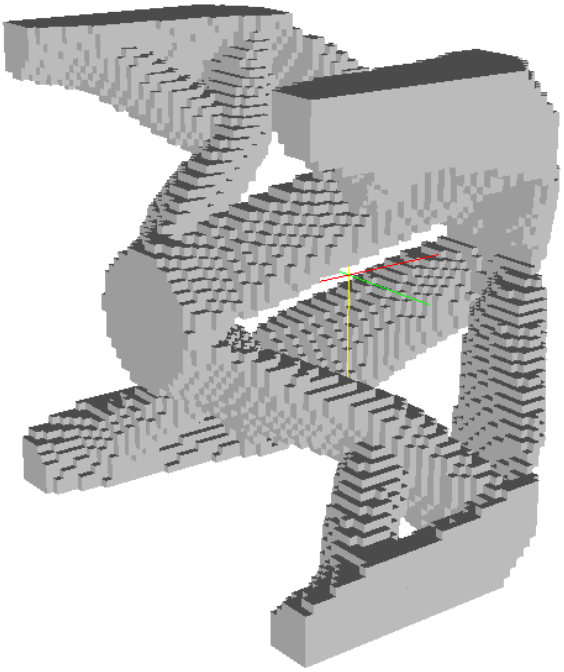

Ph.D. Thesis

Oded Amir

March 2011

Efficient Reanalysis Procedures in Structural Topology Optimization

Oded Amir

Department of Mathematics

Technical University of Denmark

Title of Thesis:
Efficient Reanalysis Procedures in Structural Topology Optimization

Ph.D. student:
Oded Amir
Department of Mathematics
Technical University of Denmark
Address: Matematiktorvet, Building 303S, DK-2800 Lyngby, Denmark
E-mail: o.amir@mat.dtu.dk

Supervisors:
Mathias Stolpe
Department of Mathematics
Technical University of Denmark
Address: Matematiktorvet, Building 303S, DK-2800 Lyngby, Denmark
E-mail: m.stolpe@mat.dtu.dk

Ole Sigmund
Department of Mechanical Engineering, Section of Solid Mechanics
Technical University of Denmark
Address: Nils Koppels Allé, Building 404, DK-2800 Lyngby, Denmark
E-mail: sigmund@mek.dtu.dk

Preface

This thesis is submitted in partial fulfillment of the requirements for obtaining the degree of Ph.D. at the Technical University of Denmark. The Ph.D. project was funded by the Technical University of Denmark and carried out at the Department of Mathematics during the period September 15th 2007 - December 21st 2010. Supervisors on the project were Associate Professor Mathias Stolpe from the Department of Mathematics and Professor, dr. techn. Ole Sigmund from the Department of Mechanical Engineering.

I would first like to thank my supervisors for their invaluable guidance and for many interesting discussions throughout the work on this thesis. Many thanks to Martin P. Bendsøe who opened DTU's doors to me, exposed me to the fascinating world of topology optimization and served as my main supervisor for the first 16 months. I am grateful to Tom Høholdt and Martin again for helping me out with various non-academic challenges, especially in the early stages of my studies. I wish to thank also my colleagues at the Department of Mathematics and at the TOPOPT group for the stimulating working environment and for the Danish *"hygge"*.

Finally, I would like to express my deep gratitude to my family: to Adi for all her love and support; and to Zohar and Omri for reminding me what is most important.

Kgs. Lyngby, December 2010

Oded Amir

Summary

This thesis examines efficient solution procedures for the structural analysis problem within topology optimization. The research is motivated by the observation that when the nested approach to structural optimization is applied, most of the computational effort is invested in repeated solutions of the analysis equations. For demonstrative purposes, the discussion is limited to topology optimization problems within the field of structural mechanics. Nevertheless, the results can be relevant for a wide range of problems in structural and topology optimization.

The main focus of the thesis is on the utilization of various approximations to the solution of the analysis problem, where the underlying model corresponds to linear elasticity. For computational environments that enable the direct solution of large linear equation systems using matrix factorization, we propose efficient procedures based on approximate reanalysis. For cases where memory limitations require the utilization of iterative equation solvers, we suggest efficient procedures based on alternative termination criteria for such solvers. These approaches are tested on two- and three-dimensional topology optimization problems including minimum compliance design and compliant mechanism design. The topologies generated by the approximate procedures are practically identical to those obtained by the standard approach. At the same time, it is shown that the computational cost can be reduced by up to one order of magnitude. The main observation in the context of optimal design of linear structures is that relatively rough approximations are acceptable, in particular in early stages of the optimization process.

The thesis also addresses topology optimization of structures exhibiting nonlinear response. In such cases, the computational effort invested in the solution of the nested problem is even more dominant since nonlinear equation systems are to be solved repeatedly. Efficient procedures for nonlinear structural analysis are proposed, based on transferring solutions and factorized tangent stiffnesses from one design cycle to the following one. This approach is demonstrated on several design problems involving either geometric or material nonlinearities. The suggested procedures are shown to be effective mainly for problems that do not involve path-dependent solutions.

Resumé (in Danish)

I denne afhandling undersøges effektive løsningsprocedurer for strukturalanalyse i topologioptimering. Forskningen motiveres af følgende: når den indlejrede fremgangsmåde til konstruktionsoptimering anvendes, bliver storstedelen af den investerede beregningsindsats brugt til gentagne løsninger af analyseligningerne. For illustrationens skyld, er diskussionen begrænset til topologioptimering inden for konstruktionsmekanik. Resultaterne kan dog alligevel være relevante for flere problemer i konstruktionsoptimering og topologioptimering.

Hovedvægten i afhandlingen ligger på anvendelsen af forskellige approksimationer til løsning af analyseproblemet, hvor den underliggende model svarer til lineær elasticitet. For beregningsmiljøer, der gør det muligt at løse store lineære ligningssystemer ved matrixdekomposition, foreslår vi effektive procedurer baseret på approksimativ genanalyse. I tilfælde af hukommelsesbegrænsninger der kræver udnyttelse af iterative metoder, foreslår vi effektive procedurer baseret på alternative afslutningskriterier for disse løsningsmetoder. Approksimative procedurer er testet på topologioptimering af konstruktioner i to og tre dimensioner, nemlig *minimum compliance design* og *compliant mecahnism design*. Konstruktionerne genererede af de approksimative procedurer er næsten identiske med dem, der opnås med standardmetoden. Samtidig er det påvist, at beregningsomkostningen kan reduceres med op til en hel størrelsesorden. Den vigtigste bemærkning i forbindelse med topologioptimering af lineære konstruktioner er, at relativt grove tilnærmelser er acceptable, især i tidlige faser af optimeringsprocessen.

Afhandlingen omhandler også topologioptimering af konstruktioner der udviser ikke-lineær respons. I sådanne tilfælde er den beregningsindsats, der investeres i gentagne løsninger af de indlejrede problemer endnu mere dominerende, da ikke-lineære ligningssystemer skal løses gentagne gange. Effektive procedurer for ikke-lineær strukturalanalyse er foreslået. Fremgangsmåden er baseret på overførsel af information fra en optimeringsfase til den efterfølgende. Denne fremgangsmåde er påvist for flere problemer i topologioptimering med geometriske eller materielle ikke-lineæritet. De foreslåede procedurer viste sig at være effektive især for konstruktioner, som ikke indeholder vej-afhængige løsninger.

Contents

Part I

Background

Introduction

The presented thesis deals with efficient solution procedures for the structural analysis problem within topology optimization. In topology optimization, the nested approach is frequently applied, meaning optimization is performed in the design variables only while the equilibrium equations are solved separately. In such cases, the computational effort involved in repeated solutions of the structural analysis equations dominates the computational cost of the whole process. This motivates the search for efficient approaches aimed at reducing the computational effort invested in the analysis. Ultimately, applying efficient procedures can enable the solution of larger and more complex models compared to standard procedures.

The thesis addresses structural topology optimization problems in which the underlying analysis model is either linear or nonlinear. For linear problems, the proposed procedures are based on utilizing various approximations to the solution of the analysis equations. For nonlinear problems, the discussion is restricted to re-using information when performing sequences of nonlinear analyses, thus the obtained solutions are accurate.

The thesis is organized as follows. Part I gives a general background to the topic. In Chapter 1, structural analysis procedures are briefly reviewed, with particular reference to methods and formulations employed in the thesis. Chapter 2 introduces structural topology optimization. The emphasis is put on the problem formulations, objective functions and sensitivity analysis procedures considered in the various test cases that are examined. Finally, Chapter 3 includes a summary of the results; an assessment of the contribution of the work; and a discussion regarding ideas for future work. Part II includes 5 research articles. Chapters 4, 5 and 6 discuss various approximate procedures for linear structural analysis in topology optimization. Chapter 8 deals with efficient computational schemes for nonlinear structural analysis based on re-using information. Chapter 7 is given as a background for Chapter 8, where one of the considered problems involving material nonlinearities is presented.

Chapter 1

Structural Analysis Procedures

The main objective of this thesis is to investigate efficient solution procedures for the structural analysis problem in structural optimization. In particular, the focus is on topology optimization where the general layout of the structure is determined.

One approach to structural optimization is to formulate the problem in the design variables space only. Then the aim is to find optimal values of the design variables such that the objective function is minimized and the constraints are satisfied. The corresponding optimization problem has the form (Kirsch, 1993)

$$\begin{aligned} \min_{\mathbf{x}} \quad & f(\mathbf{x}) \\ \text{s.t.:} \quad & g_i(\mathbf{x}) \leq 0 \qquad i = 1, ..., m \end{aligned}$$

where f is the objective function and g_i $(i = 1, ..., m)$ are general inequality constraints. Following this approach, the response of the structure (which can be formulated as a set of equality constraints) is computed separately for any value of the design variables by solving the analysis equations. The result of the analysis can then be used to evaluate the objective and the constraints. This results in a two-level procedure, where the first level consists of solving the structural analysis problem and in the second level the design is modified by mathematical programming. This is also known as the nested approach (Kirsch, 1993), since the analysis is nested in the optimization procedure and repeatedly solved for a sequence of trial designs. In topology optimization, typically only a few constraints are considered. This means that the optimization problem can be solved efficiently even if the number of design variables is large, using methods such as the one described in Section 2.3.2. Consequently, the main computational burden is in the structural analysis.

In this thesis, various approaches aimed at reducing the computational cost associated with solving the structural analysis problem are presented. This chapter provides the reader with the necessary background regarding structural analysis of both linear and nonlinear systems. A brief review of common methods and procedures for structural analysis is given. Furthermore, the concept of structural reanalysis, referring to multiple repeated analyses is presented. The main purpose is to establish a connection between standard analysis procedures, approximate reanalysis and the efficient procedures discussed in Chapters 4, 5, 6 and 8.

The main purpose of structural analysis is to determine the displacements, internal forces and stresses of a structure under a set of applied loads. The resulting internal forces in the structure must satisfy equilibrium conditions and the displacements should be compatible with the continuity of the structure and with its boundary conditions. In practice, the most common numerical method used for structural analysis is the finite element method (FEM). Using FEM, two-dimensional and three-dimensional continuum structures such as plates, shells and solids, as well as trusses and frames, can be modeled and analyzed. The main feature of FEM is the

assumption of the displacement field within a small element as a combination of a few simple functions, known as shape functions. The actual structure is replaced by a discrete model, divided into small elements, also known as finite elements, which are connected together at their boundaries. According to the shape functions used, the stiffness matrix of each element in the model is calculated and then the stiffness matrix of the whole structure can be assembled. Equilibrium at every node of the discrete structure is satisfied by solving a set of simultaneous algebraic equations and obtaining the nodal displacements. The results are then post-processed to determine the stresses and internal forces at each element. Various textbooks on FEM-based structural analysis are available. For the purpose of this thesis, the books by Bathe (1996), Zienkiewicz and Taylor (2000), Crisfield (1991) and Cook (1981) are followed.

Generally speaking, structural analysis can be divided into three types: linear static analysis, nonlinear static analysis and dynamic analysis, which itself can also be divided into linear and nonlinear cases. In linear static analysis, we assume linear relations between the applied loads and the displacements of the structure. This assumption is based on linear material laws (e.g. Hooke's law) and linear kinematics (small displacements, rotations and strains). A linear finite element linear analysis ends up in solving a set of linear algebraic equations. In nonlinear analysis, one or more of these assumptions may not be suitable: the material law could be nonlinear; the kinematics could be nonlinear (e.g. large displacements and rotations); or the boundary conditions might change (e.g. contact problems). In order to perform a nonlinear finite element analysis, a set of nonlinear algebraic equations should be solved. The solution is usually found by employing an incremental-iterative linearization technique.

1.1 Linear structural analysis

In any linear static finite element analysis (FEA), the system of algebraic equations to be solved is

$$\mathbf{K}\mathbf{u} = \mathbf{f} \tag{1.1}$$

where $\mathbf{K}$ is the global stiffness matrix, $\mathbf{u}$ is the unknown displacements vector and $\mathbf{f}$ is the external load vector. $\mathbf{K}$ has the following properties: It is symmetric; it is positive definite; and it is sparse. Exploiting symmetry and sparsity, the stiffness matrix is stored in memory in a very compact manner. The solution of (1.1) is obtained by employing either a direct or an iterative equation solver. In general, direct solvers are more robust and are preferred when the factorized form of $\mathbf{K}$ can be stored in memory. This is the case for small and medium scale 2-D FE problems. For 3-D models, $\mathbf{K}$ usually has a relatively large bandwidth so that iterative solvers are more appropriate due to their low memory requirements. Iterative schemes are also easier to parallelize and therefore are more suitable for high performance computing (Saad, 2003).

Direct solution methods Direct solution methods are algorithms based on Gauss elimination. Due to its symmetry and positive definiteness, the stiffness matrix can be decomposed using the Cholesky factorization

$$\mathbf{K} = \mathbf{U}^T\mathbf{U} \tag{1.2}$$

where $\mathbf{U}$ is an upper triangular matrix. Then, the vector of displacements $\mathbf{u}$ is obtained in two steps, involving only forward and backward substitutions

$$\begin{aligned} \mathbf{U}^T\mathbf{v} &= \mathbf{f} \\ \mathbf{U}\mathbf{u} &= \mathbf{v} \end{aligned}$$

When the matrix's half-bandwidth b is much smaller than the number of degrees of freedom n, the number of flops required for a Cholesky factorization is roughly $\frac{nb^2}{2}$ (Golub and Van Loan, 1983). The decomposed matrix can then be stored in a $n \times (b+1)$ array. In various applications,

such as structural optimization, a sequence of analysis equations of the form (1.1) is generated and should be solved. In the nested approach to topology optimization, the overall computational effort is typically dominated by the cost of solving the analysis equations. The relatively high cost of matrix factorization in large-scale problems, in particular in three-dimensional FEA, motivates the development of efficient procedures that avoid repeated factorizations. The idea of re-using the Cholesky factors from Eq. (1.2) is the underlying principal of the reanalysis approach described in Section 1.3. Investigations regarding re-using Cholesky factors, in the context of solving sequences of linear systems arising in topology optimization, are reported in Chapters 4 and 6.

Iterative solution methods Iterative methods for solving large sparse linear systems have been gaining popularity over direct methods. In earlier times, iterative methods were usually developed for particular applications and their performance depended on the actual problem parameters. Nowadays, various general-purpose iterative solvers are available, among which the family of Krylov subspace solvers is applied most extensively. For 3-D models and parallel high performance computers, Krylov iterative solvers are much more efficient than direct solvers (Saad, 2003). Therefore in the context of reducing computational effort in topology optimization, it is essential to address the use of such solvers for solving the structural analysis equations.

Among the family of Krylov subspace solvers, the most appropriate method for solving symmetric positive definite systems such as (1.1) is the conjugate gradient (CG) method (Hestenes and Stiefel, 1952). Since it was introduced by Hestenes and Stiefel as an alternative to Gauss elimination, many studies were dedicated to the method's convergence properties and error analysis, (see for example Golub and Van Loan (1983); Kelley (1995); Saad (2003)). The rate of convergence depends on the condition number of the system matrix $\mathbf{K}$, therefore it is necessary to use effective preconditioning in order to achieve fast convergence. Demonstrated with symmetric preconditioning, this means that in practice CG will be applied to solve

$$\widetilde{\mathbf{K}}\widetilde{\mathbf{u}} = \widetilde{\mathbf{f}}$$

where

$$\begin{aligned} \widetilde{\mathbf{K}} &= \mathbf{M}^{-T}\mathbf{K}\mathbf{M}^{-1} \\ \widetilde{\mathbf{u}} &= \mathbf{M}\mathbf{u} \\ \widetilde{\mathbf{f}} &= \mathbf{M}^{-T}\mathbf{f} \end{aligned}$$

The preconditioner $\mathbf{M}$ can be, for example, an incomplete factor of $\mathbf{K}$ so that the eigenvalue distribution of $\widetilde{\mathbf{K}}$ is much better than that of $\mathbf{K}$. The resulting preconditioned conjugate gradient (PCG) procedure aimed at solving the linear system can be outlined as follows:

1. Set the initial guess $\mathbf{u}_1$.
2. Compute the initial residual $\mathbf{r}_1$ and direction vector $\mathbf{p}_1$: $\mathbf{r}_1 = \mathbf{f} - \mathbf{K}\mathbf{u}_1$, $\mathbf{y} = \mathbf{M}^{-T}\mathbf{r}_1$, $\mathbf{z}_1 = \mathbf{M}^{-1}\mathbf{y}$, $\mathbf{p}_1 = \mathbf{z}_1$.
3. For `i = 1:maxiter` do
   (a) $\alpha_i = \frac{\mathbf{r}_i^T\mathbf{z}_i}{(\mathbf{K}\mathbf{p}_i)^T\mathbf{p}_i}$
   (b) $\mathbf{u}_{i+1} = \mathbf{u}_i + \alpha_i\mathbf{p}_i$
   (c) $\mathbf{r}_{i+1} = \mathbf{r}_i - \alpha_i\mathbf{K}\mathbf{p}_i$
   (d) If $\|\mathbf{r}_{i+1}\|_2 < \epsilon\,\|\mathbf{f}\|_2$ break.

(e) $\mathbf{y} = \mathbf{M}^{-T}\mathbf{r}_{i+1}$, $\mathbf{z}_{i+1} = \mathbf{M}^{-1}\mathbf{y}$.

(f) $\beta_i = \frac{\mathbf{r}_{i+1}^T \mathbf{z}_{i+1}}{\mathbf{r}_i^T \mathbf{z}_i}$

(g) $\mathbf{p}_{i+1} = \mathbf{z}_{i+1} + \beta_i \mathbf{p}_i$

Solving the system of equilibrium equations (1.1) is equivalent to the minimization of the quadratic functional ϕ which represents the potential energy in the structure

$$\phi(\mathbf{u}) = \frac{1}{2}\mathbf{u}^T\mathbf{K}\mathbf{u} - \mathbf{f}^T\mathbf{u}$$

The fundamental principal behind the derivation of CG is that it successively minimizes ϕ along a set of directions $\{\mathbf{p}_1, \mathbf{p}_2, ...\}$. This can also be seen as successively minimizing the following norm (Kelley, 1995)

$$\|\mathbf{u}_k - \mathbf{u}^*\|_K = \sqrt{(\mathbf{u}_k - \mathbf{u}^*)^T\mathbf{K}(\mathbf{u}_k - \mathbf{u}^*)} \tag{1.3}$$

where $\mathbf{u}_k$ is the k-th iterate of CG and $\mathbf{u}^*$ is the exact solution. The iterative process is typically terminated when the relative residual is small, as stated in the procedure outlined above. It can be shown that the norm of the error given in Eq. (1.3) reduces faster than the relative norm of the residuals (Kelley, 1995)

$$\frac{\|\mathbf{r}_k\|_2}{\|\mathbf{r}_1\|_2} \leq \sqrt{\frac{\lambda_1}{\lambda_N}} \frac{\|\mathbf{u}_k - \mathbf{u}^*\|_K}{\|\mathbf{u}_1 - \mathbf{u}^*\|_K}$$

where λ_1 and λ_N are the largest and the smallest eigenvalues of $\mathbf{K}$ respectively. It is important to note that in the context of compliance minimization in topology optimization, the norm (1.3) is related to the error in compliance. This is useful when seeking early termination criteria for PCG. Efficient use of PCG for solving the linear analysis equations in topology optimization, based on such early termination criteria, is the topic of Chapter 5.

1.2 Nonlinear structural analysis

Linear static analysis is based on the assumptions that the displacements of the structure are infinitesimally small, the material is linearly elastic and the boundary conditions remain unchanged under loading. When one of these assumptions is inappropriate, a nonlinear static analysis is required (Bathe, 1996). Since this thesis focuses on efficient procedures for structural analysis for the purpose of topology optimization, the discussion regarding structural nonlinearities is limited to the following demonstrative classes of problems:

- Geometric nonlinearity (GNL) - large displacements and rotations but small strains. In particular, the total Lagrangian formulation is employed and material linearity is assumed.

- Material nonlinearity (MNL) - the stress-strain relationship is nonlinear. In particular, various elasto-plastic formulations are utilized.

When examining computational procedures, it is important to emphasize one major difference between large deformations analysis and elasto-plasticity. Elasto-plastic response is path-dependent by nature, meaning that the evolution of plastic strains under a certain load intensity depends on the history of plastic straining and cannot be computed correctly in one load stage. Therefore an incremental solution scheme is mandatory for problems in elasto-plasticity and this implies that also sensitivity analysis must be performed in increments. For large deformations this is not the case and in principal the response can be computed in a single load step.

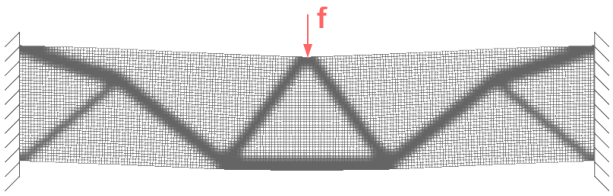

Figure 1.1: Optimized design of a clamped beam considering large deformations. The deflection at the loaded point is 1/10 of the beam height and 1/50 of the beam length.

1.2.1 Large deformations

In large deformation continuum mechanics, equilibrium should be satisfied in the deformed geometry which is unknown beforehand. One approach to large deformation analysis is the so-called total Lagrangian formulation, where all finite element computations are performed with respect to the original configuration. For this purpose, the Green-Lagrange strain tensor is defined as

$$ {}^{n}_{0}\epsilon_{ij} = \frac{1}{2}({}^{n}_{0}u_{i,j} + {}^{n}_{0}u_{j,i} + {}^{n}_{0}u_{k,i}{}^{n}_{0}u_{k,j}) \tag{1.4} $$

where u is the displacement field; i, j and k represent the cartesian axes; $u_{l,m} = \frac{\partial u_l}{\partial m}$; and Einstein summation convention is applied. The ${}^{n}_{0}$ notation means evaluation at "time" n in the initial coordinate system corresponding to "time" 0. The term "time" is used here to represent the incrementation of loads or displacements. The third term in (1.4) is neglected in linear structural analysis since it is assumed that the displacements are small.

In the following, the derivation of the finite element equations is briefly outlined following the complete derivation by Bathe (1996). Applying the principal of virtual work with respect to an unknown deformed configuration at "time" n results in the basic equation

$$ \int_{{}_0V} {}^{n}_{0}S_{ij}\delta{}^{n}_{0}\epsilon_{ij}d^0V = {}^{n}_{0}\mathscr{R} \tag{1.5} $$

where ${}^{n}_{0}S_{ij}$ is the second Piola-Kirchoff stress tensor and ${}^{n}_{0}\mathscr{R}$ is the external virtual work. For simplicity it is assumed that loading is deformation-independent. The stresses and strains are decomposed into their known parts (from a previous configuration) and unknown parts (corresponding to the current increment)

$$ \begin{aligned} {}^{n}_{0}S_{ij} &= {}^{n-1}_{0}S_{ij} + {}_0S_{ij} \\ {}^{n}_{0}\epsilon_{ij} &= {}^{n-1}_{0}\epsilon_{ij} + {}_0\epsilon_{ij} \end{aligned} $$

Furthermore, the incremental strains are decomposed into linear and nonlinear terms, denoted ${}_0e_{ij}$ and ${}_0\eta_{ij}$ respectively

$$ \begin{aligned} {}_0\epsilon_{ij} &= {}_0e_{ij} + {}_0\eta_{ij} \\ {}_0e_{ij} &= \frac{1}{2}({}_0u_{i,j} + {}_0u_{j,i} + {}^{n-1}_{0}u_{k,i}{}_0u_{k,j} + {}_0u_{k,i}{}^{n-1}_{0}u_{k,j}) \\ {}_0\eta_{ij} &= \frac{1}{2}{}_0u_{k,i}{}_0u_{k,j} \end{aligned} $$

Inserting the incremental decompositions into (1.5) and using $\delta{}^{n}_{0}\epsilon_{ij} = \delta_0\epsilon_{ij}$ leads to

$$ \int_{{}_0V} {}_0S_{ij}\delta_0\epsilon_{ij}d^0V + \int_{{}_0V} {}^{n-1}_{0}S_{ij}\delta_0\eta_{ij}d^0V = {}^{n}_{0}\mathscr{R} - \int_{{}_0V} {}^{n-1}_{0}S_{ij}\delta_0e_{ij}d^0V \tag{1.6} $$

The only nonlinear term with respect to incremental strains in (1.6) is ${}_0S_{ij}\delta_0\epsilon_{ij}d^0V$. Using the approximations ${}_0S_{ij} = {}_0D_{ijrs0}e_{rs}$ and $\delta_0\epsilon_{ij} = \delta_0 e_{ij}$, the linearized equation is obtained

$$\int_{{}_0V} {}_0D_{ijrs0}e_{rs}\delta_0 e_{ij}d^0V + \int_{{}_0V} {}^{n-1}_0S_{ij}\delta_0\eta_{ij}d^0V = {}^n_0\mathscr{R} - \int_{{}_0V} {}^{n-1}_0S_{ij}\delta_0 e_{ij}d^0V \tag{1.7}$$

where ${}_0D_{ijrs}$ is the constitutive tensor in the original configuration.

Obtaining the discretized FE equations from (1.7) follows standard FE procedures. The corresponding linearized algebraic equation system can be written as

$${}^{n-1}_0\mathbf{K}_L\Delta\mathbf{u} + {}^{n-1}_0\mathbf{K}_{NL}\Delta\mathbf{u} = {}^n\mathbf{f}_{ext} - {}^{n-1}_0\mathbf{f}_{int} \tag{1.8}$$

where ${}^{n-1}_0\mathbf{K}_L$ and ${}^{n-1}_0\mathbf{K}_{NL}$ are the linear and nonlinear parts of the stiffness matrix, based on the known configuration at "time" $n-1$; $\Delta\mathbf{u}$ is the displacements increment at "time" step n; ${}^n\mathbf{f}_{ext}$ is the external load vector at "time" step n; and ${}^{n-1}_0\mathbf{f}_{int}$ is the internal forces vector corresponding to the known configuration at "time" $n-1$. Eq. (1.8) constitutes the starting point for an iterative solution, where the stiffness and internal forces from step $n-1$ are used as initial approximations for the solution at step n. These are then corrected iteratively until the external and internal forces are balanced. At any iteration within step n, the tangent stiffness matrix and the internal forces are computed as follows

$$\begin{aligned}
{}^n_0\mathbf{K} &= {}^n_0\mathbf{K}_L + {}^n_0\mathbf{K}_{NL} = \int_{{}_0V} \{{}^n_0\mathbf{B}_L^T\}\{{}_0\mathbf{D}\}\{{}^n_0\mathbf{B}_L\}d^0V + \\
&\quad \int_{{}_0V} \{{}^n_0\mathbf{B}_{NL}^T\}\{{}^n_0\mathbf{S}\}\{{}^n_0\mathbf{B}_{NL}\}d^0V \\
{}^n_0\mathbf{f}_{int} &= \int_{{}_0V} \{{}^n_0\mathbf{B}_L^T\}\{{}^n_0\widehat{\mathbf{S}}\}d^0V
\end{aligned}$$

where ${}^n_0\mathbf{B}_L$ is the strain-displacement transformation matrix, corresponding to linear terms of incremental strains; ${}^n_0\mathbf{B}_{NL}$ is the strain-displacement transformation matrix, corresponding to nonlinear terms of incremental strains; ${}_0\mathbf{D}$ is the constitutive tensor; ${}^n_0\mathbf{S}$ represents the second Piola-Kirchoff stresses in matrix format; and ${}^n_0\widehat{\mathbf{S}}$ represents the same stresses in vector format. As mentioned above, the complete derivation of ${}^n_0\mathbf{B}_L$ and ${}^n_0\mathbf{B}_{NL}$ follows standard FE procedures and is omitted for brevity.

For evaluating the second Piola-Kirchoff stresses, it is necessary to compute the Green-Lagrange strain tensor. This can be conveniently performed using the deformation gradient ${}^n_0\mathbf{X}$ (Bathe, 1996)

$${}^n_0\boldsymbol{\epsilon} = \frac{1}{2}({}^n_0\mathbf{X}^T {}^n_0\mathbf{X} - \mathbf{I})$$

where

$${}^n_0\mathbf{X} = \begin{bmatrix} \frac{\partial^n x_1}{\partial^0 x_1} & \frac{\partial^n x_1}{\partial^0 x_2} & \frac{\partial^n x_1}{\partial^0 x_3} \\ \frac{\partial^n x_2}{\partial^0 x_1} & \frac{\partial^n x_2}{\partial^0 x_2} & \frac{\partial^n x_2}{\partial^0 x_3} \\ \frac{\partial^n x_3}{\partial^0 x_1} & \frac{\partial^n x_3}{\partial^0 x_2} & \frac{\partial^n x_3}{\partial^0 x_3} \end{bmatrix} \tag{1.9}$$

The partial derivatives in (1.9) are evaluated using derivatives of the shape functions at "time" 0.

1.2.2 Elasto-plasticity

For the purpose of studying topology optimization procedures involving nonlinear structural analysis, elasto-plasticity is examined as a representative case of material nonlinearity. In particular, design problems involving classical rate-independent plasticity are addressed. The underlying principal of elasto-plastic behavior is that the material has a yield limit in terms of strain and stress. Up to the yield limit, the response is linear elastic (though it could also be nonlinear

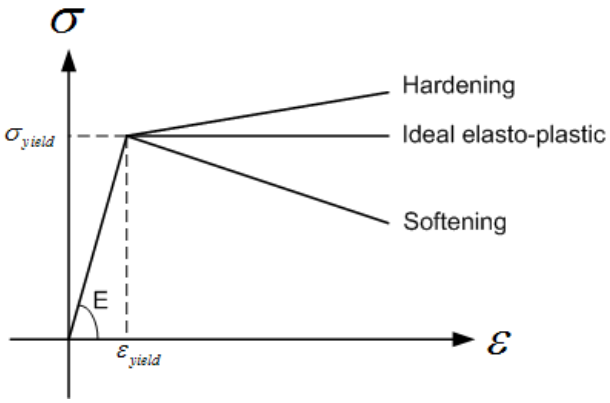

Figure 1.2: Uniaxial stress-strain relationship of elasto-plastic materials

elastic in general). Once yielding occurs, the material loses much of its stiffness in an irreversible manner. In some cases, ideal elasto-plastic behavior is assumed, meaning no stiffness remains after yielding. Many models consider a more general case where the material exhibits hardening or softening beyond the limit stress. This is demonstrated using uniaxial stress-strain curves in Figure 1.2.

1.2.2.1 Classical rate-independent plasticity

In rate-independent plasticity, it is assumed that the stress-strain relationship is independent of the rate of loading but does depend on the loading sequence (path-dependency). The process is conveniently represented as a flow evolving in time, where each "time" step corresponds to an incremental load or displacement. The formulation of the governing equations in continuum stress-space (assuming stresses as the independent variables) is hereby presented, based on the textbooks by Simo and Hughes (1998) and Zienkiewicz and Taylor (2000).

The governing equations are essentially composed of the following assumptions and rules: elastic stress-strain relationships; a yield condition, defining the elastic domain; a flow rule and hardening law; Kuhn-Tucker complementarity conditions; and a consistency condition. We first assume that the total strain tensor can be split into its elastic and plastic parts

$$\boldsymbol{\epsilon} = \boldsymbol{\epsilon}^{el} + \boldsymbol{\epsilon}^{pl}$$

Furthermore, we relate the stress tensor to the elastic strains using the elastic constitutive tensor

$$\boldsymbol{\sigma} = \mathbf{D}\boldsymbol{\epsilon}^{el} \tag{1.10}$$

The yield criterion is a function that defines the admissible stress states

$$f(\boldsymbol{\sigma}, \mathbf{q}) \leq 0$$

where $\mathbf{q}$ are internal variables related to the plastic strains and to the hardening parameters. The elastic domain is defined by the interior of the yield criterion where $f < 0$; the yield surface is defined by $f = 0$; and the stress state corresponding to $f > 0$ is considered non-admissible.

The irreversible plastic flow is governed by the evolution of plastic strains and internal variables

$$\dot{\boldsymbol{\epsilon}}^{pl} = \dot{\lambda}\mathbf{r}(\boldsymbol{\sigma}, \mathbf{q}) \tag{1.11}$$

$$\dot{\mathbf{q}} = -\dot{\lambda}\mathbf{h}(\boldsymbol{\sigma}, \mathbf{q}) \tag{1.12}$$

where $\mathbf{r}$ and $\mathbf{h}$ are functions defining the direction of plastic flow and the hardening of the material. The parameter λ is typically called the *consistency parameter* or *plastic multiplier*. Together with the yield criterion, $\dot{\lambda}$ must satisfy the Kuhn-Tucker complementarity conditions

$$\begin{aligned} \dot{\lambda} &\geq 0 \\ f(\boldsymbol{\sigma}, \mathbf{q}) &\leq 0 \\ \dot{\lambda} f(\boldsymbol{\sigma}, \mathbf{q}) &= 0 \end{aligned} \tag{1.13}$$

as well as the consistency requirement

$$\dot{\lambda} \dot{f}(\boldsymbol{\sigma}, \mathbf{q}) = 0$$

The consistency requirement means that during plastic loading, the stress state must remain on the yield surface, meaning $\dot{f} = 0$ if $\dot{\lambda} > 0$.

All possible loading or unloading situations at a certain time can be represented by the Kuhn-Tucker and consistency conditions as follows:

1. Elastic loading, meaning $f < 0$ so necessarily $\dot{\lambda} = 0$. This means there is no plastic flow, i.e. $\dot{\boldsymbol{\epsilon}}^{pl} = 0$ and $\dot{\mathbf{q}} = 0$.
2. Neutral loading, where $f = 0$, $\dot{f} = 0$ and $\dot{\lambda} = 0$.
3. Plastic loading, where $f = 0$, $\dot{f} = 0$ and $\dot{\lambda} > 0$.
4. Elastic unloading just after yielding, meaning $f = 0$ but $\dot{f} < 0$ so $\dot{\lambda} = 0$.

J_2 flow theory A widely accepted model of plasticity in metals is usually known as J_2 flow theory or simply J_2-plasticity. It is based on the von Mises yield criterion (von Mises, 1928) that relates the yielding of the material to the deviatoric stresses, measured by the second deviatoric stress invariant J_2. In this thesis, topology optimization of structures exhibiting elasto-plastic response governed by J_2-plasticity is considered in Chapter 8 for the purpose of studying efficient computational procedures. The model is hereby presented as a particular case of rate-independent plasticity.

The yield criterion is the von Mises yield function expressed as

$$f(\boldsymbol{\sigma}, \kappa) = \sqrt{3J_2} - \sigma_y(\kappa) \leq 0 \tag{1.14}$$

where the expression $\sqrt{3J_2}$ is usually named the *von Mises stress* or *equivalent stress*. σ_y is the yield stress in uniaxial tension, which depends on a single internal parameter κ according to an isotropic hardening function. Kinematic hardening is not considered in the current work. A popular choice for the hardening rule is the bi-linear function

$$\sigma_y(\kappa) = \sigma_y^0 + HE\kappa \tag{1.15}$$

where σ_y^0 is the initial yield stress, H is a scalar (usually in the order of 10^{-2}) and E is Young's modulus. An associative flow rule is assumed, meaning that the flow of plastic strains is in a direction normal to the yield surface

$$\dot{\boldsymbol{\epsilon}}^{pl} = \dot{\lambda} \frac{\partial f}{\partial \boldsymbol{\sigma}} \tag{1.16}$$

Finally, the internal variable governing the hardening is the equivalent plastic strain, evolving according to the rule

$$\dot{\kappa} = \sqrt{\frac{2}{3}} \left\| \dot{\boldsymbol{\epsilon}}^{pl} \right\|_2 \tag{1.17}$$

The factor $\sqrt{\frac{2}{3}}$ is introduced so that for the particular one-dimensional case (involving uniaxial plastic deformation), the obvious relation will be obtained, i.e. $\dot{\kappa} = \dot{\epsilon^{pl}}$.

Drucker-Prager elasto-plastic model The Drucker-Prager yield criterion (Drucker and Prager, 1952) is widely used to model the behavior of pressure-dependent materials such as soils, rock or plain concrete. Moreover, the von Mises yield criterion can be seen as a particular case of the Drucker-Prager criterion. The Drucker-Prager yield function is expressed as

$$f(\boldsymbol{\sigma}, \kappa) = \sqrt{3J_2} + \alpha(\kappa) I_1 - \sigma_y(\kappa) \leq 0 \tag{1.18}$$

where I_1 is the first invariant (trace) of the stress tensor. α is a material property depending on the internal hardening parameter κ according to some hardening function. When $\alpha = 0$, the von Mises yield criterion is obtained.

The relations (1.15), (1.16) and (1.17) corresponding to the J_2 flow model are not necessarily suitable for defining plasticity mechanisms in pressure-dependent materials. Nevertheless, the framework for deriving the governing equations according to classical rate-independent plasticity is the same as for the J_2 model. In the study presented in Chapter 7, a Drucker-Prager model with simplified flow and hardening rules is utilized for interpolating the nonlinear behavior of two candidate materials, whose yielding is defined by the Drucker-Prager and von Mises criteria. Efficient computational procedures for the corresponding topology optimization problems are discussed in Chapter 8.

1.2.2.2 Adopted computational approach

Within the finite element framework, elasto-plastic structural analysis is typically performed using an incremental-iterative scheme. The "time" interval is divided into sufficiently small increments. The displacements at each step of incremental load (or prescribed displacement) are computed at the global level and corrected iteratively. These displacements are used to compute incremental strains according to standard kinematic relations. For a given incremental strain, the state variables - stresses, plastic strains and internal variables - can be computed by solving the constitutive equations on the local level. In the context of FEA, this is performed at every Gauss point in the mesh. The state variables are then used to compute global internal forces and equilibrium can be tested. This global-local cycle is repeated until force equilibrium is satisfied.

Assuming that the total strains, plastic strains and internal variables are known at a certain time t, the local constitutive problem consists of updating these values at time $t + \Delta t$ according to the flow rules (1.11) and (1.12). The updated values must comply with the Kuhn-Tucker complementarity conditions (1.13). This continuum problem is transformed into a discrete constrained optimization problem by applying an implicit backward-Euler difference scheme. The central feature of this scheme is the introduction of a trial elastic state. For any given incremental displacement field, it is first assumed that there is no plastic flow between time t_n and the next time step t_{n+1}, meaning the incremental elastic strains are the incremental total strains. Then, for convex yield functions, it can be shown (Simo and Hughes, 1998)

$$f_{n+1}^{trial} \geq f_{n+1}$$

Consequently, the trial state can be utilized to determine the loading/unloading situation which is governed by the Kuhn-Tucker conditions. If $f_{n+1}^{trial} < 0$, then necessarily $f_{n+1} < 0$. This means that for this time step there cannot be any plastic flow, i.e. $\lambda_{n+1} - \lambda_n = 0$ and the step is elastic. If $f_{n+1}^{trial} > 0$, then the second Kuhn-Tucker condition is violated. This implies that the elastic strains are not equal to the total strains and therefore $\lambda_{n+1} - \lambda_n > 0$. Accordingly, we must have $f_{n+1} = 0$ meaning that the time step is plastic. Once this occurs, the new state variables can be found by solving a nonlinear equation system resulting from the time discretization of the governing equations. This is typically performed by a return-mapping algorithm, where the equation system is reduced to a scalar nonlinear equation that is solved by Newton's method.

As mentioned above, two types of elasto-plastic models are considered in this thesis: a J_2 flow model and a simplified rate-independent model based on the Drucker-Prager yield criterion. For solving the local constitutive problem corresponding to J_2 plasticity, a return-mapping algorithm by Simo and Taylor (1986) is employed. This procedure is tailored particularly for plane stress conditions which are the only case considered in this thesis. One obstacle encountered when utilizing a return-mapping algorithm is the need to differentiate the resulting elasto-plastic tangent modulus for the purpose of sensitivity analysis in topology optimization. This results in a tedious sensitivity analysis procedure and apparently some simplifying assumptions must be made (Maute et al., 1998). Consequently, for the purpose of sensitivity analysis a coupled approach is followed, according to the framework suggested by Michaleris et al. (1994). In the coupled approach, the local constitutive problem is again represented in the form of a system of nonlinear equations aimed at finding the new plastic state once plastic flow is predicted by the elastic trial state. For the simplified Drucker-Prager model, the coupled approach is followed for both the analysis and the sensitivity analysis. In the following, the time-discretized governing equations for the J_2 flow model are presented. For the Drucker-Prager model, the coupled equation system is presented in Chapter 7.

J_2 flow theory In the coupled approach, for every increment n in the transient analysis, we determine the unknowns $\mathbf{u}_n$ and $\mathbf{v}_n$ that satisfy the residual equations

$$
\begin{aligned}
{}^{n}\mathbf{R}({}^{n}\mathbf{u}, {}^{n-1}\mathbf{u}, {}^{n}\mathbf{v}, {}^{n-1}\mathbf{v}) = 0 \\
{}^{n}\mathbf{H}({}^{n}\mathbf{u}, {}^{n-1}\mathbf{u}, {}^{n}\mathbf{v}, {}^{n-1}\mathbf{v}) = 0
\end{aligned}
$$

where $\mathbf{u}$ is the displacements vector and $\mathbf{v}$ are the internal variables

$$
{}^{n}\mathbf{v} = \begin{bmatrix} {}^{n}\boldsymbol{\epsilon}^{pl} \\ {}^{n}\kappa \\ {}^{n}\boldsymbol{\sigma} \\ {}^{n}\lambda \end{bmatrix}
$$

The internal variables considered in this model are as follows: ${}^{n}\boldsymbol{\epsilon}^{pl}$ are the plastic strains, ${}^{n}\kappa$ is the equivalent plastic strain, ${}^{n}\boldsymbol{\sigma}$ are the stresses and ${}^{n}\lambda$ is the plastic multiplier, all corresponding to a "time" increment n.

Neglecting body forces, ${}^{n}\mathbf{R}$ is defined as the difference between external and internal forces and depends explicitly on ${}^{n}\mathbf{v}$ only

$$
{}^{n}\mathbf{R}({}^{n}\mathbf{v}) = {}^{n}\mathbf{f}_{ext} - {}^{n}\mathbf{f}_{int} = {}^{n}\mathbf{f}_{ext} - \int_{V} \mathbf{B}^{T\,n}\boldsymbol{\sigma}\, dV \tag{1.19}
$$

where $\mathbf{B}$ is the standard strain-displacement matrix in the context of finite element procedures. The nonlinear equilibrium equation (1.19) is solved by one of the methods described in Section 1.2.3. The residual ${}^{n}\mathbf{H}$ is defined as the collection of four incremental residuals, resulting from the time linearization of the governing constitutive equations

$$
\begin{aligned}
{}^{n}\mathbf{H}_1 &= {}^{n-1}\boldsymbol{\epsilon}^{pl} + ({}^{n}\lambda - {}^{n-1}\lambda)(\frac{\partial f}{\partial {}^{n}\boldsymbol{\sigma}})^{T} - {}^{n}\boldsymbol{\epsilon}^{pl} \\
{}^{n}\mathbf{H}_2 &= {}^{n-1}\kappa + ({}^{n}\lambda - {}^{n-1}\lambda)\sqrt{\frac{2}{3}(\frac{\partial f}{\partial {}^{n}\boldsymbol{\sigma}})^{T}(\frac{\partial f}{\partial {}^{n}\boldsymbol{\sigma}})} - {}^{n}\kappa \\
{}^{n}\mathbf{H}_3 &= {}^{n-1}\boldsymbol{\sigma} + \mathbf{D}\left[\mathbf{B}^{n}\mathbf{u} - \mathbf{B}^{n-1}\mathbf{u} - ({}^{n}\boldsymbol{\epsilon}^{pl} - {}^{n-1}\boldsymbol{\epsilon}^{pl})\right] - {}^{n}\boldsymbol{\sigma} \\
{}^{n}\mathbf{H}_4 &= J_2 - \frac{1}{3}(\sigma_y(\kappa))^2
\end{aligned} \tag{1.20}
$$

where the first three equations follow from (1.16), (1.17) and (1.10) respectively; the fourth equation represents the requirement that once a plastic step is identified, the stress state lies on

the yield surface. The local nonlinear equations ${}^n\mathbf{H} = 0$ are solved implicitly. An elastic trial stress is first assumed and then the true stresses and plastic strains are found iteratively using a Newton-Raphson procedure. Clearly, if an elastic increment is predicted by the elastic trial state, then this equation system is satisfied trivially: ${}^n\lambda = {}^{n-1}\lambda$ so ${}^n\boldsymbol{\epsilon}^{pl} = {}^{n-1}\boldsymbol{\epsilon}^{pl}$ and ${}^n\kappa = {}^{n-1}\kappa$, and the stresses are computed using the elastic constitutive tensor and the elastic trial stresses.

Concluding the discussion regarding J_2 flow theory, it is noted that the return-mapping algorithm by Simo and Taylor (1986) and the coupled approach presented above are completely equivalent (Michaleris et al., 1994). Therefore, it is possible to perform the structural analysis with the compact formulation of the return-mapping algorithm, and then employ the coupled approach for a convenient and general formulation of the sensitivity analysis.

1.2.3 Solving nonlinear equation systems

In general, when solving the global nonlinear equilibrium equations, an incremental-iterative solution scheme is employed. In the case of elasto-plasticity incrementation is mandatory since the solution is path-dependent so the overall load (or displacement if the solution is controlled by prescribed displacements) must be divided into sufficiently small increments. In the case of geometric nonlinearities, one increment may be sufficient but it is sometimes more efficient to divide the load into several increments that converge relatively fast.

Newton-Raphson schemes The basic equation to be solved is force equilibrium at the "time" increment n where the unknowns are the nodal displacements $\mathbf{u}^*$

$$\mathbf{R}(\mathbf{u}^*) = {}^n\mathbf{f}_{ext} - {}^n\mathbf{f}_{int}(\mathbf{u}^*) = \mathbf{0}$$

Here, ${}^n\mathbf{f}_{ext}$ and ${}^n\mathbf{f}_{int}$ are the vectors of external and internal nodal forces. For simplicity, it is assumed that only the internal forces depend on the displacements; this dependence is nonlinear. Assuming we have evaluated an approximation of the displacements at a certain iterate $i-1$ to obtain ${}^n\mathbf{u}^{i-1}$, we can expand the Taylor series

$$\mathbf{R}(\mathbf{u}^*) = \mathbf{R}({}^n\mathbf{u}^{i-1}) + \left.\frac{\partial \mathbf{R}}{\partial \mathbf{u}}\right|_{{}^n\mathbf{u}^{i-1}} (\mathbf{u}^* - {}^n\mathbf{u}^{i-1}) + \text{higher order terms}$$

This leads to the equation

$$\left.\frac{\partial \mathbf{f}_{int}}{\partial \mathbf{u}}\right|_{{}^n\mathbf{u}^{i-1}} (\mathbf{u}^* - {}^n\mathbf{u}^{i-1}) = {}^n\mathbf{f}_{ext} - {}^n\mathbf{f}_{int}^{i-1}$$

Introducing the tangent stiffness matrix we obtain the typical iterative equation system

$${}^n\mathbf{K}^{i-1}\Delta\mathbf{u} = {}^n\mathbf{f}_{ext} - {}^n\mathbf{f}_{int}^{i-1} \tag{1.21}$$

The iterative evaluation of the displacements is then updated

$${}^n\mathbf{u}^i = {}^n\mathbf{u}^{i-1} + \Delta\mathbf{u}$$

Accordingly, also the internal forces and tangent stiffness are evaluated for the next iterative step.

The resulting iterative procedure is terminated once a certain measure reaches a required tolerance. Throughout this study, a relative norm of the residual forces is utilized for this purpose

$$\frac{\left\| {}^n\mathbf{f}_{ext} - {}^n\mathbf{f}_{int}^{i-1} \right\|_2}{\left\| {}^n\mathbf{f}_{ext} - {}^{n-1}\mathbf{f}_{ext} \right\|_2} \leq \epsilon$$

In words, the value of the iterative unbalanced forces is measured relatively to the external forces added in the current increment. Once this measure is smaller than ϵ (typically 10^{-6} or smaller), it is said that the incremental solution converged.

Direct solvers One possibility is to solve (1.21) by a direct solver, utilizing factorizations of the tangent stiffness matrix. If we choose to factorize $\mathbf{K}$ at every iteration, the procedure is known as *Full Newton-Raphson* (FNR). Another possibility is to re-use available factorizations. For example, one may choose to factorize $\mathbf{K}$ at the beginning of the increment n and then use this factorization for all iterations i within this increment. This is referred to as the *Modified Newton-Raphson* procedure (MNR). Clearly, convergence will slow down but fewer factorizations will be performed. It is difficult to know beforehand which of the two procedures will lead to a lower computational cost, but it is clear that FNR is more likely to converge to the desired solution.

When nonlinear structural analysis is performed for the purpose of topology optimization, the MNR procedure can be interpreted in a broader manner. Following the nested approach, nonlinear analysis is performed within every design cycle. This means that it is possible to re-use factorizations corresponding to previous design cycles in a modified Newton-Raphson procedure. This is shown to be useful in reducing the overall number of matrix factorizations. Reducing computational cost in nonlinear analysis within topology optimization procedures by means of re-using information is discussed in Chapter 8.

In nonlinear structural analysis the stiffness matrix may lose positive definiteness. This happens, for example, during buckling or when encountering a limit point. In such cases, the Cholesky decomposition cannot be utilized to solve the linearized equation (1.21). Instead, the following symmetric decomposition is used

$$\mathbf{K} = \mathbf{L}\mathbf{D}\mathbf{L}^T$$

where L is a lower-triangular matrix and D is a diagonal matrix.

Iterative solvers For large-scale 3-D problems, a direct solution of (1.21) may be impractical due to the memory requirement and an iterative solver is used instead. These methods are usually known as *Inexact Newton Methods* (Kelley, 1995) since the linear systems may not be solved to full accuracy. If the iterative linear solver is based on the family of Krylov subspace solvers this is referred to as *Newton-Krylov methods*, see for example Kelley (2003). The main challenge when employing these methods is the desire to reduce the number of iterations performed by the Krylov solver for each linear system. Investigating efficient procedures for nonlinear structural analysis within topology optimization, based on Newton-Krylov methods, is beyond the scope of this thesis. Nevertheless, it is a natural extension of Chapter 8 thesis and an interesting topic for future work.

Displacement control When performing a nonlinear structural analysis for the purpose of topology optimization, it is sometimes useful to increment a prescribed displacement rather than a given load. This observation is further discussed in Chapter 2. Controlling the displacement can also improve the numerical stability, for example when a small additional load corresponds to a large additional displacement or when limit points are encountered (Crisfield, 1991). When applying displacement control, the incrementation parameter n represents the magnitude of the displacement at a particular degree of freedom for which incremental displacements are prescribed. Replacing Eq. (1.21), the iterative equilibrium equation corresponding to "time" n then has the form

$$^n\mathbf{K}^{i-1}\Delta\mathbf{u} = {}^n\theta\widehat{\mathbf{f}}_{ext} - {}^n\mathbf{f}_{int}^{i-1}$$

where θ is an *unknown* load factor that multiplies the *fixed* external load vector $\widehat{\mathbf{f}}_{ext}$. The total number of unknowns remains unchanged since one of the entries in $\Delta\mathbf{u}$ is prescribed. In order to maintain symmetry of the resulting linear equation system, a special incremental displacement algorithm is used. Following Batoz and Dhatt (1979), the procedure within a single increment can be outlined as follows

1. Set current displacements and load factor $\mathbf{u}^0, \theta^0$.

2. Set the incremental prescribed displacement at the p-th degree of freedom Δu_p.
3. Solve $\mathbf{K}^0 \Delta \mathbf{u_1} = \widehat{\mathbf{f}}_{ext}$ where $\mathbf{K}^0$ corresponds to $\mathbf{u}^0$.
4. Compute $\Delta\theta = \frac{\Delta u_p}{\Delta u_{1_p}}$.
5. Set $\mathbf{u}^1 = \mathbf{u}^0 + \Delta\theta\Delta\mathbf{u_1}$, $\theta^1 = \theta^0 + \Delta\theta$.
6. Repeat:
   (a) Compute internal forces $\mathbf{f}_{int}^i$ and residual $\mathbf{R} = \theta^i \widehat{\mathbf{f}}_{ext} - \mathbf{f}_{int}^i$.
   (b) Check for convergence.
   (c) Compute the tangent stiffness matrix $\mathbf{K}^i$.
   (d) Solve simultaneously $\mathbf{K}^i \Delta \mathbf{u_1} = \widehat{\mathbf{f}}_{ext}$, $\mathbf{K}^i \Delta \mathbf{u_2} = \mathbf{R}$.
   (e) Compute $\Delta\theta = -\frac{\Delta u_{2_p}}{\Delta u_{1_p}}$.
   (f) Set $\mathbf{u}^{i+1} = \mathbf{u}^i + \Delta\mathbf{u_2} + \Delta\theta\Delta\mathbf{u_1}$, $\theta^{i+1} = \theta^i + \Delta\theta$.
   (g) `i = i + 1`.

1.3 Structural reanalysis

In the nested approach to structural optimization, a sequence of linear systems of the form (1.1) is solved. Typically, the stiffness matrix $\mathbf{K}$ depends on the design variables and hence the displacements $\mathbf{u}$ should be evaluated successively within every design cycle. The process of re-solving such sequences of structural analysis problems is also known as *structural reanalysis*. In this section, an approximate reanalysis approach introduced by Kirsch (1991) is briefly described. In particular, the connection to the investigations presented in Chapters 4, 6 and 8 is emphasized.

The main idea is to re-use an available factorization from a previous linear system when solving the current system. The equation system (1.1) can be rewritten

$$(\mathbf{K}_0 + \Delta\mathbf{K})\mathbf{u} = \mathbf{f} \tag{1.22}$$

where $\mathbf{K}_0$ is the stiffness matrix corresponding to a certain previous optimization step and $\Delta\mathbf{K} = \mathbf{K} - \mathbf{K}_0$. $\mathbf{K}_0$ is given in its factorized form, meaning the Cholesky factor $\mathbf{U}_0$ is known. After rearranging, a recurrence relation is defined

$$\mathbf{u}_k = \mathbf{K}_0^{-1}\mathbf{f} - \mathbf{K}_0^{-1}\Delta\mathbf{K}\mathbf{u}_{k-1} \tag{1.23}$$

Therefore the solution can be determined by the following series expansion

$$\mathbf{u} = (\mathbf{I} - \mathbf{B} + \mathbf{B}^2 - \mathbf{B}^3 + ...)\mathbf{u}_1 \tag{1.24}$$

where

$$\mathbf{u}_1 = \mathbf{K}_0^{-1}\mathbf{f}$$
$$\mathbf{B} \equiv \mathbf{K}_0^{-1}\Delta\mathbf{K}$$

In Kirsch's Combined Approximations (CA) approach, a small number of series terms from (1.24) is taken. These are then used as basis vectors in a reduced basis solution. For a detailed description of the solution procedure and a variety of applications, the reader is referred to the monograph by Kirsch (2008).

Integrating a reanalysis procedure into topology optimization seems quite natural. First, the sequence of stiffness matrices share a common structure. Second, when design changes are small then a reanalysis procedure can yield an accurate solution using only a few recurrence terms. The integration of CA into standard topology optimization procedures is the subject of Chapter 4.

Chapter 6 discusses a procedure where only one factorization is utilized throughout the entire design process. An approximation of the displacements is obtained by simple iterative corrections inspired by the modified Newton-Raphson procedure for nonlinear equations

$$\mathbf{u}_k = \mathbf{u}_{k-1} - \mathbf{K}_0^{-1}(\mathbf{K}(\boldsymbol{\rho})\mathbf{u}_{k-1} - \mathbf{f}) \tag{1.25}$$

where $\mathbf{K}(\boldsymbol{\rho})$ corresponds to the current design cycle and $\mathbf{K}_0$ is the stiffness matrix that was factorized. It will now be shown that both recurrences (1.23) and (1.25) are identical. Rearranging (1.23) leads to

$$\mathbf{u}_k = \mathbf{K}_0^{-1}\mathbf{f} - \mathbf{K}_0^{-1}(\mathbf{K}(\boldsymbol{\rho}) - \mathbf{K}_0)\mathbf{u}_{k-1} = \mathbf{K}_0^{-1}\mathbf{f} + \mathbf{u}_{k-1} - \mathbf{K}_0^{-1}\mathbf{K}(\boldsymbol{\rho})\mathbf{u}_{k-1}$$

while the same expression is obtained when rearranging (1.25)

$$\mathbf{u}_k = \mathbf{u}_{k-1} - \mathbf{K}_0^{-1}\mathbf{K}(\boldsymbol{\rho})\mathbf{u}_{k-1} + \mathbf{K}_0^{-1}\mathbf{f} = \mathbf{K}_0^{-1}\mathbf{f} + \mathbf{u}_{k-1} - \mathbf{K}_0^{-1}\mathbf{K}(\boldsymbol{\rho})\mathbf{u}_{k-1}$$

The equivalence established here between both recurrence formulas is important since (1.25) is not suitable for practical implementation. The corresponding series of iterates converges slowly or even diverges, depending on the proximity of $\mathbf{K}_0$ to $\mathbf{K}(\boldsymbol{\rho})$. This also holds for the series expansion used in CA (Kirsch, 2008). In practical CA procedures, the basis vectors originating from the series expansion (1.24) are orthonormalized with respect to $\mathbf{K}(\boldsymbol{\rho})$. This results in a stable and more effective numerical procedure. Another possibility is to implement a PCG procedure, based on the equivalence between CA and PCG shown by Kirsch et al. (2002). This approach was taken in Chapter 6, where the equation systems of the form (1.1) were solved using PCG with the Cholesky factor of $\mathbf{K}_0$ as a preconditioner. The preconditioner was constructed once in the beginning of the optimization and re-used for all subsequent equation systems.

Nonlinear analysis as a reanalysis problem As described above, applying Newton's method in nonlinear structural analysis leads to the typical iterative equation (1.21). This can also be rewritten as a reanalysis equation, with equivalence to Eq. (1.22) in the linear case

$$(\mathbf{K}_0 + \Delta\mathbf{K})\Delta\mathbf{u} = {}^n\mathbf{f}_{ext} - {}^n\mathbf{f}_{int}^{i-1} \tag{1.26}$$

The aim is to avoid factorizing the tangent stiffness matrix ${}^n\mathbf{K}^{i-1}$ every Newton iteration. Instead, the factorization of $\mathbf{K}_0$ is utilized in a reanalysis procedure identical to that performed in linear reanalysis. As for the choice of $\mathbf{K}_0$, it could be for example the tangent stiffness matrix corresponding to the beginning of a load/displacement increment (same as in MNR). Then the same factorization is used for all iterations within this particular increment. The application of CA for solving Eq. (1.26) was investigated by Amir (2007).

When nonlinear structural analysis is performed for the purpose of structural optimization, $\mathbf{K}_0$ could also correspond to a previous design cycle. Then the matrix $\Delta\mathbf{K}$ corresponds to differences in stiffness due to design changes as well as due to nonlinear effects. Essentially, applying CA yields an approximation to the solution of (1.26). Due to the equivalence of CA and PCG, the resulting procedure can be seen as a particular Newton-Krylov method and theoretical results derived for such methods can be used. Such procedures, together with other means of re-using information in topology optimization of nonlinear structures, are explored in Chapter 8.

References

O. Amir. Nonlinear analysis and reanalysis of structures using combined approximations. Master's thesis, Faculty of Civil and Environmental Engineering, Technion - Israel Institute of Technology, Haifa, Israel, 2007.

K.-J. Bathe. *Finite Element Procedures*. Prentice Hall, Upper Saddle River, New Jersey, 1996.

J.-L. Batoz and G. Dhatt. Incremental displacement algorithms for nonlinear problems. *International Journal for Numerical Methods in Engineering*, 14:1262–1267, 1979.

R. D. Cook. *Concepts and Applications of Finite Element Analysis*. John Wiley & Sons, 2 edition, 1981.

M. A. Crisfield. *Non-linear Finite Element Analysis of Solids and Structures*, volume 1. John Wiley & Sons, 1991.

D. C. Drucker and W. Prager. Soil mechanics and plastic analysis or limit design. *Quarterly of Applied Mathematics*, 10(2):157–165, 1952.

G. H. Golub and C. F. Van Loan. *Matrix Computations*. The Johns Hopkins University Press, Baltimore, Maryland, 1983.

M. R. Hestenes and E. Stiefel. Methods of conjugate gradients for solving linear systems. *Journal of Research of the National Bureau of Standards*, 49(6):409–436, 1952.

C. T. Kelley. *Iterative Methods for Linear and Nonlinear Equations*. SIAM, Philadelphia, 1995.

C. T. Kelley. *Solving Nonlinear Equations with Newton's Method*. SIAM, Philadelphia, 2003.

U. Kirsch. Reduced basis approximations of structural displacements for optimal design. *AIAA Journal*, 29:1751–1758, 1991.

U. Kirsch. *Structural Optimization*. Springer-Verlag, Berlin Heidelberg, 1993.

U. Kirsch. *Reanalysis of Structures*. Springer, Dordrecht, 2008.

U. Kirsch, M. Kocvara, and J. Zowe. Accurate reanalysis of structures by a preconditioned conjugate gradient method. *International Journal for Numerical Methods in Engineering*, 55:233–251, 2002.

K. Maute, S. Schwarz, and E. Ramm. Adaptive topology optimization of elastoplastic structures. *Structural Optimization*, 15(2):81–91, 1998.

P. Michaleris, D. A. Tortorelli, and C. A. Vidal. Tangent operators and design sensitivity formulations for transient non-linear coupled problems with applications to elastoplasticity. *International Journal for Numerical Methods in Engineering*, 37:2471–2499, 1994.

Y. Saad. *Iterative Methods for Sparse Linear Systems, Second Edition*. SIAM, 2003.

J. Simo and T. Hughes. *Computational Inelasticity*. Springer, New York, 1998.

J. Simo and R. Taylor. A return mapping algorithm for plane stress elastoplasticity. *International Journal for Numerical Methods in Engineering*, 22:649–670, 1986.

R. von Mises. Mechanics of the ductile form changes of crystals. *Zeitschrift für Angewandte Mathematik und Mechanik*, 8:161–185, 1928.

O. C. Zienkiewicz and R. L. Taylor. *The Finite Element Method (5th edition) Volume 2 - Solid Mechanics*. Elsevier, 2000.

Chapter 2

Structural Topology Optimization

Structural optimization is concerned with improving the performance of load-bearing structures and is nowadays widely applied in various industries. In particular, topology optimization deals with finding the optimal distribution of material in the design space. Typically, it is applied at the conceptual design phase to obtain the best layout of material. Once the topology of the structure is determined, the design can be further refined by shape and sizing optimization methods. Classical applications of structural optimization are, for example, weight minimization of structural elements in an airplane and stiffness maximization of an automobile frame.

In this thesis, the discussion is limited to problems concerning topological design in structural mechanics. The main purpose of this section is to give a brief introduction regarding the computational approach to the solution of such problems. It is important to note that topology optimization has been applied successfully in various other fields involving a wide variety of physical settings. Therefore it is possible that some of the resulting observations are applicable to problems from other fields that are solved by the same computational approach. Moreover, the focus of this thesis is on a particular part of the computational procedure in structural topology optimization, namely the repeated solution of the state (structural equilibrium) equations. This means that the conclusions may be relevant also to other classes of structural optimization that utilize similar computational procedures.

2.1 Problem formulation and objective functions

Throughout this thesis, the material distribution method for topological design is applied. It was first introduced as a computational tool by Bendsøe and Kikuchi (1988) and was thoroughly reviewed in the monograph by Bendsøe and Sigmund (2003). The purpose is to find the optimal layout of a continuum structure in a given domain. The existence of material in space is conveniently approximated using a standard FEM mesh. This means that every finite element represents a material point and could consist of either material or void. The resulting optimization problem is discrete and is practically impossible to solve on sufficiently fine FE meshes. Therefore in practice a relaxation of the original problem is solved, where the material density at each finite element may vary continuously between 0 (void) to 1 (material). In order to drive the design toward a material-void layout, an interpolation scheme for solid isotropic material is applied, widely recognized as SIMP - Solid Isotropic Material with Penalization (M. P. Bendsøe, 1989). Consequently, the problem formulation resembles a sizing problem, where the material density of each finite element is a size design variable.

When seeking the optimal distribution of material in a continuum domain, considering a set of applied loads and boundary conditions, we are implicitly interested in two fields: The optimal density distribution ρ and the corresponding displacement field u. The same FE discretization is used for both fields with ρ usually set as constant in each element. The displacements are determined from structural equilibrium and depend on the stiffness distribution, which is a

function of the density. Finding the structural equilibrium is usually referred to as the *analysis problem*. One possibility is to solve for both fields simultaneously following the so-called SAND approach (Simultaneous ANalysis and Design). A more popular approach in the context of topology optimization is the nested approach, where the analysis problem is solved separately. Then the optimization problem is reduced to finding only the density distribution. For any given density distribution, a finite element analysis is performed to determine the displacements, which are then used to evaluate the objective and to compute the sensitivity of the objective with respect to the design variables.

The resulting generic form of the topology optimization problems addressed by this thesis is

$$\begin{aligned} \min_{\boldsymbol{\rho}} \quad & c(\boldsymbol{\rho}, \mathbf{u}) \\ \text{s.t.:} \quad & \sum_{e=1}^{N_e} v_e \rho_e \leq V \\ & g_i(\boldsymbol{\rho}, \mathbf{u}) \leq 0 \qquad i = 1, ..., m \\ & 0 \leq \rho_e \leq 1 \qquad e = 1, ..., N_e \\ \text{with:} \quad & \mathbf{R}(\boldsymbol{\rho}, \mathbf{u}) = \mathbf{0} \end{aligned} \tag{2.1}$$

where v_e is the element volume, N_e is the number of finite elements, V is the total available volume and g_i $(i = 1, ..., m)$ are (optional) additional constraints. The element densities ρ_e are collected in the vector $\boldsymbol{\rho}$ and $\mathbf{u}$ is the displacements vector. The nested analysis problem is stated here as a residual problem, $\mathbf{R}(\boldsymbol{\rho}, \mathbf{u}) = \mathbf{0}$, and takes different forms according to the physical model.

2.1.1 Linear elasticity

In linear elasticity the residual problem is a set of linear algebraic equations representing static equilibrium

$$\mathbf{R}(\boldsymbol{\rho}, \mathbf{u}) = \mathbf{f} - \mathbf{K}(\boldsymbol{\rho})\mathbf{u} = \mathbf{0} \tag{2.2}$$

where $\mathbf{f}$ is the external load vector, $\mathbf{u}$ is the displacements vector, and $\mathbf{K}(\boldsymbol{\rho})$ is the stiffness matrix. For simplifying the presentation, it is assumed here that $\mathbf{f}$ is independent upon the design. Using a modified SIMP scheme that can accommodate two material phases, the interpolated Young's modulus is defined as

$$E(\rho_e) = E_{min} + (E_{max} - E_{min})\rho_e^p \tag{2.3}$$

In general, E_{min} and E_{max} are the values of Young's modulus of two candidate materials which should be distributed in the design domain. For the case of distributing a single material and void, E_{min} is set to a small positive value and E_{max} is typically set to 1. p is a penalization factor required to drive the design toward a 0-1 layout. The stiffness matrix is then assembled as follows

$$\mathbf{K}(\boldsymbol{\rho}) = \sum_{e=1}^{N_e} E(\rho_e)\mathbf{K}_e \tag{2.4}$$

where $\mathbf{K}_e$ is the element stiffness matrix corresponding to the Young's modulus value of 1.

The equation system (2.2) is solved using methods described in Section 1.1. Topology optimization problems typically involve a large number of design variables and only a limited number of constraints. Consequently, for medium and large scale problems, the computational cost of the whole optimization process is frequently dominated by the effort involved in repeated solutions of (2.2). The main objective of this thesis is to examine alternative approaches that avoid the costly repeated solutions of the equilibrium equations.

For the purpose of studying efficient solution approaches to the analysis problem, several example problems in structural topology optimization are examined. For maximizing the stiffness of a linear elastic structure, a widely applied objective is to minimize the compliance which is defined as $c(\boldsymbol{\rho}, \mathbf{u}) = \mathbf{f}^T\mathbf{u}$. Another design problem achieving much attention is the force inverter design (Sigmund, 1997) where the aim is to maximize a certain output displacement in the direction opposite to the input force. The corresponding objective is defined as $c(\boldsymbol{\rho}, \mathbf{u}) = \mathbf{l}^T\mathbf{u}$ where $\mathbf{l}$ is a vector with the value of 1 at the output displacement degree of freedom and zeros otherwise.

Topology optimization of linear elastic structures is addressed in Chapters 4, 5 and 6. In the study described in Chapter 4, an approximate reanalysis procedure replaces the exact solution of the nested analysis equations. This approach is demonstrated on two- and three-dimensional minimum compliance problems as well as on two-dimensional force inverters. Efficient use of iterative equation solvers to obtain an approximation to the solution of (2.2) is the topic of Chapter 5. Three-dimensional minimum compliance and force inverter designs are used there as test cases. The same test cases are utilized also to demonstrate the performance of another approximate procedure, based on a single factorization of the stiffness matrix throughout the entire design process. This is presented in Chapter 6.

2.1.2 Large deformations

In large deformations analysis, the residual problem is a set of nonlinear algebraic equations, representing static equilibrium corresponding to the final level of the applied load or prescribed displacement. In a load-controlled analysis, the nested residual problem takes the form

$$\mathbf{R}(\boldsymbol{\rho}, \mathbf{u}) = \mathbf{f}_{ext} - \mathbf{f}_{int}(\boldsymbol{\rho}, \mathbf{u}) = \mathbf{0} \tag{2.5}$$

where $\mathbf{f}_{ext}$ and $\mathbf{f}_{int}(\boldsymbol{\rho}, \mathbf{u})$ are the external and internal force vectors, respectively. In the following it is assumed that $\mathbf{f}_{ext}$ does not depend neither on $\boldsymbol{\rho}$ nor on $\mathbf{u}$. In a displacement-controlled analysis the definition is slightly modified

$$\mathbf{R}(\boldsymbol{\rho}, \mathbf{u}, \theta) = \theta\widehat{\mathbf{f}}_{ext} - \mathbf{f}_{int}(\boldsymbol{\rho}, \mathbf{u}) = \mathbf{0} \tag{2.6}$$

where θ is the load factor multiplying the *constant* reference external load vector $\widehat{\mathbf{f}}_{ext}$. The nonlinear systems of equations (2.5), (2.6) are typically linearized and solved using a Newton-Raphson procedure with the necessary modifications for prescribed displacements, see Section 1.2.3.

In linear elastic cases, assembly of the stiffness matrix took a particularly simple form (2.4), using one standard element stiffness matrix. This cannot be extended to problems with large deformations since the strain-displacement matrix $\mathbf{B}$ depends on the element displacements. Therefore the stiffness values are collected on a Gauss-point level with the material properties interpolated using Eq. (2.3).

When the aim of optimization is to find the stiffest design while considering structural nonlinearities, it is in some cases beneficial to keep a measure of the displacements fixed and maximize the load intensity, rather than fixing the load intensity and minimizing the displacements. This is possible if the designer has some knowledge regarding the expected deformation, and can also be seen as a way of imposing a required deflection at a certain point. Moreover, a fixed load intensity throughout the optimization process may cause difficulties in solving the nonlinear analysis equations for intermediate designs that are very flexible. This calls for using displacement control for the nonlinear analysis, meaning keeping the displacement at a selected degree of freedom (DOF) prescribed for all design cycles.

One challenging aspect of utilizing displacement control is in defining an appropriate objective function. For the simple case of a single point load at the prescribed DOF, an appropriate

objective for achieving maximum stiffness is

$$c(\boldsymbol{\rho}, \mathbf{u}, \theta) = -\theta \widehat{f}_{ext,p} u_p \tag{2.7}$$

where p denotes the prescribed DOF. This means the aim is to maximize the end-compliance, corresponding to the final level of the prescribed displacement. More intuitively, this can be seen as maximizing the load intensity that corresponds to a given deflection at a certain DOF. A similar objective as well as other related measures were studied by Buhl et al. (2000) and later by Kemmler et al. (2005). However, in these studies the opposite sign was used since the nonlinear analysis was load-controlled, therefore minimization of the end-compliance was the proper objective.

If the external forces are applied at other degrees of freedom besides the prescribed one, generalizing (2.7) is not straightforward. Since the displacement is prescribed at a single DOF while the same load factor θ multiplies all nodal loads, minimizing $-\theta \widehat{\mathbf{f}}_{ext}^T \mathbf{u}$ may result in a structure that is very stiff with respect to bearing the load at the prescribed DOF but very flexible with respect to all other loads. One possible remedy is to couple the displacements of all loaded degrees of freedom to the prescribed displacement (Maute et al., 1998). Maute et al. added a stiff connection to the design domain in order to achieve such coupling. This practical approach is applicable when the loads are in close proximity to each other. For example, if a concentrated load is locally distributed between several adjacent nodes in order to avoid stress concentrations or local buckling modes, coupling the displacements is sensible. On the other hand, if we wish to optimize a beam structure subject to a general distributed load, this approach could not be applied since it interferes with the design process. Another possibility is to keep the objective (2.7), meaning to optimize a particular contribution to the compliance and not the global measure. Finally, it is also possible to utilize a prescribed displacement in the analysis, but to view the optimization problem, and in particular the sensitivity analysis, *as if* load control was used. Then the stiffest design is achieved by simply minimizing the end-compliance in a load-controlled setting ${\mathbf{f}_{ext}}^T \mathbf{u}$. This hybrid problem formulation is further discussed in Section 2.2.4.

Topology optimization of continuum structures exhibiting large deformations is considered in Chapter 8. Efficient analysis procedures are achieved by re-using information available from a certain design cycle in the solution of the analysis problem corresponding to the next design cycle. In the context of re-using information, it is important to note that typically in problems involving large deformations only the final equilibrium point should be found. Once nonlinear equilibrium is established for a certain design cycle, the corresponding stiffness matrix and displacements vector can be stored. Then they can be utilized as approximations of the stiffness and displacements corresponding to the required final equilibrium in the next design cycle. This procedure, as well as other variants of re-using information, are discussed in Chapter 8.

2.1.3 Elasto-plasticity

In elasto-plastic analysis, the residual problem can be seen as a set of transient, coupled and nonlinear algebraic equations corresponding to incremental levels of load or prescribed displacement

$$\begin{aligned} {}^n\mathbf{R}({}^n\mathbf{v}, {}^n\theta) &= \mathbf{0} \qquad n = 1, ..., N \\ {}^n\mathbf{H}({}^n\mathbf{u}, {}^{n-1}\mathbf{u}, {}^n\mathbf{v}, {}^{n-1}\mathbf{v}, \boldsymbol{\rho}) &= \mathbf{0} \qquad n = 1, ..., N \end{aligned} \tag{2.8}$$

where N is the number of increments and the load factor ${}^n\theta$ is only used for displacement-controlled analysis. The first residual in (2.8) denoted by ${}^n\mathbf{R}$ is satisfied on a global level and represents static equilibrium at increment n. For load control this is identical to (1.19), while for displacement control the expression is slightly modified

$${}^n\mathbf{R}({}^n\mathbf{v}, {}^n\theta) = {}^n\theta \widehat{\mathbf{f}}_{ext} - {}^n\mathbf{f}_{int} = {}^n\theta \widehat{\mathbf{f}}_{ext} - \int_V \mathbf{B}^T {}^n\boldsymbol{\sigma} dV = \mathbf{0} \tag{2.9}$$

The second residual in (2.8) denoted by ${}^n\mathbf{H}$ is satisfied on a local (Gauss-point) level and represents the constitutive elasto-plastic problem. For the J_2 flow model the corresponding equations are given in (1.20). Unlike the global equilibrium equation, the constitutive equations should be derived for each particular material model.

A rather open topic is the extension of the SIMP interpolation scheme to elasto-plastic material properties. Observing the von Mises yield function (1.14) and the bi-linear hardening law (1.15), we find three material parameters that can potentially vary according to the element density: E, H and σ_y^0. A SIMP approach to the interpolation of the three parameters was originally suggested by Maute et al. (1998). The resulting interpolating functions can be written as follows

$$\begin{aligned} E(\rho_e) &= E_{min} + (E_{max} - E_{min})\rho_e^{p_E} \qquad (2.10)\\ H(\rho_e) &= H_{min} + (H_{max} - H_{min})\rho_e^{p_H} \\ \sigma_y^0(\rho_e) &= \sigma_{y,min}^0 + (\sigma_{y,max}^0 - \sigma_{y,min}^0)\rho_e^{p_{\sigma y}} \qquad (2.11) \end{aligned}$$

where p_E, p_H and p_{σ_y} are separate penalty factors for each material parameter. In this work, p_H was typically set to zero since the hardening stiffness is already penalized through the value of $E(\rho_e)$. As for p_{σ_y}, from a physical point of view it should be equal to p_E. This implies that the yield strain will be constant regardless of the density ρ, which makes sense for an isotropic material. Yuge and Kikuchi (1995) observed similar behavior also for a material with a microstructure consisting of a square hole. On the other hand, for the purpose of numerical stability, it is beneficial to set p_{σ_y} to be smaller than p_E. This means that for low-density elements, yielding is somewhat delayed artificially. The overall solution remains unaffected since low-density elements have little impact on the global response. At the same time, ill-conditioning of the local equation system for such elements is avoided. In their numerical examples, Maute et al. (1998) also used a reduced penalty factor for the uniaxial yield stress.

A new extension to the SIMP interpolation scheme is utilized in Chapter 7. The goal is to distribute two nonlinear materials, whose response can be represented by either the von Mises yield function or by the Drucker-Prager yield function. This can be achieved by using a Drucker-Prager function (1.18) with the interpolations (2.10) and (2.11) and adding the following interpolating function

$$\alpha(\rho_e) = \alpha_{max} - (\alpha_{max} - \alpha_{min})\rho_e^{p_\alpha}$$

For the choice $\alpha_{min} = 0$, the von Mises yield surface is obtained for the material corresponding to $\rho = 1$. For $\rho = 0$ we obtain the Drucker-Prager yield surface with the material parameter $\alpha = \alpha_{max}$. A potential application is conceptual design of reinforced concrete, where the distribution of concrete and steel is optimized. Further details regarding this class of elasto-plastic problems can be found in Chapter 7.

When aiming at finding the stiffest structural layout, an appropriate objective function is again maximization of the end-compliance with a prescribed displacement

$$c(\boldsymbol{\rho}, \mathbf{u}, \theta) = -{}^N\theta\, \widehat{f}_{ext,p}\, {}^N u_p \qquad (2.12)$$

where the superscript N denotes the final increment, corresponding to the total prescribed displacement. As explained in the previous section, some complications arise when $\widehat{\mathbf{f}}_{ext}$ consists of loads at non-prescribed DOF. The treatment of such cases is essentially the same as for problems in large deformations.

Alternatively, the "stiffest" structure can also be interpreted as the one that absorbs the most energy. Then an appropriate objective would be to maximize the integral of the strain energy as suggested by Swan and Kosaka (1997) and by Maute et al. (1998). The same outcome is achieved by minimizing the complementary elastic work as suggested by Buhl et al. (2000). Using equilibrium in the case of a single load at the prescribed DOF, the objective function can

be written in terms of external forces and displacements

$$c(\boldsymbol{\rho}, \mathbf{u}, \theta) = -\sum_{n=1}^{N} \frac{1}{2}({}^{n}\theta + {}^{n-1}\theta)\widehat{f}_{ext,p}({}^{n}u_p - {}^{n-1}u_p) \tag{2.13}$$

Another possible goal in engineering design could be to minimize plastic deformation while maintaining relatively high stiffness. This can be posed as an optimization problem aimed at minimizing plasticity subject to a constraint on the end-compliance or on the total energy absorption. Then the measures from (2.12) or (2.13) are constrained to a certain prescribed value while minimization of plasticity can be defined using the equivalent plastic strain, for example

$$c(\boldsymbol{\rho}, \mathbf{v}) = \sum_{e=1}^{N_e} \sum_{k=1}^{4} {}^{N}\kappa_{e,k}$$

In this case, the optimized quantity is simply the sum of the Gauss-point equivalent plastic strains. In case a non-uniform mesh is utilized, meaning the element volumes may differ, it is possible to multiply the Gauss-point value by the corresponding area.

2.2 Sensitivity analysis

The optimization problem (2.1) is typically solved using a first-order nonlinear program. For each design cycle, an approximate problem is solved based on the sensitivities of the objective function to a change in the design variables. In practical topology optimization procedures, where the number of design variables is typically much larger than the number of constraints, it is beneficial to compute the sensitivities following the adjoint method. In this section, the expressions for computing design sensitivities are given, with correspondence to the classes of problems and objectives presented in Section 2.1.

2.2.1 Linear elasticity

The minimum compliance objective is hereby utilized for demonstrating adjoint sensitivity analysis for problems in linear elasticity. First an *augmented* objective function is formed, by adding a zero term to the original objective

$$\widehat{c}(\boldsymbol{\rho}, \mathbf{u}) = \mathbf{f}^T\mathbf{u} - \boldsymbol{\lambda}^T\mathbf{R}(\boldsymbol{\rho}, \mathbf{u})$$

where $\boldsymbol{\lambda}$ is an arbitrary vector containing the *adjoint variables* and $\mathbf{R}(\boldsymbol{\rho}, \mathbf{u})$ is the zero residual corresponding to the nested analysis equations. Writing the nested equation system explicitly leads to

$$\widehat{c}(\boldsymbol{\rho}, \mathbf{u}) = \mathbf{f}^T\mathbf{u} - \boldsymbol{\lambda}^T(\mathbf{f} - \mathbf{K}(\boldsymbol{\rho})\mathbf{u})$$

Assuming the load is design-independent, differentiation with respect to a certain element density gives

$$\frac{\partial \widehat{c}}{\partial \rho_e} = \mathbf{f}^T\frac{\partial \mathbf{u}}{\partial \rho_e} + \boldsymbol{\lambda}^T\frac{\partial \mathbf{K}}{\partial \rho_e}\mathbf{u} + \boldsymbol{\lambda}^T\mathbf{K}(\boldsymbol{\rho})\frac{\partial \mathbf{u}}{\partial \rho_e} \tag{2.14}$$

In order to avoid computing $\frac{\partial \mathbf{u}}{\partial \rho_e}$ explicitly, it is required that all terms involving this derivative sum to zero

$$\mathbf{f}^T\frac{\partial \mathbf{u}}{\partial \rho_e} + \boldsymbol{\lambda}^T\mathbf{K}(\boldsymbol{\rho})\frac{\partial \mathbf{u}}{\partial \rho_e} = 0$$

Since $\mathbf{K}(\boldsymbol{\rho}) = \mathbf{K}(\boldsymbol{\rho})^T$, this leads to the adjoint equation system

$$\mathbf{K}(\boldsymbol{\rho})\boldsymbol{\lambda} = -\mathbf{f}$$

So for the minimum compliance objective, evidently $\boldsymbol{\lambda} = -\mathbf{u}$. Inserting this result back into (2.14) gives the required gradient

$$\frac{\partial \widehat{c}}{\partial \rho_e} = -\mathbf{u}^T \frac{\partial \mathbf{K}}{\partial \rho_e} \mathbf{u}$$

where the derivative $\frac{\partial \mathbf{K}}{\partial \rho_e}$ takes a particularly simple form using (2.3) and (2.4).

For the second objective function used in this work, $c(\boldsymbol{\rho}, \mathbf{u}) = \mathbf{l}^T \mathbf{u}$, the same procedure is applied leading to the equation system

$$\mathbf{K}(\boldsymbol{\rho})\boldsymbol{\lambda} = -\mathbf{l}$$

and the corresponding design sensitivities are then given by

$$\frac{\partial \widehat{c}}{\partial \rho_e} = \boldsymbol{\lambda}^T \frac{\partial \mathbf{K}}{\partial \rho_e} \mathbf{u}$$

The increase in computational effort associated with the solution of another linear system (in addition to the analysis equations) depends on the type of linear solver. For direct solvers, this only requires two more triangular solves since the factors of $\mathbf{K}(\boldsymbol{\rho})$ are available from the solution of the analysis equations. When using a Krylov subspace solver, in principal every additional right-hand-side (r.h.s.) requires roughly the same effort as the first, since the search space is generated according to the r.h.s. vector. Nevertheless, in practice the cost does not rise proportionally to the number of r.h.s. vectors since a block solver is utilized (O'Leary, 1980). When solving for many r.h.s. vectors, advanced techniques can be used that significantly reduce the extra cost related to every additional r.h.s. (Saad et al., 2000).

Remarks about efficient procedures In the context of the current work, it is important to stress that the adjoint sensitivity analysis presented here is not actually performed in any of the studies investigating problems in linear elasticity. This is because the nested analysis equations are not solved accurately. Chapter 4 addresses the use of approximate reanalysis, replacing an exact solution of the nested problem. Sensitivity analysis is consistent with the actual problem that is accurately solved, which in this case is a reduced equation system. In Chapters 5 and 6, iterative solvers are employed for solving the nested problem. In both cases, the convergence criterion for the iterative solver is relaxed, meaning the residual $\mathbf{R}$ from (2.2) is not the zero vector. Nevertheless, design sensitivities are computed by the same procedure outlined above *as if* the analysis equations were solved accurately; this of course means there is some error in the value of the sensitivities. An important observation arising from these studies is that the errors in design sensitivities are insignificant for the purpose of optimization: the results obtained are practically identical to those obtained with accurate gradients. An interesting direction for future work is to investigate the performance of the optimization program when inaccurate gradients are supplied to it. Hopefully, such an investigation can provide analytical arguments that support the experimental observations.

2.2.2 Large deformations

Sensitivity analysis for problems that involve large deformations is in principal the same as for problems in linear elasticity, in cases that the objective depends on the final equilibrium only and disregards the solution path. For the minimum end-compliance objective using load-controlled analysis, the augmented objective is

$$\widehat{c}(\boldsymbol{\rho}, \mathbf{u}) = \mathbf{f}_{ext}^T \mathbf{u} - \boldsymbol{\lambda}^T (\mathbf{f}_{ext} - \mathbf{f}_{int}(\boldsymbol{\rho}, \mathbf{u}))$$

Differentiation with respect to a certain element density gives

$$\frac{\partial \widehat{c}}{\partial \rho_e} = \mathbf{f}_{ext}^T \frac{\partial \mathbf{u}}{\partial \rho_e} - \boldsymbol{\lambda}^T (-\frac{\partial \mathbf{f}_{int}}{\partial \rho_e} - \frac{\partial \mathbf{f}_{int}}{\partial \mathbf{u}} \frac{\partial \mathbf{u}}{\partial \rho_e}) \tag{2.15}$$

Using the tangent stiffness matrix corresponding to the final equilibrium point $\mathbf{K} = \frac{\partial \mathbf{f}_{int}}{\partial \mathbf{u}}$ and exploiting symmetry, the following equation is obtained

$$\mathbf{K}\boldsymbol{\lambda} = -\mathbf{f}_{ext}$$

Finally, the solution for $\boldsymbol{\lambda}$ is inserted back into (2.15) to give the design sensitivities

$$\frac{\partial \widehat{c}}{\partial \rho_e} = \boldsymbol{\lambda}^T \frac{\partial \mathbf{f}_{int}}{\partial \rho_e}$$

Introducing displacement control in the nonlinear analysis leads to a slightly different procedure. Demonstrating on the maximum end-compliance objective (2.7) and using (2.6), the augmented objective function is

$$\widehat{c}(\boldsymbol{\rho}, \mathbf{u}, \theta) = -\theta \widehat{f}_{ext,p} u_p - \boldsymbol{\lambda}^T (\theta \widehat{\mathbf{f}}_{ext} - \mathbf{f}_{int}(\boldsymbol{\rho}, \mathbf{u}))$$

Since u_p is prescribed, it does not depend on the design variables. Adding the subscript f denoting free non-prescribed DOF, differentiation with respect to a certain element density gives

$$\frac{\partial \widehat{c}}{\partial \rho_e} = -\frac{\partial \theta}{\partial \rho_e} \widehat{f}_{ext,p} u_p - \lambda_p \widehat{f}_{ext,p} \frac{\partial \theta}{\partial \rho_e} + \boldsymbol{\lambda}^T \frac{\partial \mathbf{f}_{int}}{\partial \rho_e} + \boldsymbol{\lambda}^T \frac{\partial \mathbf{f}_{int}}{\partial \mathbf{u}_f} \frac{\partial \mathbf{u}_f}{\partial \rho_e} \tag{2.16}$$

This means the value of the adjoint variable at the prescribed DOF is simply $\lambda_p = -u_p$. This is then used to determine the other adjoint variables by solving the equation system

$$\mathbf{K}_{ff}\boldsymbol{\lambda}_f + \mathbf{K}_{fp}\lambda_p = \mathbf{0}$$

Finally, the adjoint vector is inserted back into (2.16) to obtain the design sensitivities

$$\frac{\partial \widehat{c}}{\partial \rho_e} = \boldsymbol{\lambda}^T \frac{\partial \mathbf{f}_{int}}{\partial \rho_e}$$

Applying external loads to non-prescribed DOF leads to a more complicated procedure for sensitivity analysis. As discussed in the previous section, defining a suitable objective for such cases is a problem on its own. Therefore the adjoint sensitivity analysis will only be outlined in the following, without reference to a particular objective function. The augmented objective is

$$\widehat{c}(\boldsymbol{\rho}, \mathbf{u}, \theta) = c(\boldsymbol{\rho}, \mathbf{u}, \theta) - \boldsymbol{\lambda}^T (\theta \widehat{\mathbf{f}}_{ext} - \mathbf{f}_{int}(\boldsymbol{\rho}, \mathbf{u}))$$

Utilizing the subscripts p and f to denote the prescribed and non-prescribed DOF, differentiation of the augmented objective gives

$$\frac{\partial \widehat{c}}{\partial \rho_e} = \frac{\partial c}{\partial \rho_e} + \frac{\partial c}{\partial \mathbf{u}_f}\frac{\partial \mathbf{u}_f}{\partial \rho_e} + \frac{\partial c}{\partial \theta}\frac{\partial \theta}{\partial \rho_e} - \boldsymbol{\lambda}^T \frac{\partial \theta}{\partial \rho_e}\widehat{\mathbf{f}}_{ext} + \boldsymbol{\lambda}^T \frac{\partial \mathbf{f}_{int}}{\partial \rho_e} + \boldsymbol{\lambda}^T \frac{\partial \mathbf{f}_{int}}{\partial \mathbf{u}_f}\frac{\partial \mathbf{u}_f}{\partial \rho_e}$$

This leads to a *coupled* system of adjoint equations

$$\begin{aligned} \widehat{\mathbf{f}}_{ext}^T \boldsymbol{\lambda} &= \frac{\partial c}{\partial \theta} \\ \mathbf{K}_{ff}\boldsymbol{\lambda}_f + \mathbf{K}_{fp}\lambda_p &= -\frac{\partial c}{\partial \mathbf{u}_f}^T \end{aligned} \tag{2.17}$$

Comparing to the case of a single load at the prescribed DOF, this procedure is less convenient since de-coupling the equations by isolating λ_p destroys the symmetry of the stiffness matrix. This makes it more complicated to re-use the factorization of the stiffness matrix in subsequent design cycles as suggested in Chapter 8.

Applying a hybrid approach, where the analysis is displacement-controlled but the objective and sensitivity analysis correspond to a load-controlled setting, may eliminate the difficulties arising when utilizing displacement control. Such an approach is discussed in Section 2.2.4

Remarks about efficient procedures Efficient procedures for nonlinear structural analysis within topology optimization procedures are discussed in Chapter 8. The main idea is to re-use information from a certain design cycle when solving the analysis problem in the next design cycle. Such information can be, for example, the converged displacements and the factorized form of the tangent stiffness matrix. For this purpose, the stiffness matrix that is factorized for solving the adjoint equations is the best candidate, since it corresponds to $\mathbf{R} = \mathbf{0}$ and not to an intermediate Newton iteration. Utilizing displacement control in the analysis introduces some difficulty, since the matrix must be modified for solving the adjoint equations when there are loads in non-prescribed degrees of freedom. However, if adjoint sensitivity analysis is performed considering a load-controlled setting, this problem can be overcome. The topic is further discussed in Chapter 8.

2.2.3 Elasto-plasticity

Sensitivity analysis for topology optimization problems involving elasto-plasticity takes a completely different form due to path-dependency of the nonlinear response. As mentioned earlier, the framework presented by Michaleris et al. (1994) is followed when deriving the backwards-incremental adjoint procedure for such problems. Beginning with forming the augmented response functional using (2.8) and without reference to a particular objective

$$\begin{aligned}\widehat{c}(\boldsymbol{\rho},\mathbf{u},\mathbf{v},\theta) &= c(\boldsymbol{\rho},\mathbf{u},\mathbf{v},\theta) - \sum_{n=1}^{N} {}^{n}\boldsymbol{\lambda}^{T\,n}\mathbf{R}({}^{n}\mathbf{v},{}^{n}\theta) \\ &\quad - \sum_{n=1}^{N} {}^{n}\boldsymbol{\gamma}^{T\,n}\mathbf{H}({}^{n}\mathbf{u},{}^{n-1}\mathbf{u},{}^{n}\mathbf{v},{}^{n-1}\mathbf{v},\boldsymbol{\rho})\end{aligned}$$

Here, ${}^{n}\boldsymbol{\lambda}$ and ${}^{n}\boldsymbol{\gamma}$ are the adjoint vectors to be found for all increments $n = 1, ..., N$. Assuming the initial responses ${}^{0}\mathbf{u}$, ${}^{0}\mathbf{v}$ do not depend on the design variables, the explicit terms in the derivative of the response functional with respect to an element density are

$$\frac{\partial \widehat{c}_{exp}}{\partial \rho_e} = \frac{\partial c}{\partial \rho_e} - \sum_{n=1}^{N} {}^{n}\boldsymbol{\gamma}^{T}\frac{\partial {}^{n}\mathbf{H}}{\partial \rho_e}$$

The adjoint vectors ${}^{n}\boldsymbol{\gamma}$ are related to the adjoint vectors ${}^{n}\boldsymbol{\lambda}$ and both sets are chosen so that the implicit terms of the derivative vanish. The implicit terms of the derivative with respect to a certain element density ρ_e are as follows

$$\begin{aligned}\frac{\partial({}^{1}\widehat{c}_{imp})}{\partial \rho_e} &= -\left[{}^{1}\boldsymbol{\gamma}^{T}\frac{\partial({}^{1}\mathbf{H})}{\partial({}^{1}\mathbf{u})} + {}^{2}\boldsymbol{\gamma}^{T}\frac{\partial({}^{2}\mathbf{H})}{\partial({}^{1}\mathbf{u})} - \frac{\partial c}{\partial({}^{1}\mathbf{u})}\right]\frac{\partial({}^{1}\mathbf{u})}{\partial \rho_e} \\ &\quad - \left[{}^{1}\boldsymbol{\lambda}^{T}\frac{\partial({}^{1}\mathbf{R})}{\partial({}^{1}\theta)} - \frac{\partial c}{\partial({}^{1}\theta)}\right]\frac{\partial({}^{1}\theta)}{\partial \rho_e} \\ &\quad - \left[{}^{1}\boldsymbol{\lambda}^{T}\frac{\partial({}^{1}\mathbf{R})}{\partial({}^{1}\mathbf{v})} + {}^{1}\boldsymbol{\gamma}^{T}\frac{\partial({}^{1}\mathbf{H})}{\partial({}^{1}\mathbf{v})} + {}^{2}\boldsymbol{\gamma}^{T}\frac{\partial({}^{2}\mathbf{H})}{\partial({}^{1}\mathbf{v})} - \frac{\partial c}{\partial({}^{1}\mathbf{v})}\right]\frac{\partial({}^{1}\mathbf{v})}{\partial \rho_e} \\ &\vdots \\ \frac{\partial({}^{n}\widehat{c}_{imp})}{\partial \rho_e} &= -\left[{}^{n}\boldsymbol{\gamma}^{T}\frac{\partial({}^{n}\mathbf{H})}{\partial({}^{n}\mathbf{u})} + {}^{n+1}\boldsymbol{\gamma}^{T}\frac{\partial({}^{n+1}\mathbf{H})}{\partial({}^{n}\mathbf{u})} - \frac{\partial c}{\partial({}^{n}\mathbf{u})}\right]\frac{\partial({}^{n}\mathbf{u})}{\partial \rho_e} \\ &\quad - \left[{}^{n}\boldsymbol{\lambda}^{T}\frac{\partial({}^{n}\mathbf{R})}{\partial({}^{n}\theta)} - \frac{\partial c}{\partial({}^{n}\theta)}\right]\frac{\partial({}^{n}\theta)}{\partial \rho_e} \\ &\quad - \left[{}^{n}\boldsymbol{\lambda}^{T}\frac{\partial({}^{n}\mathbf{R})}{\partial({}^{n}\mathbf{v})} + {}^{n}\boldsymbol{\gamma}^{T}\frac{\partial({}^{n}\mathbf{H})}{\partial({}^{n}\mathbf{v})} + {}^{n+1}\boldsymbol{\gamma}^{T}\frac{\partial({}^{n+1}\mathbf{H})}{\partial({}^{n}\mathbf{v})} - \frac{\partial c}{\partial({}^{n}\mathbf{v})}\right]\frac{\partial({}^{n}\mathbf{v})}{\partial \rho_e} \\ &\vdots\end{aligned}$$

$$\begin{aligned}\frac{\partial({}^N\widehat{c}_{imp})}{\partial\rho_e} &= -\left[{}^N\boldsymbol{\gamma}^T\frac{\partial({}^N\mathbf{H})}{\partial({}^N\mathbf{u})}-\frac{\partial c}{\partial({}^N\mathbf{u})}\right]\frac{\partial({}^N\mathbf{u})}{\partial\rho_e}\\ &\quad -\left[{}^N\boldsymbol{\lambda}^T\frac{\partial({}^N\mathbf{R})}{\partial({}^N\theta)}-\frac{\partial c}{\partial({}^N\theta)}\right]\frac{\partial({}^N\theta)}{\partial\rho_e}\\ &\quad -\left[{}^N\boldsymbol{\lambda}^T\frac{\partial({}^N\mathbf{R})}{\partial({}^N\mathbf{v})}+{}^N\boldsymbol{\gamma}^T\frac{\partial({}^N\mathbf{H})}{\partial({}^N\mathbf{v})}-\frac{\partial c}{\partial({}^N\mathbf{v})}\right]\frac{\partial({}^N\mathbf{v})}{\partial\rho_e}\end{aligned}$$

The adjoint equations result from the requirement that all the terms involving derivatives of the type $\frac{\partial({}^n\mathbf{u})}{\partial\rho_e}$, $\frac{\partial({}^n\theta)}{\partial\rho_e}$ and $\frac{\partial({}^n\mathbf{v})}{\partial\rho_e}$ $(n=1,...,N)$ will sum up to zeros. The first adjoint equations to be solved are the ones corresponding to the last load increment denoted by N. We begin by recognizing

$$\frac{\partial({}^N\mathbf{H})}{\partial({}^N\mathbf{v})}^T{}^N\boldsymbol{\gamma}=-\frac{\partial({}^N\mathbf{R})}{\partial({}^N\mathbf{v})}^T{}^N\boldsymbol{\lambda}+\frac{\partial c}{\partial({}^N\mathbf{v})}^T \tag{2.18}$$

Then a coupled system to be solved for ${}^N\boldsymbol{\lambda}$ can be derived

$$\begin{aligned}\left[-\frac{\partial({}^N\mathbf{R})}{\partial({}^N\mathbf{v})}\frac{\partial({}^N\mathbf{H})}{\partial({}^N\mathbf{v})}^{-1}\frac{\partial({}^N\mathbf{H})}{\partial({}^N\mathbf{u})}\right]^T{}^N\boldsymbol{\lambda} &= \frac{\partial c}{\partial({}^N\mathbf{u})}^T-\left[\frac{\partial c}{\partial({}^N\mathbf{v})}\frac{\partial({}^N\mathbf{H})}{\partial({}^N\mathbf{v})}^{-1}\frac{\partial({}^N\mathbf{H})}{\partial({}^N\mathbf{u})}\right]^T\\ \frac{\partial({}^N\mathbf{R})}{\partial({}^N\theta)}^T{}^N\boldsymbol{\lambda} &= \frac{\partial c}{\partial({}^N\theta)}\end{aligned} \tag{2.19}$$

where $\left[\frac{\partial({}^N\mathbf{R})}{\partial({}^N\mathbf{v})}\frac{\partial({}^N\mathbf{H})}{\partial({}^N\mathbf{v})}^{-1}\frac{\partial({}^N\mathbf{H})}{\partial({}^N\mathbf{u})}\right]$ is the tangent stiffness matrix corresponding to the converged state at increment N (Michaleris et al., 1994). The system (2.19) strongly resembles the system (2.17) and is solved by the same approach. In a load-controlled procedure, only the first equation remains since θ is not a variable. Once ${}^N\boldsymbol{\lambda}$ is known, ${}^N\boldsymbol{\gamma}$ can be determined by solving (2.18) on a Gauss-point level. Then the next set of adjoint equations corresponding to the increment $N-1$ is addressed. Again we recognize

$$\frac{\partial({}^{N-1}\mathbf{H})}{\partial({}^{N-1}\mathbf{v})}^T{}^{N-1}\boldsymbol{\gamma}=-\frac{\partial({}^{N-1}\mathbf{R})}{\partial({}^{N-1}\mathbf{v})}^T{}^{N-1}\boldsymbol{\lambda}-\frac{\partial({}^N\mathbf{H})}{\partial({}^{N-1}\mathbf{v})}^T{}^N\boldsymbol{\gamma}+\frac{\partial c}{\partial({}^{N-1}\mathbf{v})}^T$$

Then the coupled system to be solved for ${}^{N-1}\boldsymbol{\lambda}$ can be derived

$$\begin{aligned}\left[-\frac{\partial({}^{N-1}\mathbf{R})}{\partial({}^{N-1}\mathbf{v})}\frac{\partial({}^{N-1}\mathbf{H})}{\partial({}^{N-1}\mathbf{v})}^{-1}\frac{\partial({}^{N-1}\mathbf{H})}{\partial({}^{N-1}\mathbf{u})}\right]^T{}^{N-1}\boldsymbol{\lambda} &= \frac{\partial c}{\partial({}^{N-1}\mathbf{u})}^T\\ -\left[\frac{\partial c}{\partial({}^{N-1}\mathbf{v})}\frac{\partial({}^{N-1}\mathbf{H})}{\partial({}^{N-1}\mathbf{v})}^{-1}\frac{\partial({}^{N-1}\mathbf{H})}{\partial({}^{N-1}\mathbf{u})}\right]^T &- \left[\frac{\partial({}^N\mathbf{H})}{\partial({}^{N-1}\mathbf{u})}-\frac{\partial({}^N\mathbf{H})}{\partial({}^{N-1}\mathbf{v})}\frac{\partial({}^{N-1}\mathbf{H})}{\partial({}^{N-1}\mathbf{v})}^{-1}\frac{\partial({}^{N-1}\mathbf{H})}{\partial({}^{N-1}\mathbf{u})}\right]^T{}^N\boldsymbol{\gamma}\\ \frac{\partial({}^{N-1}\mathbf{R})}{\partial({}^{N-1}\theta)}^T{}^{N-1}\boldsymbol{\lambda} &= \frac{\partial c}{\partial({}^{N-1}\theta)}\end{aligned} \tag{2.20}$$

Comparing (2.20) to its equivalent from increment N (2.19), it can be seen that there now is an extra loading term which is path-dependent, meaning ${}^N\boldsymbol{\gamma}$ must be determined prior to the solution for ${}^{N-1}\boldsymbol{\lambda}$.

So in general, in the $n-th$ increment we first solve the coupled adjoint equations to determine ${}^n\boldsymbol{\lambda}$

$$\begin{aligned}\left[-\frac{\partial({}^n\mathbf{R})}{\partial({}^n\mathbf{v})}\frac{\partial({}^n\mathbf{H})}{\partial({}^n\mathbf{v})}^{-1}\frac{\partial({}^n\mathbf{H})}{\partial({}^n\mathbf{u})}\right]^T {}^n\boldsymbol{\lambda} &= \frac{\partial c}{\partial({}^n\mathbf{u})}^T \\ -\left[\frac{\partial c}{\partial({}^n\mathbf{v})}\frac{\partial({}^n\mathbf{H})}{\partial({}^n\mathbf{v})}^{-1}\frac{\partial({}^n\mathbf{H})}{\partial({}^n\mathbf{u})}\right]^T &- \left[\frac{\partial({}^{n+1}\mathbf{H})}{\partial({}^n\mathbf{u})}-\frac{\partial({}^{n+1}\mathbf{H})}{\partial({}^n\mathbf{v})}\frac{\partial({}^n\mathbf{H})}{\partial({}^n\mathbf{v})}^{-1}\frac{\partial({}^n\mathbf{H})}{\partial({}^n\mathbf{u})}\right]^T {}^{n+1}\boldsymbol{\gamma} \\ \frac{\partial({}^n\mathbf{R})}{\partial({}^n\theta)}^T {}^n\boldsymbol{\lambda} &= \frac{\partial c}{\partial({}^n\theta)}\end{aligned}$$

The global adjoint vector ${}^n\boldsymbol{\lambda}$ is then used to find the local adjoint vector ${}^n\boldsymbol{\gamma}$ on a Gauss-point level

$$\frac{\partial({}^n\mathbf{H})}{\partial({}^n\mathbf{v})}^T {}^n\boldsymbol{\gamma} = -\frac{\partial({}^n\mathbf{R})}{\partial({}^n\mathbf{v})}^T {}^n\boldsymbol{\lambda} - \frac{\partial({}^{n+1}\mathbf{H})}{\partial({}^n\mathbf{v})}^T {}^{n+1}\boldsymbol{\gamma} + \frac{\partial c}{\partial({}^n\mathbf{v})}^T$$

Once ${}^n\boldsymbol{\gamma}$ is determined, its contribution to the design sensitivities ${}^n\boldsymbol{\gamma}^T\frac{\partial^n\mathbf{H}}{\partial\rho_e}$ is computed. Then the procedure continues to the previous increment denoted by $n-1$. This is repeated until all contributions are collected to obtain the required design sensitivities.

For performing the backwards-incremental adjoint procedure, the derivatives of the global and local residuals with respect to the analysis variables are required. The derivatives $\frac{\partial({}^n\mathbf{R})}{\partial({}^n\mathbf{v})}$ and $\frac{\partial({}^n\mathbf{R})}{\partial({}^n\theta)}$ can be easily obtained from the general form of the global residual (1.19) or (2.9). On the other hand, the derivatives $\frac{\partial({}^n\mathbf{H})}{\partial({}^n\mathbf{u})}$, $\frac{\partial({}^{n+1}\mathbf{H})}{\partial({}^n\mathbf{u})}$, $\frac{\partial({}^n\mathbf{H})}{\partial({}^n\mathbf{v})}$, $\frac{\partial({}^{n+1}\mathbf{H})}{\partial({}^n\mathbf{v})}$ and $\frac{\partial({}^n\mathbf{H})}{\partial\rho_e}$ are related to the particular elasto-plastic model and to the choice of the internal variables $\mathbf{v}$. An explicit example of these derivatives, corresponding to the classical J_2 flow theory with the governing equations (1.20), is given in Chapter 8. Another example, corresponding to a simple Drucker-Prager model, is presented in Chapter 7 and briefly reviewed in Chapter 8.

When implementing the adjoint procedure, the derivatives of the local residuals ${}^n\mathbf{H}$ and ${}^{n+1}\mathbf{H}$ should maintain consistency with respect to the analysis. In essence, four situations are possible at a certain sequence of increments $n, n+1$:

1. Both increments are elastic.
2. Increment n is elastic and transition to plasticity occurs at increment $n+1$.
3. Both increments are plastic.
4. Increment n is plastic and transition to elasticity occurs at increment $n+1$ (elastic unloading).

The actual situation encountered affects the computation of the derivatives of the respective residuals ${}^n\mathbf{H}$ and ${}^{n+1}\mathbf{H}$. For example, in an elastic state only equation ${}^n\mathbf{H}_3$ in (1.20) should be differentiated and the stresses ${}^n\boldsymbol{\sigma}$ are the only variables considered in ${}^n\mathbf{v}$. So in general, the derivatives of the local residual are matrices of varying sizes, depending on the situation which is determined exclusively by the elastic trial state as described in Section 1.2.2.2.

Remark about existence of design sensitivities Several authors addressed the issue of existence of design sensitivities in elasto-plastic response, e.g. Michaleris et al. (1994) and Kleiber et al. (1997). At a given material point, it is theoretically possible that a certain design change will result in plastic behavior while an opposite design change will result in elastic behavior. This means that design sensitivities may be non-existent at all points which just reach the yield surface - a situation known as neutral loading, see also the Kuhn-Tucker conditions in Section 1.2.2.1. However, in practice this situation seldom occurs. One reason is because in finite

element analysis we only monitor Gauss points and not all material points in the continuum structure, meaning there are much fewer material points where the Kuhn-Tucker conditions are evaluated. Furthermore, in computer implementation it is unlikely that we will have exactly $f = 0$ and $\dot{\lambda} = 0$ at a certain increment. In practice, the transition from elastic to plastic will usually occur *within* a certain increment so that small design changes, in any direction, will still lead to plastic behavior at the same time step. Therefore for practical implementation it is assumed that design sensitivities exist.

Remarks about efficient procedures As described above for GNL problems, it is suggested in Chapter 8 to re-use information from a certain design cycle when solving the nonlinear analysis problem in the next design cycle. Again, the stiffness matrix that is factorized for solving the adjoint equations is the best candidate since it corresponds to a *converged* incremental residual. Unfortunately, path-dependency of the elasto-plastic response poses an obstacle when trying to formulate such efficient solution procedures. Transferring information between design cycles requires that displacement vectors and factorized stiffness matrices from all increments will be stored. This may not be realistic due to memory limitations, especially when concerning 3-D FE meshes. The topic is further discussed in Chapter 8.

2.2.4 Special treatment of displacement-controlled problems

When addressing optimal design of nonlinear structures within this thesis, a hybrid approach is applied in several cases. This means a displacement-controlled nonlinear analysis is performed while the objective is defined according to a load-controlled setting. As a consequence, defining a proper objective is more straightforward; sensitivity analysis takes a simpler form; and realizing the re-use of information is easier.

The hybrid approach is hereby demonstrated on a small example that can be solved analytically. It is shown that in this case, the optimum achieved for a certain prescribed displacement is identical to the optimum achieved if the corresponding load is applied. The design sensitivities, however, are of course different - even though they drive the design toward the same optimum.

The example problem consists of two springs whose stiffnesses depend on the amount of material distributed to each spring. This can be formulated as an optimization problem with one design variable ρ and a total material volume of 1. One of the spring stiffnesses also depends on the spring elongation so the equilibrium equations are nonlinear. Both degrees of freedom are loaded with different load intensities in order to imitate a general loading condition. A sketch of the model is presented in Figure 2.1.

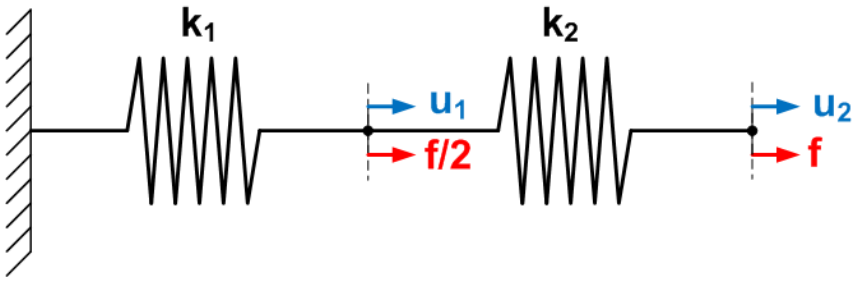

Figure 2.1: A simple two-spring model

The spring stiffnesses are defined as

$$\begin{aligned} k_1 &= \rho \\ k_2 &= (1-\rho)(1+(u_2-u_1)) \end{aligned}$$

Force equilibrium at the two nodes gives

$$\begin{aligned} k_1 u_1 - k_2(u_2 - u_1) - \frac{f}{2} &= 0 \\ k_2(u_2 - u_1) - f &= 0 \end{aligned}$$

This nonlinear equation system can be solved either by prescribing a load intensity, meaning f is known and the two unknowns are u_1 and u_2; or by prescribing a displacement, say u_2, and then the two unknowns are f and u_1. In both cases explicit expressions for the unknowns as functions of ρ can be obtained.

We begin by setting the prescribed displacement, $u_2 = 0.1$. Then, the analysis equations are solved analytically to find f and u_1 as functions of ρ. Finally, the objective function for a displacement-controlled setting, $-fu_2$, corresponding to the end-compliance of the prescribed DOF, can be expressed as a function of ρ only. This objective is plotted in Figure 2.2(a) for $0.01 \leq \rho \leq 0.99$. The minimum point is found by differentiation and occurs at $\rho = 0.561131$. The minimum objective value is -0.00206025, corresponding to a load intensity $f = 0.0206025$. In the second stage, we solve the nonlinear analysis equations using the load intensity at the achieved optimum. Then u_1 and u_2 are found as functions of ρ. Finally, the objective function for a load-controlled setting, fu_2, can be expressed as a function of ρ only. This objective is plotted in Figure 2.2(b) for $0.01 \leq \rho \leq 0.99$. The minimum point is found by differentiation and again occurs at $\rho = 0.561131$, corresponding to the objective value of 0.00206025. Hence an identical optimal design is obtained by both procedures.

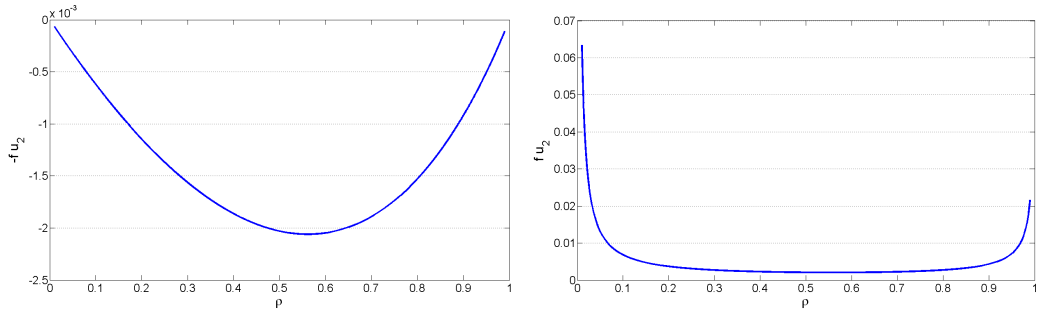

(a) Displacement-controlled setting (b) Load-controlled setting

Figure 2.2: End-compliance as a function of ρ, two-spring example

It can be seen that for this case, the strategy chosen for the nonlinear analysis does not affect the optimal solution. From observing the plots of the objective functions and of the design sensitivities (see Figure 2.3), it is clear that the following approach is valid: we can evaluate a design using one strategy and then update the design using gradients that are computed as if the other strategy was applied. Attempting to establish the validity of this observation in the general case is beyond the scope of this work. However, from an intuitive point of view it seems that this approach can be applied as long as the force-displacement relationship is unique. The results of this simple example also demonstrate the advantage of using displacement control in early stages of the design process: when still far from the optimum, the load-controlled objective is extremely high while the variation in the displacement-controlled objective is small throughout the entire feasible range.

In conclusion, if displacement control is preferred for the nonlinear analysis, optimization can still be performed using sensitivities for a load-controlled analysis. The procedure can be outlined as follows:

1. Set the value of the prescribed displacement (to be kept constant throughout the design process).

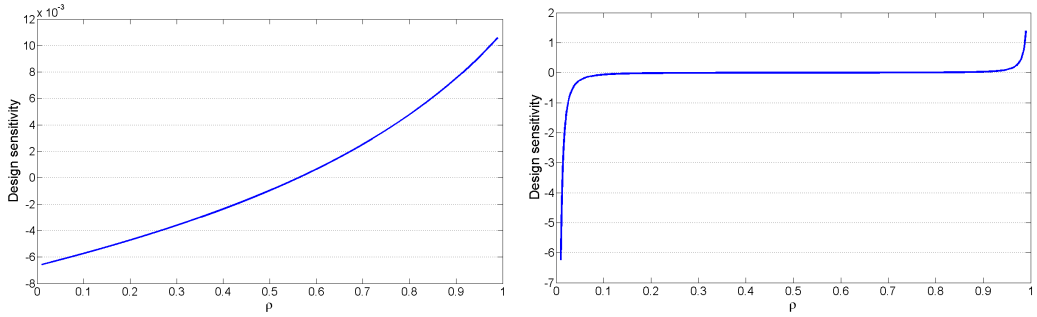

(a) Displacement-controlled setting (b) Load-controlled setting

Figure 2.3: Design sensitivity as a function of ρ, two-spring example

2. Within every design cycle until convergence:

   (a) Perform nonlinear structural analysis using displacement control.

   (b) Perform sensitivity analysis assuming a load-controlled solution, using the load intensity resulting from the nonlinear analysis.

   (c) Update the design.

In Figure 2.4, this procedure is demonstrated on a compliance objective in a single degree of freedom space. For comparison, the standard procedures for either load or displacement control are also sketched. It can be seen that the hybrid approach is equivalent to a load-controlled approach where the load intensity varies throughout the optimization process. In particular, the varying load level is determined implicitly by the displacement-controlled analysis.

2.3 Additional computational components

Besides structural analysis and sensitivity analysis, implementing a topology optimization program requires two additional components, namely a regularization scheme and a nonlinear mathematical program. In all numerical experiments conducted for the purpose of this thesis, density filtering was applied for regularization and the Method of Moving Asymptotes (MMA) was the nonlinear program employed. Both components are hereby shortly introduced.

2.3.1 Density filtering

Applying a regularization scheme is a crucial component in practical topology optimization procedures. Without regularization, black and white checkerboard patterns tend to appear in the resulting layouts. Another problem that must be addressed is the dependency of the results on the resolution of the finite element mesh. Throughout this work, all topology optimization procedures included a classical density filter that is easy to implement and successfully eliminates these problems. The necessary modifications to the overall procedure are shortly presented in this section.

The main idea behind density filtering is to modify each element's density according to the element densities in its surrounding neighborhood. This was initially proposed by Bruns and Tortorelli (2001) and mathematically analyzed by Bourdin (2001). The presentation here follows Sigmund (2007). The filtered element density is given by

$$\widetilde{\rho}_e = \frac{\sum\limits_{i \in N_e} w(\mathbf{x}_i) v_i \rho_i}{\sum\limits_{i \in N_e} w(\mathbf{x}_i) v_i} \tag{2.21}$$

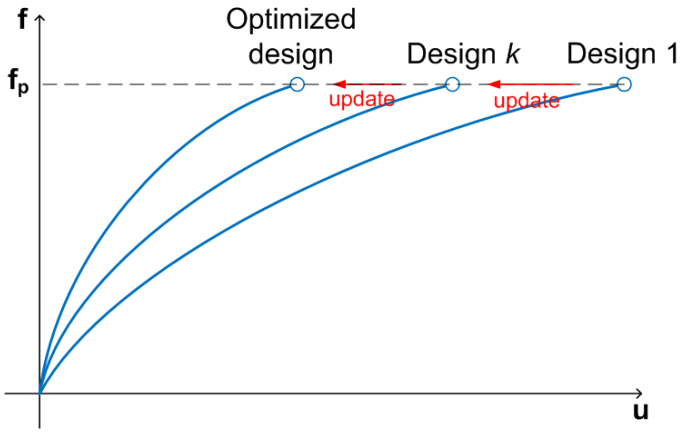

(a) Load-controlled setting

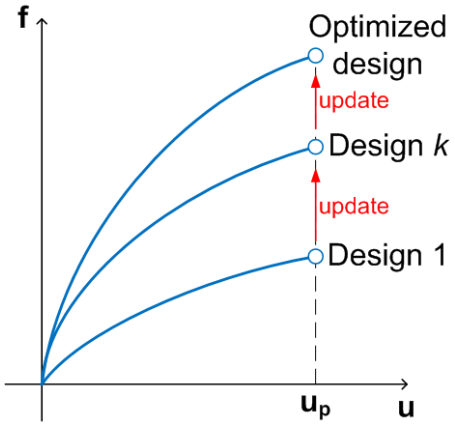

(b) Displacement-controlled setting

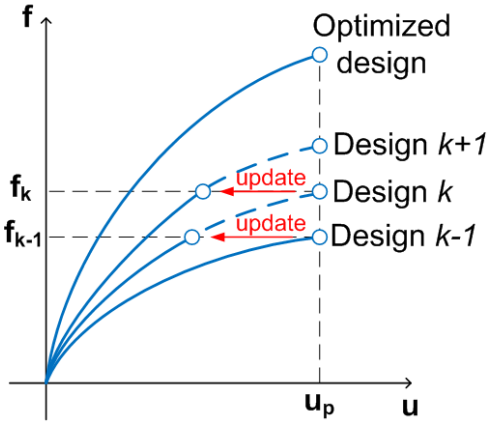

(c) Hybrid approach

Figure 2.4: Comparison of approaches for optimal design considering structural nonlinearities. In a load-controlled setting (top), the designs are evaluated at the same load level and updated accordingly. In a displacement-controlled setting (middle), the designs are evaluated at the same displacement level and updated accordingly. In the hybrid approach (bottom), each design is evaluated at the prescribed displacement level, but then updated according to the corresponding load level.

where N_e is the element's neighborhood and $w(\mathbf{x}_i)$ is a weighting function depending on the distance between element e and its neighboring element i. In this work, the most simple weighting functions were used, i.e. a constant and a linear function. Nevertheless, more sophisticated functions were utilized in other studies.

Applying the density filter means that the original densities $\boldsymbol{\rho}$ have no physical meaning and are only used as mathematical variables in the optimization program. The material interpolation, structural analysis and sensitivity analysis are all performed with the filtered densities $\widetilde{\boldsymbol{\rho}}$. Then, the design sensitivities with respect to the original densities are computed by the chain rule

$$\frac{\partial c}{\partial \rho_e} = \sum_{i \in N_e} \frac{\partial c}{\partial \widetilde{\rho}_i} \frac{\partial \widetilde{\rho}_i}{\partial \rho_e}$$

with $\frac{\partial c}{\partial \widetilde{\rho}_i}$ obtained using the adjoint procedures presented in Section 2.2. Finally, differentiating (2.21) gives

$$\frac{\partial \widetilde{\rho}_i}{\partial \rho_e} = \frac{w(\mathbf{x}_e) v_e}{\sum\limits_{j \in N_i} w(\mathbf{x}_j) v_j}$$

where $w(\mathbf{x}_e)$ is the weight of element e in the neighborhood of element i.

2.3.2 The Method of Moving Asymptotes

MMA was introduced by Svanberg (1987) and is considered an extension of CONLIN (Fleury and Braibant, 1986), both generating a sequence of separable convex approximate subproblems based on first-order sensitivities. In this section, the basic idea behind MMA will be briefly reviewed. The presentation here is based on the monographs by Bendsøe and Sigmund (2003) and by Christensen and Klarbring (2009), supplementing the original article.

Following the nested approach where the structural analysis problem is solved separately, any topology optimization problem can be written in the general form

$$\begin{aligned} \min_{\mathbf{x}} \quad & f_0(\mathbf{x}) \\ \text{s.t.:} \quad & f_i(\mathbf{x}) \leq 0 \qquad i = 1, ..., m \\ & x_j^{min} \leq x_j \leq x_j^{max} \qquad j = 1, ..., n \end{aligned}$$

In MMA the original objective function and constraints f_i $(i = 0, 1, ..., m)$ are approximated around a given iteration $\mathbf{x}^k$ by the function

$$f_i^k(\mathbf{x}) = r_i^k + \sum_{j=1}^{n} \left(\frac{p_{ij}^k}{U_j^k - x_j} + \frac{q_{ij}^k}{x_j - L_j^k} \right)$$

where n is the number of design variables in $\mathbf{x}$. The numbers p_{ij}^k, q_{ij}^k and r_i^k are chosen as

$$\text{if} \quad \frac{\partial f_i}{\partial x_j}(\mathbf{x}^k) > 0 \quad \text{then} \quad p_{ij}^k = (U_j^k - x_j^k)^2 \frac{\partial f_i}{\partial x_j}(\mathbf{x}^k) \quad \text{and} \quad q_{ij}^k = 0$$

$$\text{if} \quad \frac{\partial f_i}{\partial x_j}(\mathbf{x}^k) < 0 \quad \text{then} \quad p_{ij}^k = 0 \quad \text{and} \quad q_{ij}^k = -(x_j^k - L_j^k)^2 \frac{\partial f_i}{\partial x_j}(\mathbf{x}^k)$$

$$r_i^k = f_i(\mathbf{x}^k) - \sum_{j=1}^{n} \left(\frac{p_{ij}^k}{U_j^k - x_j^k} + \frac{q_{ij}^k}{x_j^k - L_j^k} \right)$$

U_j^k and L_j^k are parameters that give vertical asymptotes for the approximating functions and thus control the range for which the approximation is reasonable. These values are updated in order to stabilize or accelerate the convergence, depending on the iteration history.

MMA (as well as CONLIN) has some nice features that make it extremely suitable for topology optimization:

1. The functions f_i^k are first-order approximations, i.e. $f_i^k(\mathbf{x}^k) = f_i(\mathbf{x}^k)$ and $\frac{\partial f_i^k}{\partial x_j}(\mathbf{x}^k) = \frac{\partial f_i}{\partial x_j}(\mathbf{x}^k)$.

2. The functions f_i^k are separable since they are constructed as a sum of functions of one variable. This means that the optimality conditions of the approximate subproblem can be established separately for each design variable.

3. The functions f_i^k are convex since $\nabla^2 f_i^k$ is positive semidefinite. This means that a dual method can be utilized to solve the subproblems.

Topology optimization problems typically have a large number of design variables and a limited number of constraints. For such cases, separability and convexity both lead to a very efficient solution of the optimization problem.

In the original implementation (Svanberg, 1987), the MMA subproblem is solved using Lagrangian duality. First, the approximate subproblem at a certain iteration k can be written as (omitting the k index)

$$\begin{aligned} \min_{\mathbf{x}} \quad & \sum_{j=1}^{n} \left(\frac{p_{0j}}{U_j - x_j} + \frac{q_{0j}}{x_j - L_j} \right) + r_0 \\ \text{s.t.:} \quad & \sum_{j=1}^{n} \left(\frac{p_{ij}}{U_j - x_j} + \frac{q_{ij}}{x_j - L_j} \right) - b_i \leq 0 \qquad i = 1, ..., m \\ & \alpha_j \leq x_j \leq \beta_j \qquad j = 1, ..., n \end{aligned} \tag{2.22}$$

where α_j and β_j are move limits that satisfy $L_j < \alpha_j \leq \beta_j < U_j$. The Lagrangian function $\mathcal{L}$ corresponding to the MMA subproblem (2.22) is

$$\mathcal{L}(\mathbf{x}, \boldsymbol{\lambda}) = r_0 - \boldsymbol{\lambda}^T \mathbf{b} + \sum_{j=1}^{n} \left(\frac{p_{0j} + \boldsymbol{\lambda}^T \mathbf{p}_j}{U_j - x_j} + \frac{q_{0j} + \boldsymbol{\lambda}^T \mathbf{q}_j}{x_j - L_j} \right) = r_0 - \boldsymbol{\lambda}^T \mathbf{b} + \sum_{j=1}^{n} \mathcal{L}_j(x_j, \boldsymbol{\lambda})$$

where $\boldsymbol{\lambda}$ is the vector of m non-negative Lagrange multipliers, $\mathbf{b} = (b_1, ..., b_m)^T$, $\mathbf{p}_j = (p_{1j}, ..., p_{mj})^T$ and $\mathbf{q}_j = (q_{1j}, ..., q_{mj})^T$. The dual objective function is

$$\varphi(\boldsymbol{\lambda}) = \arg\min_{\mathbf{x}} \mathcal{L}(\mathbf{x}, \boldsymbol{\lambda}) = r_0 - \boldsymbol{\lambda}^T \mathbf{b} + \sum_{j=1}^{n} \arg\min_{x_j} \mathcal{L}_j(x_j, \boldsymbol{\lambda})$$

The problem of finding the dual objective $\varphi(\boldsymbol{\lambda})$ is now reduced to separately finding $\arg\min_{x_j} \mathcal{L}_j(x_j, \boldsymbol{\lambda})$ for all $j = 1, ..., n$. Due to convexity, these minimizations have particularly simple solutions depending on the signs of the first derivatives $\mathcal{L}_j'(x_j, \boldsymbol{\lambda})$ at the limits α_j and β_j. Denoting these minimum points by $x_j(\boldsymbol{\lambda})$, the dual objective is now written as

$$\varphi(\boldsymbol{\lambda}) = r_0 - \boldsymbol{\lambda}^T \mathbf{b} + \sum_{j=1}^{n} \left(\frac{p_{0j} + \boldsymbol{\lambda}^T \mathbf{p}_j}{U_j - x_j(\boldsymbol{\lambda})} + \frac{q_{0j} + \boldsymbol{\lambda}^T \mathbf{q}_j}{x_j(\boldsymbol{\lambda}) - L_j} \right)$$

The dual objective is always concave and gives lower bounds on the optimal solution of (2.22) (Boyd and Vandenberghe, 2004). Therefore the dual problem to be solved is

$$\begin{aligned} \max_{\boldsymbol{\lambda}} \quad & \varphi(\boldsymbol{\lambda}) \\ \text{s.t.:} \quad & \lambda_i \geq 0 \qquad i = 1, ..., m \end{aligned}$$

For a limited number of constraints, this is a small and relatively "easy" optimization problem to solve. Once the dual variables $\boldsymbol{\lambda}$ are determined, the optimal values $x_j(\boldsymbol{\lambda})$ can be computed

to give the optimal solution of (2.22). This constitutes a new iterate $\mathbf{x}^{k+1}$, which is used for structural analysis and sensitivity analysis. Then the next subproblem is constructed, and the process continues until a certain convergence measure is satisfied.

In later implementations of MMA, reflected also in the MATLAB code used for numerical experiments within this work, the subproblem (2.22) is solved using a primal-dual interior point method. Such methods solve the primal and the dual problems simultaneously. This is achieved by applying Newton's method to find a solution that satisfies a modified version of the KKT (Karush-Kuhn-Tucker) optimality conditions (Wright, 1997).

References

M. P. Bendsøe and N. Kikuchi. Generating optimal topologies in structural design using a homogenization method. *Computer Methods in Applied Mechanics and Engineering*, 71:197–224, 1988.

M. P. Bendsøe and O. Sigmund. *Topology Optimization - Theory, Methods and Applications*. Springer, Berlin, 2003.

B. Bourdin. Filters in topology optimization. *International Journal for Numerical Methods in Engineering*, 50:2143–2158, 2001.

S. Boyd and L. Vandenberghe. *Convex Optimization*. Cambridge University Press, 2004.

T. E. Bruns and D. A. Tortorelli. Topology optimization of non-linear elastic structures and compliant mechanisms. *Computer Methods in Applied Mechanics and Engineering*, 190:3443–3459, 2001.

T. Buhl, C. Pedersen, and O. Sigmund. Stiffness design of geometrically nonlinear structures using topology optimization. *Structural and Multidisciplinary Optimization*, 19(2):93–104, 2000.

P. W. Christensen and A. Klarbring. *An Introduction to Structural Optimization*. Springer, 2009.

C. Fleury and V. Braibant. Structural optimization - a new dual method using mixed variables. *International Journal for Numerical Methods in Engineering*, 23(3):409–428, 1986.

R. Kemmler, A. Lipka, and E. Ramm. Large deformations and stability in topology optimization. *Structural and Multidisciplinary Optimization*, 30:459–476, 2005.

M. Kleiber, H. Antúnez, T. Hien, and P. Kowalczyk. *Parameter Sensitivity in Nonlinear Mechanics*. John Wiley & Sons, Chichester, 1997.

M. P. Bendsøe. Optimal shape design as a material distribution problem. *Structural Optimization*, 1:193–202, 1989.

K. Maute, S. Schwarz, and E. Ramm. Adaptive topology optimization of elastoplastic structures. *Structural Optimization*, 15(2):81–91, 1998.

P. Michaleris, D. A. Tortorelli, and C. A. Vidal. Tangent operators and design sensitivity formulations for transient non-linear coupled problems with applications to elastoplasticity. *International Journal for Numerical Methods in Engineering*, 37:2471–2499, 1994.

D. P. O'Leary. The block conjugate gradient algorithm and related methods. *Linear Algebra and its Applications*, 29:293–322, 1980.

Y. Saad, M. Yeung, J. Erhel, and F. Guyomarch. A deflated version of the conjugate gradient algorithm. *SIAM Journal on Scientific Computing*, 21:1909–1926, 2000.

O. Sigmund. On the design of compliant mechanisms using topology optimization. *Mechanics Based Design of Structures and Machines*, 25:493–524, 1997.

O. Sigmund. Morphology-based black and white filters for topology optimization. *Structural and Multidisciplinary Optimization*, 33:401–424, 2007.

K. Svanberg. The method of moving asymptotes - a new method for structural optimization. *International Journal for Numerical Methods in Engineering*, 24:359–373, 1987.

C. Swan and I. Kosaka. Voigt-Reuss topology optimization for structures with nonlinear material behaviors. *International Journal for Numerical Methods in Engineering*, 40(20):3785–3814, 1997.

S. J. Wright. *Primal-Dual Interior-Point Methods*. SIAM, Philadelphia, 1997.

K. Yuge and N. Kikuchi. Optimization of a frame structure subjected to a plastic deformation. *Structural Optimization*, 10:197–208, 1995.

Chapter 3

Conclusion

The presented thesis suggests various procedures that can reduce the computational effort involved in repeated solutions of the structural analysis equations. The discussion is focused on applications of topology optimization in structural mechanics but the results can be relevant for a wide range of problems in structural optimization. The main contribution is related to the solution of linear systems while the investigation regarding efficient nonlinear structural analysis only reached a preliminary stage.

This concluding chapter is organized as follows. First, a summary of the articles and the main results is given in Section 3.1. Then, the contribution of the work and its potential impact are assessed in Section 3.2. Finally, ideas for future work related to this thesis are discussed in Section 3.3.

3.1 Summary of the results

The main results from the appended articles are hereby presented. As of the date of submission of the thesis, Articles 1 and 2 were published in printed form and Article 3 was published online, all in peer-reveiwed international journals. Articles 4 and 5 are intended for submission in the near future.

Article 1: Approximate reanalysis in topology optimization (Chapter 4 of the thesis)
In this study, we integrate an approximate reanalysis procedure into the general framework of topology optimization of continuum structures. The goal is to reduce the number of stiffness matrix factorizations performed throughout the design process. It is shown that accurate results can be obtained with one factorization every 10 to 20 design cycles in average.
When reanalysis is performed instead of a standard analysis, the nested optimization problem is re-formulated accordingly. Design sensitivities are derived in a consistent manner, meaning that the errors related to the use of an approximation to the displacement vector are taken into account in the sensitivity analysis. It is shown that as a consequence, relatively rough approximations are acceptable.
The implementation is tested on several small- and medium-scale problems, including two and three dimensional minimum compliance problems and two dimensional compliant force inverter problems. For minimum compliance problems, the approximate procedure yields very accurate results and offers significant savings in computing time. When dealing with compliant mechanism design, the approximate procedure does not yield exactly the same solution as the standard procedure. More work is needed in order to improve the applicability of the approximate approach for this class of problems.

Article 2: Efficient use of iterative solvers in nested topology optimization (Chapter 5 of the thesis)
In this study, it is suggested to reduce the computational effort associated with solving the nested analysis equations by using an approximation to the solution of the analysis problem. The approximation is generated by a Krylov subspace iterative solver and therefore the resulting procedure is highly suitable for parallel computing. When comparing to a standard approach, it is shown that the optimized designs are practically identical while the time spent on the analysis is reduced by roughly 40%.
The key to achieving accurate results efficiently is the early termination criteria for the iterative solver. By defining criteria that are strongly related to the optimization objective and to the design sensitivities, it is possible to terminate the iterative solution of the nested equations earlier compared to traditional convergence measures. The approach is demonstrated on several large-scale 3-D topology optimization problems. In some cases, such as compliant mechanism design where many local minima exist, the approximate procedure leads to slightly different optimized layouts. The accuracy can be further improved by adapting the tolerance of the suggested termination criteria according to the progress of the optimization.

Article 3: On reducing computational effort in topology optimization: how far can we go? (Chapter 6 of the thesis)
In this study, an approximate approach to solving the nested analysis equations in topology optimization is proposed. The procedure consists of one matrix factorization for the whole design process and a small number of iterative corrections for each design cycle. It is shown that the computational cost can be reduced by one order of magnitude while the optimized layouts are practically identical to those generated using standard procedures.
The procedure suggested in this article is in part related to the procedures presented in Articles 1 and 2. We use one matrix factorization in the beginning of the design process, meaning that the solution of the first nested problem is accurate but all subsequent solutions are approximate. The iterative correction procedure is equivalent to the reanalysis approach used in Article 1 but it is re-formulated as a PCG method which is utilized in Article 2. Convergence of the iterative equation solver is not enforced and it is simply terminated after a prescribed number of iterations. It is observed that the errors in the design sensitivities do not affect the progress of the optimization. This raises an important question regarding the required accuracy of the gradients when using a first-order nonlinear program such as MMA.

Article 4: Conceptual design of reinforced concrete using topology optimization with nonlinear material modeling (Chapter 7 of the thesis)
This article gives the background necessary for appreciating one of the demonstrative problems considered in Article 5. In the article, a computational procedure for optimal conceptual design of reinforced concrete structures is presented, based on an extension of the SIMP approach to topology optimization.
The main idea is to consider both concrete and steel as elasto-plastic materials. The different failure criteria corresponding to the nonlinear response of concrete and steel are taken into account, using material interpolation rules for post-yielding behavior in addition to the standard interpolation of elastic properties.
For the case of distributing steel within a full concrete beam, the optimized placement of reinforcement resembles traditional design and agrees with common engineering knowledge. When distributing concrete, steel and void, it is shown that optimized strut-and-tie models can be generated. However, the modeling should be further improved in order for the procedure to be applicable for practical design. Considering strain softening in the concrete model and realistic volume fractions of the steel phase are among the necessary extensions.

Article 5: Re-using solutions and tangent stiffnesses for efficient nonlinear structural analysis in topology optimization (Chapter 8 of the thesis)
In this article we propose efficient solution procedures for nonlinear structural analysis within topology optimization. The suggested computational schemes are based on re-using information throughout the optimization process. It is shown that the computational effort can be decreased, either by reducing the number of iterations in a standard Newton-Raphson procedure or by reducing the number of matrix factorizations using a modified Newton-Raphson procedure.

In the proposed schemes, the solution of the nonlinear structural analysis corresponding to a certain design cycle is used as a starting point for the analysis in the next design cycle. This is shown to be effective in reducing the number of Newton iterations necessary for convergence. When the design changes between two subsequent cycles are small, it is suggested to re-use also the factorization of the tangent stiffness matrix. These procedures are shown to be effective especially for design problems involving geometric nonlinearities, for which savings of up to 50% are achieved. For problems involving elasto-plasticity, the results are less promising due to difficulties arising from the path-depenedent nature of the desired solution.

3.2 Contribution and impact

The main contributions of this work are the various approximate procedures suggested for reducing the computational effort in topology optimization involving linear structural analysis. Even though further studies are necessary for establishing a robust scheme that can be implemented in practice, we believe that this thesis provides a step toward this goal.

Despite the differences between the procedures described in Chapters 4, 5 and 6, one main conclusion arises from the three studies. As stated in the discussion in Chapter 6, we observe that in some cases it may be unnecessary to solve the nested problem accurately. Hopefully, the promising results presented in the thesis can stimulate further research toward the development of an effective computational procedure that can facilitate the solution of larger problems in shorter time. Some ideas regarding future work on this topic are discussed in the next section.

On a more detailed level, the main contribution in Chapter 4 is the consistent integration of an approximate reanalysis approach into topology optimization procedures. To the best of our knowledge, this is the first study connecting Kirsch's Combined Approximations with practical topology optimization procedures. In Chapter 5, the main contributions are the alternative stopping criteria for iterative equation solvers, which can be effective in the context of nested structural optimization. Finally, the main contribution in Chapter 6 is the utilization of relatively rough approximations. The purpose is mainly demonstrative: by showing that acceptable results are obtained with only one stiffness matrix factorization for the whole design process, we hope to raise attention to the prospects of utilizing approximations.

Concluding the discussion regarding topology optimization involving linear structural analysis, it must be stressed that the main drawback of the procedures presented in Chapters 5 and 6 is the lack of theoretical insight. The actual contribution of these studies is in providing ideas and positive conclusions based on numerical experiments, and hopefully in stimulating more fundamental investigations into the topic.

The thesis offers additional contributions to the topic of topology optimization of elasto-plastic structures, as well as in relation to efficient procedures for nonlinear structural analysis in topology optimization.

Topology optimization of elasto-plastic structures is a relatively immature research topic, if judging by the number of publications and the developments reported over the last decade. The challenges arising in the sensitivity analysis constitute one difficulty. The layouts obtained when considering elasto-plastic response are another "problem": often they resemble the layouts

obtained with linear elastic modeling [1]. With these obstacles in mind, we see the main contribution in relation to this topic in the implementation of a general sensitivity analysis procedure for path-dependent response. Within the work on this thesis, perfectly accurate design sensitivities were computed for various elasto-plastic models. In several relevant publications, it was stated that some simplifications were taken into account in the sensitivity analysis. In other articles, some errors in the design sensitivities are reported. Therefore it is possible that the procedure implemented here offers a step forward with respect to consistent sensitivity analysis.

With respect to the examination of computational procedures for nonlinear structural analysis in topology optimization, the study presented in Chapter 8 is by all means preliminary. Nevertheless, the contribution is in opening the topic for discussion and suggesting ideas for efficient treatment of the nonlinear structural analysis. Up to date, investigations regarding topology optimization of structures exhibiting nonlinear response were focused on various challenging aspects of the design problem. This thesis is presumably the first to address the computational challenge arising from the need to perform repeated nonlinear structural analyses. The ideas expressed in Chapter 8 may provide the basis for further investigation into this topic.

3.3 Future work

Several ideas for future work related to the results of this thesis are hereby presented.

Unified approach for approximate linear structural analysis The results from Chapters 4, 5 and 6 can provide the starting point for developing a unified computational procedure that is both robust and efficient. Based on the experience gained during the work on the present thesis, we believe the following components are essential for such a procedure to be realized:

1. *Formulation as a Krylov solver*. All three procedures discussed in this thesis can be formulated as a Krylov subspace solver with preconditioning. The choice of preconditioner depends on the computational environment: the more memory is available, the closer it can be to a factorization. If computer memory is not a limitation, the preconditioner can be a factorization (as in Chapters 4 and 6).

2. *Automatic control over updates of the preconditioner*. One of the parameters governing the accuracy and efficiency of such a Krylov solver is the quality of the preconditioner. In standard procedures, it is updated every design cycle (as in Chapter 5). Otherwise, it can be updated once every several design cycles (as in Chapter 4) or in the extreme case, it can be kept constant throughout the whole design process (as in Chapter 6). The key point to investigate is how to control the frequency of updates so that sufficient accuracy is achieved in an efficient manner.

3. *Effective stopping criterion*. Another parameter affecting the accuracy and efficiency is the number of iterations performed by the Krylov solver. This is determined by the stopping criterion and the required tolerance. An effective criterion could be based on the suggestions in Chapter 5, but such a choice must be supported by strong analytical arguments. A possible direction to explore is relating the stopping criterion and the tolerance to information given from the optimization program. When the optimization process is still far from converging, it is expected that relatively large errors in the analysis can be tolerated. This means that the convergence tolerance of the Krylov solver can be tightened as we approach a solution to the optimization problem. By digging a bit deeper into the optimization program, it may also be possible to relate the quality of the approximations there

[1] This was observed when investigating the problem of maximizing energy absorption with a J_2 plasticity material model, which seems to be the most popular design problem in the relevant literature.

to the quality of the approximations required in the nested analysis. The question is: do we really need to solve the analysis accurately, and compute accurate design sensitivities, knowing that the optimization itself is based on first-order approximations?

Reanalysis applied to robust topology optimization An important extension of the classical topology optimization method is the consideration of uncertainties related to manufacturing processes. These are taken into account in the so-called robust topology optimization approach. The corresponding optimization problem is formulated as a worst case design problem, where for each design cycle a set of similar designs are evaluated. We expect that a reanalysis approach, such as the one utilized in Chapters 4 and 6, will be highly effective in this setting. Using a reanalysis procedure, it may be possible to evaluate accurately only one "base" design within every design cycle. The other designs, generated according to the considered manufacturing errors, will then be evaluated using efficient reanalysis.

Comparative study regarding sensitivity analysis for elasto-plasticity As discussed in the previous section, one of the obstacles encountered during the work was sensitivity analysis for problems involving elasto-plastic response. In the majority of publications, the so-called variational adjoint approach is taken while in the current study a different approach was preferred. As mentioned above, in previous studies that followed the former approach some simplifications were considered and some errors were reported. We find it interesting to conduct a thorough study that will compare all suggested approaches, with emphasis on the consistency of the formulation. Furthermore, computational efficiency should also be examined, due to the relatively high cost of adjoint sensitivity analysis for path-dependent response.

Efficient nonlinear structural analysis in topology optimization using Newton-Krylov methods The study presented in Chapter 8 is restricted to the use of direct methods for solving linear systems, based on matrix factorization. However, practical topology optimization procedures should be suitable for high performance parallel computing so that large-scale 3-D problems could be tackled. Therefore it is crucial to extend the ideas suggested in Chapter 8 for the case that an iterative solver is used to solve the linear systems. The nonlinear structural analysis will then be performed by a Newton-Krylov method. It may be possible to use advanced techniques, such as deflation and recycling of subspaces, for achieving efficient solution procedures based on re-using information.

Part II

Articles

Chapter 4

Approximate reanalysis in topology optimization

Amir O, Bendsøe MP and Sigmund O. Approximate reanalysis in topology optimization. *International Journal for Numerical Methods in Engineering* 2009, vol. 78, pp. 1474-1491.

Abstract In the nested approach to structural optimization, most of the computational effort is invested in the solution of the finite element analysis equations. In this study, the integration of an approximate reanalysis procedure into the framework of topology optimization of continuum structures is investigated. The nested optimization problem is re-formulated to accommodate the use of an approximate displacement vector and the design sensitivities are derived accordingly. It is shown that relatively rough approximations are acceptable since the errors are taken into account in the sensitivity analysis. The implementation is tested on several small and medium scale problems, including two and three dimensional minimum compliance problems and two dimensional compliant force inverter problems. Accurate results are obtained and the savings in computation time are promising.

Keywords Approximate reanalysis, Topology optimization, Structural reanalysis

4.1 Introduction

Despite rapid improvements in computer performance over the last few decades, there is still room for advances in computational efficiency for handling structural optimization applications due to the high computational cost involved in the optimization process. In general, the total computational cost of the optimization procedure is governed by the complexity of three aspects: the model, the analysis and the optimization (Venkataraman and Haftka, 2004). Solving problems that are characterized by high complexities in all three aspects is presently still limited, thus motivating the search for methods and procedures that require reduced computational resources but yield high quality results.

In this paper, the implementation of an approximate reanalysis method in structural topology optimization is investigated. We follow the material distribution approach for topological design (Bendsøe and Kikuchi, 1988) together with the solid isotropic material with penalization (SIMP) interpolation (Bendsøe, 1989). Furthermore, we apply the so-called nested approach where optimization is performed in the design variables only and where the equilibrium equations are treated as function calls. The aim of using approximate reanalysis is to reduce the computational effort involved in repeated solutions of the equilibrium equations, which for large problems will dominate the computational cost of the whole process. The approximate

reanalysis performed here follows the Combined Approximations (CA) approach, originally proposed by Kirsch (1991) for linear static reanalysis. The main feature of CA is the utilization of a local series expansion in a global reduced basis solution. When using CA for repeated structural analysis, one can substantially reduce the number of required factorizations of the stiffness matrix, thus removing a significant portion of the computational effort. It has been shown that the CA method is theoretically equivalent to the preconditioned conjugate gradient method (Kirsch et al., 2002). Therefore, available results from one method, such as convergence criteria and error bounds, can be used also in the other method. Accurate results and significant savings in computational effort have been reported; for further details the reader is referred to (Kirsch, 2002) and (Kirsch, 2008). The approach has also been applied successfully in several classes of structural reanalysis problems, e.g. vibration reanalysis (Kirsch and Bogomolni, 2004), dynamic reanalysis (Kirsch and Bogomolni, 2006) and nonlinear reanalysis (Amir et al., 2008). In connection with topology optimization, it was shown that CA can be utilized in the reanalysis of truss structures undergoing topological changes, even when the structural model is altered and the number of degrees of freedom is changed (Kirsch and Papalambros, 2001).

The main purpose of this study is to examine the integration of linear static reanalysis by CA into the widely used procedures for topology optimization using a distribution of material approach. The investigation focuses on the two most important aspects of an approximate procedure - its accuracy, meaning in this case the possibility to obtain the same topological designs as would be generated by a standard procedure; and its efficiency, meaning that the approximate procedure should offer significant savings in computation time when compared to a standard procedure.

The article is organized as follows. First, the Combined Approximations approach for structural reanalysis is briefly reviewed for the sake of completeness in Section 4.2. Then, in Section 4.3, formulations of topology optimization problems into which approximate reanalysis is integrated are presented for two different types of problems, including the corresponding sensitivity analysis. Computational considerations regarding the implementation of the procedure are discussed in Section 4.4, followed by several numerical examples and efficiency estimates. Finally, some conclusions are drawn in Section 4.5.

4.2 Reanalysis by combined approximations

In this study, approximate reanalysis is performed following the Combined Approximations (CA) approach, originally proposed by Kirsch (1991). As mentioned earlier, the formulation of linear reanalysis by CA is repeated here for the sake of completeness.

Consider the linear system of equilibrium equations resulting from a finite element discretization of the computational domain, corresponding to a certain iterative step of the optimization process

$$\mathbf{K}\mathbf{u} = \mathbf{f} \tag{4.1}$$

where $\mathbf{K}$ is the stiffness matrix, $\mathbf{u}$ is the unknown displacement vector and $\mathbf{f}$ is the external force vector. We assume here that $\mathbf{f}$ does not depend on the optimization and remains constant throughout the whole process; this does not lead to any loss of generality. Now, instead of solving the full system of equations, it is possible to efficiently find an approximate solution $\widetilde{\mathbf{u}}$ that will be sufficiently accurate for the purpose of optimization

$$\widetilde{\mathbf{u}} \approx \mathbf{u}$$
$$\mathbf{K}\widetilde{\mathbf{u}} \approx \mathbf{f}$$

According to the Combined Approximations approach, the approximate solution is obtained as follows. We denote $\mathbf{K}_0$ as the stiffness matrix corresponding to a certain previous optimization

step and given in its factorized form. The equation system (4.1) can be rewritten

$$(\mathbf{K}_0 + \Delta\mathbf{K})\mathbf{u} = \mathbf{f}$$

and hence

$$\mathbf{K}_0\mathbf{u} = \mathbf{f} - \Delta\mathbf{K}\mathbf{u}$$

Here, $\Delta\mathbf{K}$ represents the matrix of changes in stiffness due to changes in the values of the design variables. Defining the following recurrence relation

$$\mathbf{K}_0\mathbf{u}^k = \mathbf{f} - \Delta\mathbf{K}\mathbf{u}^{k-1}$$

leads to the so-called binomial series expansion

$$\mathbf{u} = (\mathbf{I} - \mathbf{B} + \mathbf{B}^2 - \mathbf{B}^3 + ...)\mathbf{u}_1 \tag{4.2}$$

where

$$\begin{aligned} \mathbf{u}_1 &= \mathbf{K}_0^{-1}\mathbf{f} \\ \mathbf{B} &\equiv \mathbf{K}_0^{-1}\Delta\mathbf{K} \\ \mathbf{u}_i &= -\mathbf{B}\mathbf{u}_{i-1} \end{aligned}$$

It is important to note that the first term $\mathbf{u}_1$ is already known from a previous optimization step and the following terms $\mathbf{u}_i$ can be easily computed by forward and backward substitutions based on the factorization of $\mathbf{K}_0$. The main feature of CA is the utilization of the series terms from (4.2) as basis vectors in a reduced basis solution. Considering only the first s series terms, the approximate solution can now be expressed as

$$\widetilde{\mathbf{u}} = y_1\mathbf{u}_1 + y_2\mathbf{u}_2 + ... + y_s\mathbf{u}_s = \mathbf{R}_B\mathbf{y} \tag{4.3}$$

where $\mathbf{R}_B$ is an n x s matrix containing the basis vectors $\mathbf{u}_1, \mathbf{u}_2, ..., \mathbf{u}_s$ and $\mathbf{y}$ is a vector of s unknowns. Replacing $\mathbf{u}$ in (4.1) with $\widetilde{\mathbf{u}}$ from (4.3) and premultiplying both sides by $\mathbf{R}_B^T$

$$\mathbf{R}_B^T\mathbf{K}\mathbf{R}_B\mathbf{y} = \mathbf{R}_B^T\mathbf{f} \tag{4.4}$$

This ends up in a reduced system of equations, with s equations instead of n

$$\mathbf{K}_R\mathbf{y} = \mathbf{f}_R$$

where

$$\begin{aligned} \mathbf{K}_R &= \mathbf{R}_B^T\mathbf{K}\mathbf{R}_B \\ \mathbf{f}_R &= \mathbf{R}_B^T\mathbf{f} \end{aligned}$$

In many cases it is beneficial to orthonormalize the basis vectors, for example by an algorithm usually known as the modified Gram-Schmidt procedure (for details see Golub and Van Loan (1983)). Then, an explicit expression for the approximate vector can be obtained

$$\widetilde{\mathbf{u}} = \mathbf{V}_B\mathbf{z} = \sum_{i=1}^{s} \mathbf{v}_i(\mathbf{v}_i^T\mathbf{f})$$

where the n x s matrix $\mathbf{V}_B$ contains the set of orthonormal basis vectors.

It is important to point out that the computational benefit of this procedure is due to the fact that the basis vectors are easily generated by solving a linear system where the stiffness matrix is already given in its factorized form. The computational cost of the reanalysis procedure is then dominated by the cost of orthonormalization, and is therefore much smaller than the cost of a complete new analysis, which is dominated by the cost of a matrix factorization.

4.3 Topology optimization and sensitivity analysis

The integration of the CA method for approximate reanalysis into a topology optimization procedure is presented in this section. First, for demonstrating the issues to be addressed, we present the formulation for minimum compliance problems, aimed at finding the optimal distribution of elastic material in a certain domain so that the stiffest structure is obtained. Second, the sensitivity analysis for this problem is formulated. Finally, a brief description of the utilization of CA in another class of topology optimization problems is presented.

4.3.1 Problem formulation: minimum compliance

When applying the so-called nested approach, where optimization is performed in the design variables only and where the equilibrium equations are treated as function calls, the optimization problem is formulated as follows

$$\begin{aligned} \min_{\boldsymbol{\rho}} c(\boldsymbol{\rho}) &= \mathbf{f}^T\mathbf{u} \\ \text{s.t.:} \quad & \sum_{e=1}^{N} v_e\rho_e \leq V \\ & 0 < \rho_{min} \leq \rho_e \leq 1, \qquad e = 1, ..., N \\ \text{with:} \quad & \mathbf{K}(\boldsymbol{\rho})\mathbf{u} = \mathbf{f} \end{aligned}$$

where $\mathbf{K}(\boldsymbol{\rho})$ is the stiffness matrix whose entries depend on the design variables $\boldsymbol{\rho}$. When using the SIMP interpolation and element-wise constant densities scheme, $\mathbf{K}(\boldsymbol{\rho})$ can be rewritten as a sum over all elements

$$\mathbf{K}(\boldsymbol{\rho}) = \sum_{e=1}^{N} \rho_e^p \mathbf{K}_e$$

where $\mathbf{K}_e$ is a standard element stiffness matrix referring to an element density equal to 1.

When applying approximate reanalysis, this formulation accurately represents the problem only for optimization cycles in which the full equation system is solved to satisfy the structural equilibrium. For each optimization cycle in which an approximate reanalysis is performed by CA, an appropriate optimization problem is formulated in terms of the approximate solution of the equilibrium equations, $\widetilde{\mathbf{u}}$. The objective function can be expressed as follows

$$\begin{aligned} c(\boldsymbol{\rho}) &= \mathbf{f}^T\mathbf{u} \approx \widetilde{\mathbf{u}}^T\mathbf{K}(\boldsymbol{\rho})\widetilde{\mathbf{u}} \\ \widetilde{\mathbf{u}} &= \mathbf{R}_B\mathbf{y} \\ c(\boldsymbol{\rho}) &= \mathbf{y}^T\mathbf{R}_B^T\mathbf{K}(\boldsymbol{\rho})\mathbf{R}_B\mathbf{y} \end{aligned}$$

When performing approximate reanalysis within a certain optimization cycle, a set of s basis vectors is generated and utilized according to the CA procedure. The size of this set is determined in the reanalysis stage and is then fixed for the sensitivity analysis. In this case the optimization problem will have the form

$$\begin{aligned} \min_{\boldsymbol{\rho}} c(\boldsymbol{\rho}) &= \mathbf{y}^T\mathbf{R}_B^T\mathbf{K}(\boldsymbol{\rho})\mathbf{R}_B\mathbf{y} \\ \text{s.t.:} \quad & \sum_{e=1}^{N} v_e\rho_e \leq V \\ & 0 < \rho_{min} \leq \rho_e \leq 1, \qquad e = 1, ..., N \\ \text{with:} \quad & \mathbf{R}_B^T\mathbf{K}(\boldsymbol{\rho})\mathbf{R}_B\mathbf{y} = \mathbf{R}_B^T\mathbf{f} \\ & \mathbf{K}_0(\boldsymbol{\rho}_0)\mathbf{u}_1 = \mathbf{f} \\ & \mathbf{K}_0(\boldsymbol{\rho}_0)\mathbf{u}_i = -\Delta\mathbf{K}(\boldsymbol{\rho}, \boldsymbol{\rho_0})\mathbf{u}_{i-1}, \qquad i = 2, ..., s \end{aligned} \tag{4.5}$$

It can be seen that the nested equations are the reduced reanalysis system of Equation (4.4) and the equation systems governing the generation of the basis vectors, based on the available factorization of the stiffness matrix $\mathbf{K}_0(\boldsymbol{\rho}_0)$ corresponding to a previous design cycle. In this nested problem, the matrix $\mathbf{R}_B$ contains the basis vectors

$$\mathbf{R}_B = [\mathbf{u}_1, ..., \mathbf{u}_s]$$

and the matrix $\mathbf{K}(\boldsymbol{\rho})$ is split into two parts, the first corresponding to a previous factorization and the second to the changes in stiffness due to changes in the design

$$\mathbf{K}(\boldsymbol{\rho}) = \mathbf{K}_0(\boldsymbol{\rho}_0) + \Delta\mathbf{K}(\boldsymbol{\rho}, \boldsymbol{\rho_0})$$

When using the SIMP interpolation and element-wise constant densities scheme, both matrices can be rewritten as a sum over all elements

$$\begin{aligned} \mathbf{K}_0(\boldsymbol{\rho}_0) &= \sum_{e=1}^{N} \rho_{e,[0]}^p \mathbf{K}_e \\ \Delta\mathbf{K}(\boldsymbol{\rho}, \boldsymbol{\rho_0}) &= \sum_{e=1}^{N} (\rho_e^p - \rho_{e,[0]}^p) \mathbf{K}_e \end{aligned}$$

In many cases, the approximate displacement vector $\widetilde{\mathbf{u}}$ is obtained by solving the reduced system of equations resulting from the utilization of the orthonormal set of basis vectors generated according to the modified Gram-Schmidt procedure. However, the optimization problem is formulated in terms of the original basis vectors $\mathbf{R}_B$ and the corresponding reduced solution $\mathbf{y}$ since this simplifies the sensitivity analysis. Therefore, the reduced solution vector $\mathbf{y}$ should be extracted from the reduced solution vector $\mathbf{z}$. This can be achieved by solving a small (s x s) linear system

$$\mathbf{A}\mathbf{y} = \mathbf{z} \tag{4.6}$$

where the coefficients $\mathbf{A}_{ij}$ are computed when performing the modified Gram-Schmidt orthonormalization. It is important to pay attention to possible ill-conditioning of this system, an issue that will be addressed in the next section.

4.3.2 Sensitivity analysis: minimum compliance

Clearly, when a full analysis is performed within a certain optimization cycle, the sensitivity can be easily obtained using the adjoint method (Bendsøe and Sigmund, 2003), leading to the well-known expression

$$\frac{\partial c}{\partial \rho_e} = -\mathbf{u}^T \frac{\partial \mathbf{K}}{\partial \rho_e} \mathbf{u}$$

Within optimization cycles in which approximate reanalysis is performed, the reduced solution in terms of the original basis vectors is obtained according to (4.6) and then the corresponding sensitivity analysis can be performed by the adjoint method. Introducing adjoint variables $\widetilde{\mathbf{y}}$, λ_i (i = 1,...,s, s being the number of basis vectors used in the reanalysis), the following modified objective function is obtained by adding zero terms

$$\begin{aligned} c(\rho_e) &= \mathbf{y}^T \mathbf{R}_B^T \mathbf{K} \mathbf{R}_B \mathbf{y} - 2\widetilde{\mathbf{y}}^T (\mathbf{R}_B^T \mathbf{K} \mathbf{R}_B \mathbf{y} - \mathbf{R}_B^T \mathbf{f}) - \\ &\quad \lambda_1^T (\mathbf{K}_0 \mathbf{u}_1 - \mathbf{f}) - \sum_{i=2}^{s} \lambda_i^T (\mathbf{K}_0 \mathbf{u}_i + \Delta\mathbf{K} \mathbf{u}_{i-1}) \end{aligned}$$

When differentiating the objective function with respect to a certain design variable, derivatives of the adjoint variables are obviously eliminated and the derivative will be

$$\begin{aligned}\frac{\partial c}{\partial \rho_e} &= 2\frac{\partial \mathbf{y}^T}{\partial \rho_e}\mathbf{R}_B^T\mathbf{K}\mathbf{R}_B\mathbf{y} + 2\mathbf{y}^T\frac{\partial \mathbf{R}_B^T}{\partial \rho_e}\mathbf{K}\mathbf{R}_B\mathbf{y} + \mathbf{y}^T\mathbf{R}_B^T\frac{\partial \mathbf{K}}{\partial \rho_e}\mathbf{R}_B\mathbf{y} + 2\widetilde{\mathbf{y}}^T\frac{\partial \mathbf{R}_B^T}{\partial \rho_e}\mathbf{f} - \\ & 2\widetilde{\mathbf{y}}^T\frac{\partial \mathbf{R}_B^T}{\partial \rho_e}\mathbf{K}\mathbf{R}_B\mathbf{y} - 2\widetilde{\mathbf{y}}^T\mathbf{R}_B^T\frac{\partial \mathbf{K}}{\partial \rho_e}\mathbf{R}_B\mathbf{y} - 2\widetilde{\mathbf{y}}^T\mathbf{R}_B^T\mathbf{K}\frac{\partial \mathbf{R}_B}{\partial \rho_e}\mathbf{y} - \\ & 2\widetilde{\mathbf{y}}^T\mathbf{R}_B^T\mathbf{K}\mathbf{R}_B\frac{\partial \mathbf{y}}{\partial \rho_e} - \lambda_1^T\frac{\partial \mathbf{K}_0}{\partial \rho_e}\mathbf{u}_1 - \lambda_1^T\mathbf{K}_0\frac{\partial \mathbf{u}_1}{\partial \rho_e} - \\ & \sum_{i=2}^{s}\lambda_i^T[\frac{\partial \mathbf{K}_0}{\partial \rho_e}\mathbf{u}_i + \mathbf{K}_0\frac{\partial \mathbf{u}_i}{\partial \rho_e} + \frac{\partial \Delta\mathbf{K}}{\partial \rho_e}\mathbf{u}_{i-1} + \Delta\mathbf{K}\frac{\partial \mathbf{u}_{i-1}}{\partial \rho_e}]\end{aligned}$$

As is the case for the standard (full) problem, the adjoint variable vector that should be chosen such that the derivatives of the solution vector are eliminated, is simply the solution vector itself, meaning that for the approximate problem

$$\widetilde{\mathbf{y}} \equiv \mathbf{y}$$

By defining the vector of residual forces due to approximation errors

$$\Delta\mathbf{f} = \mathbf{f} - \mathbf{K}\mathbf{R}_B\mathbf{y} \tag{4.7}$$

and applying the following equalities

$$\begin{aligned}2\mathbf{y}^T\frac{\partial \mathbf{R}_B^T}{\partial \rho_e}\Delta\mathbf{f} &= \sum_{i=1}^{s} 2y_i\frac{\partial \mathbf{u}_i^T}{\partial \rho_e}\Delta\mathbf{f} \\ \frac{\partial \mathbf{K}_0}{\partial \rho_e} &= \mathbf{0} \\ \frac{\partial \Delta\mathbf{K}}{\partial \rho_e} &= \frac{\partial \mathbf{K}}{\partial \rho_e}\end{aligned}$$

the following expression for the sensitivity is obtained as

$$\begin{aligned}\frac{\partial c}{\partial \rho_e} &= -\mathbf{y}^T\mathbf{R}_B^T\frac{\partial \mathbf{K}}{\partial \rho_e}\mathbf{R}_B\mathbf{y} - \sum_{i=2}^{s}\lambda_i^T\frac{\partial \mathbf{K}}{\partial \rho_e}\mathbf{u}_{i-1} - \sum_{i=1}^{s-1}\frac{\partial \mathbf{u}_i^T}{\partial \rho_e}[\mathbf{K}_0\lambda_i + \Delta\mathbf{K}\lambda_{i+1} - 2y_i\Delta\mathbf{f}] - \\ & \frac{\partial \mathbf{u}_s^T}{\partial \rho_e}[\mathbf{K}_0\lambda_s - 2y_s\Delta\mathbf{f}]\end{aligned}$$

It can be seen that derivatives of the basis vectors can be eliminated by solving the adjoint problems, where $i = 1, ..., s-1$:

$$\begin{aligned}\mathbf{K}_0\lambda_s &= 2y_s\Delta\mathbf{f} \\ \mathbf{K}_0\lambda_i &= 2y_i\Delta\mathbf{f} - \Delta\mathbf{K}\lambda_{i+1}\end{aligned}$$

Therefore the final expression for the sensitivity is

$$\frac{\partial c}{\partial \rho_e} = -\mathbf{y}^T\mathbf{R}_B^T\frac{\partial \mathbf{K}}{\partial \rho_e}\mathbf{R}_B\mathbf{y} - \sum_{i=2}^{s}\lambda_i^T\frac{\partial \mathbf{K}}{\partial \rho_e}\mathbf{u}_{i-1}$$

Several interesting observations can be made when examining this expression. First, it can be seen that if there are no approximation errors, then the first term is identical to the sensitivity in the standard problem and the second term is eliminated. Second, once approximation errors occur, they are accounted for in the sensitivity analysis, meaning that relatively large inaccuracies could be tolerated. Third, the number of adjoint problems to be solved is $s-1$ since the first basis vector does not depend on changes in the design; so the additional computational cost is very low considering the availability of the factorized stiffness matrix. Finally, it should be noted that the sensitivities computed following this derivation were found to be perfectly compatible with calculations using finite differences.

4.3.3 Optimization problem and sensitivity analysis: maximizing output displacements

The utilization of CA reanalysis is not restricted to the class of minimum compliance problems. As another demonstrative case, the problem of compliant mechanism design (Bendsøe and Sigmund, 2003) is examined. At this point, only linear response is considered. This may not be sufficiently accurate when designing an actual device but will suffice for the purpose of demonstrating the formulation with approximate reanalysis. Consider the optimization problem of maximizing a particular output displacement

$$\begin{aligned} \max_{\boldsymbol{\rho}} c(\boldsymbol{\rho}) &= \mathbf{l}^T\mathbf{u} \\ \text{s.t.:} \quad & \sum_{e=1}^{N} v_e\rho_e \le V \\ & 0 < \rho_{min} \le \rho_e \le 1, \qquad e = 1, ..., N \\ \text{with:} \quad & \mathbf{K}(\boldsymbol{\rho})\mathbf{u} = \mathbf{f} \end{aligned} \tag{4.8}$$

where $\mathbf{l}$ is a vector with the value of 1 at the output DOF and zeros otherwise.

The formulation (4.8) holds for optimization cycles that include a full structural analysis. When the approximate problem is solved, the corresponding objective function can be expressed as follows

$$\begin{aligned} c(\boldsymbol{\rho}) &= \mathbf{l}^T\mathbf{u} \approx \mathbf{l}^T\widetilde{\mathbf{u}} \\ \widetilde{\mathbf{u}} &= \mathbf{R}_B\mathbf{y} \\ c(\boldsymbol{\rho}) &= \mathbf{l}^T\mathbf{R}_B\mathbf{y} = \mathbf{y}^T\mathbf{R}_B^T\mathbf{l} \end{aligned}$$

Then, the appropriate optimization problem will have the form

$$\begin{aligned} \max_{\boldsymbol{\rho}} c(\boldsymbol{\rho}) &= \mathbf{y}^T\mathbf{R}_B^T\mathbf{l} \\ \text{s.t.:} \quad & \sum_{e=1}^{N} v_e\rho_e \le V \\ & 0 < \rho_{min} \le \rho_e \le 1, \qquad e = 1, ..., N \\ \text{with:} \quad & \mathbf{R}_B^T\mathbf{K}(\boldsymbol{\rho})\mathbf{R}_B\mathbf{y} = \mathbf{R}_B^T\mathbf{f} \\ & \mathbf{K}_0(\boldsymbol{\rho}_0)\mathbf{u}_1 = \mathbf{f} \\ & \mathbf{K}_0(\boldsymbol{\rho}_0)\mathbf{u}_i = -\Delta\mathbf{K}(\boldsymbol{\rho}, \boldsymbol{\rho}_0)\mathbf{u}_{i-1}, \qquad i = 2, ..., s \end{aligned} \tag{4.9}$$

Design sensitivities can be derived in a similar fashion as for the minimum compliance problem. When the full system is analyzed, the design sensitivities are (Bendsøe and Sigmund, 2003)

$$\frac{\partial c}{\partial \rho_e} = -\lambda^T\frac{\partial \mathbf{K}}{\partial \rho_e}\mathbf{u}$$

where λ is the solution to the adjoint problem

$$\mathbf{K}\lambda = \mathbf{l}$$

When the reduced reanalysis problem is solved, the design sensitivities are found by

$$\frac{\partial c}{\partial \rho_e} = -\widetilde{\mathbf{y}}^T\mathbf{R}_B^T\frac{\partial \mathbf{K}}{\partial \rho_e}\mathbf{R}_B\mathbf{y} - \sum_{i=2}^{s}\lambda_i^T\frac{\partial \mathbf{K}}{\partial \rho_e}\mathbf{u}_{i-1}$$

Here, $\widetilde{\mathbf{y}}$ is the solution of the *reduced* adjoint problem

$$\mathbf{R}_B^T\mathbf{K}\mathbf{R}_B\widetilde{\mathbf{y}} = \mathbf{R}_B^T\mathbf{l} \tag{4.10}$$

In order to avoid the solution of an ill-conditioned system, the orthonormal basis is utilized again and the reduced vector $\widetilde{\mathbf{y}}$ can be obtained as in (4.6). The adjoints for the basis vectors are found by solving the following linear systems, where $i = 1, ..., s-1$:

$$\begin{aligned} \mathbf{K}_0 \lambda_s &= \widetilde{y}_s \Delta\mathbf{f} + y_s \Delta\mathbf{l} \\ \mathbf{K}_0 \lambda_i &= \widetilde{y}_i \Delta\mathbf{f} + y_i \Delta\mathbf{l} - \Delta\mathbf{K}\lambda_{i+1} \end{aligned}$$

where $\Delta\mathbf{f}$ and $\Delta\mathbf{l}$ can be seen as residual vectors due to approximation errors, the former corresponding to the reanalysis (same as in (4.7)) and the latter corresponding to the reduced adjoint problem (4.10)

$$\Delta\mathbf{l} = \mathbf{l} - \mathbf{K}\mathbf{R}_B\widetilde{\mathbf{y}}$$

Finally, it should be noted that also for this class of problems the sensitivities computed by the presented derivation were found to be perfectly compatible with calculations using finite differences.

4.4 Numerical implementation and examples

4.4.1 Computational considerations

Solving an optimization problem in which the actual stiffness matrix is factorized only once within a certain number of design iterations can be seen as solving a series of 'short' optimization problems, each one of them a valid optimization problem on its own. Each 'short' optimization problem begins with a matrix factorization and therefore an accurate design iteration; then it continues with a sequence of approximate design iterations based on an approximate reanalysis and its corresponding (exact) sensitivities.

The main goal of using approximate reanalysis is to achieve an accurate result efficiently. When considering the accuracy of the proposed procedure, the somewhat limited scope of the 'short' problems should be taken into account. On the one hand, it is clear that an approximate procedure cannot accommodate extremely large changes in stiffness so these should be bounded in some way. This results in the use of an outdated physical model, so that in many cases the approximate problem (4.5) cannot reach the true optimum and will converge to a higher value (assuming minimization is considered). On the other hand, in certain cases the approximate solution is not accurate enough and the optimization process leads to unreliable results, sometimes with a better objective value than the final optimum. Due to these shortcomings, a certain frequency of updating the factorized matrix (and terminating the current 'short' problem) should be defined if we seek a stable convergence leading to the same optimum as found by solving the full problem. Considering the efficiency of the procedure, matrix factorizations are the most expensive part so the number of updates should be minimized. Therefore the key for achieving an accurate result efficiently is choosing the right time to stop a sequence of reanalyses and perform a new factorization. Possible options for controlling the procedure could be:

1. State a fixed frequency of matrix factorizations, which will be performed regardless of the convergence of the 'short' problem.

2. Perform a new matrix factorization when the current design variable vector $\boldsymbol{\rho}_{[k]}$ is significantly different from the design variable vector corresponding to the factorized matrix, $\boldsymbol{\rho}_{[0]}$. This can be done by examining the angle between the two vectors.

3. Perform a new matrix factorization when the 'short' problem reaches a certain convergence criterion. Such a criterion could be, for example, the relative change in the value of the objective function within the 'short' problem.

In the current study, only the first two options were investigated.

In addition to the frequency of matrix factorizations, the size of the reduced basis also has a direct impact on the accuracy and efficiency of the procedure. Adding basis vectors improves the approximate representation of the problem; however, the computational cost rises significantly since the cost of orthonormalization is proportional to s^2 (s being the number of basis vectors). Therefore it is important to state a certain criterion that will help us determine the sufficient number of basis vectors. In this study, it is suggested to examine the relative magnitude of the residual forces (meaning the error due to approximation, see (4.7)) for this purpose. If the relative magnitude of this residual (measured by the ratio between the Euclidean norms of the residual and the external force vector) exceeds a certain permitted tolerance value, another basis vector is generated, until the residual satisfies the criterion or the predefined maximum number of basis vectors is reached. The relative magnitude of the force residual for which no more basis vectors would be generated was set to 1e-2 for minimum compliance problems and 1e-4 for the force inverter problem. The former class of problems is considered more simple to solve since it is self-adjoint and all sensitivities have the same sign. On the other hand, the force inverter problems require higher accuracy in the solution of the reanalysis equations and therefore the tighter tolerance value. [1]

All the solutions presented in this section were obtained using a nonlinear optimization program based on the Method of Moving Asymptotes (Svanberg, 1987). The external move limit associated with the use of this method in topology optimization had to be treated with some care in order to obtain convergence to meaningful results. For this purpose, the design update was bounded by two external move limits: one referring to the previous design cycle (as defined in most cases) and the other referring to the design corresponding to the last 'full' cycle, in which a full analysis was performed

$$\rho_{e,[k]}^{max} = \min\left\{1, \min\left\{\rho_{e,[0]} + \delta, \rho_{e,[k-1]} + \delta/2\right\}\right\} \tag{4.11}$$

$$\rho_{e,[k]}^{min} = \max\left\{\rho_{min}, \max\left\{\rho_{e,[0]} - \delta, \rho_{e,[k-1]} - \delta/2\right\}\right\} \tag{4.12}$$

Here, $\rho_{e,[k]}^{max}$ and $\rho_{e,[k]}^{min}$ are the upper and lower external bounds for the MMA update of the element density in the k-th design cycle; $\rho_{e,[0]}$ is the element density referring to the last factorized stiffness matrix; $\rho_{e,[k-1]}$ is the element density referring to the previous design cycle; and δ is a user-defined external move limit, usually equal to 0.2 or 0.3. Equations (4.11), (4.12) imply that the design changes computed by MMA will be limited so that they are not too far away from the last accurately computed design values, thus imposing an implicit limit on the values of $\Delta\mathbf{K}$. This relates also to the limited scope of an approximate solution as discussed above: in order to avoid large inaccuracies which may lead to unreliable objective values, we impose an external limit on the magnitude of changes, knowing that the next factorization will enable us to further improve the objective without the risk of unreliable results.

Finally, in order to obtain regularized mesh-independent designs and to avoid checkerboard patterns, a density filter was applied (Bruns and Tortorelli, 2001; Bourdin, 2001). In all the examples solved, the underlying FE model consisted of square, four-noded, bi-linear plane stress elements.

4.4.2 Numerical examples

In this section, several numerical results are presented. The problems that are addressed are minimum compliance problems in two and three dimensions and a force inverter problem in two dimensions. It is shown that accurate results can be obtained when using the approximate procedure. Moreover, promising computational savings are achieved due to a significant reduction in the number of matrix factorizations. A detailed discussion regarding the actual savings and several CPU time measurements are presented in Section 4.4.3.

[1] It is well known in the structural optimization community that this is a more complicated class of problems.

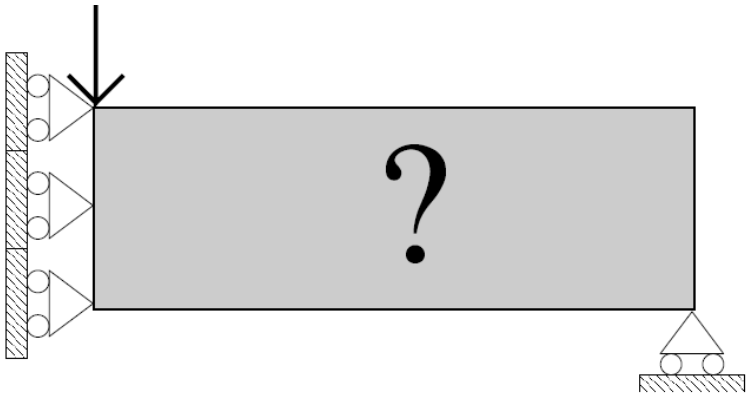

Figure 4.1: MBB beam (symmetric half)

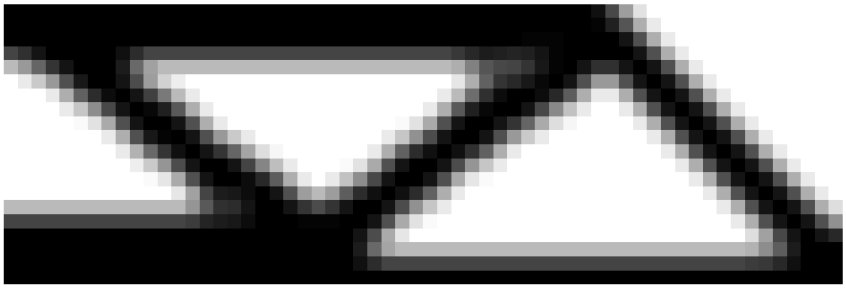

Figure 4.2: Final topology of the MBB beam, 60*20 mesh (symmetric half)

4.4.2.1 Example 1: minimum compliance of a 2-D beam.

As a first demonstrative example, we present the solution for the minimum compliance of a beam subjected to a concentrated vertical load. This example follows the benchmark problem from Sigmund (2001), usually known as the MBB-beam, see Figure 4.1. For a qualitative examination, we focus on the solution obtained with a 60×20 FE mesh, consisting of square elements with a side length equal to 1. The maximum value of Young's modulus (corresponding to the maximum density) was set to 1; Poisson's ratio was set to 0.3; the allowed volume fraction was 0.5; and the penalization factor used in the SIMP interpolation was set to 3. A linear weighting density filter was used with the radius of 2.1. The MMA move limit was set to 0.2 when solving by the standard procedure and 0.3 when solving by the approximate procedure.

When implementing the standard topology optimization procedure, convergence was obtained after 92 iterations (meaning that 92 factorizations were performed) to an objective value of 221.5535. When implementing approximate reanalysis, the frequency of matrix factorizations was fixed to once every 10 iterations and the maximum number of basis vectors was set to 4. Convergence was obtained after 190 iterations (meaning that 19 factorizations were performed) to an objective value of 221.5544. The final topology in terms of filtered densities is presented in Figure 4.2 and is practically identical for the two solutions.

In Figure 4.3, the number of basis vectors used in the approximate procedure is plotted, as well as the convergence of the optimization process. In the top figure, it can be seen that as the optimization proceeds, the required number of basis vectors is reduced since the design changes are small and fewer vectors are needed in order to obtain a sufficiently accurate representation of the true stiffness. The differences between the number of vectors used for reanalysis and the number of vectors used for sensitivity analysis (e.g. during iterations 35-40 and 45-50) is due to elimination of vectors when ill-conditioning of the linear system in Equation (4.6) is observed. Elimination is required in order to ensure that the coefficient vector $\mathbf{y}$ is calculated accurately. By examining the bottom of the figure, the concept of 'short' optimization problems can be clarified.

Between two consecutive factorizations, a certain convergence curve can be observed. In some cases, the value of the objective is *lower* than the final minimum (e.g. iterations 31-40); this is corrected after the next factorization, which 'directs' the objective back to the desired value, so that the final optimum is accurate.

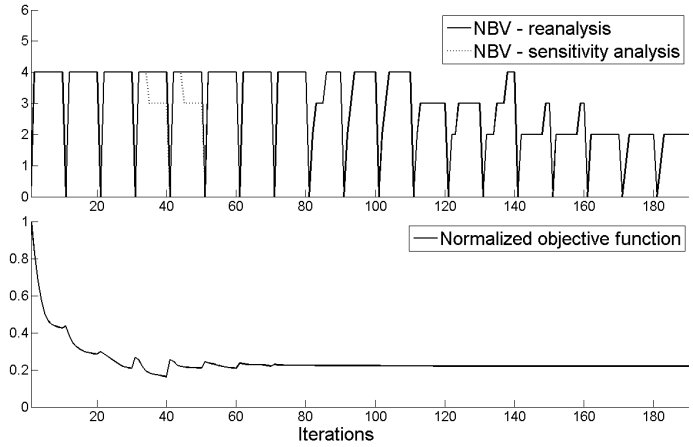

Figure 4.3: Number of basis vectors (top) and objective convergence (bottom), 60×20 half MBB beam

Some interesting properties of the approximate procedure are demonstrated in Figure 4.4. In the upper part of the figure, the approximation errors are documented, in terms of the Euclidean norm of the force residual relative to the norm of the external forces. It can be observed that relatively large errors can be tolerated, with some values even exceeding the magnitude of the external forces. This leads to the conclusion that a relatively rough approximation in the reanalysis is sufficient for the purpose of optimization, as long as consistent sensitivities are derived which take the approximation errors into account.

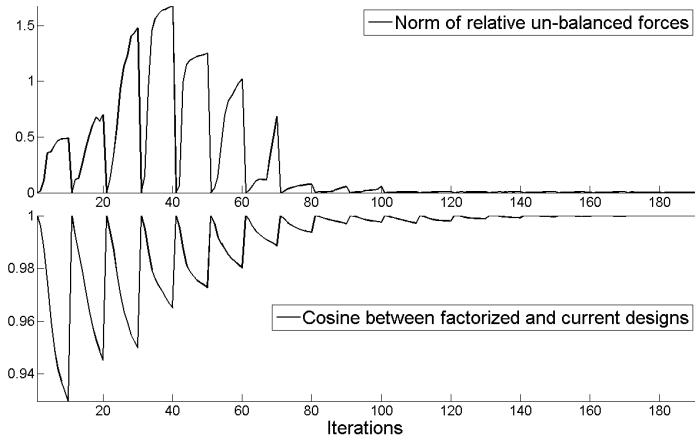

Figure 4.4: Relative force residuals (top) and angles between factorized and current designs (bottom), 60×20 half MBB beam

Another interesting property to examine is the measure of the design changes, which influences the magnitude of the values in $\Delta\mathbf{K}$ and therefore affects the accuracy of the approximation. In the bottom of Figure 4.4, the cosine of the angle between design variable vectors is plotted. In principle, the value of the cosine is reduced the further we are from the previous matrix factorization, since the changes in the design variables grow larger. However, as the optimization proceeds, these changes become very small (e.g. iterations 81 and further); this means that it may make sense to adapt the frequency of matrix factorizations according to the

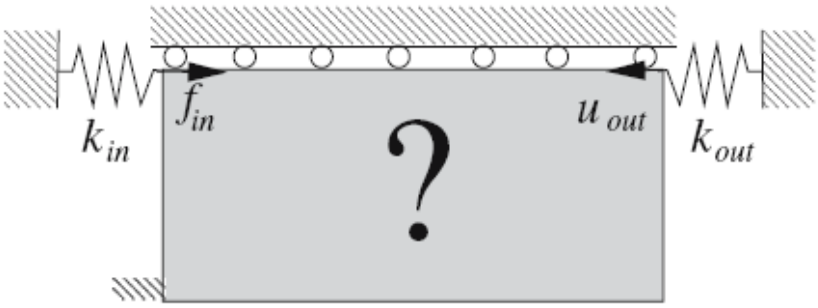

Figure 4.5: Force inverter (symmetric half)

magnitude of the design changes, as described above in Section 4.4.1. In the beginning of the optimization process, more frequent factorizations are required; but from a certain stage, the frequency can be reduced significantly. This control option was tested on the same example problem, but a minimum frequency of factorizations was set to once every 20 iterations and a constraint on the cosine between design vectors was introduced. After 200 iterations (the maximum number of iterations), the objective reached the value of 221.5701 (compared to 221.5535 in the standard solution, 0.007% error) and only 15 factorizations were performed.

4.4.2.2 Example 2: maximum output of a 2-D force inverter.

As a second demonstrative example, we present the solution for the maximum output displacement of a force inverter. This example follows the benchmark problem examined in Sigmund (2007), see Figure 4.5. The displacement to be maximized is negative in global FE coordinates so the optimization problems (see (4.8), (4.9)) are automatically modified into minimization problems. For a qualitative examination, we focus on the solution obtained with a 40×20 FE mesh consisting of square elements with a side length equal to 1. The maximum value of Young's modulus (corresponding to the maximum density) was set to 1; Poisson's ratio was set to 0.3; the allowed volume fraction was 0.3; and the penalization factor used in the SIMP interpolation was set to 3. A linear weighting density filter was used with the radius of 2.1. The MMA move limit was set to 0.2 when solving both by the standard procedure and by the approximate procedure.

When implementing the standard topology optimization procedure, convergence was obtained after 159 iterations (meaning that 159 factorizations were performed) to an objective value of -1.7413. When implementing approximate reanalysis, an adaptive control was used: the minimum frequency of factorizations was set to once every 15 iterations with a constraint on the cosine between design vectors, and the maximum number of basis vectors to be generated was set to 6. These values represent a more accurate, but less efficient, adaptive procedure than the one used for the MBB-beam; this is due to the more complicated nature of the inverter problem as explained earlier in Section 4.4.1. After 300 iterations (the maximum number of iterations), the objective reached the value of -1.7281 (an error of 0.76%) but only 24 factorizations were performed. The final topologies in terms of filtered densities are presented in Figure 4.6. It can be seen that for this case the approximate procedure does not yield exactly the same solution as the standard procedure. Moreover, numerical experience shows that the results for this problem are very sensitive to the choice of the solution parameters, mainly: the MMA move limit; the force residual tolerance; and of course, the frequency of matrix factorizations and the number of basis vectors. Therefore, when seeking an approximate solution for this class of problems, these parameters should be treated with care. However, the solution to this problem is sensitive to the choice of parameters (such as the MMA move limit) also when solving with a

Figure 4.6: Final topology of the force inverter - approximate solution (left), standard solution (right), 40×20 mesh (symmetric half)

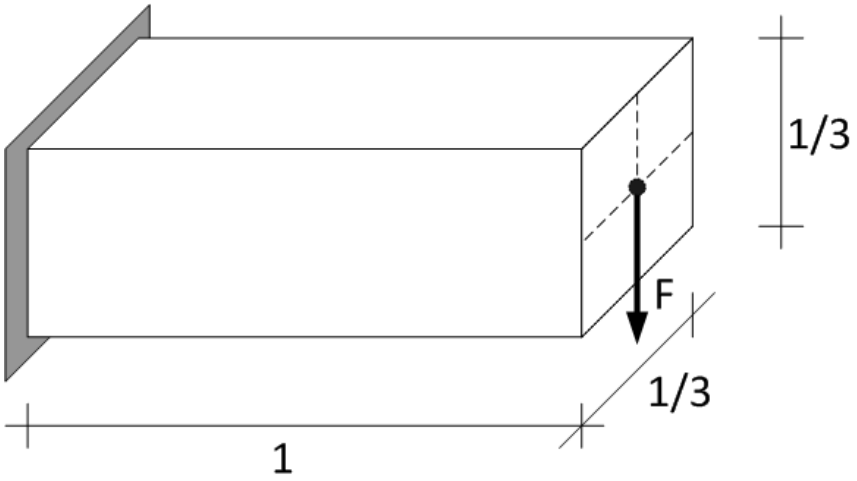

Figure 4.7: 3-D cantilever beam

full analysis, so the inaccuracies should not be referred only to the use of approximate reanalysis but also to the difficulties inherent in this class of problems.

4.4.2.3 Example 3: minimum compliance of a 3-D cantilever beam.

In this example, we present the solution for the minimum compliance of a cantilever beam subjected to a concentrated vertical load at the center of its free face. The parametric sizes and the shape of the physical domain are presented in Figure 4.7. Clearly, this can be seen as a direct extension of the MBB-beam problem to three dimensions. For a qualitative examination, we focus on the solution obtained with a 48×16×16 FE mesh consisting of cubic elements with a side length equal to 1. The maximum value of Young's modulus (corresponding to the maximum density) was set to 1; Poisson's ratio was set to 0.3; the allowed volume fraction was 0.5; and the penalization factor used in the SIMP interpolation was set to 3. A linear weighting density filter was used with the radius of 2.01. The MMA move limit was set to 0.2 when solving by the standard procedure and 0.3 when solving by the approximate procedure.

As for the 2-D case, very accurate results were obtained for this example problem. When implementing the standard topology optimization procedure, convergence was obtained after 152 iterations (meaning that 152 factorizations were performed) to an objective value of 13.300. When implementing approximate reanalysis, the frequency of matrix factorizations was fixed to once every 10 iterations and the maximum number of basis vectors was set to 4. Convergence was obtained after 151 iterations (meaning 16 factorizations were performed) to an objective value of 13.304. The final layout for a 48×16×16 mesh is presented in Figure 4.8, and was practically identical for both the full and the approximate solution procedures. It can be seen that the topology indeed changes and a hole is created by the fixed wall. The computational efficiency of the approximate procedure will be discussed in more detail in the following section.

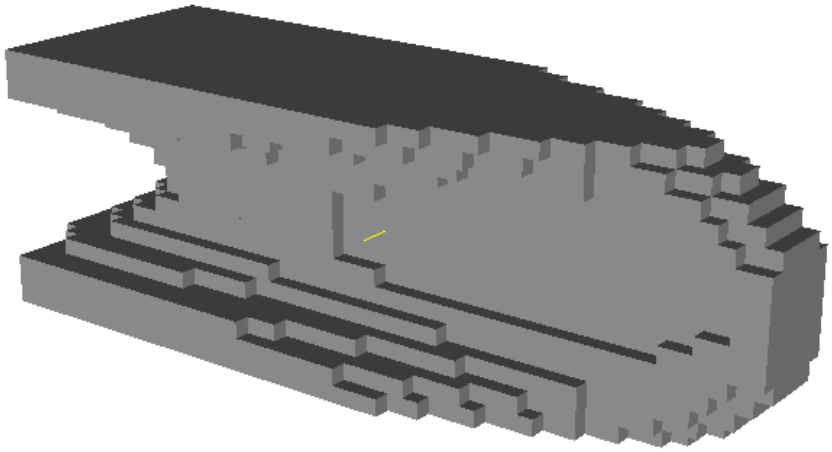

Figure 4.8: Final topology of the 3-D cantilever, 48×16×16 mesh

4.4.3 Computational efficiency

4.4.3.1 Estimated efficiency by FLOPS count.

The savings in computational effort that can be achieved when implementing the approximate procedure can be roughly estimated by examining the FLOPS count. Focusing on the nested analysis/reanalysis problem and referring to the banded structure of the stiffness matrix, the cost related to the standard procedure is dominated by factorization where the number of FLOPS performed is in the order of nb^2 (n being the number of DOF and b the half-bandwidth of the stiffness matrix). In the approximate procedure, the cost of approximate reanalysis is dominated by the cost of generation and orthonormalization of the basis, where the FLOPS count includes terms in the order of nbs and nbs^2 (s being the number of basis vectors). Therefore we expect savings in computer run time when $s^2 < b$.

In practice, the FLOPS count can only provide a rough estimate since many other factors influence the actual efficiency of an implemented algorithm, especially if sparsity of the stiffness matrix is taken into account. Efficient programming and memory usage, which take full advantage of the matrix's sparsity, should also be taken into account but are out of the scope of this work. However, an approximate FLOPS count assuming banded structure of the stiffness matrix together with several promising CPU time measurements should be sufficient in order to demonstrate the potential savings offered by the approximate procedure.

4.4.3.2 Actual efficiency by CPU time measurements.

In Table 4.1, some results obtained when solving the 2-D MBB-beam problem (Example 1) using several mesh resolutions are presented. For all cases the FE mesh consists of square elements with a side length equal to 1. Other numerical parameters were identical to those used in Example 1. Both standard and approximate procedures were implemented in Fortran utilizing sparse solver routines available from the Sun Performance Library (Sun, 2005), and were executed on a Sun UNIX terminal. For all runs, the frequency of matrix factorizations was fixed to once every 10 iterations and the maximum number of basis vectors was set to 4. As demonstrated above, more savings could be achieved if an adaptive control would have been used.

For each example problem, two measurements of CPU time were taken: one for the solution of the finite element equations (by standard analysis or approximate reanalysis) and one for the whole optimization process. It can be observed that approximate reanalysis can save significant time spent on the solution of the FE analysis equations. However, the total speedups achieved

Table 4.1: 2-D MBB beam, fixed CA (4/10)

Problem size	90×30	180×60	300×100
Design variables	2,700	7,200	30,000
Degrees of freedom	5,642	22,082	60,802
Final objective, CA	225.187	227.834	230.374
Iterations, CA	200	200	200
Final objective, full solution	224.749	227.111	230.608
Iterations, full solution	200	200	200
Error	0.19%	0.32%	0.10%
FE speedup	2.22	2.37	3.14
Total speedup	0.90	1.36	1.48

for the whole optimization process are not very high since the problem sizes are relatively small, meaning that the time spent on solving the FE equations is not completely dominant. It is expected that when dealing with large scale problems the total speedup will be similar to the speedup achieved for the solution of the FE equations. As for the accuracy of the approximate procedure, it can be seen that the relative errors are small and the results can be regarded as accurate for any practical purpose.

More promising speedups are achieved when solving three-dimensional problems. In Table 4.2 some results obtained when solving the minimum compliance problem of a 3-D cantilever beam (see Example 3) using several mesh resolutions are presented. For all cases the FE mesh consists of cubic elements with a side length equal to 1. Other numerical parameters were identical to those used in Example 3. Again, the results are very accurate and the relative errors when comparing to standard procedures are negligible. When solving with a $24\times8\times8$ and a $36\times12\times12$ mesh, the approximate procedure converged after fewer iterations than the standard procedure. In these cases, the speedup factors were scaled so that the faster convergence is not taken into account. Otherwise the results may be misleading, showing too high and not necessarily realistic speedups.

It can be seen that for 3-D cases, the potential savings are higher than for 2-D cases since factorization is more costly and also more dominant. For problem sizes of the order of 10e4, a total speedup factor higher than 5 can be achieved compared to approximately 1.5 for 2-D problems of the same size. Focusing on the FE speedup factor, it is clear that it rises as the mesh is finer, as expected from the FLOPS estimation. In theory, for a very large problem the FE speedup should approach the value of 10 since the cost of the CA iterations will be negligible in comparison to the full iterations.

4.5 Conclusions

An effective procedure for integrating approximate reanalysis into the topology optimization framework was proposed. It was shown that accurate optimization results can be obtained even if the reanalysis problem is not solved very accurately. This is due to the derivation of design sensitivites which are consistent with the use of an approximate solution. The current study focuses on applications within the field of topology optimization but the approach could be extended to other classes of structural optimization. The approximate procedure offers significant savings in computational effort compared to the standard procedure, especially in 3-dimensional problems.

Table 4.2: 3-D cantilever, fixed CA (4/10)

Problem size	24×8×8	36×12×12	48×16×16
Design variables	1,536	5,184	12,288
Degrees of freedom	6,075	18,759	42,483
Final objective, CA	25.649	16.155	13.304
Iterations, CA	100	90	151
Final objective, full solution	25.635	16.136	13.300
Iterations, full solution	125	170	152
Error	0.05%	0.12%	0.03%
FE speedup	4.56	5.28	6.85
Total speedup	3.24	3.84	5.66

More work is needed in order to improve the accuracy of the approximate procedure when dealing with the compliant mechanism class of problems. Compared to minimum compliance problems, these are much more challenging from the point of view of utilizing approximations. Moreover, the efficiency of the approximate procedure can also be improved by introducing adaptive controls that can reduce the total number of matrix factorizations to be performed during the whole optimization process. Possible controls were proposed here but their implementation was not yet investigated thoroughly.

In the future, an effort will be made to extend the application of the Combined Approximations approach also to topology optimization problems where the structural response is nonlinear and transient.

4.6 Acknowledgments

This work received support from the Eurohorcs/ESF European Young Investigator Award (EURYI, www.esf.org/euryi) through the grant “Synthesis and topology optimization of optomechanical systems”. The first author would like to thank Michael Bogomolny for many fruitful discussions about the topic. We are also grateful to Krister Svanberg for allowing us to use the MMA code.

References

O. Amir, U. Kirsch, and I. Sheinman. Efficient non-linear reanalysis of skeletal structures using combined approximations. *International Journal for Numerical Methods in Engineering*, 73: 1328–1346, 2008.

M. P. Bendsøe. Optimal shape design as a material distribution problem. *Structural Optimization*, 1:193–202, 1989.

M. P. Bendsøe and N. Kikuchi. Generating optimal topologies in structural design using a homogenization method. *Computer Methods in Applied Mechanics and Engineering*, 71:197–224, 1988.

M. P. Bendsøe and O. Sigmund. *Topology Optimization - Theory, Methods and Applications*. Springer, Berlin, 2003.

B. Bourdin. Filters in topology optimization. *International Journal for Numerical Methods in Engineering*, 50:2143–2158, 2001.

T. E. Bruns and D. A. Tortorelli. Topology optimization of non-linear elastic structures and compliant mechanisms. *Computer Methods in Applied Mechanics and Engineering*, 190:3443–3459, 2001.

G. H. Golub and C. F. Van Loan. *Matrix Computations*. The Johns Hopkins University Press, Baltimore, Maryland, 1983.

U. Kirsch. Reduced basis approximations of structural displacements for optimal design. *AIAA Journal*, 29:1751–1758, 1991.

U. Kirsch. *Design-Oriented Analysis of Structures*. Kluwer Academic Publishers, Dordrecht, 2002.

U. Kirsch. *Reanalysis of Structures*. Springer, Dordrecht, 2008.

U. Kirsch and M. Bogomolni. Procedures for approximate eigenproblem reanalysis of structures. *International Journal for Numerical Methods in Engineering*, 60:1969–1986, 2004.

U. Kirsch and M. Bogomolni. Nonlinear dynamic reanalysis of structures by combined approximations. *Computer Methods in Applied Mechanics and Engineering*, 195:4420–4432, 2006.

U. Kirsch and P. Y. Papalambros. Structural reanalysis for topological modifications - a unified approach. *Structural and Multidisciplinary Optimization*, 21:333–344, 2001.

U. Kirsch, M. Kocvara, and J. Zowe. Accurate reanalysis of structures by a preconditioned conjugate gradient method. *International Journal for Numerical Methods in Engineering*, 55:233–251, 2002.

O. Sigmund. A 99 line topology optimization code written in matlab. *Structural and Multidisciplinary Optimization*, 21:120–127, 2001.

O. Sigmund. Morphology-based black and white filters for topology optimization. *Structural and Multidisciplinary Optimization*, 33:401–424, 2007.

Sun Performance Library Reference Manual. Sun Microsystems Inc., 2005.

K. Svanberg. The method of moving asymptotes - a new method for structural optimization. *International Journal for Numerical Methods in Engineering*, 24:359–373, 1987.

S. Venkataraman and R. T. Haftka. Structural optimization complexity: what has Moore's law done for us? *Structural and Multidisciplinary Optimization*, 28:375–387, 2004.

Chapter 5

Efficient use of iterative solvers in nested topology optimization

Amir O, Stolpe M and Sigmund O. Efficient use of iterative solvers in nested topology optimization. *Structural and Multidisciplinary Optimization* 2010, vol. 42, pp. 55-72.

Abstract In the nested approach to structural optimization, most of the computational effort is invested in the solution of the analysis equations. In this study, it is suggested to reduce this computational cost by using an approximation to the solution of the analysis problem, generated by a Krylov subspace iterative solver. By choosing convergence criteria for the iterative solver that are strongly related to the optimization objective and to the design sensitivities, it is possible to terminate the iterative solution of the nested equations earlier compared to traditional convergence measures. The approximation is computationally shown to be sufficiently accurate for the purpose of optimization though the nested equation system is not necessarily solved accurately. The approach is tested on several large-scale topology optimization problems, including minimum compliance problems and compliant mechanism design problems. The optimized designs are practically identical while the time spent on the analysis is reduced significantly.

Keywords Topology optimization, Nested approach, Iterative equation solvers, PCG, Approximations

5.1 Introduction

Over the past few years there has been much progress in the application of structural optimization (and topology optimization in particular) to large-scale problems, especially due to the increasing availability of high performance parallel computers (see e.g. Kim et al. (2004), Vemaganti and Lawrence (2005), Mahdavi et al. (2006), Wang et al. (2007) and Evgrafov et al. (2008)). In cases in which the number of inequality constraints is considerably smaller than the number of design variables, the nested approach is usually applied, meaning that optimization is performed in the design variables only and that the equilibrium equations are treated by function calls and solved separately. When following this approach, the computational cost of the whole optimization process is frequently dominated by the effort involved in repeated solutions of large systems of equilibrium equations, obtained after applying the firnite element method to solve the underlying PDE. For the purpose of solving large-scale linear systems, iterative solvers based on various Krylov subspace methods (for a review of these methods, see for example (Saad, 2003)) are now gaining popularity over direct methods since they are easier to parallelize and have modest memory requirements. This study examines the use of such solvers in the repeated solution of the analysis problem.

The issue of reducing the computational effort invested in repeated solutions of the nested analysis problem was recently addressed in several studies. Wang et al. (2007) applied a Krylov subspace solver with recycling, where parts of the search space corresponding to a certain design cycle were reused in the solution of the next design cycle. This approach leads to a reduction in the number of iterations performed in the solution of the nested problem, especially when the design changes between two optimization steps are small. In (Amir et al., 2009a) an approximate reanalysis procedure, based on the Combined Approximations method (Kirsch, 1991), was integrated into nested topology optimization procedures. It was shown that relatively rough approximations are acceptable since the errors are taken into account in the sensitivity analysis which is consistent with the approximation utilized. For example, in some design cycles the residual forces due to inaccurate solution of the equation system were of the same magnitude as the external forces. The approximation is obtained efficiently so this approach can lead to significant savings in computer run time, especially for three-dimensional problems.

In the current study, we suggest using an approximation to the solution vector generated by a Krylov subspace solver. This approximation corresponds to an intermediate stage of the iterative procedure, meaning that the iterate does not satisfy the common convergence criterion that measures the relative norm of the residuals. Two different ways of choosing the approximate solution and ensuring sufficient accuracy of the optimization process are discussed. One possibility is to obtain the approximation by introducing a relatively slack convergence tolerance for the iterative equation solver. Then the adjoint method for sensitivity analysis is applied in a consistent manner, so that the design sensitivities are accurate with respect to the approximation that is utilized. Throughout this article, this will be referred to as the *consistent* approach. Another possibility is to obtain the approximation by disregarding the traditional convergence criterion for the iterative solver and introducing alternative convergence criteria. These measures are strongly related to the objective function of the optimization problem we are aiming to solve and to the corresponding design sensitivities. Following this approach, sensitivity analysis is approximate since it is performed assuming that the nested equations are solved accurately. The approximations obtained in this manner are too rough for the purpose of analysis, but are indeed sufficiently accurate for the practical purpose of optimization. This approach will be referred to as the *approximate* approach and is the main focus of this article. It is shown that the computational effort invested in solving the nested analysis problem can be reduced significantly, without affecting the accuracy of the optimization process. Some preliminary results were recently presented by Amir et al. (2009b). This article gives more insight into the proposed procedures, including a full derivation of the consistent apporach and new examples.

The concepts presented in this article are demonstrated on, and applied to topology optimization problems within the field of structural mechanics. In this class of problems, the nested linear equation system has a symmetric positive definite matrix. Therefore we only use the conjugate gradients (CG) method (Hestenes and Stiefel, 1952) combined with effective preconditioning (PCG) which is the most appropriate choice from the family of Krylov subspace solvers. However, in some studies other methods are applied (Wang et al., 2007), and we note that the approach proposed here also can be applied to other Krylov methods and to other physical models even though it will only be demonstrated for PCG and systems from linear elasticity.

The article is organized as follows. First, the idea of obtaining approximations by forcing early termination of the iterative solver is presented in section 5.2. Then, in section 5.3, the consistent approach for sensitivity analysis is described and demonstrated. The approximate approach is presented and demonstrated in section 5.4, including a detailed discussion regarding alternative convergence measures for different types of topology optimization problems. Finally, is section 5.5 we present solutions to several large scale topology optimization problems.

5.2 Considered optimization problems with approximations based on early termination of PCG

In this study, an approximation to the solution of the nested problem is utilized instead of the exact solution. This approximation is obtained by forcing early termination of the iterative equation solver intended to solve the nested equation system. This means that the nested equation system is not solved accurately and that its corresponding residual is not negligible.

Throughout this article the approximate procedures will be demonstrated on two types of topology optimization problems. The first type is minimum compliance design, aimed at finding the stiffest structural layout given a limited amount of material. This class is chosen since it represents a very fundamental and well established application of topology optimization (for an extensive report on topology optimization, see the book by Bendsøe and Sigmund (2003)). The second type is compliant mechanism design, aimed at maximizing a certain output displacement given a certain input force (Sigmund, 1997). This class is chosen since it is much more demanding from an optimization point of view: it is not self-adjoint and possibly possesses several strong local minima. Therefore it is expected that larger approximation errors could be tolerated in minimum compliance problems compared to compliant mechanism problems. This was also observed in the study presented in (Amir et al., 2009a).

In both cases, we follow the material distribution approach for topological design (Bendsøe and Kikuchi, 1988) together with the SIMP interpolation scheme (Bendsøe, 1989). For the case of minimizing compliance, the optimization problem will have the following form

$$\begin{aligned} \min_{\boldsymbol{\rho}} c_1(\boldsymbol{\rho}) &= \mathbf{f}^T \mathbf{u}_m \\ \text{s.t.:} \quad & \sum_{e=1}^{N} v_e \rho_e \leq V \\ & 0 \leq \rho_e \leq 1 \qquad e = 1, ..., N \\ \text{with:} \quad & \mathbf{K}(\boldsymbol{\rho}) \mathbf{u}_m \approx \mathbf{f} \end{aligned} \tag{5.1}$$

where $\mathbf{f}$ is the external load vector, $\mathbf{u}_m$ is an approximation to the displacements vector, v_e is the element volume, V is the total available volume and $\mathbf{K}(\boldsymbol{\rho})$ is the stiffness matrix corresponding to the element densities $\boldsymbol{\rho}$

$$\mathbf{K}(\boldsymbol{\rho}) = \sum_{e=1}^{N} (E_{min} + (E_{max} - E_{min}) \rho_e^p) \mathbf{K}_e$$

In general, E_{min} and E_{max} are the values of Young's modulus of two materials which should be distributed in the design domain. For the case of distributing a single material and void, E_{min} is set to a small positive value and E_{max} is typically set to 1. $\mathbf{K}_e$ represents the element stiffness matrix corresponding to the Young's modulus value E_{max} and p is a penalization factor required to drive the design towards a 0-1 layout. $\mathbf{K}(\boldsymbol{\rho})$ results from a finite element discretization of the governing PDEs which define equilibrium in linear elasticity. Therefore it is symmetric and positive-semidefinite. Since the value of E_{min} is larger than zero, $\mathbf{K}(\boldsymbol{\rho})$ is strictly positive-definite.

Within the class of optimizing compliant mechanisms, we focus on the design of a force inverter, where the objective is to maximize a displacement in the negative global direction so

the problem will have the form

$$\begin{aligned} \min_{\boldsymbol{\rho}} c_2(\boldsymbol{\rho}) \quad &= \quad \mathbf{l}^T \mathbf{u}_m \\ \text{s.t.:} \quad & \sum_{e=1}^{N} v_e \rho_e \leq V \\ & 0 \leq \rho_e \leq 1 \qquad e = 1, ..., N \\ \text{with:} \quad & \mathbf{K}(\boldsymbol{\rho}) \mathbf{u}_m \approx \mathbf{f} \end{aligned} \tag{5.2}$$

where $\mathbf{l}$ is a vector with the value of 1 at the output displacement degree of freedom and zeros otherwise. In both cases, the index m corresponds to an intermediate PCG iteration, for which the corresponding iterative solution $\mathbf{u}_m$ does not necessarily satisfy equilibrium accurately.

5.3 Consistent sensitivity analysis

In order to maintain consistency even though the analysis problem is not solved accurately, we derive design sensitivities in a manner that takes the approximation errors into account. Therefore, when applying the adjoint method for sensitivity analysis, the complete iterative procedure performed in order to obtain the approximation is taken into account. Then the design sensitivities are accurate and consistent with respect to the approximate representation of the problem.

When solving optimization problems such as (5.1) and (5.2), the PCG solver will be called once every optimization iteration to solve the analysis equations. The PCG procedure aimed at solving the linear system $\mathbf{M}^{-1}\mathbf{K}\mathbf{u} = \mathbf{M}^{-1}\mathbf{f}$, where $\mathbf{M}$ is the preconditioner, can be outlined as follows

1. Set the initial guess $\mathbf{u}_1$.
2. Compute the initial residual $\mathbf{r}_1$ and direction vector $\mathbf{p}_1$: $\mathbf{r}_1 = \mathbf{f} - \mathbf{K}\mathbf{u}_1$, $\mathbf{z}_1 = \mathbf{M}^{-1}\mathbf{r}_1$, $\mathbf{p}_1 = \mathbf{z}_1$.
3. For `i = 1:maxiter` do
   (a) $\alpha_i = \frac{\mathbf{r}_i^T \mathbf{z}_i}{(\mathbf{K}\mathbf{p}_i)^T \mathbf{p}_i}$
   (b) $\mathbf{u}_{i+1} = \mathbf{u}_i + \alpha_i \mathbf{p}_i$
   (c) $\mathbf{r}_{i+1} = \mathbf{r}_i - \alpha_i \mathbf{K}\mathbf{p}_i$
   (d) If $\|\mathbf{r}_{i+1}\|_2 < \epsilon \|\mathbf{f}\|_2$ break.
   (e) $\mathbf{z}_{i+1} = \mathbf{M}^{-1}\mathbf{r}_{i+1}$.
   (f) $\beta_i = \frac{\mathbf{r}_{i+1}^T \mathbf{z}_{i+1}}{\mathbf{r}_i^T \mathbf{z}_i}$
   (g) $\mathbf{p}_{i+1} = \mathbf{z}_{i+1} + \beta_i \mathbf{p}_i$

A common criterion for convergence of a PCG procedure (and other Krylov methods) is based on the norm of the residual $\mathbf{r}_i$, measured relatively to the norm of the right hand side $\mathbf{f}$. It is said that the iterate $\mathbf{u}_k$ converged if the following condition is satisfied

$$\frac{\|\mathbf{f} - \mathbf{K}\mathbf{u}_k\|_2}{\|\mathbf{f}\|_2} = \frac{\|\mathbf{r}_k\|_2}{\|\mathbf{f}\|_2} < \epsilon \tag{5.3}$$

where a common value for the tolerance ϵ is 10^{-6}. Now let us assume that after $m-1$ iterations we obtain an iterate $\mathbf{u}_m$ that did not converge to satisfy equilibrium, meaning

$$\frac{\|\mathbf{f} - \mathbf{K}\mathbf{u}_m\|_2}{\|\mathbf{f}\|_2} = \frac{\|\mathbf{r}_m\|_2}{\|\mathbf{f}\|_2} > \epsilon$$

It will be shown later that typically, the relative norm of residuals corresponding to the iterate $\mathbf{u}_m$ will be several orders of magnitude larger than ϵ. Despite the inaccuracy in the solution of the equation system, it will be shown that the approximation $\mathbf{u}_m$ can be sufficiently accurate for the purpose of optimization.

In order to maintain accuracy of the optimization process, we derive design sensitivities in a manner that is consistent with the approximation that was introduced. Following the adjoint method, this means that all the expressions used for computing the PCG variables throughout the iterative procedure (until the early termination step) should be multiplied by a corresponding adjoint variable and added to the objective function. Then the augmented objective function for minimum compliance problems will have the form

$$\begin{aligned}\widehat{c}_1(\boldsymbol{\rho}) &= \mathbf{f}^T\mathbf{u}_m + \widetilde{\mathbf{r}_1}^T(\mathbf{r}_1 - \mathbf{f} + \mathbf{K}\mathbf{u}_1) + \widetilde{\mathbf{z}_1}^T(\mathbf{M}\mathbf{z}_1 - \mathbf{r}_1) + \\ &\quad \widetilde{\mathbf{p}}_1^T(\mathbf{p}_1 - \mathbf{z}_1) + \sum_{i=1}^{m-1}\widetilde{\alpha}_i(\alpha_i - \frac{\mathbf{r}_i^T\mathbf{z}_i}{(\mathbf{K}\mathbf{p}_i)^T\mathbf{p}_i}) + \\ &\quad \sum_{i=2}^{m}\widetilde{\mathbf{u}}_i^T(\mathbf{u}_i - \mathbf{u}_{i-1} - \alpha_{i-1}\mathbf{p}_{i-1}) + \sum_{i=2}^{m}\widetilde{\mathbf{r}}_i^T(\mathbf{r}_i - \mathbf{r}_{i-1} + \\ &\quad \alpha_{i-1}\mathbf{K}\mathbf{p}_{i-1}) + \sum_{i=2}^{m-1}\widetilde{\mathbf{z}}_i^T(\mathbf{M}\mathbf{z}_i - \mathbf{r}_i) + \\ &\quad \sum_{i=1}^{m-2}\widetilde{\beta}_i(\beta_i - \frac{\mathbf{r}_{i+1}^T\mathbf{z}_{i+1}}{\mathbf{r}_i^T\mathbf{z}_i}) + \\ &\quad \sum_{i=2}^{m-1}\widetilde{\mathbf{p}}_i^T(\mathbf{p}_i - \mathbf{z}_i - \beta_{i-1}\mathbf{p}_{i-1}) \end{aligned} \tag{5.4}$$

For the case of the force inverter, we only need to replace $\mathbf{f}$ with $\mathbf{l}$ in the first term; otherwise the augmented objective is identical.

When differentiating the augmented objective function we wish to remain with explicit derivatives of the stiffness matrix and the preconditioner only. For that purpose, we should solve a set of adjoint equations that will eliminate all other derivatives. The complete set of adjoint equations to be solved is presented in Appendix A, but we note here that this approach leads to an iterative CG-like adjoint procedure that should be performed in a reverse manner, beginning in the m-th cycle and ending in the first cycle. After performing the complete adjoint procedure, the design sensitivities include only explicit derivatives of the stiffness matrix and of the preconditioner that can be computed efficiently on an element level

$$\begin{aligned}\frac{\partial\widehat{c}_1}{\partial\rho_e} &= \widetilde{\mathbf{r}_1}^T\frac{\partial\mathbf{K}}{\partial\rho_e}\mathbf{u}_1 + \sum_{i=1}^{m-1}\frac{\widetilde{\alpha}_i\mathbf{r}_i^T\mathbf{z}_i}{((\mathbf{K}\mathbf{p}_i)^T\mathbf{p}_i)^2}\mathbf{p}_i^T\frac{\partial\mathbf{K}}{\partial\rho_e}\mathbf{p}_i + \\ &\quad \sum_{i=2}^{m}\alpha_{i-1}\widetilde{\mathbf{r}}_i^T\frac{\partial\mathbf{K}}{\partial\rho_e}\mathbf{p}_{i-1} + \sum_{i=1}^{m-1}\widetilde{\mathbf{z}}_i^T\frac{\partial\mathbf{M}}{\partial\rho_e}\mathbf{z}_i \end{aligned} \tag{5.5}$$

The accuracy of the consistent approach is demonstrated in the following example. We examine the solution of a 2D minimum compliance problem modeled with a 45×15 mesh. This example follows the benchmark problem from (Sigmund, 2001), usually known as the MBB-beam, see Figure 5.1(a). We use an SSOR (Symmetric Successive Over Relaxation) preconditioner (Saad, 2003) which is based on a splitting of the stiffness matrix and therefore can be easily constructed and differentiated with little extra cost. When solving by the approximate procedure, the convergence tolerance for PCG was set to 10^{-1} compared to 10^{-6} when solving by the full procedure. Moreover, the initial guesses for PCG were zero vectors when solving by the approximate procedure, but when solving by the full procedure the solution corresponding

to the previous design cycle was used as the initial guess for the current cycle. This may reduce the number of PCG iterations, especially once the topology is well defined and the design changes are small. After 50 design iterations, the full procedure reaches an objective value of 228.823 while the approximate procedure reaches a value of 226.343 (approximately 1% error). Observing Figure 5.1(b), it is evident that both convergence curves are very similar though not perfectly identical. As for the number of PCG iterations, the approximate procedure requires nearly 40% fewer iterations: a total of 4,527 compared to 7,436 required by the standard procedure. The complete history of PCG iterations performed in each design cycle throughout the optimization process is presented in Figure 5.1(c).

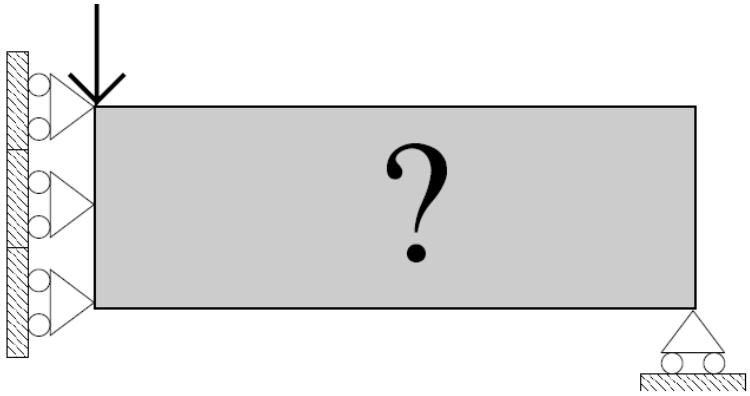

(a) MBB beam (symmetric half)

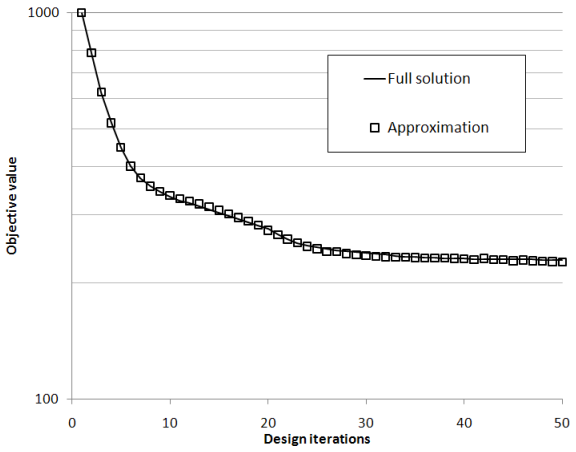

(b) Convergence curve for 50 design iterations

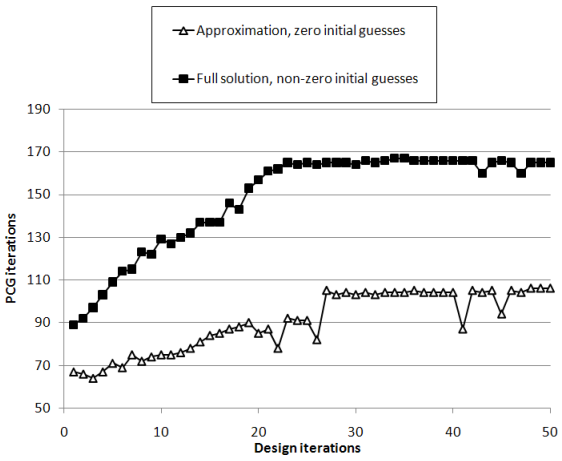

(c) PCG iterations for 50 design iterations

Figure 5.1: Minimum compliance of a 2D MBB-beam: the approximate procedure with consistent sensitivities vs. the full procedure.

Unfortunately, some difficulties are encountered when implementing this approach. First, for efficient computation of the design sensitivities one would like to use a preconditioner that can be differentiated on an element level. Therefore diagonal and SSOR preconditioners are suitable but incomplete factorizations (Meijerink and van der Vorst, 1977) are less preferable. Second, from the the authors' experience it seems to be difficult to find the appropriate tolerance ϵ such that the adjoint procedure will be both efficient and robust. In some cases when a slack ϵ is used, the adjoint procedure does not reach the correct solution because the number of PCG iterations is too small. This typically happens when a reasonable initial guess is used. Such a guess could, for example, consist of the solution to the analysis problem corresponding to the previous design cycle. When employed, the slack convergence tolerance may be reached after only a few iterations. Then the adjoint iterates are not sufficiently distributed across the FE

mesh and the adjoint variables are computed incorrectly. Third and most important, achieving actual savings in computation time when applying the consistent approach is not guaranteed. The adjoint procedure itself requires one matrix-vector multiplication per iteration. Another matrix-vector product per PCG iteration is required for regenerating the vectors $\mathbf{u}_i$, $\mathbf{r}_i$, $\mathbf{p}_i$ and $\mathbf{z}_i$ while performing the adjoint procedure in reverse. These vectors are required for computing the adjoint variables and it is assumed that we cannot store in memory the complete history for all i iterations. This means that the number of matrix-vector products per PCG iteration will be three, compared to a single product in standard PCG. Therefore the consistent approach can be competitive only if the number of PCG iterations is reduced to less than one third of the iterations required by standard PCG. Unfortunately, such a reduction leads to very high residual norms due to the accelerated convergence rate typically exhibited by PCG (van der Sluis and van der Vorst, 1986). Therefore in this study the consistent approach was only implemented and tested for small problems, mainly for the purpose of gaining insight about the behavior of the adjoint procedure and for comparing to the approximate approach.

5.4 Approximate sensitivity analysis

When following the approximate approach, the design sensitivities are computed again using the adjoint method but it is *assumed* that the nested analysis problem is solved accurately. This is of course not the case when using the approximation $\mathbf{u}_m$; nevertheless, we use the same design sensitivity expressions *as if* the nested problem was solved accurately. This is possible due to the particular decision of when to terminate the PCG procedure and choose $\mathbf{u}_m$, which is the main focus of this section.

The compliance case is self-adjoint, meaning that the adjoint vector is the displacements vector. Then the element design sensitivity is

$$\frac{\partial c_1}{\partial \rho_e} \approx -\mathbf{u}_m^T \frac{\partial \mathbf{K}}{\partial \rho_e} \mathbf{u}_m \tag{5.6}$$

For the force inverter case, the element design sensitivity is

$$\frac{\partial c_2}{\partial \rho_e} \approx -\boldsymbol{\lambda}_n^T \frac{\partial \mathbf{K}}{\partial \rho_e} \mathbf{u}_m \tag{5.7}$$

where $\boldsymbol{\lambda}_n$ is an *approximation* to the solution of the adjoint problem (m and n are not necessarily equal)

$$\mathbf{K}\boldsymbol{\lambda}_n \approx \mathbf{l}$$

This leads to the utilization of approximations in two levels. First, the analysis equations are not solved accurately; second, the design sensitivities are not computed accurately nor are they consistent with the use of an approximation in the nested problem. These shortcomings can be overcome by carefully choosing the termination point of the PCG procedure.

The common convergence criterion for PCG (5.3) is measured in terms of residual forces, which is a natural choice since the equations to be solved are force equilibrium equations. However, in order to utilize the approximate sensitivities (5.6) and (5.7) the primary concern should be the accuracy of the design sensitivities. It will be shown here that the approximations $\mathbf{u}_m$ and $\boldsymbol{\lambda}_n$ can be chosen in a manner that ensures that these sensitivities are indeed sufficiently accurate. This is due to the observation that their values in practice converge to the accurate value *before* the norm of the residuals converges according to the criterion in (5.3).

5.4.1 Application to minimum compliance problems

When optimizing compliance, instead of examining the residual forces we suggest to determine convergence of PCG by measuring the change in the **K**-norm of the iterative solution *within the PCG iterations*

$$\frac{\mathbf{u}_m^T\mathbf{K}\mathbf{u}_m - \mathbf{u}_{m-1}^T\mathbf{K}\mathbf{u}_{m-1}}{\mathbf{u}_{m-1}^T\mathbf{K}\mathbf{u}_{m-1}} < \epsilon \tag{5.8}$$

In physical terms, the **K**-norm is the energy norm of the displacements. This value is extremely important in compliance problems: When PCG converges, it is the true value of the objective function; and on an element level, it is simply a scaling of the design sensitivity. Moreover, the conjugate gradients method is an optimal Krylov method in the sense that it minimizes the energy norm of the error, which is also the error in compliance, so in theory it is the most suitable method for this particular convergence measure.

The reasoning behind this particular choice of convergence criterion is first demonstrated on a small minimum compliance problem. Again, we examine the 2D MBB-beam, modeled with a 60×20 mesh. For preconditioning, an incomplete Cholesky factorization (Meijerink and van der Vorst, 1977) with zero fill-in is used. We focus on an early design cycle where the optimization problem (5.1) is far from being solved. Nevertheless, the authors' experience is that the behavior presented here is common to all design iterations. In the first case, the initial guess for PCG is the zero vector and we examine the change in the energy norm of the displacements $\mathbf{u}_i^T\mathbf{K}\mathbf{u}_i$ within the PCG iterations. In Figure 5.2 this energy norm is plotted, together with the relative norm of residual forces which is frequently used to determine convergence. It can be seen that the relative norm of residual forces improves very slowly in the beginning and speeds up toward the end, converging to a tolerance of 10^{-6} after 98 iterations. At the same time, the value of $\mathbf{u}_i^T\mathbf{K}\mathbf{u}_i$ hardly changes after 55 iterations and effectively converges after approximately 60 iterations.

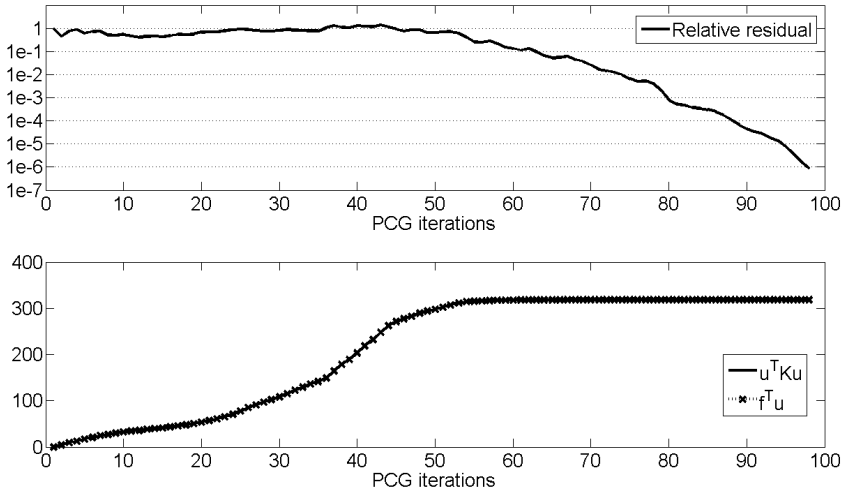

Figure 5.2: Typical behavior of PCG when applied to a nested analysis problem within a minimum compliance problem. The initial guess is the zero vector. Top: The relative norm of residual forces vs. PCG iterations; Bottom: Compliance and energy norm of the displacements vs. PCG iterations

A close look at the convergence of the design sensitivities for the same case is presented in Figure 5.3. We examine the development in the values of the Euclidean and infinity norms over all element sensitivities and in the values of four element design sensitivities *within PCG iterations* for one particular design cycle. Element #1 is located near the loading point and therefore has a maximum density from an early stage of the optimization process. The other elements, #415, #805 and #1158 are boundary elements in the connecting areas of the bars

which will eventually have a high density. However, at this particular optimization iteration these elements still have intermediate densities and therefore it is crucial to compute their design sensitivities correctly. It can be seen that for the four elements, as well as for the norms over all elements, accurate values are obtained after 65-70 PCG iterations. Beyond that, these values hardly change but the PCG procedure continues since force equilibrium is obtained only after 98 iterations.

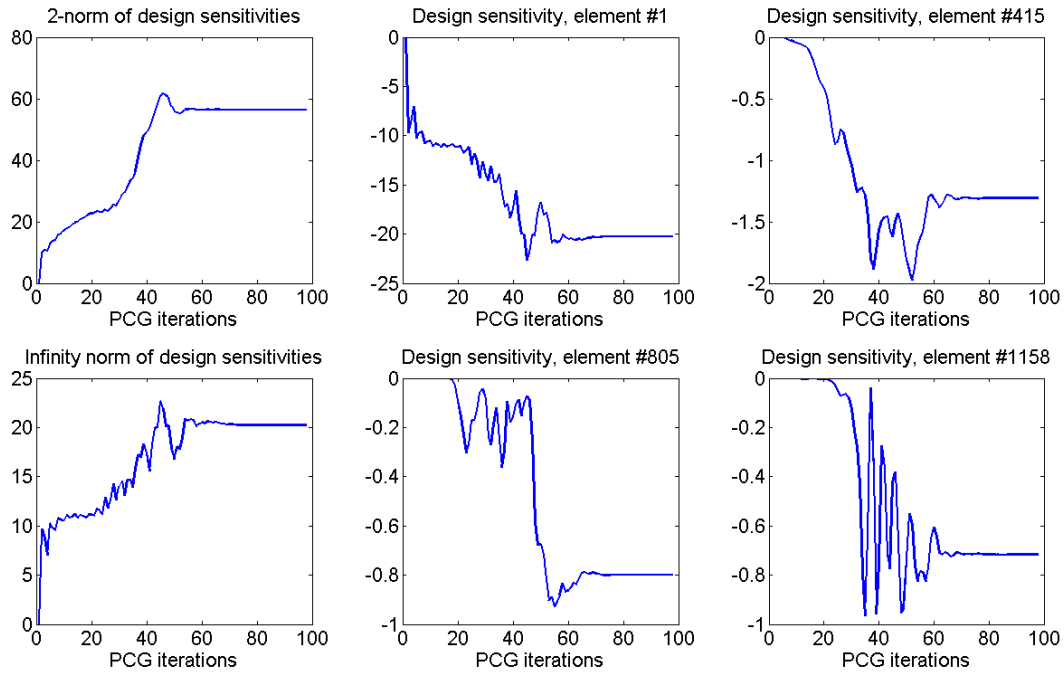

Figure 5.3: Norms of the design sensitivities and sensitivities for four particular finite elements vs. PCG iterations within a minimum compliance problem. The initial guess for PCG is the zero vector.

In this particular case, if the PCG solution would be terminated after approximately 70 iterations, when the criterion in (5.8) is satisfied, it is most likely that both the objective value and the design sensitivities will be sufficiently accurate, even though the relative norm of residual forces is larger than 10^{-2}. Such an error is clearly too large if our aim is to solve the equation system. However, for the purpose of solving the compliance optimization problem this approximation could be sufficient. This means that determining PCG convergence according to the relative norm of the residual is somewhat conservative, leading to performing unnecessary PCG iterations.

The convergence criterion suggested in (5.8) should only be used when the initial guess for the PCG procedure is a zero vector. It is interesting to see that in such a case $\mathbf{f}^T\mathbf{u}_i = \mathbf{u}_i^T\mathbf{K}\mathbf{u}_i$ for all PCG iterations. This means that within PCG, measuring the compliance as it is expressed in the objective function $\mathbf{f}^T\mathbf{u}_i$, is identical to measuring the energy norm of the displacements $\mathbf{u}_i^T\mathbf{K}\mathbf{u}_i$, whose error is minimized by PCG. This property of PCG results from the orthogonality of the residuals $\mathbf{r}_i$ and the direction vectors $\mathbf{p}_j$ ($\forall j < i$) and is not affected by preconditioning; a detailed derivation of this equality can be found in Appendix B.

Within an optimization process, the solution of the nested problem corresponding to the previous design cycle is often used as an initial guess for the iterative solution of the current nested problem. In that case, $\mathbf{f}^T\mathbf{u}_i$ and $\mathbf{u}_i^T\mathbf{K}\mathbf{u}_i$ have different values, and are equal only when the equilibrium equations are satisfied. Measuring the convergence of $\mathbf{u}_i^T\mathbf{K}\mathbf{u}_i$ is not sufficient, since when the design changes are small the value corresponding to the initial guess will be

very close to the value corresponding to the converged PCG solution. However, it is possible to determine convergence by measuring also the relative difference between the compliance and the energy norm of the displacements

$$\frac{\left|\mathbf{f}^T\mathbf{u}_m - \mathbf{u}_m^T\mathbf{K}\mathbf{u}_m\right|}{\mathbf{u}_m^T\mathbf{K}\mathbf{u}_m} < \epsilon \tag{5.9}$$

The reasoning behind this criterion for choosing the termination point is demonstrated in Figure 5.4. Again, we focus on a certain design cycle of the same 2D MBB-beam minimum compliance problem, where PCG was called to solve the analysis equation system. Since a sensible initial guess is used, the relative norm of the residual forces improves rapidly in the first PCG iterations, but then the convergence slows down and speeds up again only after the error is smaller than 10^{-2}. The final convergence tolerance of 10^{-6} is satisfied after 95 iterations, while 98 iterations were required when the initial guess was zero. This means that using a reasonable initial guess does not necessarily reduce the final number of PCG iterations significantly, especially when the design changes are not very small and the structural topology is not yet determined. It can be seen that in this case, the values of $\mathbf{f}^T\mathbf{u}_i$ and $\mathbf{u}_i^T\mathbf{K}\mathbf{u}_i$ are nearly equal after 60 iterations and effectively converge after 65-70 iterations.

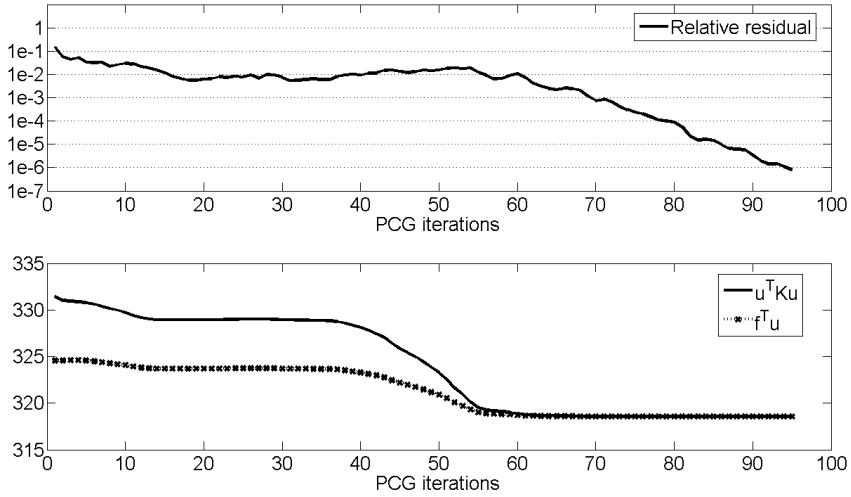

Figure 5.4: Typical behavior of PCG when applied to a nested analysis problem within a minimum compliance problem. The initial guess is the solution from the analysis in the previous design cycle. Top: The relative norm of residual forces vs. PCG iterations; Bottom: Compliance and energy norm of the displacements vs. PCG iterations

The development of the element design sensitivities within PCG iterations is presented in Figure 5.5, for the case where an initial guess was utilized. Again, we examine the Euclidean and infinity norms over all element sensitivities and the design sensitivities for the same set of four elements as in the previous example. As it was already demonstrated for the case of a zero initial guess, now too we obtain accurate values of the design sensitivities after 65-70 PCG iterations. Beyond that, these values hardly change but the PCG procedure continues since force equilibrium is obtained only after 95 iterations.

Concluding this section regarding minimum compliance problems, it is clear that in practice we can reduce the number of PCG iterations performed on the nested analysis problem. This is possible by using an approximation to the solution vector $\mathbf{u}_m$ that corresponds to the point in which at least one of the criteria suggested in (5.8) and (5.9) is satisfied. Even though the solution is approximate in terms of residual forces, it is sufficiently accurate for the purpose of optimization. This is because PCG is terminated at a point when the objective value, and most likely the design sensitivities, are computed accurately.

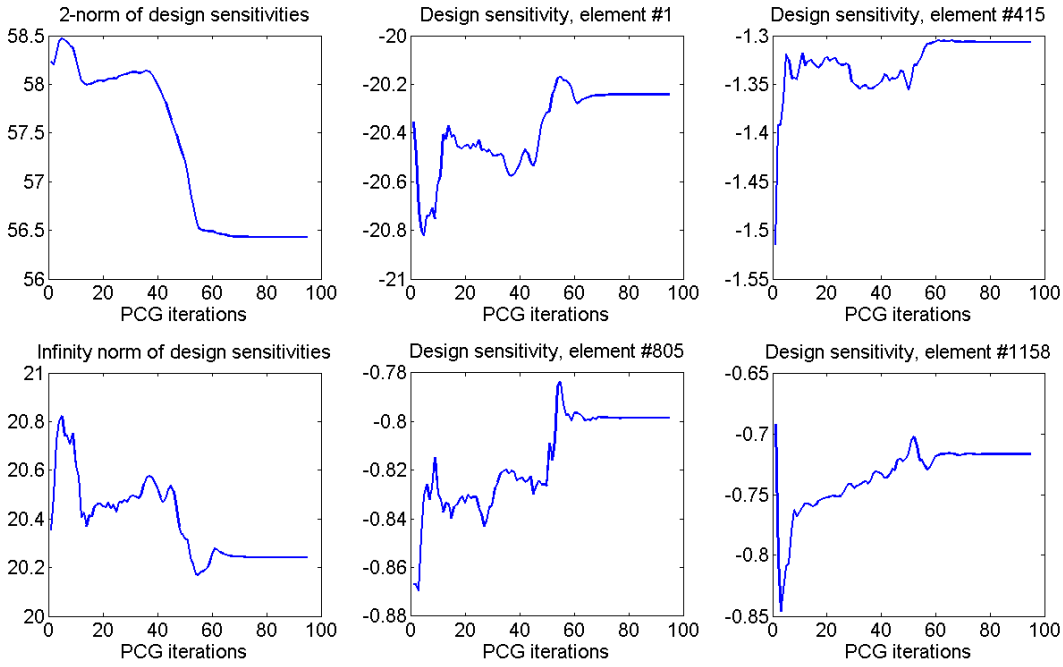

Figure 5.5: Norms of the design sensitivities and sensitivities for four particular finite elements vs. PCG iterations within a minimum compliance problem. The initial guess is the solution from the analysis in the previous design cycle.

5.4.2 Application to other classes of problems

The alternative convergence measures proposed above (5.8) and (5.9) are tailored for the particular case of minimum compliance problems, where the optimality of PCG as a minimizer of the energy norm of the error plays a major role. For other objective functions, these measures are less natural and one should search for more suitable ones that are related to the particular objective function we are trying to optimize. As a demonstrative case we focus on the design of a force inverter, under the simplifying assumption of small displacements. The corresponding optimization problem and design sensitivities were given above (5.2), (5.7). This example follows the benchmark problem originally examined in (Sigmund, 1997), see Figure 5.6. At this stage, we did not attempt to apply the same concepts to other objectives or physical models, but this certainly is a challenging topic for future studies.

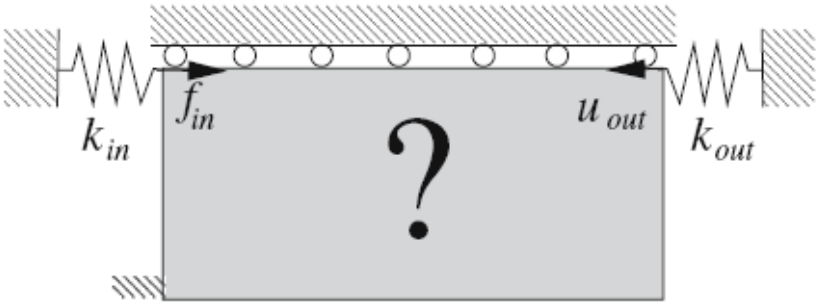

Figure 5.6: Design of a 2D force inverter: Design domain, boundary conditions and external load

In order to compute the design sensitivities in the force inverter problem, an adjoint equation system must be solved in addition to the solution of the nested analysis equations. This is not necessary in minimum compliance problems which are self-adjoint. The analysis problem consists of a load vector $\mathbf{f}$ (a point load at the input degree of freedom) and the corresponding displacements $\mathbf{u}$, while the adjoint problem consists of a load vector $\mathbf{l}$ (a point load at the output degree of freedom) and the corresponding displacements $\boldsymbol{\lambda}$. Since both equation systems have the same stiffness matrix and since their right hand side vectors are independent of each other, it is worthwhile to use a block-PCG procedure (O'Leary, 1980) instead of calling PCG twice separately. It is important to point out that due to the ground structure's aspect ratio and the location of loads and supports (see Figure 5.6), the analysis problem tends to converge faster than the adjoint problem in terms of residual forces. The horizontal support in the lower left corner is closer to the input force and therefore the residual in the analysis problem is reduced earlier in terms of PCG iterations. Eventually this leads to earlier convergence of the analysis problem compared to the adjoint problem. If this occurs while solving by block-PCG, all further iterations of the PCG procedure will be performed only on the adjoint problem.

In this class of optimization problems we suggest to focus on the development *within PCG* of the quantities $\mathbf{l}^T\mathbf{u}_i$, $\mathbf{f}^T\boldsymbol{\lambda}_i$ and $\boldsymbol{\lambda}_i^T\mathbf{K}\mathbf{u}_i$. If both the analysis and the adjoint problems are solved to full accuracy, then these quantities are all equal. Same as for the compliance case, the latter has an element-wise relation to the design sensitivities. This means that besides measuring the convergence of the objective value, in an indirect manner we are also measuring the convergence of the sensitivity values.

We examine a small 2D force inverter modeled with a 40×20 mesh. For preconditioning, an incomplete Cholesky factorization with zero fill-in is used. We focus on the seventh design cycle, where the distribution of material begins to become clear but the optimization problem (5.2) is far from being solved. In the first case the initial guesses for PCG are two zero vectors and we examine the change in the values $\mathbf{l}^T\mathbf{u}_i$, $\mathbf{f}^T\boldsymbol{\lambda}_i$ and $\boldsymbol{\lambda}_i^T\mathbf{K}\mathbf{u}_i$ within PCG iterations. In Figure 5.7 these quantities are plotted, together with the relative norms of residual forces for both problems - analysis and adjoint.

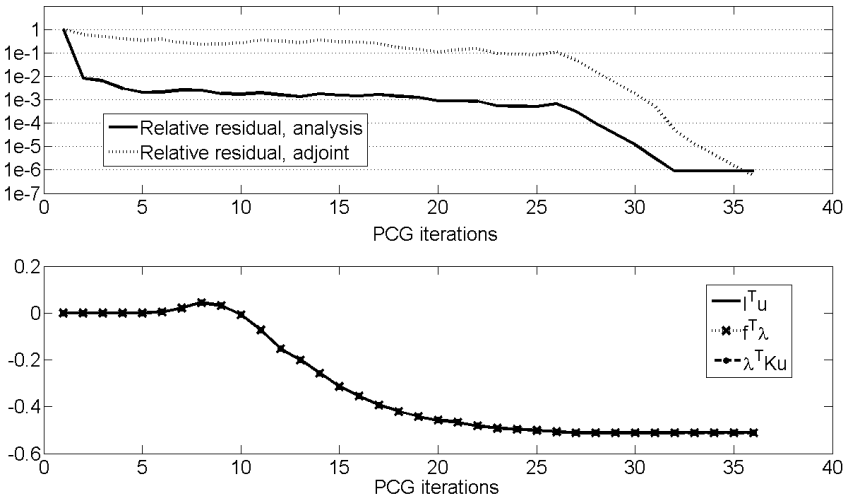

Figure 5.7: Typical behavior of PCG when applied to the nested analysis and adjoint problems within a force inverter design problem. The initial guesses for the block-PCG procedure are the zero vectors. Top: The relative norms of residual forces vs. PCG iterations; Bottom: $\mathbf{l}^T\mathbf{u}_i$, $\mathbf{f}^T\boldsymbol{\lambda}_i$ and $\boldsymbol{\lambda}_i^T\mathbf{K}\mathbf{u}_i$ vs. PCG iterations

As expected, the analysis problem converges faster, mainly due to a significant reduction in residual forces within the first PCG iterations. It is noted that also for this problem the

three quantities $\mathbf{l}^T\mathbf{u}_i$, $\mathbf{f}^T\boldsymbol{\lambda}_i$ and $\boldsymbol{\lambda}_i^T\mathbf{K}\mathbf{u}_i$ are equal throughout the PCG procedure. This is again due to orthogonality of residuals and direction vectors (which is maintained also for block-PCG iterations, (O'Leary, 1980)) and due to the utilization of a zero vector as an initial guess. A detailed derivation of this equality can be found in Appendix B. As for the convergence of these values, it can be seen that they hardly change after 25 iterations and effectively converge after approximately 30 iterations. At the same time, the analysis problem is close to convergence but the adjoint problem still has a significant residual, with a relative norm between 10^{-2} and 10^{-3}.

When examining a few representative design sensitivities we observe similar behavior to that of compliance problems, see Figure 5.8. We focus on the Euclidean and infinity norms of the design sensitivities over all elements and on four particular finite elements. Elements #1 and #200 will eventually be part of high-density regions. On the other hand, elements #495 and #497 are located in the vicinity of the main joint and in the final design element #495 will be void while element #497 will have full density. At this particular design cycle, they both have intermediate densities so it is very important that their design sensitivities will be computed accurately. It can be seen that for the four elements, as well as for the global measures, accurate values are obtained after 28-30 PCG iterations. Beyond that, these values hardly change but the PCG procedure continues since force equilibrium is obtained after 36 iterations.

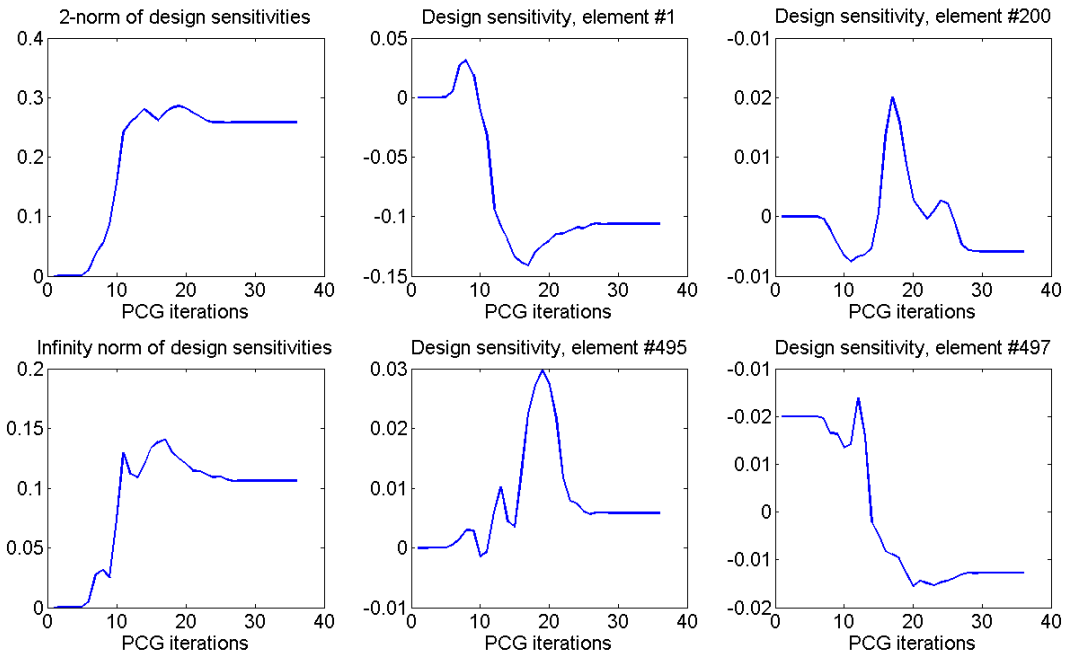

Figure 5.8: Norms of the design sensitivities and sensitivities for four particular finite elements vs. PCG iterations within a force inverter design problem. The initial guesses for the block-PCG procedure are the zero vectors.

As it can be seen in Figure 5.8, the design sensitivities are computed accurately before the PCG procedure converges in terms of residual forces, and there is a clear correlation between their point of convergence and the convergence of the global quantities. This means that for the purpose of optimizing a force inverter, it may be sufficient to determine convergence of PCG

according to the following criteria

$$\left|\frac{\boldsymbol{\lambda}_m^T\mathbf{K}\mathbf{u}_m - \boldsymbol{\lambda}_{m-1}^T\mathbf{K}\mathbf{u}_{m-1}}{\boldsymbol{\lambda}_{m-1}^T\mathbf{K}\mathbf{u}_{m-1}}\right| < \epsilon \tag{5.10}$$

$$\left|\frac{\mathbf{l}^T\mathbf{u}_m - \mathbf{l}^T\mathbf{u}_{m-1}}{\mathbf{l}^T\mathbf{u}_{m-1}}\right| < \epsilon \tag{5.11}$$

$$\left|\frac{\mathbf{f}^T\boldsymbol{\lambda}_m - \mathbf{f}^T\boldsymbol{\lambda}_{m-1}}{\mathbf{f}^T\boldsymbol{\lambda}_{m-1}}\right| < \epsilon \tag{5.12}$$

which are equivalent when zero vectors are used as initial guesses. When a non-zero initial guess is used for PCG, the criteria (5.10)-(5.12) may not be sufficient. However, several different combinations of convergence criteria are available, based on measuring the absolute differences between the three values as well as their convergence. For example, we can add the following measure

$$\left|\frac{\mathbf{l}^T\mathbf{u}_m - \mathbf{f}^T\boldsymbol{\lambda}_m}{\mathbf{f}^T\boldsymbol{\lambda}_m}\right| < \epsilon \tag{5.13}$$

When examining the same 2D force inverter problem but for the case of non-zero initial guesses, similar conclusions arise. The convergence of residual forces as well as $\mathbf{l}^T\mathbf{u}_i$, $\mathbf{f}^T\boldsymbol{\lambda}_i$ and $\boldsymbol{\lambda}_i^T\mathbf{K}\mathbf{u}_i$ are plotted in Figure 5.9. We note that in this case, $\mathbf{f}^T\boldsymbol{\lambda}_i$ and $\boldsymbol{\lambda}_i^T\mathbf{K}\mathbf{u}_i$ follow a similar convergence path beginning from the first PCG iteration. This is because the residual corresponding to the iterative solution of $\mathbf{K}\mathbf{u} = \mathbf{f}$ is small from the beginning due to a good initial guess. Therefore the development of these two quantities is governed mainly by the iterative development of $\boldsymbol{\lambda}_i$. The convergence of the design sensitivities is presented in Figure 5.10. The three quantities we focus on, as well as the design sensitivities, effectively converge after approximately 30 PCG iterations. At the same time, the relative norm of the residual is 10^{-5} for the analysis problem but only slightly smaller than 10^{-2} for the adjoint problem.

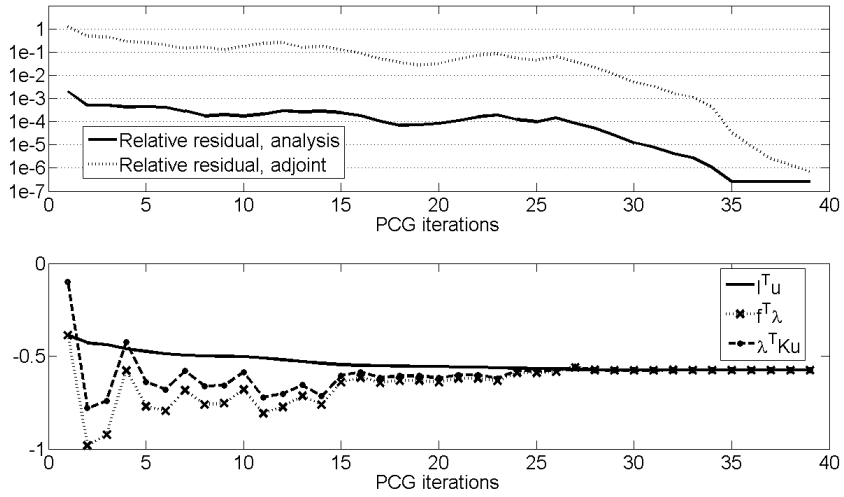

Figure 5.9: Typical behavior of PCG when applied to the nested analysis and adjoint problems within a force inverter design problem. The initial guesses for the block-PCG procedure are the solutions of the analysis and adjoint problems from the previous design cycle. Top: The relative norms of residual forces vs. PCG iterations; Bottom: $\mathbf{l}^T\mathbf{u}_i$, $\mathbf{f}^T\boldsymbol{\lambda}_i$ and $\boldsymbol{\lambda}_i^T\mathbf{K}\mathbf{u}_i$ vs. PCG iterations

In conclusion, choosing the solution vectors $\mathbf{u}_m$ and $\boldsymbol{\lambda}_m$, corresponding to the point in which the criteria suggested in (5.10), (5.11), (5.12) and (5.13) are satisfied, can lead to a significant reduction in the number of PCG iterations performed on the adjoint problem and a slight

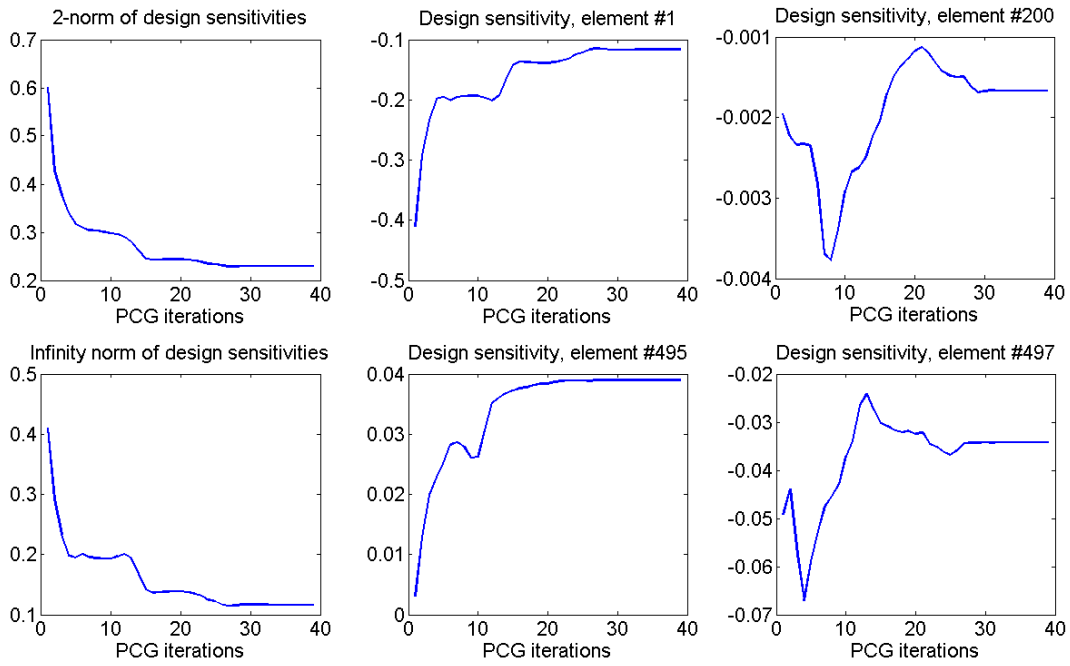

Figure 5.10: Norms of the design sensitivities and sensitivities for four particular finite elements vs. PCG iterations within a force inverter design problem. The initial guesses for the block-PCG procedure are the solutions of the analysis and adjoint problems from the previous design cycle.

reduction in the number of PCG iterations performed on the analysis problem. Clearly, these alternative convergence criteria are tailored for only one particular class of topology optimization problems, but it should be possible to define similar criteria for other types. The guideline for defining such criteria is that the quantity whose convergence is measured should have a correlation to the objective value and to the design sensitivities. Then it should be possible to find approximations that may not be accurate in terms of residuals in the nested equation system, but are sufficiently accurate for the evaluation of the objective and the sensitivities.

5.5 3D Examples

In this section, several large-scale three-dimensional examples are presented. The problems that are addressed are minimum compliance problems and a force inverter problem. It is shown that accurate results can be obtained efficiently when using approximations generated by PCG in the analysis and sensitivity analysis. All the results presented in this section were obtained using an incomplete Cholesky factorization with zero fill-in as preconditioner. The optimization is performed by a nonlinear optimization program based on the Method of Moving Asymptotes (Svanberg, 1987). In order to obtain regularized designs and to avoid checkerboard patterns, a density filter was applied (Bourdin, 2001; Bruns and Tortorelli, 2001).

5.5.1 3D minimum compliance

In this example, we present the solution for the minimum compliance design of a cantilever beam subjected to a concentrated vertical load at the bottom of its free face, see Figure 5.11(a). The cantilever has a length of 1 and its width and height are equal to 1/3. It is fixed to the wall only at the four corners. Exploiting the symmetry of the problem, we solve only one half of the

structure modeled with a 180×30×60 FE mesh consisting of 8-node cubic elements. The values of E_{min} and E_{max} were set to 10^{-9} and 1 and Poisson's ratio was set to 0.3. The allowed volume fraction was 0.35 and the penalization factor p used in the SIMP interpolation was set to 3. A linear weighting density filter was used with the radius of 6 times an element length. The MMA move limit was fixed throughout the optimization process to the value of 0.2.

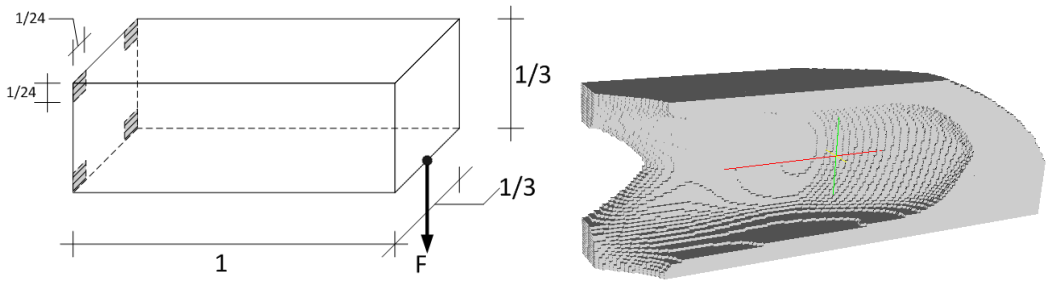

(a) Design domain, boundary conditions and external load

(b) Layout after 50 design iterations, inner part of symmetric half

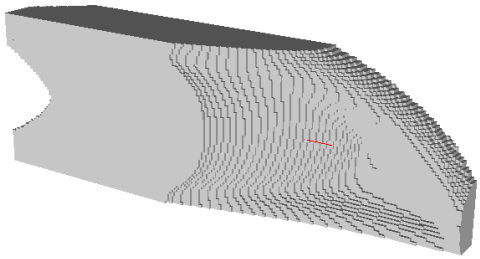

(c) Layout after 50 design iterations, outer part of symmetric half

Figure 5.11: Minimum compliance design of a 3D cantilever beam

In Figures 5.12(a) and 5.12(b) we compare the performance of the approximate approach against standard procedures. In the approximate scheme, zero vectors are utilized as initial guesses for the PCG iterations so the criterion suggested in (5.8) is employed, with a tolerance ϵ of 10^{-4}. At the final design iteration of the approximate procedure, PCG was driven to full convergence for the purpose of obtaining an accurate evaluation of the objective. When using the standard convergence criterion for the PCG iterations, given in (5.3), the tolerance was set to the common value of 10^{-6} and the solution corresponding to the current design design cycle was the initial guess for the following cycle. Using the alternative convergence criterion leads to approximately 38% reduction in the total number of PCG iterations: 9,898 compared to 15,864 using the standard criterion. This comes with little compromise on the quality of the results: after 50 design iterations, the full procedure reaches an objective value of 859.713 and the approximate procedure reaches 859.558 (0.02% error). The final objectives and the convergence curves of the optimization problems are practically identical (see Figure 5.12(a)) as are also the resulting designs. It can be seen that when supports are available only at the corners of the wall, the preferred design is a shell with a large inner void. This is opposed to the I-section design which is frequently the optimal shape when the complete wall area is supported (see for example Wang et al. (2007); Amir et al. (2009a)).

In order to gain more insight about the accuracy and efficiency of the approximate approach, we solved the same problem with a coarse mesh (90×15×30) and tighter design convergence tolerance. The optimization process was terminated when the maximum change in an element density did not exceed 0.001 or after 500 design iterations. The results are presented in Table 5.1. It should be noted that these results depend strongly on the behavior of the optimization program (MMA) which also incorporates approximations and therefore direct comparison can

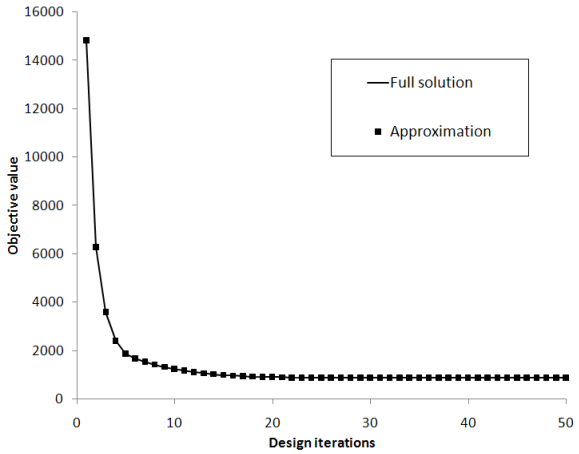

(a) Convergence curve, 50 design iterations

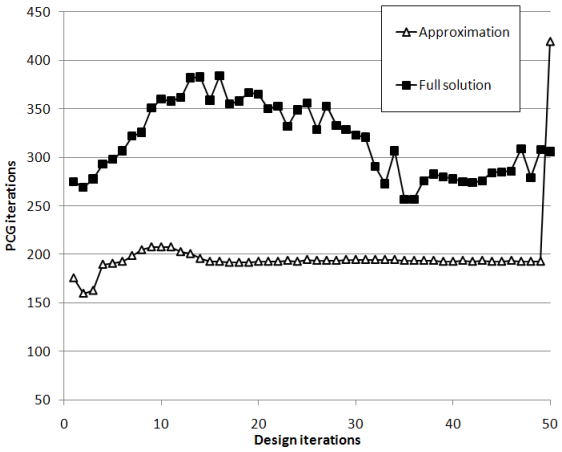

(b) PCG iterations vs. design iterations

Figure 5.12: Results of the 3D cantilever minimum compliance problem, 324,000 elements and 1.03×10^6 DOF

be misleading. For example, in this particular problem the approximate procedures reached the stopping criterion earlier than the full procedure, a result that is somewhat unexpected. This may be related to the use of a physical stopping criterion rather than a mathematical one. Moreover, when solving by approximate procedures also the final objective values were computed approximately. When using non-zero initial guesses, this objective is nearly accurate since the final relative residual norm is smaller than 1×10^{-5} (see Figure 5.13). However, when using zeros as initial guesses the true objective is expected to be higher, according to the behavior of PCG as presented earlier. In any case, it is possible to identify some general trends. The approximate procedures reach accurate objective values, with relative errors of 0.04% and 0.006%. Moreover, the number of PCG iterations (measured per design iteration for a more reliable comparison, see last column in Table 5.1) can be reduced significantly, especially if non-zero initial guesses are utilized in the advanced stages of the optimization process.

Table 5.1: Results of the 3D cantilever minimum compliance problem, 40,500 elements and 1.35×10^5 DOF

Procedure	Design iterations	Objective	Total PCG iterations	PCG iterations per design iteration
Full	500	679.61215	53,691	107.38
Approximate, zero initial guesses	389	679.34588 [a]	40,286	103.56
Approximate, non-zero initial guesses	440	679.65369 [a]	15,855	36.03

[a] Final objective values computed by the *approximate* procedures.

The same coarse mesh was also utilized when investigating the influence of the lower bound E_{min} on the behavior of the approximate procedure. It was found that reducing E_{min} leads to a very minor increase in computational effort, measured through the total number of matrix-vector products. When solving by the approximate procedure, the number of matvecs performed with $E_{min} = 10^{-6}$ was 2.6% higher than with $E_{min} = 10^{-3}$; when setting $E_{min} = 10^{-9}$ the number of matvecs performed was 3.6% higher than with $E_{min} = 10^{-3}$. Moreover, the relative

error in the objective value obtained by the approximate procedure was roughly 0.01% in all three cases, while the number of matrix-vector products was reduced by roughly 52% compared to the full procedure.

Concluding this example, we find it interesting to examine the actual accuracy of the approximations with respect to the solution of the nested equation system. In Figure 5.13, the relative norms of residuals for the whole design process are plotted for the two types of approximate procedures. For each design iteration, the value plotted is the relative norm of the residual corresponding to the early termination point of PCG, meaning the point when either (5.8) or both (5.8) and (5.9) were satisfied. When using zeros as initial guesses, the values of this norm are between 1×10^{-2} and 2×10^{-2} throughout the whole design process. However, when utilizing a sensible initial guess in every design iteration (an approximation to the solution corresponding to the previous design cycle) the relative norm of residuals tends to reduce as the design process advances. This means that as we get closer to the optimal design, we also get closer to an accurate solution of the nested system. This explains the superior accuracy and efficiency of this procedure compared to a procedure using zeros as initial guesses.

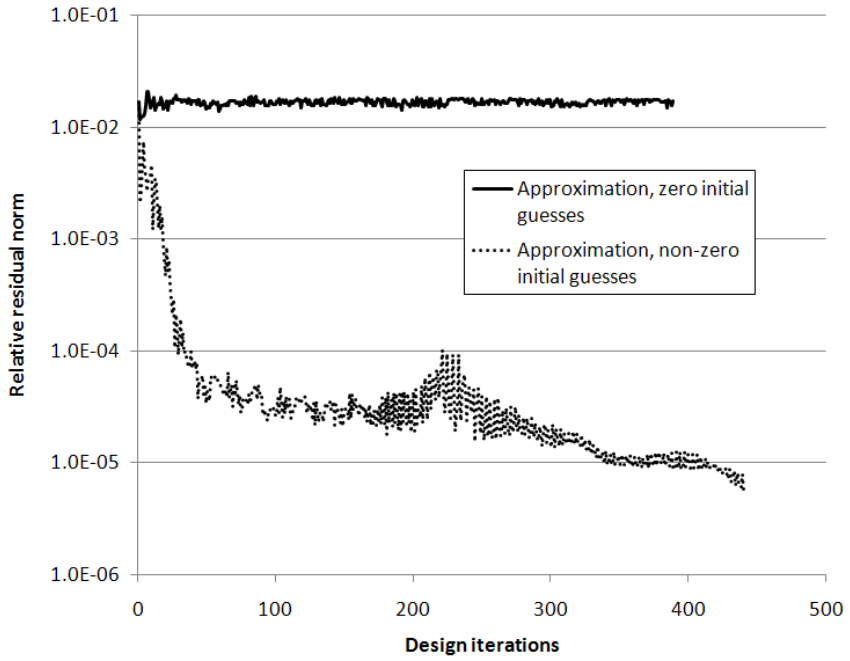

Figure 5.13: The relative norm of residual forces vs. design iterations when approximate procedures are applied to a minimum compliance design of a 3D cantilever, 40,500 elements and 1.35×10^5 DOF

5.5.2 3D multiple load case minimum compliance

In this example, we examine the solution for the minimum compliance design of a cantilever beam subjected to two separate load scenarios. The objective is to minimize the worst case compliance so the problem has a min-max form which differs slightly from the single load case

considered above (5.1)

$$
\begin{aligned}
\min_{\boldsymbol{\rho},\tau} \quad & \tau \\
\text{s.t.:} \quad & \mathbf{f_1}^T \mathbf{u_1}_m \leq \tau \\
& \mathbf{f_2}^T \mathbf{u_2}_m \leq \tau \\
& \sum_{e=1}^{N} v_e \rho_e \leq V \\
& 0 \leq \rho_e \leq 1 \qquad e = 1, ..., N \\
\text{with:} \quad & \mathbf{K}(\boldsymbol{\rho}) \left[\mathbf{u_1} \;\; \mathbf{u_2}\right]_m \approx \left[\mathbf{f_1} \;\; \mathbf{f_2}\right]
\end{aligned}
$$

The first load case consists of vertical loads at the four corners of the free face, each with a magnitude of 0.01. The second load case is the same but with horizontal loads acting in the transverse direction of the beam. The cantilever has a length of 1, its width is 2/15, its height is 1/5, and it is completely fixed to a wall in one end, see Figure 5.14(a). We model the structure with a 150×20×30 FE mesh consisting of 8-node cubic elements. The values of E_{min} and E_{max} were set to 10^{-6} and 1 and Poisson's ratio was set to 0.3. The allowed volume fraction was 0.5 and the penalization factor p used in the SIMP interpolation was set to 3. A linear weighting density filter was used with the radius of 5 times an element length. The MMA move limit was fixed throughout the optimization process to the value of 0.2.

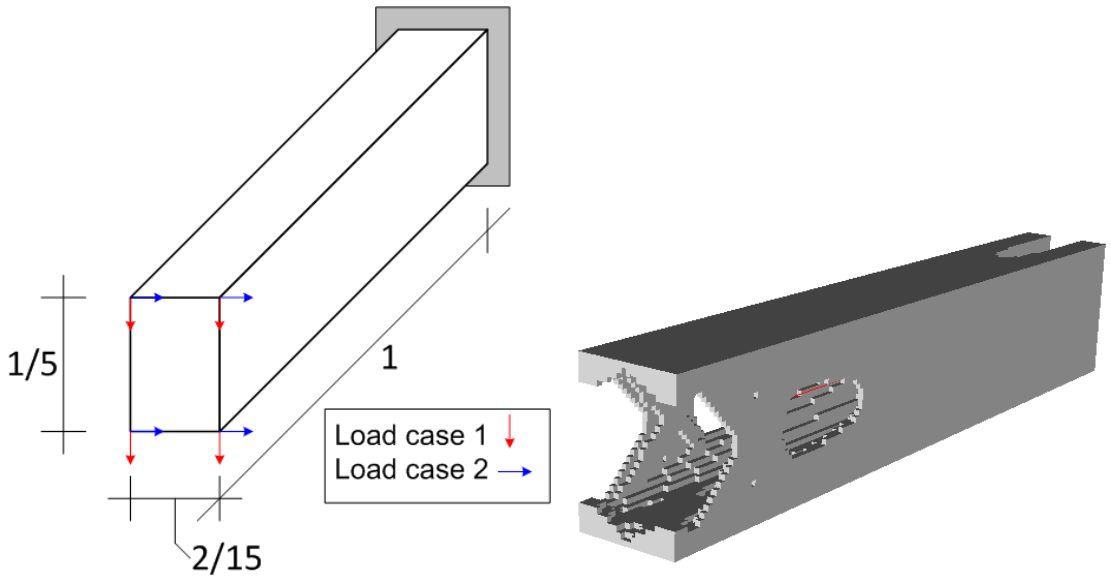

(a) Design domain, boundary conditions and external load

(b) Layout after 100 design iterations

Figure 5.14: Two load case worst-case minimum compliance of a 3D cantilever beam

This example problem was solved by both standard and approximate procedures, utilizing non-zero initial guesses for the block-PCG iterations. When using the standard convergence criterion for the PCG iterations, given in (5.3), the tolerance was set to the common value of 10^{-6}. In the approximate procedure, PCG was terminated when both criteria (5.8) and (5.9) were satisfied to a tolerance of 10^{-4}. The design process was stopped after 100 iterations in both cases. Again, using the alternative convergence criteria leads to significant reductions in computation time: 39,854 matrix-vector products compared to 67,859 when solving by the standard procedure (approximately 41% reduction). The objective values after 100 design iterations are

practically the same: 21.0854 and 21.0865 in the approximate and standard procedures, respectively. Finally, as was observed also for the single load minimum compliance problem, the relative norm of residuals tends to reduce as the design process advances, see Figure 5.15.

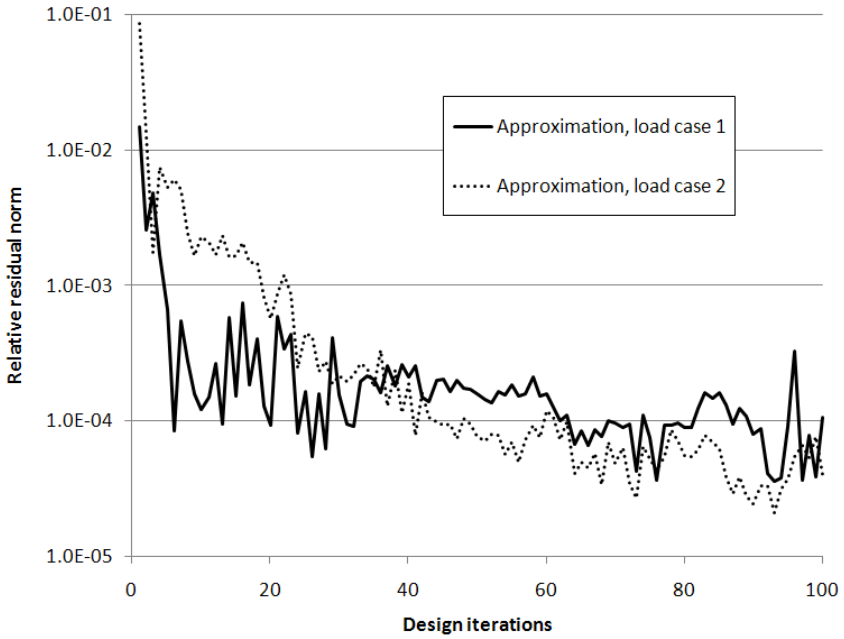

Figure 5.15: The relative norm of residual forces vs. design iterations when an approximate procedure is applied to a two load case minimum compliance design of a 3D cantilever, 90,000 elements and 2.95×10^5 DOF

5.5.3 3D force inverter

As a third demonstrative example, we present the solution for the maximum output displacement of a three dimensional force inverter. Exploiting symmetry, we model only one quarter of the structure with a $60\times30\times30$ FE mesh consisting of 8-node cubic elements. The spring stiffnesses were set to 0.1 for the input spring and 0.01 for the output spring. The values of E_{min} and E_{max} were set to 10^{-4} and 1 and Poisson's ratio was set to 0.3. The allowed volume fraction was 0.15 and the penalization factor p used in the SIMP interpolation was set to 3. A linear weighting density filter was used with the radius of 3 times an element length and the MMA move limit was fixed throughout the optimization process to the value of 0.2.

The force inverter problem was solved by both standard and approximate procedures, utilizing non-zero initial guesses for the block-PCG iterations. When using the standard convergence criterion for the PCG iterations, given in (5.3), the tolerance was set to the common value of 10^{-6}. In the approximate procedure, PCG was terminated when the criteria (5.10), (5.11), (5.12) and (5.13) were satisfied to a tolerance of 10^{-4}. The design process was stopped after 200 iterations in both cases. Again, using the alternative convergence criteria leads to significant reductions in computation time: 23,484 matrix-vector products compared to 41,668 when solving by the standard procedure (approximately 44% reduction). The objective values after 200 design iterations are practically the same: -0.52733 and -0.52759 in the approximate and standard procedures, respectively. However, there are some differences between the two solutions. First, the convergence curves (see Figure 5.17(a)) are not identical - when using the approximations, the local minimum with the objective value of 0 is overcome faster than when using the full solutions. This of course is related to the performance of the optimizer (MMA) and should not be seen as a general observation. Second, the optimized designs obtained after

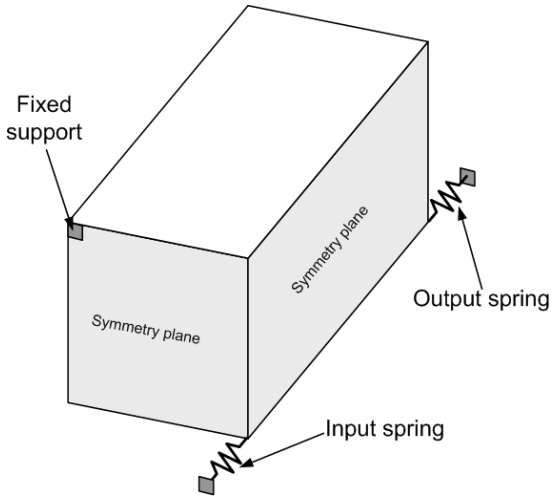

(a) Design domain and boundary conditions, upper left symmetric quarter

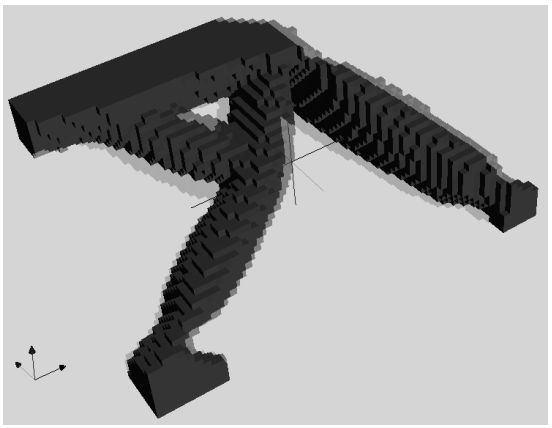

(b) Comparison between force inverter designs obtained by both full (black + light grey regions) and approximate (black + dark grey regions) procedures. Results are presented on the symmetric quarter only

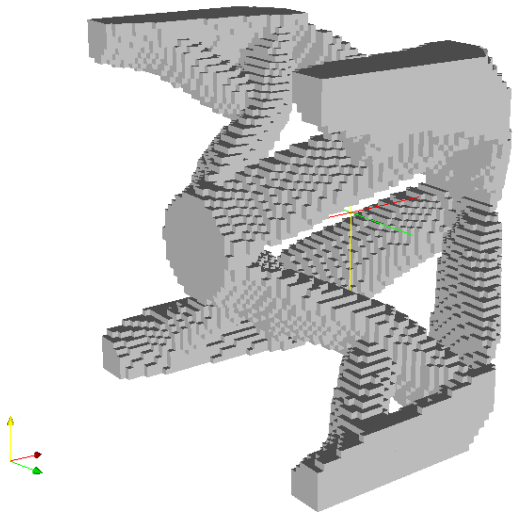

(c) Layout after 200 design iterations, whole structure

Figure 5.16: Design of a 3D force inverter

200 iterations are not identical. In Figure 5.16(b) both designs are displayed in one merged figure. It can be seen that the designs share the same topology but do not have the exact same shape. Nevertheless, their performance at this stage of the optimization is practically identical - the relative error in the objective value is 0.05%.

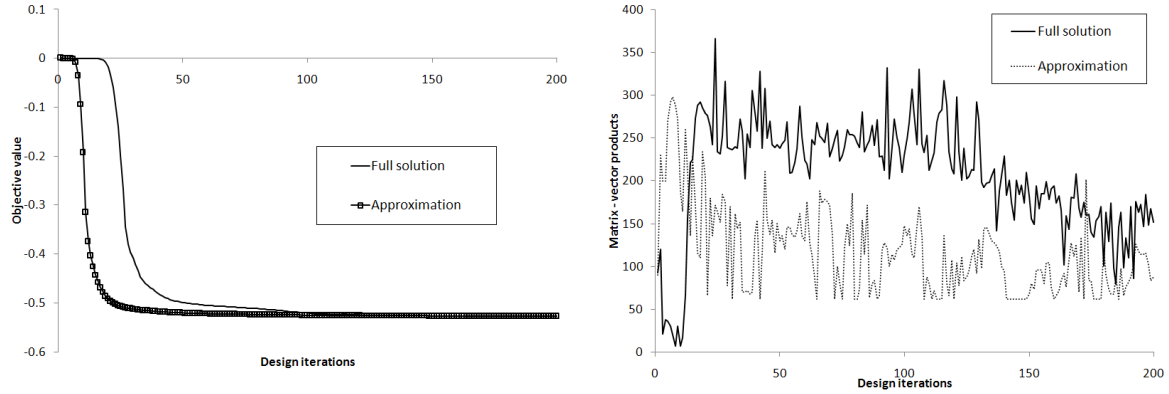

(a) Convergence curve, 200 design iterations

(b) PCG matvecs vs. design iterations

Figure 5.17: Results of the 3D force inverter design problem, 54,000 elements and 1.76×10^5 DOF

Concluding the examples section, in Table 5.2 we present a summary of the results obtained for the three example problems. As noted earlier, these results depend strongly on the behavior of the optimization program and direct comparison of objective values can be misleading. For example, in the minimum compliance case the approximate procedure reaches a lower objective than the full procedure - a result that in general is not expected. Moreover, in the force inverter and the multiple load case problems the final objective values were computed by the approximate procedures, meaning that they differ slightly from the true values. With these limitations in mind, it can be observed that for all example problems accurate results are obtained while computer time, reflected in the number of PCG matrix-vector multiplications, can be reduced significantly.

Table 5.2: Accuracy and efficiency of the approximate approach

Problem description	PCG convergence criteria	Design iterations	Objective	PCG matvecs
Minimum compliance	Eq. (5.3)	50	859.713	15,864
	Eq. (5.8)	50	859.558 [a]	9,898
Force inverter	Eq. (5.3)	200	-0.52759	41,668
	Eqs. (5.10),(5.11),(5.12),(5.13)	200	-0.52733 [b]	23,484
Multiple load case minimum compliance	Eq. (5.3)	100	21.0865	67,859
	Eqs. (5.8),(5.9)	100	21.0854 [b]	39,854

[a] Final objective value computed accurately.

[b] Final objective values computed by the *approximate* procedures.

5.6 Summary and conclusions

An effective approximate approach for solving the nested analysis problem in topology optimization was presented. The approximation is based on a sensible early termination of the

iterative equation solver intended to solve the analysis equations. It was shown that accurate optimization results can be obtained together with significant reduction in the computational effort invested in repeated solutions of the analysis equations. This is due to the particular choice of when to terminate the equation solver.

In some cases, such as compliant mechanism design where many local minima exist, the approximate approach leads to slightly different optimized layouts. Nevertheless, the approximate approach can be utilized in order to obtain a good initial design efficiently while for the final design an accurate approach will be used. This can lead to significant savings in computer run time especially when many design iterations are required in order to converge.

The current study focuses on applications of topology optimization in structural mechanics but the approach could be applied to other classes of topology and structural optimization.

5.7 Acknowledgments

We are grateful to Krister Svanberg for allowing us to use the MMA code.

References

O. Amir, M. P. Bendsøe, and O. Sigmund. Approximate reanalysis in topology optimization. *International Journal for Numerical Methods in Engineering*, 78:1474–1491, 2009.

O. Amir, M. Stolpe, and O. Sigmund. Efficient use of iterative solvers in nested topology optimization. In *Proceedings of the 8th World Congress on Structural and Multidisciplinary Optimization, Lisbon, Portugal.*, 2009.

M. P. Bendsøe. Optimal shape design as a material distribution problem. *Structural Optimization*, 1:193–202, 1989.

M. P. Bendsøe and N. Kikuchi. Generating optimal topologies in structural design using a homogenization method. *Computer Methods in Applied Mechanics and Engineering*, 71:197–224, 1988.

M. P. Bendsøe and O. Sigmund. *Topology Optimization - Theory, Methods and Applications*. Springer, Berlin, 2003.

B. Bourdin. Filters in topology optimization. *International Journal for Numerical Methods in Engineering*, 50:2143–2158, 2001.

T. E. Bruns and D. A. Tortorelli. Topology optimization of non-linear elastic structures and compliant mechanisms. *Computer Methods in Applied Mechanics and Engineering*, 190:3443–3459, 2001.

A. Evgrafov, C. J. Rupp, K. Maute, and M. L. Dunn. Large-scale parallel topology optimization using a dual-primal substructuring solver. *Structural and Multidisciplinary Optimization*, 36: 329–345, 2008.

M. R. Hestenes and E. Stiefel. Methods of conjugate gradients for solving linear systems. *Journal of Research of the National Bureau of Standards*, 49(6):409–436, 1952.

T. S. Kim, J. E. Kim, and Y. Y. Kim. Parallelized structural topology optimization for eigenvalue problems. *International Journal of Solids and Structures*, 41:2623–2641, 2004.

U. Kirsch. Reduced basis approximations of structural displacements for optimal design. *AIAA Journal*, 29:1751–1758, 1991.

A. Mahdavi, R. Balaji, M. Freckerand, and E. M. Mockensturm. Topology optimization of 2D continua for minimum compliance using parallel computing. *Structural and Multidisciplinary Optimization*, 32:121–132, 2006.

J. A. Meijerink and H. A. van der Vorst. An iterative solution method for linear equation systems of which the coefficient matrix is a symmetric M-matrix. *Mathematics of Computation*, 31: 148–162, 1977.

D. P. O'Leary. The block conjugate gradient algorithm and related methods. *Linear Algebra and its Applications*, 29:293–322, 1980.

Y. Saad. *Iterative Methods for Sparse Linear Systems, Second Edition*. SIAM, 2003.

O. Sigmund. On the design of compliant mechanisms using topology optimization. *Mechanics Based Design of Structures and Machines*, 25:493–524, 1997.

O. Sigmund. A 99 line topology optimization code written in matlab. *Structural and Multidisciplinary Optimization*, 21:120–127, 2001.

K. Svanberg. The method of moving asymptotes - a new method for structural optimization. *International Journal for Numerical Methods in Engineering*, 24:359–373, 1987.

A. van der Sluis and H. A. van der Vorst. The rate of convergence of conjugate gradients. *Numerische Mathematik*, 48:543–560, 1986.

K. Vemaganti and E. W. Lawrence. Parallel methods for optimality criteria-based topology optimization. *Computer Methods in Applied Mechanics and Engineering*, 194:3637–3667, 2005.

S. Wang, E. de Sturler, and G. H. Paulino. Large-scale topology optimization using preconditioned Krylov subspace methods with recycling. *International Journal for Numerical Methods in Engineering*, 69:2441–2468, 2007.

Appendix A: Adjoint procedure for consistent sensitivity analysis

When differentiating the augmented objective function (5.4) we wish to remain with explicit derivatives of the stiffness matrix only. This means we need to eliminate all derivatives of the iterative residuals $\mathbf{r}_i$, displacements $\mathbf{u}_i$, scalars α_i, direction vectors $\mathbf{p}_i$, scalars β_i and preconditioned residuals $\mathbf{z}_i$. Eliminating a particular derivative is achieved by collecting all the terms in the augmented objective function which include this derivative and equate them to zero. This leads to a set of adjoint equations that can be solved iteratively. The unknowns are a set of adjoint variables $\widetilde{\mathbf{r}}_i$, $\widetilde{\mathbf{u}}_i$, $\widetilde{\alpha}_i$, $\widetilde{\mathbf{p}}_i$, $\widetilde{\beta}_i$ and $\widetilde{\mathbf{z}}_i$, some of which are explicitly required for computing the design sensitivities (5.5). The full set of adjoint equations is as follows:

Collecting the derivatives of the residuals $\frac{\partial \mathbf{r}_m}{\partial \rho_e}$:

$$\frac{\partial \mathbf{r}_m^T}{\partial \rho_e}\widetilde{\mathbf{r}}_m = 0$$

Solving for $\widetilde{\mathbf{r}}_m$:

$$\widetilde{\mathbf{r}}_m = \mathbf{0}$$

Collecting the derivatives of the residuals $\frac{\partial \mathbf{r}_{m-1}}{\partial \rho_e}$:

$$\frac{\partial \mathbf{r}_{m-1}^T}{\partial \rho_e}\widetilde{\mathbf{r}}_{m-1} - \frac{\partial \mathbf{r}_{m-1}^T}{\partial \rho_e}\widetilde{\mathbf{z}}_{m-1} - \frac{\partial \mathbf{r}_{m-1}^T}{\partial \rho_e}\widetilde{\mathbf{r}}_m - \frac{\partial \mathbf{r}_{m-1}^T}{\partial \rho_e}\mathbf{z}_{m-1}\left(\frac{\widetilde{\alpha}_{m-1}}{(\mathbf{K}\mathbf{p}_{m-1})^T\mathbf{p}_{m-1}} + \frac{\widetilde{\beta}_{m-2}}{\mathbf{r}_{m-2}^T\mathbf{z}_{m-2}}\right) = 0$$

Solving for $\widetilde{\mathbf{r}}_{m-1}$:

$$\widetilde{\mathbf{r}}_{m-1} = \widetilde{\mathbf{r}}_m + \widetilde{\mathbf{z}}_{m-1} + (\frac{\widetilde{\alpha}_{m-1}}{(\mathbf{K}\mathbf{p}_{m-1})^T\mathbf{p}_{m-1}} + \frac{\widetilde{\beta}_{m-2}}{\mathbf{r}_{m-2}^T\mathbf{z}_{m-2}})\mathbf{z}_{m-1} \tag{5.14}$$

Collecting the derivatives of the residuals $\frac{\partial \mathbf{r}_i}{\partial \rho_e}$, $i = 2, ..., m-2$:

$$\frac{\partial \mathbf{r}_i^T}{\partial \rho_e}\widetilde{\mathbf{r}}_i - \frac{\partial \mathbf{r}_i^T}{\partial \rho_e}\widetilde{\mathbf{z}}_i - \frac{\partial \mathbf{r}_i^T}{\partial \rho_e}\widetilde{\mathbf{r}}_{i+1} - \frac{\partial \mathbf{r}_i^T}{\partial \rho_e}\mathbf{z}_i(\frac{\widetilde{\alpha}_i}{(\mathbf{K}\mathbf{p}_i)^T\mathbf{p}_i} - \frac{\widetilde{\beta}_i\mathbf{r}_{i+1}^T\mathbf{z}_{i+1}}{(\mathbf{r}_i^T\mathbf{z}_i)^2} + \frac{\widetilde{\beta}_{i-1}}{\mathbf{r}_{i-1}^T\mathbf{z}_{i-1}}) = 0$$

Solving for $\widetilde{\mathbf{r}}_i$, $i = 2, ..., m-2$:

$$\widetilde{\mathbf{r}}_i = \widetilde{\mathbf{r}}_{i+1} + \widetilde{\mathbf{z}}_i + (\frac{\widetilde{\alpha}_i}{(\mathbf{K}\mathbf{p}_i)^T\mathbf{p}_i} - \frac{\widetilde{\beta}_i\mathbf{r}_{i+1}^T\mathbf{z}_{i+1}}{(\mathbf{r}_i^T\mathbf{z}_i)^2} + \frac{\widetilde{\beta}_{i-1}}{\mathbf{r}_{i-1}^T\mathbf{z}_{i-1}})\mathbf{z}_i \tag{5.15}$$

Collecting the derivatives of the residuals $\frac{\partial \mathbf{r}_1}{\partial \rho_e}$:

$$\frac{\partial \mathbf{r}_1^T}{\partial \rho_e}\widetilde{\mathbf{r}}_1 - \frac{\partial \mathbf{r}_1^T}{\partial \rho_e}\widetilde{\mathbf{z}}_1 - \frac{\partial \mathbf{r}_1^T}{\partial \rho_e}\widetilde{\mathbf{r}}_2 - \frac{\partial \mathbf{r}_1^T}{\partial \rho_e}\mathbf{z}_1(\frac{\widetilde{\alpha}_1}{(\mathbf{K}\mathbf{p}_1)^T\mathbf{p}_1} - \frac{\widetilde{\beta}_1\mathbf{r}_2^T\mathbf{z}_2}{(\mathbf{r}_1^T\mathbf{z}_1)^2}) = 0$$

Solving for $\widetilde{\mathbf{r}}_1$:

$$\widetilde{\mathbf{r}}_1 = \widetilde{\mathbf{r}}_2 + \widetilde{\mathbf{z}}_1 + (\frac{\widetilde{\alpha}_1}{(\mathbf{K}\mathbf{p}_1)^T\mathbf{p}_1} - \frac{\widetilde{\beta}_1\mathbf{r}_2^T\mathbf{z}_2}{(\mathbf{r}_1^T\mathbf{z}_1)^2})\mathbf{z}_1 \tag{5.16}$$

Collecting the derivatives of the displacements $\frac{\partial \mathbf{u}_m}{\partial \rho_e}$:

$$\frac{\partial \mathbf{u}_m^T}{\partial \rho_e}\mathbf{f} + \frac{\partial \mathbf{u}_m^T}{\partial \rho_e}\widetilde{\mathbf{u}}_m = 0$$

Solving for $\widetilde{\mathbf{u}}_m$:

$$\widetilde{\mathbf{u}}_m = -\mathbf{f} \tag{5.17}$$

Collecting the derivatives of the displacements $\frac{\partial \mathbf{u}_i}{\partial \rho_e}$, $i = 2, ..., m-1$:

$$\frac{\partial \mathbf{u}_i^T}{\partial \rho_e}\widetilde{\mathbf{u}}_i - \frac{\partial \mathbf{u}_i^T}{\partial \rho_e}\widetilde{\mathbf{u}}_{i+1} = 0$$

Solving for $\widetilde{\mathbf{u}}_i$, $i = 2, ..., m-1$:

$$\widetilde{\mathbf{u}}_i = \widetilde{\mathbf{u}}_{i+1} = -\mathbf{f} \tag{5.18}$$

We assume that the starting guess $\mathbf{u}_1$ is independent of the design. Collecting the derivatives of the scalars $\frac{\partial \alpha_i}{\partial \rho_e}$, $i = 1, ..., m-1$:

$$\frac{\partial \alpha_i}{\partial \rho_e}\widetilde{\alpha}_i - \frac{\partial \alpha_i}{\partial \rho_e}\widetilde{\mathbf{u}}_{i+1}^T\mathbf{p}_i + \frac{\partial \alpha_i}{\partial \rho_e}\widetilde{\mathbf{r}}_{i+1}^T\mathbf{K}\mathbf{p}_i = 0$$

Solving for $\widetilde{\alpha}_i$, $i = 1, ..., m-1$:

$$\widetilde{\alpha}_i = \widetilde{\mathbf{u}}_{i+1}^T\mathbf{p}_i - \widetilde{\mathbf{r}}_{i+1}^T\mathbf{K}\mathbf{p}_i \tag{5.19}$$

Collecting the derivatives of the directions $\frac{\partial \mathbf{p}_{m-1}}{\partial \rho_e}$:

$$2\frac{\partial \mathbf{p}_{m-1}^T}{\partial \rho_e}\mathbf{K}\mathbf{p}_{m-1}\frac{\widetilde{\alpha}_{m-1}\mathbf{r}_{m-1}^T\mathbf{z}_{m-1}}{((\mathbf{K}\mathbf{p}_{m-1})^T\mathbf{p}_{m-1})^2} - \alpha_{m-1}\frac{\partial \mathbf{p}_{m-1}^T}{\partial \rho_e}\widetilde{\mathbf{u}}_m + \alpha_{m-1}\frac{\partial \mathbf{p}_{m-1}^T}{\partial \rho_e}\mathbf{K}\widetilde{\mathbf{r}}_m + \frac{\partial \mathbf{p}_{m-1}^T}{\partial \rho_e}\widetilde{\mathbf{p}}_{m-1} = 0$$

Solving for $\widetilde{\mathbf{p}}_{m-1}$:

$$\widetilde{\mathbf{p}}_{m-1} = \alpha_{m-1}(\widetilde{\mathbf{u}}_m - \mathbf{K}\widetilde{\mathbf{r}}_m) - 2\frac{\widetilde{\alpha}_{m-1}\mathbf{r}_{m-1}^T\mathbf{z}_{m-1}}{((\mathbf{K}\mathbf{p}_{m-1})^T\mathbf{p}_{m-1})^2}\mathbf{K}\mathbf{p}_{m-1} \tag{5.20}$$

Collecting the derivatives of the directions $\frac{\partial \mathbf{p}_i}{\partial \rho_e}$, $i = 1, ..., m-2$

$$2\frac{\partial \mathbf{p}_i^T}{\partial \rho_e}\mathbf{K}\mathbf{p}_i\frac{\widetilde{\alpha}_i\mathbf{r}_i^T\mathbf{z}_i}{((\mathbf{K}\mathbf{p}_i)^T\mathbf{p}_i)^2} - \alpha_i\frac{\partial \mathbf{p}_i^T}{\partial \rho_e}\widetilde{\mathbf{u}}_{i+1} + \alpha_i\frac{\partial \mathbf{p}_i^T}{\partial \rho_e}\mathbf{K}\widetilde{\mathbf{r}}_{i+1} + \frac{\partial \mathbf{p}_i^T}{\partial \rho_e}\widetilde{\mathbf{p}}_i - \frac{\partial \mathbf{p}_i^T}{\partial \rho_e}\beta_i\widetilde{\mathbf{p}}_{i+1} = 0$$

Solving for $\widetilde{\mathbf{p}}_i$, $i = 1, ..., m-2$:

$$\widetilde{\mathbf{p}}_i = \alpha_i(\widetilde{\mathbf{u}}_{i+1} - \mathbf{K}\widetilde{\mathbf{r}}_{i+1}) - 2\frac{\widetilde{\alpha}_i\mathbf{r}_i^T\mathbf{z}_i}{((\mathbf{K}\mathbf{p}_i)^T\mathbf{p}_i)^2}\mathbf{K}\mathbf{p}_i + \beta_i\widetilde{\mathbf{p}}_{i+1} \tag{5.21}$$

Collecting the derivatives of the scalars $\frac{\partial \beta_i}{\partial \rho_e}$, $i = 1, ..., m-2$

$$\frac{\partial \beta_i}{\partial \rho_e}\widetilde{\beta}_i - \frac{\partial \beta_i}{\partial \rho_e}\widetilde{\mathbf{p}}_{i+1}^T\mathbf{p}_i = 0$$

Solving for $\widetilde{\beta}_i$, $i = 1, ..., m-2$:

$$\widetilde{\beta}_i = \widetilde{\mathbf{p}}_{i+1}^T\mathbf{p}_i \tag{5.22}$$

Collecting the derivatives of the residuals $\frac{\partial \mathbf{z}_{m-1}}{\partial \rho_e}$:

$$\frac{\partial \mathbf{z}_{m-1}^T}{\partial \rho_e}\mathbf{M}\widetilde{\mathbf{z}}_{m-1} - \frac{\partial \mathbf{z}_{m-1}^T}{\partial \rho_e}\widetilde{\mathbf{p}}_{m-1} - \frac{\partial \mathbf{z}_{m-1}^T}{\partial \rho_e}\mathbf{r}_{m-1}(\frac{\widetilde{\alpha}_{m-1}}{(\mathbf{K}\mathbf{p}_{m-1})^T\mathbf{p}_{m-1}} + \frac{\widetilde{\beta}_{m-2}}{\mathbf{r}_{m-2}^T\mathbf{z}_{m-2}}) = 0$$

Solving for $\widetilde{\mathbf{z}}_{m-1}$:

$$\mathbf{M}\widetilde{\mathbf{z}}_{m-1} = \widetilde{\mathbf{p}}_{m-1} + (\frac{\widetilde{\alpha}_{m-1}}{(\mathbf{K}\mathbf{p}_{m-1})^T\mathbf{p}_{m-1}} + \frac{\widetilde{\beta}_{m-2}}{\mathbf{r}_{m-2}^T\mathbf{z}_{m-2}})\mathbf{r}_{m-1} \tag{5.23}$$

Collecting the derivatives of the residuals $\frac{\partial \mathbf{z}_i}{\partial \rho_e}$, $i = 2, ..., m-2$:

$$\frac{\partial \mathbf{z}_i^T}{\partial \rho_e}\mathbf{M}\widetilde{\mathbf{z}}_i - \frac{\partial \mathbf{z}_i^T}{\partial \rho_e}\widetilde{\mathbf{p}}_i - \frac{\partial \mathbf{z}_i^T}{\partial \rho_e}\mathbf{r}_i(\frac{\widetilde{\alpha}_i}{(\mathbf{K}\mathbf{p}_i)^T\mathbf{p}_i} - \frac{\widetilde{\beta}_i\mathbf{r}_{i+1}^T\mathbf{z}_{i+1}}{(\mathbf{r}_i^T\mathbf{z}_i)^2} + \frac{\widetilde{\beta}_{i-1}}{\mathbf{r}_{i-1}^T\mathbf{z}_{i-1}}) = 0$$

Solving for $\widetilde{\mathbf{z}}_i$, $i = 2, ..., m-2$:

$$\mathbf{M}\widetilde{\mathbf{z}}_i = \widetilde{\mathbf{p}}_i + (\frac{\widetilde{\alpha}_i}{(\mathbf{K}\mathbf{p}_i)^T\mathbf{p}_i} - \frac{\widetilde{\beta}_i\mathbf{r}_{i+1}^T\mathbf{z}_{i+1}}{(\mathbf{r}_i^T\mathbf{z}_i)^2} + \frac{\widetilde{\beta}_{i-1}}{\mathbf{r}_{i-1}^T\mathbf{z}_{i-1}})\mathbf{r}_i \tag{5.24}$$

Collecting the derivatives of the residuals $\frac{\partial \mathbf{z}_1}{\partial \rho_e}$:

$$\frac{\partial \mathbf{z}_1^T}{\partial \rho_e}\mathbf{M}\widetilde{\mathbf{z}}_1 - \frac{\partial \mathbf{z}_1^T}{\partial \rho_e}\widetilde{\mathbf{p}}_1 - \frac{\partial \mathbf{z}_1^T}{\partial \rho_e}\mathbf{r}_1(\frac{\widetilde{\alpha}_1}{(\mathbf{K}\mathbf{p}_1)^T\mathbf{p}_1} - \frac{\widetilde{\beta}_1\mathbf{r}_2^T\mathbf{z}_2}{(\mathbf{r}_1^T\mathbf{z}_1)^2}) = 0$$

Solving for $\widetilde{\mathbf{z}}_1$:

$$\mathbf{M}\widetilde{\mathbf{z}}_1 = \widetilde{\mathbf{p}}_1 + (\frac{\widetilde{\alpha}_1}{(\mathbf{K}\mathbf{p}_1)^T\mathbf{p}_1} - \frac{\widetilde{\beta}_1\mathbf{r}_2^T\mathbf{z}_2}{(\mathbf{r}_1^T\mathbf{z}_1)^2})\mathbf{r}_1 \tag{5.25}$$

In summary, the adjoint PCG procedure aimed at finding $\widetilde{\mathbf{r}}_i (i = 1, ..., m)$, $\widetilde{\mathbf{z}}_i (i = 1, ..., m-1)$ and $\widetilde{\alpha}_i (i = 1, ..., m-1)$ which are required for computing the design sensitivities is performed as follows

1. First cycle:
   (a) Set $\widetilde{\mathbf{u}}$ (Equations 5.17, 5.18).
   (b) Compute $\widetilde{\alpha}_{m-1}$ (Equation 5.19).

(c) Compute $\widetilde{\mathbf{p}}_{m-1}$ (Equation 5.20).

2. For `i = (m-2):-1:1` do

   (a) Compute $\widetilde{\beta}_i$ (Equation 5.22).
   (b) Compute $\widetilde{\mathbf{z}}_{i+1}$ (Equations 5.23, 5.24).
   (c) Compute $\widetilde{\mathbf{r}}_{i+1}$ (Equations 5.14, 5.15).
   (d) Compute $\widetilde{\alpha}_i$ (Equation 5.19).
   (e) Compute $\widetilde{\mathbf{p}}_i$ (Equation 5.21).

3. Compute $\widetilde{\mathbf{z}}_1$ (Equation 5.25).

4. Compute $\widetilde{\mathbf{r}}_1$ (Equation 5.16).

Appendix B: Special CG properties

When using CG to solve the linear system $\mathbf{Ku} = \mathbf{f}$ and setting the starting guess in the CG procedure to be a zero vector, i.e. $\mathbf{u}_1 = \mathbf{0}$, the following equality holds for all CG iterations

$$\mathbf{f}^T\mathbf{u}_i = \mathbf{u}_i^T\mathbf{K}\mathbf{u}_i$$

This property of CG results from the orthogonality of the residuals $\mathbf{r}_i$ and the direction vectors $\mathbf{p}_j$ ($\forall j \neq i$). For $i > 1$ we can write

$$\mathbf{f}^T\mathbf{u}_i - \mathbf{u}_i^T\mathbf{K}\mathbf{u}_i = \mathbf{u}_i^T(\mathbf{f} - \mathbf{K}\mathbf{u}_i) = \mathbf{u}_i^T\mathbf{r}_i = (\mathbf{u}_1 + \sum_{j=1}^{i-1}\alpha_j\mathbf{p}_j)^T\mathbf{r}_i = \mathbf{u}_1^T\mathbf{r}_i$$

Therefore if $\mathbf{u}_1 = \mathbf{0}$ we obtain $\mathbf{f}^T\mathbf{u}_i = \mathbf{u}_i^T\mathbf{K}\mathbf{u}_i$, $\forall i$.

The extension to multiple right hand sides solved by a block-PCG is rather straightforward. We solve $\mathbf{Ku} = \mathbf{f}$ and $\mathbf{K}\boldsymbol{\lambda} = \mathbf{l}$ simultanously by a block-PCG procedure. We wish to show that if $\mathbf{u}_1 = \boldsymbol{\lambda}_1 = \mathbf{0}$ the following equalities hold

$$\mathbf{l}^T\mathbf{u}_i = \boldsymbol{\lambda}_i^T\mathbf{K}\mathbf{u}_i$$
$$\mathbf{f}^T\boldsymbol{\lambda}_i = \boldsymbol{\lambda}_i^T\mathbf{K}\mathbf{u}_i$$

Introducing the block-CG notation

$$\begin{aligned}\mathbf{R} &= [\mathbf{r}_u \;\; \mathbf{r}_\lambda] \\ \mathbf{P} &= [\mathbf{p}_u \;\; \mathbf{p}_\lambda]\end{aligned}$$

Orthogonality of the residuals $\mathbf{R}$ and the direction vectors $\mathbf{P}$ can be expressed as follows

$$\mathbf{R}_i^T\mathbf{P}_j = \mathbf{0}_{2\times 2}, \qquad \forall i \neq j$$

Then for $i > 1$ we can write

$$\begin{aligned}\mathbf{l}^T\mathbf{u}_i - \boldsymbol{\lambda}_i^T\mathbf{K}\mathbf{u}_i = \mathbf{u}_i^T(\mathbf{l} - \mathbf{K}\boldsymbol{\lambda}_i) = \mathbf{u}_i^T\mathbf{r}_{\lambda,i} = \\ (\mathbf{u}_1 + \sum_{j=1}^{i-1}\mathbf{p}_{u,j}\alpha_{11,j} + \sum_{j=1}^{i-1}\mathbf{p}_{\lambda,j}\alpha_{21,j})^T\mathbf{r}_{\lambda,i} = \mathbf{u}_1^T\mathbf{r}_{\lambda,i} \\ \mathbf{f}^T\boldsymbol{\lambda}_i - \boldsymbol{\lambda}_i^T\mathbf{K}\mathbf{u}_i = \boldsymbol{\lambda}_i^T(\mathbf{f} - \mathbf{K}\mathbf{u}_i) = \boldsymbol{\lambda}_i^T\mathbf{r}_{u,i} = \\ (\boldsymbol{\lambda}_1 + \sum_{j=1}^{i-1}\mathbf{p}_{u,j}\alpha_{12,j} + \sum_{j=1}^{i-1}\mathbf{p}_{\lambda,j}\alpha_{22,j})^T\mathbf{r}_{u,i} = \boldsymbol{\lambda}_1^T\mathbf{r}_{u,i}\end{aligned}$$

Therefore if $\mathbf{u}_1 = \boldsymbol{\lambda}_1 = \mathbf{0}$ we obtain $\mathbf{l}^T\mathbf{u}_i = \mathbf{f}^T\boldsymbol{\lambda}_i = \boldsymbol{\lambda}_i^T\mathbf{K}\mathbf{u}_i$, $\forall i$.

Chapter 6

On reducing computational effort in topology optimization: how far can we go?

Amir O, Sigmund O. On reducing computational effort in topology optimization: how far can we go? *Structural and Multidisciplinary Optimization*. Published online.

Abstract An approximate approach to solving the nested analysis equations in topology optimization is proposed. The procedure consists of only one matrix factorization for the whole design process and a small number of iterative corrections for each design cycle. The approach is tested on 3D topology optimization problems. It is shown that the computational cost can be reduced by one order of magnitude without affecting the outcome of the optimization process.

Keywords Topology optimization, Nested approach, Approximations

6.1 Introduction

In the nested approach to structural optimization, most of the computational effort is invested in the solution of the analysis equations. Several recent investigations focused on reducing the computational cost of repeated solutions of linear equation systems: Wang et al. (2007) suggested recycling parts of the search space in a Krylov subspace solver; Amir et al. (2009) integrated an approximate reanalysis procedure into nested topology optimization; and in (Amir et al., 2010) an alternative stopping criterion for a PCG iterative solver was proposed so that fewer iterations are performed. This note presents new results that, together with the studies mentioned, lead to the following observation: *There seems to be more room for improving the efficient treatment of the nested problem in topology optimization*. We focus here on direct solution procedures based on matrix factorization, but expect that similar schemes could be proposed based on iterative equation solvers.

In the context of direct solvers, the standard approach is to solve the equilibrium equations within every design cycle. Then the overall cost is governed by the cost of factorization multiplied by the number of design cycles. In the current study, it is suggested to perform *only one factorization* in the beginning of the design process, and then approximate the solution of all the nested problems using an iterative procedure. We do not enforce a tight tolerance on the accuracy of these iterates, since it is observed that even rough approximations of the displacements lead to fairly accurate design sensitivities. Consequently, the optimization process is practically the same even though the nested equations are never solved to full accuracy.

6.2 Considered optimization problems

The approximate procedure is demonstrated on two well known topology optimization problems: (1) Minimum compliance design; (2) Force inverting mechanism design. Some details are omitted in the following for the purpose of brevity, so readers who are not well acquainted with topology optimization are referred to the book by Bendsøe and Sigmund (2003) and references therein. The considered optimization problem has the following generic form

$$\begin{aligned} \min_{\boldsymbol{\rho}} c(\boldsymbol{\rho}) &= \mathbf{l}^T\mathbf{u} \\ \text{s.t.:} \quad & \sum_{e=1}^{N} v_e\rho_e \leq V \\ & 0 \leq \rho_e \leq 1 \qquad e = 1, ..., N \\ \text{with:} \quad & \mathbf{K}(\boldsymbol{\rho})\mathbf{u} = \mathbf{f} \end{aligned}$$

where $\mathbf{K}(\boldsymbol{\rho})$ is the stiffness matrix, $\mathbf{f}$ is the load vector, $\mathbf{u}$ is the displacements vector, v_e is the element volume and V is the total available volume. The minimum compliance case is obtained by setting $\mathbf{l} \equiv \mathbf{f}$ while for the force inverter problem $\mathbf{l}$ is a vector with the value of 1 at the output degree of freedom and zeros otherwise. Design sensitivities are computed by the adjoint method. For both cases, the sensitivity of the objective with respect to a particular element density is given by

$$\frac{\partial c}{\partial \rho_e} = -\boldsymbol{\lambda}^T \frac{\partial \mathbf{K}}{\partial \rho_e}\mathbf{u} \tag{6.1}$$

where $\mathbf{K}\boldsymbol{\lambda} = \mathbf{l}$, thus for the compliance problem $\boldsymbol{\lambda} \equiv \mathbf{u}$.

6.3 Efficient approximation to the solution of the nested analysis equations

6.3.1 Iterative correction approach

In the nested approach, the following system of analysis equations is solved within every optimization cycle

$$\mathbf{K}(\boldsymbol{\rho})\mathbf{u} = \mathbf{f} \tag{6.2}$$

Aiming at reducing the computational effort, we wish to avoid repeatedly factorizing $\mathbf{K}(\boldsymbol{\rho})$ at every design step. Assuming we have an available factorization of a similar stiffness matrix denoted by $\mathbf{K}_0$, we can define a simple iterative correction inspired by the modified Newton-Raphson procedure for nonlinear equations

$$\mathbf{u}_k = \mathbf{u}_{k-1} - \mathbf{K}_0^{-1}(\mathbf{K}(\boldsymbol{\rho})\mathbf{u}_{k-1} - \mathbf{f}) \tag{6.3}$$

Each corrective step requires only one matrix-vector multiplication (which can be performed on an element level and easily parallelized) and two triangular solves based on the factors of $\mathbf{K}_0$.

In practice, the series of iterates (6.3) converges very slow, depending on the difference between $\mathbf{K}_0$ and $\mathbf{K}(\boldsymbol{\rho})$. Therefore the procedure actually implemented in this study is a Preconditioned Conjugate Gradient (PCG) where the factors of $\mathbf{K}_0$ serve as preconditioners. The equivalence between the iterative corrections (1.25) and this particular PCG is based on the following observations: 1) The recurrence (6.3) is equivalent to the recurrence used in the Combined Approximations (CA) procedure for structural reanalysis (Kirsch, 1991); and 2) Kirsch et al. (2002) showed that CA is mathematically equivalent to a PCG with the factors of $\mathbf{K}_0$ as preconditioners in an iterative Krylov subspace solution of (6.2). The computational cost remains roughly the

same, since each PCG iteration requires one matrix-vector multiplication, two triangular solves (using the factors of $\mathbf{K}_0$) and several vector products.

This study focuses on two key aspects that can enhance the efficiency of such an iterative procedure, thus considerably reducing the overall computational cost of topology optimization: (1) Utilizing a *single* factorization / preconditioner throughout the whole optimization process; and (2) Performing only a few PCG iterations and computing design sensitivities as if an accurate $\mathbf{u}$ was computed. From a computational point of view, utilizing a factorization as a preconditioner may seem rather odd, since iterative solvers are mostly used if factorization is ruled out due to memory requirements. Therefore it is important to stress that PCG is implemented here since it is a robust and straightforward framework for the iterative corrections, based on minimization of the potential energy. Nevertheless, a purely iterative procedure with low memory requirements can be derived by choosing a different preconditioner instead of the factors of $\mathbf{K}_0$. This challenging aspect will be further discussed in Section 6.5.

6.3.2 Observations based on numerical experiments

As pointed out above, only a single factorization is performed during the whole optimization process. We choose $\mathbf{K}_0$ to be the stiffness matrix corresponding to a design domain that is entirely solid, meaning $\rho_e = 1$ for all finite elements in the computational domain. This particular choice of $\mathbf{K}_0$ possesses a nice property: when solid regions appear in the actual design, $\mathbf{K}_0$ is identical to the actual stiffness $\mathbf{K}(\boldsymbol{\rho})$ in these local regions. In numerical experiments, the residual forces reduced rather fast in solid regions. However, in regions of intermediate density, where $\mathbf{K}_0$ differed significantly from the actual $\mathbf{K}(\boldsymbol{\rho})$, the errors remained large even after many PCG iterations.

An important aspect is the accuracy of the design sensitivities computed with an approximation of $\mathbf{u}$, and the influence of using inaccurate sensitivities on the overall optimization process. In Amir et al. (2010) early termination was forced on a standard PCG solver. The design sensitivities were computed *as if* the analysis problem was solved accurately, using (6.1). This did not seriously affect the progress of optimization since the early termination criteria for PCG were related to the objective and to the sensitivities. In the current study, no such measure is taken so it is evident that there is some error associated to the design sensitivities. Nevertheless, numerical experiments show that these errors are quite small after only a few PCG iterations. Moreover, it seems that the nonlinear program (MMA, Svanberg (1987)) is not particularly sensitive to such errors and the progress of optimization remains unaffected and in some cases even improves.

6.3.3 Computational scheme

The resulting computational scheme is as follows, demonstrated using some standard Matlab commands:

1. Initialize optimization process and state the maximum number of PCG iterations. One possible choice:

   ```
   m = min([nelx,nely,nelz])
   ```

2. Compute factors of $\mathbf{K}_0$ corresponding to an entirely solid design domain:

   ```
   rho = ones
   K_0 = K(rho)
   U_0 = chol(K_0)
   ```

3. Repeat design cycle until convergence:

(a) Compute an approximation $\mathbf{u}_m$ by performing m PCG iterations on Eq. (6.2) with the current stiffness $\mathbf{K}(\boldsymbol{\rho})$, the factors of $\mathbf{K}_0$ as preconditioners and $\mathbf{u}_m$ from the previous design cycle as an initial guess:

```
u_m_old = u_m
u_m = pcg(K,f,1e-6,m,U_0',U_0,u_m_old)
```

(b) Compute approximate sensitivities using $\mathbf{u}_m$ in (6.1).

(c) Update design variables $\boldsymbol{\rho}$ by MMA.

The overall cost is dominated by stage 3(a), which for every design cycle is m times the cost of a single PCG iteration. It is not necessary to assemble $\mathbf{K}(\boldsymbol{\rho})$ and the matrix-vector product can be easily parallelized. In the force inverter case, a block-PCG solver (O'Leary, 1980) is used to compute $\mathbf{u}_m$ and $\boldsymbol{\lambda}_m$ simultaneously. Then the sensitivities (6.1) can be computed.

6.4 Numerical examples

In this section, several examples are presented. Optimization was performed using the Method of Moving Asymptotes (Svanberg, 1987) and a density filter was applied (Bourdin, 2001; Bruns and Tortorelli, 2001).

6.4.1 Accuracy of the design sensitivities

Concerning the errors in sensitivity analysis, consider Figures 6.1(a) and 6.1(b). The plots correspond to an intermediate design cycle of a small half-MBB minimum compliance problem, but the authors observed the same behavior throughout the whole design process. In Figure 6.1(a), the current (filtered) densities are plotted, while Figure 6.1(b) shows the errors in the element sensitivities after only 5 PCG iterations. The error is measured relatively to the true design sensitivity, corresponding to an accurate solution of (6.2) for this design cycle. In high density (dark) regions, the errors as computed after 5 PCG iterations are in the order of 10^{-2} to 10^{-5}. Large errors in the order of 10^{-1} or higher appear only in low density (bright) regions and are therefore less important. Numerical experiments show that errors in the order of up to a few percent do not have significant effect on the design process - meaning that the approximate sensitivities are sufficient for the purpose of obtaining an effective descent direction for optimization.

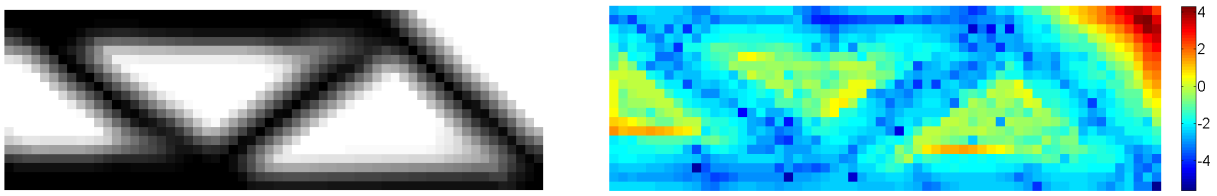

(a) Design after 30 cycles: Black = solid, white = void

(b) Relative errors in sensitivities as computed after 5 PCG iterations, logarithmic scale

Figure 6.1: Errors in design sensitivities, 60×20 half-MBB beam, after 30 design cycles

6.4.2 Computational effort in 3D problems

We present solutions of two 3D topology optimization problems, with particular emphasis on the computational effort involved in the solution of the analysis equations. Two schemes are compared: (1) Standard approach using a direct solver; (2) The proposed approach with a

single factorization and few PCG iterations per design cycle. It is important to note that for 3D problems of medium or large scale, direct solvers are in general less preferable due to the large bandwidth of the stiffness matrix. Nevertheless, 3D problems are chosen for demonstrative purposes and it is evident that also in 2D, where direct solvers are more effective, significant savings can be achieved.

We consider minimum compliance design of a cantilever beam and force inverter design, see Amir et al. (2010) for all the technical details involved. The FE meshes consist of 40,500 elements (1.35×10^5 DOF) and 54,000 elements (1.76×10^5 DOF) respectively. The number of PCG iterations in the approximate scheme was fixed to the number of elements in the shortest side of the mesh: 15 for the minimum compliance case and 30 for the force inverter case. This is no more than a good guess and does not guarantee that the approximate scheme is successful. The resulting layouts are presented in Figures 6.2 and 6.3 and are practically identical for both procedures.

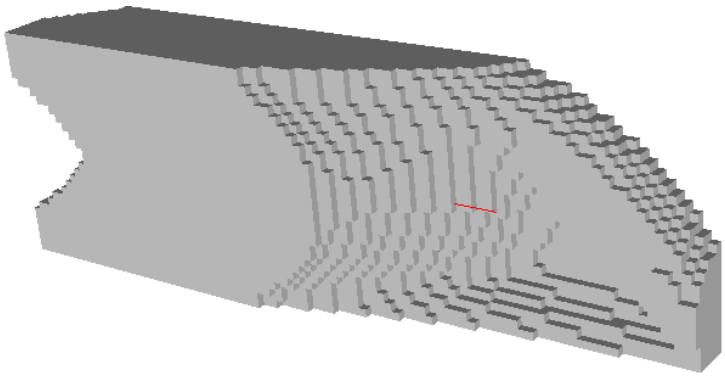

Figure 6.2: Minimum compliance design of a 3D cantilever beam: Layout of symmetric half after 200 design iterations, 90×15×30 elements

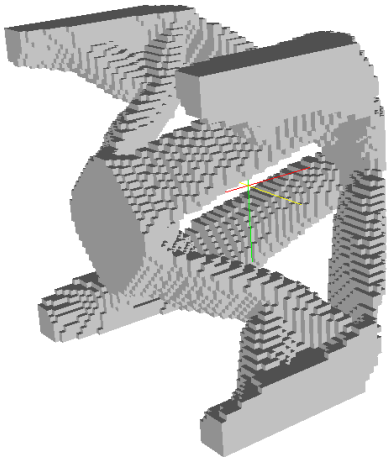

Figure 6.3: Design of a 3D force inverter: Layout after 200 design iterations, 60×30×30 elements in one symmetric quarter

The computational costs are compared in Table 6.1. Measuring CPU time for 200 design iterations, the approximate approach was 12 times faster than the standard solution in the minimum compliance problem and 4 times faster in the inverter problem. Estimated FLOPS counts based on Golub and Van Loan (1983) predict speedup ratios of 11.5 and 5.9, respectively. The actual savings for the inverter problem are lower than predicted probably since little effort was invested in optimizing the Fortran code. The quality of the results remains unaffected: The differences in objective values are very small and the designs are practically identical. The

approximate scheme was also compared to a standard iterative scheme (PCG and an incomplete Cholesky factorization as preconditioner) and was found to be twice as fast in the minimum compliance problem and slightly faster in the force inverter problem.

Table 6.1: Accuracy and efficiency of the approximate approach

Problem	Procedure	Objective	Relative time	Detailed time
Min. compliance	Standard	682.1184	12.339	99.4% direct solve, 0.6% other
	Approximate	681.6625[a]	1.000	6.1% factor, 85.9% PCG, 8% other
Force inverter	Standard	-0.5274	3.999	99.1% direct solve, 0.9% other
	Approximate	-0.5274[b]	1.000	2.0% factor, 94.7% PCG, 3.3% other

[a] Objective value resulting from accurate analysis with final design was 681.6563.

[b] Objective value resulting from accurate analysis with final design was -0.5275.

Finally, we examine the actual accuracy of the approximations with respect to the solution of the nested equation system. For this purpose we utilize the relative norm of residual forces, a common measure for iterative solvers. In Figure 6.4 the recorded norms corresponding to the approximation within each design cycle are plotted. It can be seen that the errors in the solution of the nested equations tend to reduce as the optimization proceeds. This is due to the use of each approximate displacement vector as an initial guess for the approximation in the next design cycle. In other words, as we approach an optimal design, we also approach an accurate solution of the nested system.

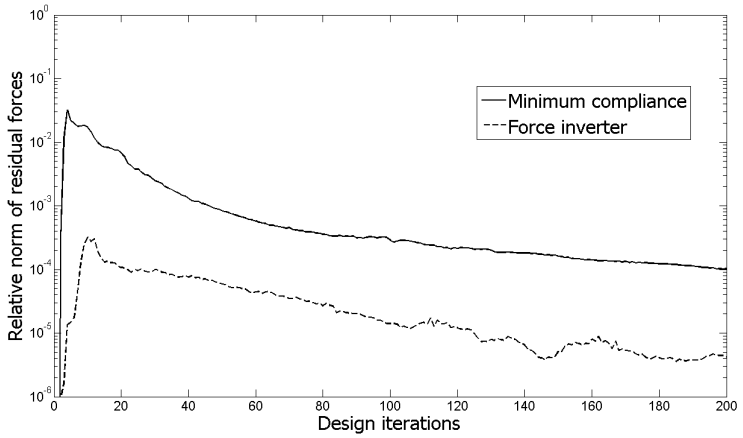

Figure 6.4: The relative norm of residual forces vs. design iterations

6.5 Discussion

An efficient computational scheme for nested topology optimization was presented. The analysis equation system is solved approximately using an iterative correction procedure, based on only one matrix factorization for the whole design process. The preliminary results presented here, together with some observations based on the numerical experience of the authors, challenge the way the analysis equations are treated in contemporary topology optimization procedures: *It may be unnecessary to solve the nested problem accurately*. Nevertheless, several questions and discussion topics arise regarding the approximate approach:

- Is it possible to generalize the proposed scheme so that the single preconditioner is not a factorization, meaning that memory requirements are lower and the overall procedure is more suitable for parallel computing?

- Can one define an effective stopping criteria for the iterative equation solver, or an upper bound on the number of iterations, so that it is guaranteed that the design sensitivities are sufficiently accurate and computational cost is reduced considerably? In some cases, it seems that the arbitrary maximum number of PCG iterations used in this study could have been even smaller.

- In the context of nonlinear programming methods: How sensitive are they to inaccurate gradient information?

- In industrial applications, problems typically involve many load cases. In such cases the cost of iterative corrections rises proportionally to the number of load cases and it may be cheaper to perform a new factorization. The actual trade-off depends on the properties of the stiffness matrix, the number of load cases and the number of iterations used in the approximate approach. The same applies to problems with multiple constraints, such as displacement constraints.

- Iterative solvers perform best for solid block FEA models. It has been shown that they are less effective for solving shell models that are typical for a wide range of industrial applications. The actual performance is dominated by the quality of the preconditioner. Therefore it is possible that more costly preconditioners and more frequent updates are required for shell models compared to solid block models.

- This article focused exclusively on reducing the cost associated with the solution of the nested analysis equations. Computational efficiency can be improved also by reducing the size of the FEA models, for example by an adaptive approach. Multilevel procedures can also contribute to reducing the problem size. Can the various approaches be combined effectively?

In conclusion, reducing the computational effort is a challenging topic of high importance for further development of topology optimization - both for academic research and as a standard design tool in industry. It is the authors' hope that this brief note will stimulate a discussion within the research community regarding further improvements of effective solution procedures.

6.6 Acknowledgments

This work received support from the Eurohorcs/ESF European Young Investigator Award (EURYI, www.esf.org/euryi) through the grant "Synthesis and topology optimization of optomechanical systems". We wish to thank the reviewers for their valuable comments and contributions to the discussion section. We are also grateful to Krister Svanberg for allowing us to use the MMA code.

References

O. Amir, M. P. Bendsøe, and O. Sigmund. Approximate reanalysis in topology optimization. *International Journal for Numerical Methods in Engineering*, 78:1474–1491, 2009.

O. Amir, M. Stolpe, and O. Sigmund. Efficient use of iterative solvers in nested topology optimization. *Structural and Multidisciplinary Optimization*, 42:55–72, 2010.

M. P. Bendsøe and O. Sigmund. *Topology Optimization - Theory, Methods and Applications*. Springer, Berlin, 2003.

B. Bourdin. Filters in topology optimization. *International Journal for Numerical Methods in Engineering*, 50:2143–2158, 2001.

T. E. Bruns and D. A. Tortorelli. Topology optimization of non-linear elastic structures and compliant mechanisms. *Computer Methods in Applied Mechanics and Engineering*, 190:3443–3459, 2001.

G. H. Golub and C. F. Van Loan. *Matrix Computations*. The Johns Hopkins University Press, Baltimore, Maryland, 1983.

U. Kirsch. Reduced basis approximations of structural displacements for optimal design. *AIAA Journal*, 29:1751–1758, 1991.

U. Kirsch, M. Kocvara, and J. Zowe. Accurate reanalysis of structures by a preconditioned conjugate gradient method. *International Journal for Numerical Methods in Engineering*, 55:233–251, 2002.

D. P. O'Leary. The block conjugate gradient algorithm and related methods. *Linear Algebra and its Applications*, 29:293–322, 1980.

K. Svanberg. The method of moving asymptotes - a new method for structural optimization. *International Journal for Numerical Methods in Engineering*, 24:359–373, 1987.

S. Wang, E. de Sturler, and G. H. Paulino. Large-scale topology optimization using preconditioned Krylov subspace methods with recycling. *International Journal for Numerical Methods in Engineering*, 69:2441–2468, 2007.

Chapter 7

Conceptual design of reinforced concrete using topology optimization with nonlinear material modeling

Bogomolny M, Amir O. Conceptual design of reinforced concrete using topology optimization with nonlinear material modeling. To be submitted.

Abstract Design of reinforced concrete structures is governed by the nonlinear behavior of concrete and by its different strengths in tension and compression. The purpose of this article is to present a computational procedure for optimal conceptual design of reinforced concrete structures, based on topology optimization with nonlinear material modeling. Concrete and steel are both considered as elasto-plastic materials, including the appropriate yield criteria and post-yielding response. The same approach can be applied also for topology optimization of other material compositions where nonlinear response must be considered. Optimized distribution of material is achieved by introducing interpolation rules for both elastic and plastic material properties. Several numerical examples illustrate the capability and potential of the proposed procedure.

Keywords Topology optimization, Material nonlinearity, Yield surface, Reinforced concrete, Strut-and-Tie

7.1 Introduction

Structural optimization techniques are now becoming an integral part of the design process and are widely applied, for example, in the automotive and aerospace industries. So far, optimal design had less impact on traditional structural engineering as practiced in the construction industry. One reason might be the difficulty in combining numerical optimization tools with models that can accurately represent the complex behavior of composite materials used by the building industry, such as reinforced concrete. The aim of this article is to present a computational procedure that enables optimal design of reinforced concrete structures. The approach can easily be generalized to accommodate other combinations of materials besides steel and concrete. By combining topology optimization with nonlinear material modeling of the candidate materials, it is possible to consider not only the different elastic stiffnesses of the candidate materials, but also their distinct yield limits and yield criteria.

The main challenge in the design of structural elements made of reinforced concrete (RC) lies in the different strengths of concrete in tension and compression. Typical concrete mixes have high resistance to compressive stresses but due to the quasi-brittle nature, any appreciable

tension (e.g. due to bending) will cause fracture and lead to failure of the structural element. Numerical analysis of RC structures is typically based on the finite element method. Since concrete itself is a composition of several materials, developing appropriate computational models is challenging and both nonlinear stress-strain relationship, as well as deformation localization effects are important. In practice, traditional plasticity formulations constitute reasonable approximations to the underlying fracturing process. A key element in plasticity formulations is the yield or failure criteria. Several yield criteria have been applied in computational models for concrete. Early studies suggest using the Mohr-Coulomb or Drucker-Prager yield surfaces (Chen, 1982). Recently, Oliver et al. (2008) proposed more advanced models, that combine the Drucker-Prager yield criterion in the compression region and the Rankine criterion in the tension region . Similarly, Pravida and Wunderlich (2002) proposed an advanced analytical surface which is a combination of several surfaces for compression and tension.

In practical design, RC members are treated as composite structures, where reinforcing steel bars are located in regions where tension (i.e. failure of plain concrete) is expected. Traditional methods may be sufficient for effectively distributing steel bars in standard structural elements such as beams, columns and slabs. However, nowadays advanced concrete technology - resulting in new and improved material properties - as well as new production methods, allow production of concrete structures of almost any shape, giving new freedom to the structural designer (Okamura and Ouchi, 2003; Stang and Geiker, 2004). This opens much room for applying structural optimization techniques, aimed at finding both the optimal shape of the concrete element as well as the optimal placement of reinforcement.

Up to date, the vast majority of studies in structural topology optimization were restricted to elastic material models (see Bendsøe and Sigmund (2003) for a comprehensive review of the field). Elastic modeling is sufficient for determining the distribution of one or more material phases in a given domain, but only as long as all material points remain in their elastic stress state. This is clearly not the case in reinforced concrete, where the concrete phase fails under relatively low tension stresses. Therefore nonlinear material modeling is necessary when aiming at optimal design of RC structures. Several studies were dedicated to topology optimization of elasto-plastic structures, for example based on the von Mises yield criterion (Swan and Kosaka, 1997; Maute et al., 1998) or the Drucker-Prager yield criterion (Swan and Kosaka, 1997). However, to the best of the authors' knowledge, this is the first study where more than one nonlinear candidate material is considered. Lately, multiphase material optimization was utilized for improving the performance of fiber reinforced concrete (Kato et al., 2009). Failure behavior of all candidate materials was considered, but the approach taken is restricted to layered structures and cannot provide general layouts as obtained using topology optimization.

One approach to visualizing the internal forces in cracked concrete beams is by a simple truss model introduced by Ritter (1899). The resulting model, widely known as the strut-and-tie model, has numerous applications in analysis and design of RC structures subjected to shear forces or torsion moments (e.g. Schlaich et al. (1987), Marti (1985)). Several researchers proposed to use a truss-like structure resulting from linear elastic topology optimization in order to predict a strut-and-tie model (Bruggi (2009), Liang et al. (2000) and Kwak and Noh (2006)). Accordingly, the truss bars under tension forces represent the location of steel reinforcement while the compressed bars represent concrete. In the current study material nonlinearity of both concrete and steel is considered , and hence a more realistic model is obtained. An interpolation scheme is proposed, such that by changing the density (design variable of the optimization problem), the material properties and the failure criteria vary between concrete and steel. The result of the optimization process is the optimal distribution of concrete and steel inside a certain domain. Therefore an efficient strut-and-tie model is directly obtained.

The article is organized as follows: topology optimization is shortly introduced in Section 7.2, with emphasis on reinforcement design. The elasto-plastic models used for concrete and steel and the nonlinear finite element analysis are discussed in Section 7.3. Section 7.4 is the

heart of this article, where we present the material interpolation, the optimization problem formulation and the sensitivity analysis. Several demonstrative examples are presented in Section 7.5 and some conclusions are drawn in Section 7.6.

7.2 Design of linear elastic reinforcement using topology optimization

In this section, we shortly review topology optimization procedures, with particular emphasis on optimal layouts consisting of two materials, see Bendsøe and Sigmund (2003) for an extensive report on topology optimization. We follow the material distribution approach for topological design (Bendsøe and Kikuchi, 1988) together with the SIMP (Solid Isotropic Material with Penalization) interpolation scheme (M. P. Bendsøe, 1989). The optimization problem aimed at finding the stiffest structural layout, usually known as the minimum compliance problem, is defined as follows

$$\begin{aligned} \min_{\boldsymbol{\rho}} c(\boldsymbol{\rho}) &= \mathbf{f}^T\mathbf{u} \\ \text{s.t.:} \quad & \sum_{e=1}^{N_e} v_e\rho_e \leq V \\ & 0 \leq \rho_e \leq 1 \qquad e = 1, ..., N_e \\ \text{with:} \quad & \mathbf{K}(\boldsymbol{\rho})\mathbf{u} = \mathbf{f} \end{aligned} \tag{7.1}$$

where $\mathbf{f}$ is the external load vector, $\mathbf{u}$ is the displacements vector, v_e is the element volume, ρ_e is the element density, V is the total available volume and $\mathbf{K}(\boldsymbol{\rho})$ is the stiffness matrix corresponding to the element densities $\boldsymbol{\rho}$

$$\mathbf{K}(\boldsymbol{\rho}) = \sum_{e=1}^{N_e}(E_{min} + (E_{max} - E_{min})\rho_e^{p_E})\mathbf{K}_e$$

In general, E_{min} and E_{max} are the values of Young's modulus corresponding to two candidate materials which should be distributed in the design domain. For the case of distributing a single material and void, E_{min} is set to a small positive value and E_{max} is typically set to 1. $\mathbf{K}_e$ represents the element stiffness matrix corresponding to the Young's modulus value of 1 and p_E is a penalization factor required to drive the design towards a 0-1 (or black and white) layout. For the purpose of clarity, filtering is not considered in the above formulation. Nevertheless, in many cases it is necessary to apply a filter in order to avoid checkerboard patterns and to obtain mesh-independent results (Bendsøe and Sigmund, 2003).

In Figure 7.1, an optimized design obtained for a single linear elastic material (E_{min} represents void) is presented. The design domain is a rectangular simply supported beam; 25% of the total volume is available; and the load consists of a single point load. The obtained layout is a typical result of single-material topology optimization: the layouts usually resemble a truss/frame structure formed of several triangles. When E_{min} and E_{max} represent two materials (E_{min} is one order smaller than E_{max}), a different layout is obtained, see Figure 7.2. Such designs are typical for sandwich structures, consisting of a soft core and stiff sheets.

The optimized topologies obtained with linear elastic material modeling cannot be used directly in some design problems involving the composition of two materials. A fundamental example is the design of reinforced concrete, where the design philosophy is based mainly on the fact that plain concrete has higher strength in compression than in tension, a property that is not captured by linear elastic modeling. In traditional reinforced concrete design, steel bars are positioned where tension stresses are expected. Therefore nonlinear material modeling is an essential component in optimal design of reinforced concrete and other compositions of

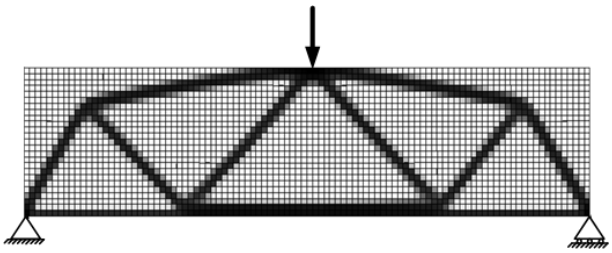

Figure 7.1: Optimized layout of a simply supported beam. Black: material, white: void.

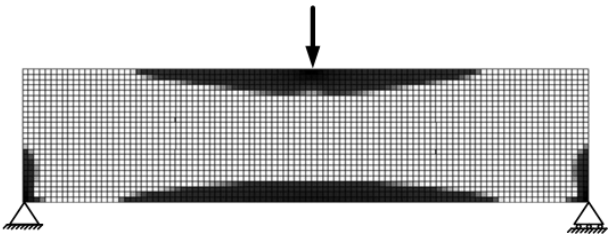

Figure 7.2: Optimized layout of a simply supported beam. Black: stiff material, white: soft material.

materials with different nonlinear properties, taking into account not only the elastic stiffnesses of the two materials but also their yield limits and post-yielding behavior.

7.3 Nonlinear material model and finite element analysis

In this section, we shortly review the elasto-plastic model utilized in our study and outline the resulting nonlinear finite element problem to be solved. Later, in Section 7.4, the connection between the topology optimization problem and the nonlinear material model will be made.

7.3.1 Elasto-plastic material model

The main purpose of this study is to optimize the distribution of two materials in a given domain, taking the different nonlinear behavior of both materials into account. The main idea is to represent the elasto-plastic response of both materials using one generic yield function that varies according to the value of the design variable. For this purpose, we utilize the Drucker-Prager yield criterion (Drucker and Prager, 1952). For certain choices of material properties, the Drucker-Prager yield function can model the behavior of materials that are much stronger in compression than in tension, such as soils, rock or plain concrete. Moreover, the von Mises yield criterion which is widely used for metals (having equal strength in tension and compression) can be seen as a particular case of the Drucker-Prager criterion.

As a demonstrative case we focus throughout this article on the distribution of concrete and steel. In essence, the purpose of utilizing nonlinear modeling is to identify the failure of concrete when tension stresses appear and then redistribute material so that such failure does not occur. Other aspects of the elasto-plastic behavior, namely yielding of steel in both stress states or yielding of concrete in compression, are categorized as less important for the purpose of this study. Therefore some simplifying assumptions are made in the formulation of the nonlinear material model, which would not be allowed if the purpose was accurate prediction of failure and damage in reinforced concrete structures.

In the following, we present the governing equations of the elasto-plastic model, leading to the local constitutive problem to be solved on a Gauss-point level. We follow classical rate-

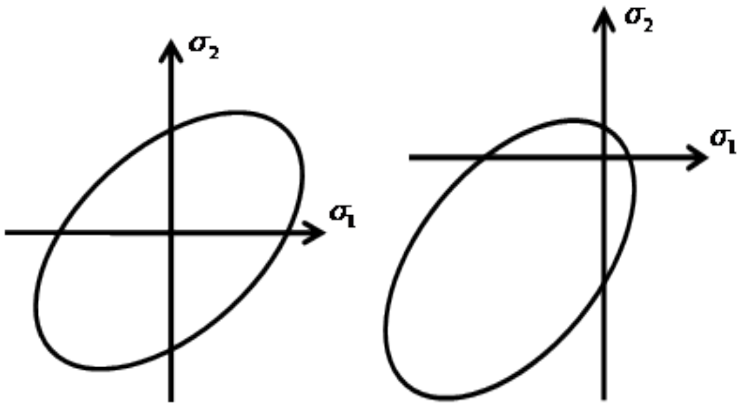

(a) von Mises (b) Drucker-Prager

Figure 7.3: Yield surfaces in 2D principal stress space.

independent plasticity formulations, based on the textbooks by Simo and Hughes (1998) and Zienkiewicz and Taylor (2000). The Drucker-Prager yield function can be expressed as

$$f(\boldsymbol{\sigma}, \kappa) = \sqrt{3J_2} + \alpha(\kappa) I_1 - \sigma_y(\kappa) \leq 0$$

where J_2 is the second invariant of the deviatoric stress tensor and I_1 is the first invariant (trace) of the stress tensor. α is a material property and σ_y is the yield stress in uniaxial tension, both functions of the internal hardening parameter κ according to some hardening functions. The expression $\sqrt{3J_2}$ is usually known as the *von Mises stress* or *equivalent stress*. When $\alpha = 0$, we obtain the von Mises yield criterion. We assume simple isotropic hardening rules

$$\alpha(\kappa) = constant \tag{7.2}$$

$$\sigma_y(\kappa) = \sigma_y^0 + HE\kappa \tag{7.3}$$

where σ_y^0 is the initial uniaxial yield stress, E is Young's modulus and H is a constant, typically in the order of 10^{-2}. The assumptions (7.2) and (7.3) are not necessarily suitable for accurate modeling of concrete but do not affect the ability to capture the most important failure in concrete, that is failure in tension. We assume an associative flow rule and a simple relation between the hardening parameter and the rate of the plastic flow

$$\begin{aligned} \dot{\boldsymbol{\epsilon}}^{pl} &= \dot{\lambda} \frac{\partial f}{\partial \boldsymbol{\sigma}} \\ \dot{\kappa} &= \dot{\lambda} \end{aligned} \tag{7.4}$$

where $\boldsymbol{\epsilon}^{pl}$ is the plastic strain tensor and the scalar λ is usually referred to as the *plastic multiplier*. The relation (7.4) does not accurately represent hardening mechanisms in metals. Nevertheless, it is accurate enough for the purpose of the current study, since post-yielding response of the steel phase should not have an effect on the optimal choice of material. Together with the yield criterion, $\dot{\lambda}$ must satisfy the Kuhn-Tucker complementarity conditions

$$\begin{aligned} \dot{\lambda} &\geq 0 \\ f(\boldsymbol{\sigma}, \kappa) &\leq 0 \\ \dot{\lambda} f(\boldsymbol{\sigma}, \kappa) &= 0 \end{aligned}$$

The continuum problem (in the temporal sense) is transformed into a discrete constrained optimization problem by applying an implicit backward-Euler difference scheme. The central

feature of this scheme is the introduction of a trial elastic state. For any given incremental displacement field, it is first assumed that there is no plastic flow between time t_n and the next time step t_{n+1}, meaning the incremental elastic strains are the incremental total strains. It can be shown that the loading/unloading situation which is governed by the Kuhn-Tucker conditions can be identified using the trial elastic state (Simo and Hughes, 1998). Once a plastic increment occurs, the new state variables can be found by solving a nonlinear equation system resulting from the time discretization of the governing equations. For the current model, the derivation of the discrete equation system is as follows. The total strain is split into its elastic and plastic parts

$$\boldsymbol{\epsilon} = \boldsymbol{\epsilon}^{el} + \boldsymbol{\epsilon}^{pl}$$

The stress rate is related to the elastic strain rate via the elastic constitutive tensor $\mathbf{D}$

$$\dot{\boldsymbol{\sigma}} = \mathbf{D}\dot{\boldsymbol{\epsilon}}^{el}$$

So for a certain "time" increment we can write the linearized equation

$$\Delta\boldsymbol{\sigma} = \mathbf{D}(\Delta\boldsymbol{\epsilon} - \Delta\boldsymbol{\epsilon}^{pl}) = \mathbf{D}(\Delta\boldsymbol{\epsilon} - \Delta\lambda\frac{\partial f}{\partial\boldsymbol{\sigma}})$$

Multiplying by $\mathbf{D}^{-1}$ leads to the first set of equations to be solved

$$\Delta\boldsymbol{\epsilon} - \mathbf{D}^{-1}\Delta\boldsymbol{\sigma} - \frac{\partial f}{\partial\boldsymbol{\sigma}}\Delta\lambda = \mathbf{0} \tag{7.5}$$

An additional equation results from the requirement that after initial yielding, the stress state should satisfy the yield condition

$$f(\boldsymbol{\sigma}, \lambda) = \sqrt{3J_2} + \alpha I_1 - \sigma_y(\lambda) = 0 \tag{7.6}$$

7.3.2 Nonlinear finite element analysis

Throughout this study, we follow the framework described by Michaleris et al. (1994) for nonlinear finite element analysis and adjoint sensitivity analysis, where the elasto-plastic nonlinear analysis is seen as a transient, nonlinear coupled problem. In the coupled approach, for every increment n in the transient analysis, we determine the unknowns $\mathbf{u}_n$ (displacements) and $\mathbf{v}_n$ (stresses and plastic multipliers) that satisfy the residual equations

$$\begin{aligned} \mathbf{R}_n(\mathbf{u}_n, \mathbf{u}_{n-1}, \mathbf{v}_n, \mathbf{v}_{n-1}) &= 0 \\ \mathbf{H}_n(\mathbf{u}_n, \mathbf{u}_{n-1}, \mathbf{v}_n, \mathbf{v}_{n-1}) &= 0 \end{aligned} \tag{7.7}$$

where $\mathbf{R}_n = 0$ is satisfied at the global level and $\mathbf{H}_n = 0$ is satisfied at each Gauss point. The transient, coupled and nonlinear system of equations is uncoupled by treating the response $\mathbf{v}$ as a function of the response $\mathbf{u}$. When solving the residual equations for the n-th "time" increment, the responses $\mathbf{u}_{n-1}$ and $\mathbf{v}_{n-1}$ are known from the previous converged increment. The independent response $\mathbf{u}_n$ is found by an iterative prediction-correction procedure in the global level, while for each iterative step the dependent response $\mathbf{v}_n(\mathbf{u}_n)$ is found by an inner iterative loop. The responses $\mathbf{u}_n$ and its dependant $\mathbf{v}_n$ are corrected until Eq. (7.7) is satisfied to sufficient accuracy. This procedure is repeated for all N increments.

Neglecting body forces, $\mathbf{R}_n$ is defined as the difference between external and internal forces and depends explicitly only on $\mathbf{v}_n$

$$\mathbf{R}_n(\mathbf{v}_n) = \mathbf{f}_n - \int_V \mathbf{B}^T\boldsymbol{\sigma}_n dV$$

where $\mathbf{B}$ is the standard strain-displacement matrix in the context of finite element procedures. The internal, Gauss-point level variables $\mathbf{v}_n$ are defined as

$$\mathbf{v}_n = \begin{bmatrix} \boldsymbol{\sigma}_n \\ \lambda_n \end{bmatrix}$$

where $\boldsymbol{\sigma}_n$ are the stresses and λ_n is the plastic multiplier. Furthermore, the residual $\mathbf{H}_n$ is defined as the collection of two incremental residuals, resulting from Eqs. (7.5),(7.6)

$$\mathbf{H}_n(\mathbf{u}_n, \mathbf{u}_{n-1}, \mathbf{v}_n, \mathbf{v}_{n-1}) = \begin{bmatrix} \mathbf{B}\mathbf{u}_n - \mathbf{B}\mathbf{u}_{n-1} - \mathbf{D}^{-1}(\boldsymbol{\sigma}_n - \boldsymbol{\sigma}_{n-1}) - \frac{\partial f}{\partial \boldsymbol{\sigma}_n}(\lambda_n - \lambda_{n-1}) \\ \sqrt{3J_2} + \alpha I_1 - \sigma_y(\lambda_n) \end{bmatrix} = \mathbf{0} \quad (7.8)$$

Here, the first equation equates total, elastic and plastic strains and the second represents the requirement that during plastic response the stress state satisfies the yield condition. In case an elastic step is predicted by the trial state, then no plastic flow occurs and $\lambda_n = \lambda_{n-1}$. Therefore the first equation is satisfied trivially by the elastic stress-strain relationship and the second equation can be disregarded.

The elasto-plastic problem is path-dependent by nature, meaning that the evolution of plastic strains under a certain load intensity depends on the history of plastic straining and cannot be computed correctly in one load stage. In practice, this means that the FE analysis must be solved incrementally. The default choice for most nonlinear FE solvers is to use *load control*, meaning that the total load is divided into a certain number of increments. Then for each increment, the current stress and strain states are required for the solution of the local elasto-plastic problem corresponding to the next load step. In some cases it is beneficial to switch to *displacement control*, for example when a small addition to the load causes a large additional displacement or when limit points are encountered (Crisfield, 1991). In the context of optimal design, a fixed load intensity throughout the optimization process may cause difficulties in solving the nonlinear analysis equations for intermediate designs that are very flexible. From this point of view, using displacement control for the nonlinear analysis is preferable. This means that the displacement at a selected degree of freedom is prescribed to a certain value for all design cycles. Choosing an appropriate value is possible if the designer has some knowledge regarding the expected deformation, and can also be seen as a way of imposing a required deflection at a certain point. Displacement control was utilized also in previous studies regarding topology optimization of elasto-plastic structures, e.g. by Swan and Kosaka (1997) and Maute et al. (1998).

For these reasons we mainly use displacement control and corresponding objective functions in this study. Then the global residual equation (7.7) takes the form

$$\mathbf{R}_n(\mathbf{v}_n, \theta_n) = \theta_n \hat{\mathbf{f}} - \int_V \mathbf{B}^T \boldsymbol{\sigma}_n dV$$

where θ_n is the (unknown) load factor in the n-th increment and $\hat{\mathbf{f}}$ is a constant reference load vector with non-zero entries only at loaded degrees of freedom. When solving the coupled equation system for each increment, a single displacement has a prescribed value and the rest, as well as the corresponding load factor θ_n, are determined from equilibrium.

7.4 Problem formulation

7.4.1 Interpolation of material properties

The main idea is to interpolate the nonlinear behavior of the two candidate materials using the density variables from the topology optimization problem. The interpolation of the elastic modulus is identical to that used in standard, linear elastic topology optimization

$$E(\rho_e) = E_{min} + (E_{max} - E_{min})\rho_e^{p_E} \quad (7.9)$$

where ρ_e is the density design variable corresponding to a certain finite element e. Interpolation of the nonlinear response is achieved by adding a dependency on the design variable ρ to the yield function, so instead of Eq. (7.6) we have

$$f(\boldsymbol{\sigma}, \lambda, \rho_e) = \sqrt{3J_2} + \alpha(\rho_e) I_1 - \sigma_y(\lambda, \rho_e) = 0 \tag{7.10}$$

Following a SIMP-type approach, the interpolating functions $\alpha(\rho_e)$ and $\sigma_y(\rho_e)$ are given by

$$\alpha(\rho_e) = \alpha_{max} - (\alpha_{max} - \alpha_{min})\rho_e^{p_\alpha} \tag{7.11}$$

$$\sigma_y(\lambda, \rho_e) = \sigma^0_{y,min} + (\sigma^0_{y,max} - \sigma^0_{y,min})\rho_e^{p_{\sigma_y}} + HE(\rho_e)\lambda \tag{7.12}$$

where p_α and p_{σ_y} are penalization factors for α and σ_y, respectively. These interpolations imply that the yield surface of one material is obtained by choosing $\rho_e = 0$, meaning $\alpha = \alpha_{max}$ and $\sigma^0_y = \sigma^0_{y,min}$, and the second yield surface is obtained by $\rho_e = 1$, meaning $\alpha = \alpha_{min}$ and $\sigma^0_y = \sigma^0_{y,max}$. As stated above, the particular case $\alpha_{min} = 0$ means that the plastic response of the second material is governed by the von Mises yield criterion. By setting also $\sigma^0_{y,max} = \sigma^0_{y,steel}$ an actual model of steel is obtained for $\rho_e = 1$. In Figure 7.4, the interpolation of the yield surfaces is demonstrated, for two materials resembling steel and concrete.

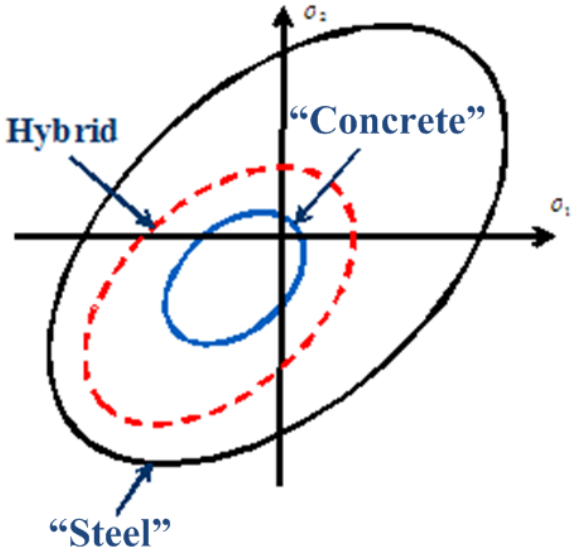

Figure 7.4: Demonstrative example of the interpolation between two yield surfaces, presented in 2D principal stress space. The "Hybrid" surface represents the behavior of an artificial mixture, corresponding to an intermediate density in topology optimization.

In order to approach optimal strut-and-tie designs, we extend this interpolation so it accommodates also void regions. Following Bendsøe and Sigmund (2003), we add another design variable x for each finite element. Void regions are represented by $x = 0$ and solid regions are represented by $x = 1$. Within the solid regions, the value of ρ determines the distribution of the two candidate materials. This leads to the following interpolation functions, replacing Eqs. (7.9), (7.10), (7.11), (7.12)

$$E(x_e, \rho_e) = x_e^{p_{Ex}}(E_{min} + (E_{max} - E_{min})\rho_e^{p_E}) \tag{7.13}$$

$$f(\boldsymbol{\sigma}, \lambda, \rho_e, x_e) = \sqrt{3J_2} + \alpha(x_e, \rho_e) I_1 - \sigma_y(\lambda, x_e, \rho_e) = 0 \tag{7.14}$$

$$\alpha(x_e, \rho_e) = x_e^{p_{\alpha x}}(\alpha_{max} - (\alpha_{max} - \alpha_{min})\rho_e^{p_\alpha}) \tag{7.15}$$

$$\sigma_y(\lambda, x_e, \rho_e) = x_e^{p_{\sigma x}}(\sigma^0_{y,min} + (\sigma^0_{y,max} - \sigma^0_{y,min})\rho_e^{p_{\sigma_y}} + HE(x_e, \rho_e)\lambda) \tag{7.16}$$

where p_{Ex}, $p_{\alpha x}$ and $p_{\sigma x}$ are penalization factors for x. In practice, one may choose to use the same penalty factors for both design variables, x and ρ.

7.4.2 Optimization problem and sensitivity analysis

In this article, we focus mainly on one demonstrative class of objective functions. The aim is to find the stiffest structural layouts given certain amounts of available material. When only linear elastic response is considered, the corresponding objective is the widely used minimum compliance problem, presented above (7.1). When nonlinear response is taken into account, one may define several different objectives that are related to the maximization of the structural stiffness (see for example Swan and Kosaka (1997), Maute et al. (1998), Buhl et al. (2000)). Since displacement control is preferred in the nonlinear FE analysis, a possible equivalent to minimizing compliance in linear elasticity is maximizing the end compliance for a given prescribed displacement. In other words, the objective is to maximize the magnitude of the load that corresponds to a certain prescribed displacement at a particular degree of freedom.

Assuming the analysis problem is solved in N increments, the optimization problem of distributing two materials in the design domain can be stated as follows

$$\begin{aligned}
\min_{\boldsymbol{\rho}} c(\boldsymbol{\rho}) \quad &= \quad -\theta_N \hat{\mathbf{f}}^T \mathbf{u}_N \\
\text{s.t.:} \qquad & \sum_{e=1}^{N_e} v_e \rho_e \leq V \\
& 0 \leq \rho_e \leq 1, \qquad e = 1, ..., N_e \\
\text{with the coupled residuals:} \qquad & \mathbf{R}_n(\mathbf{v}_n, \theta_n) = 0 \qquad n = 1, ..., N \\
& \mathbf{H}_n(\mathbf{u}_n, \mathbf{u}_{n-1}, \mathbf{v}_n, \mathbf{v}_{n-1}, \boldsymbol{\rho}) = 0 \qquad n = 1, ..., N
\end{aligned} \tag{7.17}$$

where V is the available volume of the material whose properties correspond to $\rho_e = 1$. When distributing two materials and void, the optimization problem is slightly modified

$$\begin{aligned}
\min_{\boldsymbol{\rho}, \mathbf{x}} c(\boldsymbol{\rho}, \mathbf{x}) \quad &= \quad -\theta_N \hat{\mathbf{f}}^T \mathbf{u}_N \\
\text{s.t.:} \qquad & \sum_{e=1}^{N_e} v_e x_e \leq V_1 \\
& \sum_{e=1}^{N_e} v_e \rho_e \leq V_2 \\
& 0 < x_{min} \leq x_e \leq 1, \qquad e = 1, ..., N_e \\
& 0 \leq \rho_e \leq 1, \qquad e = 1, ..., N_e \\
\text{with the coupled residuals:} \qquad & \mathbf{R}_n(\mathbf{v}_n, \theta_n) = 0 \qquad n = 1, ..., N \\
& \mathbf{H}_n(\mathbf{u}_n, \mathbf{u}_{n-1}, \mathbf{v}_n, \mathbf{v}_{n-1}, \boldsymbol{\rho}, \mathbf{x}) = 0 \qquad n = 1, ..., N
\end{aligned} \tag{7.18}$$

where V_1 is the total available volume of material, V_2 is the available volume of the material whose properties correspond to $\rho_e = 1$ ($V_2 \leq V_1$) and x_{min} is a positive lower bound used in order to avoid singularity of the stiffness matrix.

As discussed in Chapter 2, the objective function used in the problem formulations above is appropriate for stiffness maximization only in the case of a single point load. When a distributed load is applied, the load-controlled objective $\mathbf{f}_N^T \mathbf{u}_N$ should be used. Then also the sensitivity analysis is performed considering a load-controlled setting following the hybrid approach presented in Chapter 2.

As mentioned earlier, the design sensitivities are computed by the adjoint method, following the framework for transient, nonlinear coupled problems described by Michaleris et al. (1994). To the best of the authors' knowledge, this is the first implementation of this framework in topology optimization of structures with material nonlinearities. Furthermore, it is presumably the first sensitivity analysis for topology optimization of structures with material nonlinearities where no simplifying assumptions are made. An effort is made to use similar notation to that in

Michaleris et al. (1994). The procedure for sensitivity analysis is described here only for the two material and void problem (7.18) since the two-material problem can easily be deduced from it. We begin by forming the augmented objective function $\hat{c}(\boldsymbol{\rho})$

$$\begin{aligned}\hat{c}(\boldsymbol{\rho},\mathbf{x}) &= -\theta_N \hat{\mathbf{f}}^T \mathbf{u}_N - \sum_{n=1}^{N} \boldsymbol{\lambda}_n^T \mathbf{R}_n(\mathbf{v}_n,\theta_n) \\ &\quad - \sum_{n=1}^{N} \boldsymbol{\gamma}_n^T \mathbf{H}_n(\mathbf{u}_n,\mathbf{u}_{n-1},\mathbf{v}_n,\mathbf{v}_{n-1},\boldsymbol{\rho},\mathbf{x})\end{aligned}$$

where $\boldsymbol{\lambda}_n$ and $\boldsymbol{\gamma}_n$ are the adjoint vectors to be found for all increments $n = 1, ..., N$. We assume the initial responses $\mathbf{u}_0$, $\mathbf{v}_0$ do not depend on the design variables. Furthermore, it can be observed that the objective function and the nonlinear equation systems $\mathbf{R}_n = 0$ $(n = 1, ..., N)$ do not depend explicitly on the design variables. Therefore the explicit terms in the derivative of the augmented objective with respect to the design variables are

$$\begin{aligned}\frac{\partial \hat{c}_{exp}}{\partial x_e} &= -\sum_{n=1}^{N} \boldsymbol{\gamma}_n^T \frac{\partial \mathbf{H}_n}{\partial x_e} \\ \frac{\partial \hat{c}_{exp}}{\partial \rho_e} &= -\sum_{n=1}^{N} \boldsymbol{\gamma}_n^T \frac{\partial \mathbf{H}_n}{\partial \rho_e}\end{aligned}$$

The adjoint vectors $\boldsymbol{\gamma}_n$ $(n = 1, ..., N)$ are computed on a Gauss-point level by a backward incremental procedure, which is required due to path dependency of the elasto-plastic response. The backward procedure consists of the collection of equation systems resulting from the requirement that all implicit derivatives of the design variables will vanish. Further details regarding the adjoint procedure can be found in Chapter 2. For performing the backwards-incremental sensitivity analysis, the derivatives of the global and local residuals with respect to the analysis variables are required. These are given in this section for the elasto-plastic model utilized in the current study. In particular, we consider a plane stress situation, meaning the stresses and strains are collected in a vector with three entries: $\boldsymbol{\sigma} = [\sigma_{11}, \sigma_{22}, \sigma_{12}]^T$ and $\boldsymbol{\epsilon} = [\epsilon_{11}, \epsilon_{22}, \epsilon_{12}]^T$.

The derivative of the global residual is independent of the specific material model employed and is given by

$$\frac{\partial(\mathbf{R}_n)}{\partial(\mathbf{v}_n)} = \begin{bmatrix} -\mathbf{B}^T w J_{(8\times3)} & \mathbf{0}_{(8\times1)} \end{bmatrix}$$

where $\mathbf{B}$ is the standard strain-displacement matrix; w is the Gauss-point weight for numerical integration; and J is the determinant of the Jacobian at the Gauss-point. For the nonlinear material model described in Section 7.3, the derivatives of the local residual are

$$\begin{aligned}\frac{\partial(\mathbf{H}_n)}{\partial(\mathbf{u}_n)} &= \begin{bmatrix} \mathbf{B}_{(3\times8)} \\ \mathbf{0}_{(1\times8)} \end{bmatrix} \\ \frac{\partial(\mathbf{H}_{n+1})}{\partial(\mathbf{u}_n)} &= \begin{bmatrix} -\mathbf{B}_{(3\times8)} \\ \mathbf{0}_{(1\times8)} \end{bmatrix} \\ \frac{\partial(\mathbf{H}_n)}{\partial(\mathbf{v}_n)} &= \begin{bmatrix} -\mathbf{D}^{-1} - \Delta^n \lambda \frac{\partial^2 f}{\partial \boldsymbol{\sigma}_n}_{(3\times3)} & -\frac{\partial f}{\partial \boldsymbol{\sigma}_n}^T_{(3\times1)} \\ \frac{\partial f}{\partial \boldsymbol{\sigma}_n}_{(1\times3)} & -HE_{(1\times1)} \end{bmatrix} \\ \frac{\partial(\mathbf{H}_{n+1})}{\partial(\mathbf{v}_n)} &= \begin{bmatrix} \mathbf{D}^{-1}{}_{(3\times3)} & \frac{\partial f}{\partial \boldsymbol{\sigma}_{n+1}}^T_{(3\times1)} \\ \mathbf{0}_{(1\times3)} & 0_{(1\times1)} \end{bmatrix}\end{aligned}$$

where the derivative of the yield function with respect to the stress components is

$$\frac{\partial f}{\partial \boldsymbol{\sigma}} = \frac{1}{2\sqrt{3J_2}} \begin{bmatrix} 2\sigma_{11} - \sigma_{22} & 2\sigma_{22} - \sigma 11 & 6\sigma_{12} \end{bmatrix} + \alpha \begin{bmatrix} 1 & 1 & 0 \end{bmatrix}$$

In actual implementation, the derivatives of the local residuals $\mathbf{H}_n$ and $\mathbf{H}_{n+1}$ should maintain consistency with respect to the analysis. This means that some rows and columns should be disregarded in case of elastic loading or unloading. For example, if increment n is elastic, then we have $\frac{\partial(\mathbf{H}_n)}{\partial(\mathbf{u}_n)} = \left[\mathbf{B}_{(3\times 8)}\right]$ and $\frac{\partial(\mathbf{H}_n)}{\partial(\mathbf{v}_n)} = \left[-\mathbf{D}^{-1}_{(3\times 3)}\right]$.

Finally, computing the derivatives $\frac{\partial \mathbf{H}_n}{\partial x_e}$, $\frac{\partial \mathbf{H}_n}{\partial \rho_e}$ requires adding the dependency on the design variables to Eq. (7.8) and differentiating with respect to x_e and ρ_e. This leads to

$$\frac{\partial \mathbf{H}_n}{\partial x_e} = \begin{bmatrix} -\frac{\partial(\mathbf{D}(x_e,\rho_e)^{-1})}{\partial x_e}(\boldsymbol{\sigma}_n - \boldsymbol{\sigma}_{n-1}) - \frac{\partial(\frac{\partial f}{\partial \boldsymbol{\sigma}_n}(x_e,\rho_e))^T}{\partial x_e}(\lambda_n - \lambda_{n-1}) \\ \frac{\partial f(x_e,\rho_e)}{\partial x_e} \end{bmatrix}$$

$$\frac{\partial \mathbf{H}_n}{\partial \rho_e} = \begin{bmatrix} -\frac{\partial(\mathbf{D}(x_e,\rho_e)^{-1})}{\partial \rho_e}(\boldsymbol{\sigma}_n - \boldsymbol{\sigma}_{n-1}) - \frac{\partial(\frac{\partial f}{\partial \boldsymbol{\sigma}_n}(x_e,\rho_e))^T}{\partial \rho_e}(\lambda_n - \lambda_{n-1}) \\ \frac{\partial f(x_e,\rho_e)}{\partial \rho_e} \end{bmatrix}$$

where

$$\begin{aligned}
\frac{\partial(\mathbf{D}(x_e,\rho_e)^{-1})}{\partial x_e} &= -\frac{1}{E(x_e,\rho_e)}\frac{\partial E(x_e,\rho_e)}{\partial x_e}\mathbf{D}(x_e,\rho_e)^{-1} \\
\frac{\partial(\mathbf{D}(x_e,\rho_e)^{-1})}{\partial \rho_e} &= -\frac{1}{E(x_e,\rho_e)}\frac{\partial E(x_e,\rho_e)}{\partial \rho_e}\mathbf{D}(x_e,\rho_e)^{-1} \\
\frac{\partial(\frac{\partial f}{\partial \boldsymbol{\sigma}_n}(x_e,\rho_e))^T}{\partial x_e} &= \frac{\partial \alpha(x_e,\rho_e)}{\partial x_e}\begin{bmatrix} 1 \\ 1 \\ 0 \end{bmatrix} \\
\frac{\partial(\frac{\partial f}{\partial \boldsymbol{\sigma}_n}(x_e,\rho_e))^T}{\partial \rho_e} &= \frac{\partial \alpha(x_e,\rho_e)}{\partial \rho_e}\begin{bmatrix} 1 \\ 1 \\ 0 \end{bmatrix} \\
\frac{\partial f(x_e,\rho_e)}{\partial x_e} &= \frac{\partial \alpha(x_e,\rho_e)}{\partial x_e}I_1 - \frac{\partial \sigma_y(x_e,\rho_e)}{\partial x_e} \\
\frac{\partial f(x_e,\rho_e)}{\partial \rho_e} &= \frac{\partial \alpha(x_e,\rho_e)}{\partial \rho_e}I_1 - \frac{\partial \sigma_y(x_e,\rho_e)}{\partial \rho_e}
\end{aligned}$$

The above derivatives can be easily computed using the relations given in Eqs. (7.13), (7.14), (7.15), (7.16).

7.5 Examples

In this section we present several results obtained when implementing the computational approach described in this article. The purpose is to demonstrate the capabilities and potential of our approach and to gain insight regarding implementation aspects. Therefore, as preliminary examples we consider relatively small scale two-dimensional problems with no self weight. Extending to three dimensional models and incorporating more realistic loading conditions are among the goals of future work.

7.5.1 General considerations

In the following examples, both optimization problems are considered: distribution of concrete and steel (7.17) and distribution of concrete, steel and void (7.18). The material parameters resemble actual values corresponding to steel and concrete, see Table 7.1. For computing α_{max} and $\sigma^0_{y,min}$, both corresponding to the concrete phase, it was assumed that the strength of concrete in compression is ten times higher than in tension. All test cases were solved using a 2D finite element mesh consisting of square, bi-linear plane stress elements. The optimization was

performed by a nonlinear optimization program based on the Method of Moving Asymptotes - MMA (Svanberg, 1987). In order to obtain regularized designs and to avoid checkerboard patterns, a density filter was applied (Bourdin, 2001; Bruns and Tortorelli, 2001).

Table 7.1: Material properties in all test cases

Parameter	Material	Value
E_{min}	concrete	25.0 [GPa]
E_{max}	steel	200.0 [GPa]
α_{min}	steel	0.0
α_{max}	concrete	0.818
$\sigma^0_{y,min}$	concrete	5.5 [MPa]
$\sigma^0_{y,max}$	steel	300 [MPa]
ν	both	0.3
H	both	0.01

The actual computational performance of the proposed approach is affected by the choice of several numerical parameters. First, in order to ensure convergence of the Newton-Raphson iterations in the nonlinear FE analysis, one should carefully choose an appropriate value of the prescribed displacement, denoted by δ. Too large values of δ may cause difficulties in convergence, thus increasing the computing time. On the other hand, δ should be large enough to ensure that the response of the structure is indeed nonlinear. In case the nonlinear analysis fails to converge at a certain displacement level even after several increment cuts, the analysis is terminated and sensitivity analysis is performed with respect to the converged configuration.

As for the optimization program, it is well known that in topology optimization the computational performance is strongly affected by the choice of the filter radius and penalty factors. An effort was made to keep these values similar for all test cases. In some cases, the penalty factors are gradually increased and/or the filter radius is gradually decreased in order to obtain a more refined layout. The particular choice of numerical parameters for each test case is given in the corresponding text. The number of design iterations varies between test cases. According to the authors' experience, most problems require 100 to 200 design iterations to reach a converged design. After that, no significant changes in the layout can be observed and the improvement in objective value is negligible. The relatively tight convergence tolerance (1×10^{-4}) referring to the maximum change in an element density throughout the design domain was not reached.

7.5.2 Optimized concrete-steel layouts

Example 1. Simply supported beam subject to a concentrated load In this example problem, the competence of the proposed procedure in designing the reinforcement for a simply supported beam is demonstrated. We consider a beam with a length-to-height ratio equal to 4, loaded with a prescribed displacement directed downwards at the middle of the top edge, see Figure 7.5. The model of the symmetric half is discretized with a 200×100 FE mesh. The objective is to maximize the end-compliance, see (7.17). The volume fraction is 0.2 and the magnitude of the prescribed displacement is $\delta = 0.005$. The final design is achieved by gradually increasing all penalty factors and reducing the filter radius, for details see Table 7.2. This is necessary in order to remove "gray" regions of intermediate density, as well as small isolated reinforcement regions.

The layout obtained for the simply supported beam resembles actual design of reinforced concrete beams. Away from the supports, bending action is dominant so steel is necessary in the bottom fibers where tension stresses appear. Closer to the supports, shear forces are

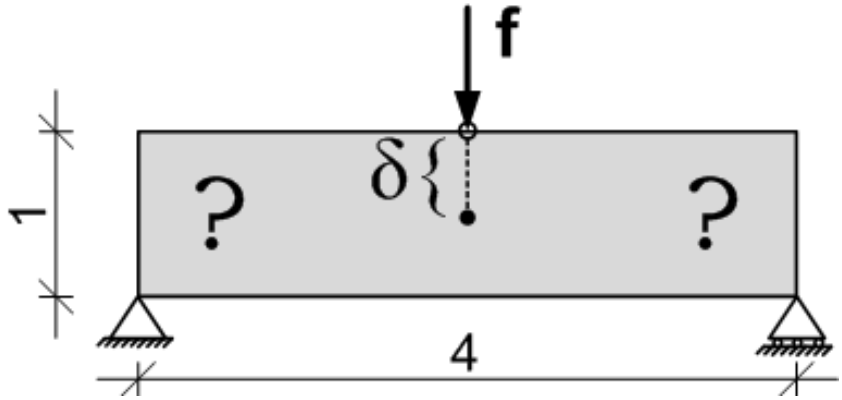

Figure 7.5: Maximum end-compliance of a simply supported beam: design domain, boundary conditions and prescribed displacement.

Table 7.2: Gradual refinement, example 1

	Design iterations	Penalty factor	Filter radius
Stage 1	100	3.0	0.015
Stage 2	50	4.0	0.010

dominant so concrete typically cracks in an angle of $45°$, corresponding to the direction of the principal stresses in pure shear. Consequently, the steel reinforcement should be bent in order to accommodate the tensile stresses due to shear. Additional reinforcement is placed at the upper fibers and at the supports. This is necessary since the load and the reaction force are concentrated at single nodes. Moreover, the relatively high available volume of steel facilitates the use of steel also in compression, both in the top fibers and in the shear-dominated regions. As will be seen in the following example, this is not the case when the volume fraction of steel is reduced and the load is distributed. Concluding this example, the benefit of employing nonlinear modeling is clear when comparing the result to the layout obtained with linear modeling, see Figure 7.2.

Example 2. Simply supported beam subject to a distributed load In this example problem, we again address the maximum end-compliance design of a simply supported beam. However, in this case the load is evenly distributed along the beam and the length-to-height ratio is larger, see Figure 7.5. This means that we expect bending action to be much more dominant than in the previous example. The model of the symmetric half is discretized with a 160×40 FE mesh; the volume fraction is set to 0.1; and the magnitude of the prescribed displacement is $\delta = 0.005$. The load is modeled as 10 equally spaced point loads on one half of the beam. As in the previous example, gradual changes in penalization and filtering are necessary for obtaining the final design, see Table 7.3 for details.

Examining this example, it can be seen that the presented procedure enables a clear distinction between tensile and compressive stresses. The optimized layout is generated accordingly: steel reinforcement is placed in the bottom fiber where tensile stresses appear due to bending, and in the vicinity of concentrated forces (at the supports in this case). Near the supports, the reinforcement is bent upwards. This improves the structure's resistance to shear failure, which is dominant in these regions.

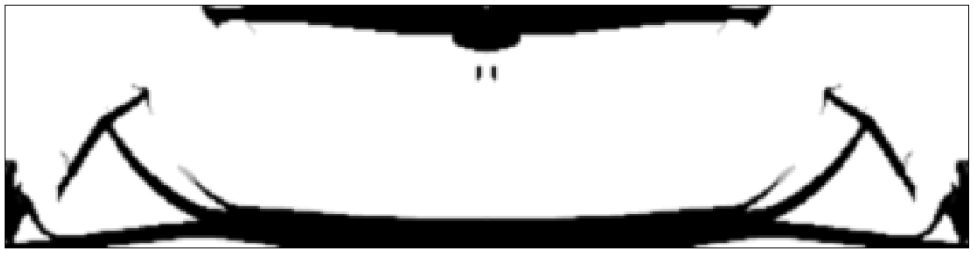

(a) Optimized layout after 100 design iterations with $p_E = 3, p_\alpha = 3, p_{\sigma_y} = 3$ and filter radius $r = 0.015$.

(b) Optimized layout after 50 further design iterations with $p_E = 4, p_\alpha = 4, p_{\sigma_y} = 4$ and filter radius $r = 0.010$.

Figure 7.6: Maximum end-compliance of a simply supported beam subject to a concentrated load. Black = steel, white = concrete. Steel consists of 20% of the total volume.

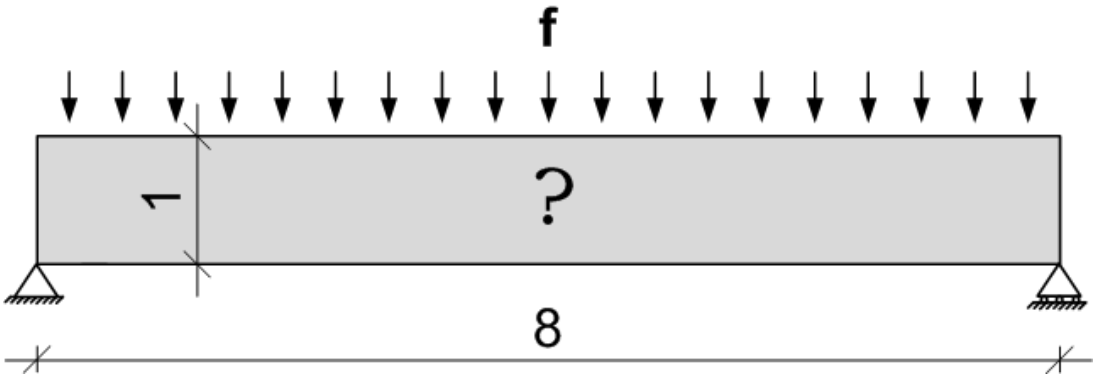

(a) Design domain and boundary conditions.

(b) Optimized layout for maximum end-compliance after 100 design iterations with $p_E = 3, p_\alpha = 3, p_{\sigma_y} = 3$ and filter radius $r = 0.040$.

(c) Optimized layout after 50 further design iterations with $p_E = 4, p_\alpha = 4, p_{\sigma_y} = 4$ and filter radius $r = 0.025$.

Figure 7.7: Maximum end-compliance of a simply supported beam subject to a distributed load. Black = steel, white = concrete. Steel consists of 10% of the total volume.

Table 7.3: Gradual refinement, example 2

	Design iterations	Penalty factor	Filter radius
Stage 1	100	3.0	0.040
Stage 2	50	4.0	0.025

Example 3. Short cantilever In this example problem, the proposed procedure is applied for designing the reinforcement in a short cantilever. The design domain is a square supported at two corners on one side and loaded with a prescribed displacement directed downwards at the opposite bottom corner, see Figure 7.8(a). The model is discretized with a 100×100 FE mesh. The objective is to maximize the end-compliance, and we present two results: one of concrete-steel distribution (see (7.17)) and another of concrete-steel-void distribution (see (7.18)). For the two-material design, the steel volume fraction is 0.2. When void is considered as well, then the total volume fraction is 0.4 and the steel volume fraction is 0.1. The prescribed displacements are set to $\delta = 0.002$ and $\delta = 0.001$ respectively. The penalty factors are set to the value of 3.0 and the filter radius is $r = 0.015$ for all design iterations.

In both cases, steel is used mainly for a cable-like member in tension, transferring the load to the upper support. This cable is then supported by either a continuous concrete domain (when no voids are possible) or by two compressed concrete bars, see Figures 7.8(b), 7.8(c). This again demonstrates the capability of the procedure to distinguish between structural elements in tension and in compression and to choose the appropriate material for each type. The layout obtained when distributing steel, concrete and void resembles strut-and-tie models that are widely used in practical analysis and design of reinforced concrete. As observed in previous examples, steel might be used also for stiffening support regions. In the short cantilever, this is the case mainly for the two material problem with no voids. To a lesser extent, this is observed also in the result of the concrete-steel-void distribution.

7.6 Discussion

Optimized conceptual design of reinforced concrete was demonstrated, based on a new approach to topology optimization with nonlinear material modeling. The different failure criteria corresponding to the nonlinear response of concrete and steel were taken into account, using material interpolation rules for post-yielding behavior in addition to the standard interpolation of elastic properties. Even though the approach was applied only to the design of steel-reinforced concrete, it can be easily applied to other compositions of materials where it is necessary to capture the nonlinear behavior for the purpose of optimizing the design.

The resulting optimized layouts clearly demonstrate the potential of this approach. When distributing steel within a concrete beam, the placement of reinforcement resembles traditional design and agrees with common engineering knowledge. When distributing concrete, steel and void, it is shown that optimized strut-and-tie models are generated. These can be used for several purposes: first, to provide the engineer an improved initial design before the detailed design stage; second, to challenge traditional practice and achieve more efficient design of reinforced concrete structures by suggesting non-traditional forms and shapes; third, to reduce weight and concrete production, by utilizing lightweight concrete in the "void" regions where no strength is required.

Future work will focus on more realistic modeling. With respect to loading conditions, it is necessary to consider also self-weight and multiple load cases. Another important issue is the constraint on the volume of reinforcing material: in practice, the relative volume of steel seldom

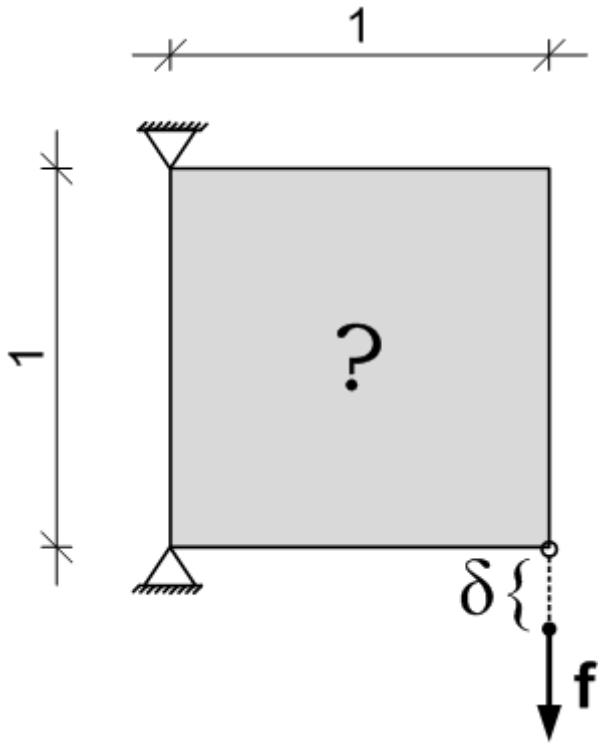

(a) Design domain, boundary conditions and prescribed displacement.

(b) Optimized layout after 500 design iterations, 80% concrete, 20% steel. Black = steel, gray = concrete.

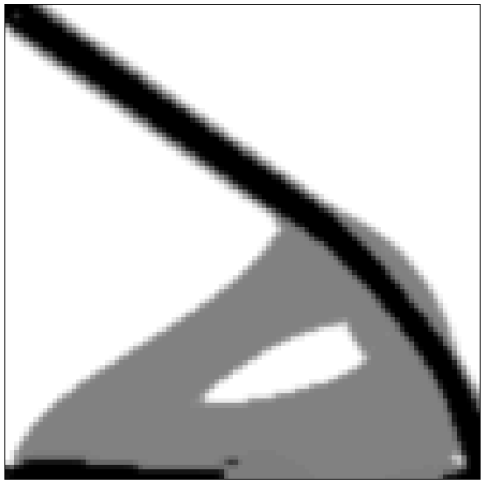

(c) Optimized layout after 200 design iterations, 30% concrete, 10% steel, 60% void. Black = steel, gray = concrete, white = void.

Figure 7.8: Maximum end-compliance of a short cantilever

exceeds 1%. This requires much more refined FE models in which thin steel bars can be properly realized. Another important extension is to consider strain softening in the concrete phase. Consequently, transferring tension forces in concrete will be even less preferable, meaning that more realistic designs can be suggested. Finally, the introduction of other objective functions will also be explored.

7.7 Acknowledgments

The work of the first author was fully funded by the Danish Council for Independent Research - Technology and Production Sciences (FTP - 274-08-0294). This support is gratefully acknowledged. The authors are grateful to Asso. Prof. Mathias Stolpe for his valuable comments on the manuscript. The authors also wish to thank Krister Svanberg for allowing them to use the MMA code.

References

M. P. Bendsøe and N. Kikuchi. Generating optimal topologies in structural design using a homogenization method. *Computer Methods in Applied Mechanics and Engineering*, 71:197–224, 1988.

M. P. Bendsøe and O. Sigmund. *Topology Optimization - Theory, Methods and Applications*. Springer, Berlin, 2003.

B. Bourdin. Filters in topology optimization. *International Journal for Numerical Methods in Engineering*, 50:2143–2158, 2001.

M. Bruggi. Generating strut-and-tie patterns for reinforced concrete structures using topology optimization. *Computers and Structures*, 87(23-24):1483–1495, 2009.

T. E. Bruns and D. A. Tortorelli. Topology optimization of non-linear elastic structures and compliant mechanisms. *Computer Methods in Applied Mechanics and Engineering*, 190:3443–3459, 2001.

T. Buhl, C. Pedersen, and O. Sigmund. Stiffness design of geometrically nonlinear structures using topology optimization. *Structural and Multidisciplinary Optimization*, 19(2):93–104, 2000.

W. F. Chen. *Plasticity in Reinforced Concrete*. McGraw-Hill Book Company, New York, 1982.

M. A. Crisfield. *Non-linear Finite Element Analysis of Solids and Structures*, volume 1. John Wiley & Sons, 1991.

D. C. Drucker and W. Prager. Soil mechanics and plastic analysis or limit design. *Quarterly of Applied Mathematics*, 10(2):157–165, 1952.

J. Kato, A. Lipka, and E. Ramm. Multiphase material optimization for fiber reinforced composites with strain softening. *Structural and Multidisciplinary Optimization*, 39(1):63–81, 2009.

H.-G. Kwak and S.-H. Noh. Determination of strut-and-tie models using evolutionary structural optimization. *Engineering Structures*, 28(10):1440–1449, 2006.

Q. Liang, Y. Xie, and G. Steven. Topology optimization of strut-and-tie models in reinforced concrete structures using an evolutionary procedure. *ACI Structural Journal*, 97(2):322–330, 2000.

M. P. Bendsøe. Optimal shape design as a material distribution problem. *Structural Optimization*, 1:193–202, 1989.

P. Marti. Truss models in detailing. *Concrete International*, 7:66–73, 1985.

K. Maute, S. Schwarz, and E. Ramm. Adaptive topology optimization of elastoplastic structures. *Structural Optimization*, 15(2):81–91, 1998.

P. Michaleris, D. A. Tortorelli, and C. A. Vidal. Tangent operators and design sensitivity formulations for transient non-linear coupled problems with applications to elastoplasticity. *International Journal for Numerical Methods in Engineering*, 37:2471–2499, 1994.

H. Okamura and M. Ouchi. Self compacting concrete: Development, application and investigations. *Journal of Advanced Concrete Technology*, 1:5–15, 2003.

J. Oliver, D. L. Linero, A. E. Huespe, and O. L. Manzoli. Two-dimensional modeling of material failure in reinforced concrete by means of a continuum strong discontinuity approach. *Computer Methods in Applied Mechanics and Engineering*, 197(5):332–348, 2008.

J. Pravida and W. Wunderlich. A plasticity based model and an adaptive algorithm for finite element analysis of reinforced concrete panels. *International Journal for Numerical Methods in Engineering*, 53(11):2445–2462, 2002.

W. Ritter. The hennebique system of construction. *Schweizerische Bauzeitung*, 33/34, 1899.

J. Schlaich, K. Schafer, and M. Jennewein. Toward a consistent design of structural concrete. *PCI Journal*, 32(3):74–150, 1987.

J. Simo and T. Hughes. *Computational Inelasticity*. Springer, New York, 1998.

H. Stang and M. Geiker. High Performance Concrete. *Arkitekten*, 12:33–35, 2004. (In Danish).

K. Svanberg. The method of moving asymptotes - a new method for structural optimization. *International Journal for Numerical Methods in Engineering*, 24:359–373, 1987.

C. Swan and I. Kosaka. Voigt-Reuss topology optimization for structures with nonlinear material behaviors. *International Journal for Numerical Methods in Engineering*, 40(20):3785–3814, 1997.

O. C. Zienkiewicz and R. L. Taylor. *The Finite Element Method (5th edition) Volume 2 - Solid Mechanics*. Elsevier, 2000.

Chapter 8

Re-using solutions and tangent stiffnesses for efficient nonlinear structural analysis in topology optimization

Amir O, Stolpe M and Sigmund O. Re-using solutions and tangent stiffnesses for efficient nonlinear structural analysis in topology optimization. To be submitted.

Abstract In the nested approach to topology optimization, most of the computational effort is invested in repeated solutions of the analysis equations. When nonlinear structural response is considered, the computational effort invested in the solution of the nested problem is even more dominant. In this study, we present efficient solution procedures for nonlinear structural analysis based on re-using information throughout the optimization process. In the proposed schemes, the solution of the nonlinear structural analysis corresponding to a certain design cycle is used as a starting point for the analysis in the next design cycle. When the design changes between two subsequent cycles are small, it is suggested to re-use also the factorization of the tangent stiffness matrix. The approach is tested on several design problems involving either geometric or material nonlinearities. Savings of up to 50% are achieved for problems involving large deformations. When considering elasto-plasticity, the results are less promising due to difficulties arising from the path-depenedent nature of the desired solution.

Keywords Topology optimization, Nonlinear structural analysis, Structural reanalysis

8.1 Introduction

The application of structural optimization, and topology optimization in particular, to large-scale problems has been advancing rapidly over the past few years, especially due to the utilization of high performance computer systems (e.g. Aage et al. (2008), Wang et al. (2007) and Evgrafov et al. (2008)). Nevertheless, improving the efficiency of computational procedures in topology optimization is still important. Reducing the computational costs can enable more realistic modeling of complex physical systems and can facilitate the solution of even larger problems, compared to standard procedures.

In many topology optimization problems, the number of inequality constraints is considerably smaller than the number of design variables. Then it is natural to apply the nested approach, where optimization is performed in the design variables only and the equilibrium

equations are solved separately by a function call. When utilizing the nested approach, the computational cost of the whole optimization process is dominated by the effort involved in repeated solutions of large systems of finite element equilibrium equations. Several studies have recently addressed the issue of reducing the computational effort invested in repeated solutions of the nested analysis problem. A common feature in these studies is that they suggest to re-use information for performing a sequence of structural analyses efficiently. One approach presented by Wang et al. (2007) is to recycle information used by a Krylov subspace solver in order to reduce the number of iterations performed when solving the analysis equations. Another approach suggests to apply an approximate reanalysis procedure (Amir et al., 2009). This means the analysis equations are not solved accurately but consistency of the optimization problem is ensured by taking the errors in the analysis into account in the sensitivity analysis. Finally, using a similar reanalysis approach, Amir and Sigmund (2010) recently presented an approximate procedure based on only one matrix factorization for the whole design process.

The studies mentioned above show that significant computing time can be saved by employing efficient solution procedures based on re-using information. However, they all focus on the particular case in which the nested analysis problem is linear. This means that for every design cycle a linear system of equations needs to be solved (in some cases an additional adjoint system is solved for the purpose of sensitivity analysis). When aiming to optimize the performance of a structure that exhibits nonlinear behavior, solving the nested problem involves the solution of a system of nonlinear finite element equations. In such cases the computational effort invested in the solution of the nested problem is even more dominant, and the need for efficient procedures for repeated solutions of the analysis problem is evident. This is the purpose of the current study. The suggested computational schemes are demonstrated on topology optimization problems involving either material or geometric nonlinearities.

Material nonlinearities in topology optimization were initially considered by Yuge and Kikuchi (1995). Layout optimization of frame structures undergoing plastic deformation was presented, based on homogenization of porous material. Swan and Kosaka (1997) suggested a framework for topology optimization of structures with material nonlinearity based on Voigt and Reuss mixing rules. The SIMP (Solid Isotropic Material with Penalization) interpolation scheme, originally proposed for linear elastic material (M. P. Bendsøe, 1989), was extended for elasto-plastic behavior by Maute et al. (1998). Although several other articles on the subject were published over the last decade, topology optimization involving elasto-plasticity is still not well established. One difficulty lies in obtaining accurate design sensitivities. In some cases, several derivative terms are neglected (Maute et al., 1998; Schwarz et al., 2001). Apparently this has no effect on the outcome of the optimization but in general these terms are not negligible. Moreover, when comparing analytical design sensitivities to finite difference calculations, errors in the order of 10^{-2} are observed (Swan and Kosaka, 1997; Yoon and Kim, 2007). Another difficulty is related to the loading conditions. All the studies mentioned above considered only point loads or distributed loads with rigid interconnections, meaning the deflections at the loaded points are coupled. This simplifies the sensitivity analysis for displacement-controlled procedures, as demonstrated in Chapter 2. In the current study, design sensitivities are computed following the framework by Michaleris et al. (1994) and are found to be perfectly compatible with numerical derivatives. Moreover, optimization in the presence of a general distributed load is made possible by combining displacement-controlled analysis with sensitivity analysis based on a load-controlled procedure. Finally, a new application of topology optimization with elasto-plastic material modeling for reinforced concrete design is used as one of the test cases. This is based on the design procedure presented in Chapter 7.

Topology optimization of geometrically nonlinear structures was first addressed by Buhl et al. (2000) for the purpose of stiffness maximization and later by Pedersen et al. (2001) and by Bruns and Tortorelli (2001) for compliant mechanism design. Numerous studies were dedicated to the challenging aspects of engineering design that arise when considering geometric nonlin-

earities, for example the snap-through phenomenon and loss of stability (Bruns and Sigmund, 2004; Kemmler et al., 2005). In the current study, we consider only stiffness maximization for structures exhibiting large deformations. The suitability of efficient analysis procedures for problems involving extreme geometric nonlinearities will be examined in future work.

The article is organized as follows. First, in Section 8.2 we briefly review the nonlinear finite element formulations for each of the problems considered in this study. Then, in Section 8.3 the topology optimization problems are presented, together with the material interpolation schemes and the procedures for sensitivity analysis. Section 8.4 is dedicated to the proposed computational schemes based on re-using information throughout the optimization process. Finally, several demonstrative examples are presented in Section 8.5 and preliminary conclusions are drawn is Section 8.6.

8.2 Considered structural nonlinearities and finite element formulations

In principal, the proposed computational procedures can be applied to any structural optimization problem involving nonlinear structural response, which is solved using the nested approach. For demonstrative purposes, this study focuses particularly on topology optimization problems where the underlying physical arises from nonlinear continuum mechanics. Standard nonlinear finite element procedures are employed for solving the structural analysis problems. In essence, the efficient procedures discussed in this article are based on re-using information from the nonlinear finite element solver, namely converged solutions and corresponding factors of tangent stiffnesses. This can be useful since in the nested approach, a sequence of nonlinear structural analyses needs to be performed, where in many cases the differences between two consecutive systems (due to design changes) are very small.

The structural nonlinearities considered in the demonstrative examples are: large deformations as a case of *geometric nonlinearity*; and rate-independent plasticity as a case of *material nonlinearity*. In this section, we briefly review the finite element formulations corresponding to the problems addressed by this study.

8.2.1 Large deformations

In large deformation continuum mechanics, equilibrium should be satisfied in the deformed geometry which is unknown beforehand. One approach to large deformation analysis is the so-called total Lagrangian formulation, where all finite element computations are performed with respect to the original configuration. For this purpose, the Green-Lagrange strain tensor is defined as

$$ {}^{n}_{0}\epsilon_{ij} = \frac{1}{2}({}^{n}_{0}u_{i,j} + {}^{n}_{0}u_{j,i} + {}^{n}_{0}u_{k,i}{}^{n}_{0}u_{k,j}) $$

where u is the displacement field; i, j and k represent the cartesian axes; $u_{l,m} = \frac{\partial u_l}{\partial m}$; and Einstein summation convention is applied. The ${}^{n}_{0}$ notation means evaluation at "time" n in the initial coordinate system corresponding to "time" 0. The term "time" is used here to represent the incrementation of loads or displacements. The derivation of the finite element equations follows Bathe (1996) and will be omitted here for the purpose of brevity.

The basic nonlinear equation system to be solved represents force equilibrium at the "time" increment n where the unknowns are the nodal displacements $\mathbf{u}$

$$ {}^{n}\mathbf{R}({}^{n}\mathbf{u}) = {}^{n}\mathbf{f}_{ext} - {}^{n}\mathbf{f}_{int} = \mathbf{0} \tag{8.1} $$

${}^{n}\mathbf{f}_{ext}$ and ${}^{n}\mathbf{f}_{int}$ are the vectors of external and internal nodal forces, respectively. For simplicity, it is assumed that only the internal forces depend on the displacements. Eq. (8.1) is typically

solved using an iterative Newton-Raphson procedure, where the tangent stiffness matrix is utilized. Even though alternative approaches may be applied (Bathe, 1996), the discussion here as well as the proposed re-use of information are limited to the context of Newton-Raphson procedures. At any iteration within step n, the tangent stiffness matrix and the internal forces are computed as follows

$$\begin{aligned} {}^{n}_{0}\mathbf{K} &= {}^{n}_{0}\mathbf{K}_L + {}^{n}_{0}\mathbf{K}_{NL} = \int_{{}_0V} \{{}^{n}_{0}\mathbf{B}^T_L\}\{{}_0\mathbf{D}\}\{{}^{n}_{0}\mathbf{B}_L\} d^0V + \\ &\quad \int_{{}_0V} \{{}^{n}_{0}\mathbf{B}^T_{NL}\}\{{}^{n}_{0}\mathbf{S}\}\{{}^{n}_{0}\mathbf{B}_{NL}\} d^0V \\ {}^{n}_{0}\mathbf{f}_{int} &= \int_{{}_0V} \{{}^{n}_{0}\mathbf{B}^T_L\}\{{}^{n}_{0}\widehat{\mathbf{S}}\} d^0V \end{aligned}$$

where ${}^{n}_{0}\mathbf{B}_L$ is the strain-displacement transformation matrix, corresponding to linear terms of incremental strains; ${}^{n}_{0}\mathbf{B}_{NL}$ is the strain-displacement transformation matrix, corresponding to nonlinear terms of incremental strains; ${}_0\mathbf{D}$ is the constitutive tensor; ${}^{n}_{0}\mathbf{S}$ represents the second Piola-Kirchoff stresses in matrix format; and ${}^{n}_{0}\widehat{\mathbf{S}}$ represents the same stresses in vector format.

8.2.2 Classical rate-independent plasticity

The derivation of the governing equations follows the textbooks by Simo and Hughes (1998) and Zienkiewicz and Taylor (2000). For the purpose of sensitivity analysis in optimal design, these equations are cast into the framework for transient, coupled and nonlinear systems suggested by Michaleris et al. (1994). In the coupled approach, for every increment n in the transient analysis, we determine the unknowns ${}^{n}\mathbf{u}$ and ${}^{n}\mathbf{v}$ that satisfy the residual equations

$$\begin{aligned} {}^{n}\mathbf{R}({}^{n}\mathbf{u}, {}^{n-1}\mathbf{u}, {}^{n}\mathbf{v}, {}^{n-1}\mathbf{v}) = 0 \\ {}^{n}\mathbf{H}({}^{n}\mathbf{u}, {}^{n-1}\mathbf{u}, {}^{n}\mathbf{v}, {}^{n-1}\mathbf{v}) = 0 \end{aligned}$$

where $\mathbf{u}$ is the displacements vector and $\mathbf{v}$ are the internal variables - stresses, plastic strains and internal hardening parameters. Neglecting body forces, ${}^{n}\mathbf{R}$ is defined as the difference between external and internal forces and depends explicitly on ${}^{n}\mathbf{v}$ only

$$ {}^{n}\mathbf{R}({}^{n}\mathbf{v}) = {}^{n}\mathbf{f}_{ext} - {}^{n}\mathbf{f}_{int} = {}^{n}\mathbf{f}_{ext} - \int_V \mathbf{B}^{T\,n}\boldsymbol{\sigma} dV \tag{8.2} $$

where $\mathbf{B}$ is the standard strain-displacement matrix in the context of finite element procedures.

For solving the local nonlinear constitutive problem, an implicit backward-Euler scheme is employed. The central feature of this scheme is the introduction of a trial elastic state. For any given incremental displacement field, it is first assumed that there is no plastic flow between time t_n and the next time step t_{n+1}, meaning the incremental elastic strains are the incremental total strains. It can be shown that the the loading/unloading situation which is governed by the Kuhn-Tucker conditions can be identified using the trial elastic state (Simo and Hughes, 1998). Once a plastic increment occurs, the new state variables can be found by solving a nonlinear equation system resulting from the time discretization of the governing equations. This results in the nonlinear system ${}^{n}\mathbf{H}$ which is derived specifically for any given elasto-plastic model.

8.2.2.1 J_2 flow theory

J_2 flow theory is a widely accepted model for predicting the elasto-plastic response of metals. It is based on the von Mises yield criterion (von Mises, 1928) which relates the yielding of the

material to the second invariant of the deviatoric stresses. The vector ${}^n\mathbf{v}$ is given by

$$ {}^n\mathbf{v} = \begin{bmatrix} {}^n\boldsymbol{\epsilon}^{pl} \\ {}^n\kappa \\ {}^n\boldsymbol{\sigma} \\ {}^n\lambda \end{bmatrix} $$

The internal variables in this model are as follows: ${}^n\boldsymbol{\epsilon}^{pl}$ are the plastic strains, ${}^n\kappa$ is the equivalent plastic strain, ${}^n\boldsymbol{\sigma}$ are the stresses and ${}^n\lambda$ is the plastic multiplier, all corresponding to a time increment n. The residual ${}^n\mathbf{H}$ is defined as the collection of four incremental residuals, resulting from the time linearization of the governing constitutive equations

$$ \begin{aligned} {}^n\mathbf{H}_1 &= {}^{n-1}\boldsymbol{\epsilon}^{pl} + ({}^n\lambda - {}^{n-1}\lambda)(\frac{\partial f}{\partial {}^n\boldsymbol{\sigma}})^T - {}^n\boldsymbol{\epsilon}^{pl} \\ {}^n\mathbf{H}_2 &= {}^{n-1}\kappa + ({}^n\lambda - {}^{n-1}\lambda)\sqrt{\frac{2}{3}(\frac{\partial f}{\partial {}^n\boldsymbol{\sigma}})^T(\frac{\partial f}{\partial {}^n\boldsymbol{\sigma}})} - {}^n\kappa \\ {}^n\mathbf{H}_3 &= {}^{n-1}\boldsymbol{\sigma} + \mathbf{D}\left[\mathbf{B}^n\mathbf{u} - \mathbf{B}^{n-1}\mathbf{u} - ({}^n\boldsymbol{\epsilon}^{pl} - {}^{n-1}\boldsymbol{\epsilon}^{pl})\right] - {}^n\boldsymbol{\sigma} \\ {}^n\mathbf{H}_4 &= J_2 - \frac{1}{3}(\sigma_y(\kappa))^2 \end{aligned} \tag{8.3} $$

The equation ${}^n\mathbf{H}_1$ represents the associative flow rule, where λ is the plastic multiplier and f is the yield function; ${}^n\mathbf{H}_2$ represents the evolution of the isotropic hardening parameter κ; ${}^n\mathbf{H}_3$ relates stresses to elastic strains through the constitutive tensor $\mathbf{D}$; and ${}^n\mathbf{H}_4$ is the yield criterion in squared form. A bi-linear hardening rule relates the yield stress to the hardening parameter

$$ \sigma_y(\kappa) = \sigma_y^0 + HE\kappa $$

where σ_y^0 is the initial yield stress, H is a scalar (usually in the order of 10^{-2}) and E is Young's modulus. As mentioned above, the local nonlinear equations ${}^n\mathbf{H} = 0$ are solved implicitly. An elastic trial stress is first assumed and then the true stresses and plastic strains are found iteratively using a Newton-Raphson procedure. Clearly, if an elastic increment is predicted by the elastic trial state, then this equation system is satisfied trivially: ${}^n\lambda = {}^{n-1}\lambda$ so ${}^n\boldsymbol{\epsilon}^{pl} = {}^{n-1}\boldsymbol{\epsilon}^{pl}$ and ${}^n\kappa = {}^{n-1}\kappa$, and the stresses are computed using the elastic constitutive tensor and the elastic trial stresses.

For plane stress situations, the local nonlinear problem (8.3) can be solved efficiently by the return-mapping algorithm by Simo and Taylor (1986). Nevertheless, for the purpose of sensitivity analysis we find it convenient to use the full representation as suggested by Michaleris et al. (1994).

8.2.2.2 A simplified model based on the Drucker-Prager yield criterion

The Drucker-Prager yield criterion (Drucker and Prager, 1952) is widely used to model the behavior of pressure-dependent materials such as soils, rock or plain concrete. Moreover, the von Mises yield criterion can be seen as a particular case of the Drucker-Prager criterion. The Drucker-Prager yield function is expressed as

$$ f(\boldsymbol{\sigma}, \kappa) = \sqrt{3J_2} + \alpha(\kappa)I_1 - \sigma_y(\kappa) \leq 0 \tag{8.4} $$

where I_1 is the first invariant (trace) of the stress tensor. α is a material property depending on the internal hardening parameter κ according to some hardening function. When $\alpha = 0$, the von Mises yield criterion is obtained.

In the study presented in Chapter 7, a Drucker-Prager model with simplified flow and hardening rules is used for interpolating the nonlinear behavior of two candidate materials. This

interpolation is utilized in a topology optimization procedure aimed at generating optimized conceptual designs of reinforced concrete structures. One of the example problems in the current study is based on the same procedure, therefore a brief review of the governing equations is given in the following. We assume simple isotropic hardening rules

$$\begin{aligned} \alpha(\kappa) &= constant && (8.5)\\ \sigma_y(\kappa) &= \sigma_y^0 + HE\kappa && (8.6) \end{aligned}$$

Furthermore, an associative flow rule is considered and the hardening parameter is simply the plastic multiplier

$$\begin{aligned} \dot{\boldsymbol{\epsilon}}^{pl} &= \dot{\lambda}\frac{\partial f}{\partial \boldsymbol{\sigma}} \\ \dot{\kappa} &= \dot{\lambda} && (8.7) \end{aligned}$$

The assumptions (8.5), (8.6) are not necessarily suitable for accurate modeling of concrete but do not affect the ability to capture the most important failure in concrete, that is failure in tension. Moreover, the relation (8.7) does not accurately represent hardening mechanisms. Nevertheless, it is accurate enough for the purpose of the current study, since post-yielding response of the steel phase should not affect the optimal choice of material. Upon time discretization, the local nonlinear equation system for this model is obtained

$$\begin{aligned} {}^n\mathbf{H}_1 &= \mathbf{B}({}^n\mathbf{u} - {}^{n-1}\mathbf{u}) - \mathbf{D}^{-1}({}^n\boldsymbol{\sigma} - {}^{n-1}\boldsymbol{\sigma}) - ({}^n\lambda - {}^{n-1}\lambda)(\frac{\partial f}{\partial {}^n\boldsymbol{\sigma}})^T \\ {}^n\mathbf{H}_2 &= \sqrt{3J_2} + \alpha I_1 - \sigma_y({}^n\lambda) \end{aligned}$$

where the internal variables $\mathbf{v}$ are

$${}^n\mathbf{v} = \begin{bmatrix} {}^n\boldsymbol{\sigma} \\ {}^n\lambda \end{bmatrix}$$

8.2.3 Load control vs. displacement control

When performing a nonlinear structural analysis it is sometimes useful to increment a prescribed displacement rather than a given load. Controlling the displacement can improve the numerical stability, for example when a small additional load corresponds to a large additional displacement or when limit points are encountered (Crisfield, 1991). When applying displacement control, the incrementation parameter n represents the magnitude of the displacement at a particular degree of freedom whose incremental displacements are prescribed, instead of representing the load intensity.

In the context of optimal design, using displacement control has some advantages but it is not necessarily suitable for practical engineering design. In most cases, the designer has prior knowledge about the loads to be applied on the structure but not about the expected deflections; it is also not known beforehand if the response is linear or nonlinear. Naturally, nonlinear behavior is not preferable in the majority of practical situations. Therefore an appropriate approach would be to apply the given loads and to optimize the structure so that the final design behaves linearly. The main obstacle when following this approach is that for intermediate designs the response can be highly nonlinear, thus posing difficulties in computing accurate sensitivities and in obtaining an overall smooth optimization procedure.

When performing a displacement-controlled nonlinear analysis, the global residuals (8.1), (8.2) are modified respectively

$$\begin{aligned} {}^n\mathbf{R}({}^n\mathbf{u}, {}^n\theta) &= {}^n\theta\widehat{\mathbf{f}}_{ext} - {}^n\mathbf{f}_{int} = \mathbf{0} \\ {}^n\mathbf{R}({}^n\mathbf{v}, {}^n\theta) &= {}^n\theta\widehat{\mathbf{f}}_{ext} - \int_V \mathbf{B}^T {}^n\boldsymbol{\sigma} dV \end{aligned}$$

where θ is an *unknown* load factor that multiplies the *fixed* external load vector $\widehat{\mathbf{f}}_{ext}$. In the context of structural optimization, prescribing a displacement can be useful if we wish to optimize the nonlinear response. By setting the magnitude of the deflection at a critical point in the structure, it is possible to ensure nonlinear response for all design cycles. Moreover, difficulties in solving the nonlinear analysis equations corresponding to early design stages are less likely to occur. This is because the load intensity corresponds to the structural stiffness, and varies throughout the optimization process.

Applying displacement control in the nonlinear analysis poses some difficulties in defining appropriate objective functions. Another problem is that sensitivity analysis becomes more demanding when non-prescribed degrees of freedom are loaded. These issues are thoroughly discussed in Chapter 2. As a consequence, the topology optimization problems addressed in this study are formulated in a hybrid manner: for the nonlinear finite element analysis, displacement control is utilized; on the other hand, sensitivity analysis is performed *as if* load control is used, based on the obtained converged solution.

8.3 Considered topology optimization problems

As mentioned above, the proposed procedures are intended for structural optimization problems that are solved using the nested approach. This means that the nonlinear structural analysis is performed separately by standard finite element procedures. The solution is then used for sensitivity analysis and the optimization problem is solved in the design variables only. In this study, the discussion is limited to structural topology optimization problems, where the design variables are densities corresponding to finite elements. We follow the material distribution approach for topological design (Bendsøe and Kikuchi, 1988) together with the SIMP interpolation scheme (M. P. Bendsøe, 1989). A generic form of such an optimization problem, aimed at minimizing a certain quantity subject to a volume constraint, is as follows

$$
\begin{aligned}
\min_{\boldsymbol{\rho}} \quad & c \\
\text{s.t.:} \quad & \sum_{e=1}^{N_e} v_e \rho_e \leq V \\
& g_i \leq 0 \qquad i = 1, ..., m \\
& 0 \leq \rho_e \leq 1 \qquad e = 1, ..., N_e \\
\text{with:} \quad & \mathbf{R} = \mathbf{0}
\end{aligned}
$$

where c is the objective function and g_i ($i = 1, ..., m$) are (optional) additional constraints. The element densities ρ_e are collected in the vector $\boldsymbol{\rho}$; N_e is the number of finite elements; v_e is the element volume; and V is the total available volume. The nested analysis problem is stated here as a residual problem, $\mathbf{R} = \mathbf{0}$, and takes different forms according to the physical model.

For demonstrative purposes, a few particular topology optimization problems are considered. Problem (I) involves geometric nonlinearities and addresses the maximization of stiffness when large deformations are considered. Problem (II) involves material nonlinearities, where the response is governed by J_2 flow theory. The aim is to find a topology that combines high stiffness with minimum plastic straining. The overall procedure can be seen as an alternative approach to achieving minimum compliance while satisfying stress constraints, which is a challenging topic attracting much attention over the years, see Bendsøe and Sigmund (2003) and recently Le et al. (2010) and references therein. Problem (III) deals with a new extension of the SIMP interpolation scheme, aiming at optimizing the distribution of two nonlinear materials whose response can be approximately represented using the Drucker-Prager yield criterion. This formulation can be utilized for generating conceptual designs of reinforced concrete structures, as initially presented in Chapter 7.

In this section, the topology optimization problems addressed in this study are shortly described. For each type of problem, the SIMP interpolating functions and the derivation of design sensitivities are presented.

8.3.1 Stiffness maximization considering large deformations

We consider the simple case of a structure subjected to a concentrated load. In order to avoid local buckling modes, the load is distributed between several adjacent nodes. The displacement at the center of the loaded region is prescribed to a value that corresponds to a large deformation so that an appropriate nonlinear formulation is required. Since the displacement is prescribed, the analysis is performed using displacement control. This may be seen as a rather academic problem because in practice one would typically design for a given load intensity. In general, the designer would ultimately prefer a linear response but it may be necessary to consider nonlinear analysis for intermediate design stages. Such topology optimization problems were initially considered by Buhl et al. (2000) and addressed in numerous later articles, for example by Kemmler et al. (2005). In the current study, we consider the prescribed displacement version since it ensures nonlinear response for all design cycles. This is useful for examining the applicability of the proposed computational procedures, which is the main purpose of this study.

Applying a distributed load while prescribing a single displacement poses a problem when defining a proper objective for stiffness maximization. As discussed in Chapter 2, maximizing the global end-compliance $\theta\widehat{\mathbf{f}}_{ext}^T\mathbf{u}$ may result in a structure that is very stiff with respect to bearing the load at the prescribed DOF but very flexible with respect to all other loads. Therefore the objective is defined as minimizing the end-compliance ${\mathbf{f}_{ext}}^T\mathbf{u}$ *as if* the analysis is load-controlled and *as if* the load intensity is constant throughout the optimization. The resulting procedure combines the advantages of both load and displacement control. On the one hand, the analysis is more stable numerically and is more likely to converge when the structural layout is relatively "soft". On the other hand, the objective is well-defined and should lead to the best global stiffness with respect to all loads. In practice, this can be seen as a load-controlled procedure, just that the load intensity varies throughout the design process to fit the prescribed displacement. Moreover, in the sensitivity analysis it is assumed that the solution was obtained using load control, which leads to a more straightforward computational procedure.

The quantity to be minimized is therefore the end-compliance, which corresponds to the final level of the prescribed displacement

$$c(\boldsymbol{\rho}, \mathbf{u}) = \mathbf{f}_{ext}^T\mathbf{u}$$

The nonlinear finite element analysis problem to be solved is given by

$$\mathbf{R}(\boldsymbol{\rho}, \mathbf{u}, \theta) = \theta\widehat{\mathbf{f}}_{ext} - \mathbf{f}_{int}(\boldsymbol{\rho}, \mathbf{u}) = \mathbf{0} \tag{8.8}$$

In principal, incrementation is not mandatory since the evolution of large deformations is not path-dependent. Therefore it is assumed that (8.8) can be solved in a single increment. If it fails to converge, the increment is cut and an automatic incrementation scheme is employed.

SIMP interpolation When assembling the tangent stiffness matrix and the internal forces vector for solving (8.8), Young's modulus is interpolated as follows

$$E(\rho_e) = E_{min} + (E_{max} - E_{min})\rho_e^{p_E} \tag{8.9}$$

In general, E_{min} and E_{max} are the values of Young's modulus of two candidate materials which should be distributed in the design domain. For the case of distributing a single material and void, E_{min} is several orders of magnitude smaller than E_{max}. Finally, p_E is a penalization factor required to drive the design toward a 0-1 layout.

Sensitivity analysis The gradients of the objective function are computed using the adjoint method. We begin by forming the augmented objective function

$$\widehat{c}(\boldsymbol{\rho}, \mathbf{u}) = \mathbf{f}_{ext}^T \mathbf{u} - \boldsymbol{\lambda}^T (\mathbf{f}_{ext} - \mathbf{f}_{int}(\boldsymbol{\rho}, \mathbf{u}))$$

Differentiation with respect to a certain element density gives

$$\frac{\partial \widehat{c}}{\partial \rho_e} = \mathbf{f}_{ext}^T \frac{\partial \mathbf{u}}{\partial \rho_e} - \boldsymbol{\lambda}^T (-\frac{\partial \mathbf{f}_{int}}{\partial \rho_e} - \frac{\partial \mathbf{f}_{int}}{\partial \mathbf{u}} \frac{\partial \mathbf{u}}{\partial \rho_e}) \tag{8.10}$$

Using the tangent stiffness matrix corresponding to the final equilibrium point $\mathbf{K} = \frac{\partial \mathbf{f}_{int}}{\partial \mathbf{u}}$ and exploiting symmetry, the following equation is obtained

$$\mathbf{K}\boldsymbol{\lambda} = -\mathbf{f}_{ext}$$

Finally, the solution for $\boldsymbol{\lambda}$ is inserted back into (8.10) to give the design sensitivities

$$\frac{\partial \widehat{c}}{\partial \rho_e} = \boldsymbol{\lambda}^T \frac{\partial \mathbf{f}_{int}}{\partial \rho_e}$$

8.3.2 Stiffness maximization considering elasto-plasticity

In the first stage of problem (II), as well as in problem (III), we find the stiffest structural layout subject to a volume constraint, given a certain prescribed displacement and a reference distributed load. Applying the hybrid approach again, the objective function considered for stiffness maximization is

$$c(\boldsymbol{\rho}, {}^N\mathbf{u}) = \mathbf{f}_{ext}^T {}^N\mathbf{u}$$

where the total number of increments performed in the analysis is denoted by N, meaning that the end-displacement vector is ${}^N\mathbf{u}$. The nested nonlinear analysis problem is now a coupled system. The residuals ${}^n\mathbf{R} = \mathbf{0}$ and ${}^n\mathbf{H} = \mathbf{0}$ should be satisfied at every displacement increment $n = 1, ..., N$. ${}^n\mathbf{R}$ and ${}^n\mathbf{H}$ are explicitly defined in Sections 8.2.2.1 and 8.2.2.2.

SIMP interpolation The constitutive model corresponding to J_2 flow theory involves three material parameters: Young's modulus E, the hardening fraction H and the initial yield stress σ_y^0. As mentioned above, an extension to the SIMP approach for interpolating the three parameters was originally presented by Maute et al. (1998). In this study, we keep H independent of the design variables so in addition to (8.9) we have

$$\sigma_y^0(\rho_e) = \sigma_{y,min}^0 + (\sigma_{y,max}^0 - \sigma_{y,min}^0)\rho_e^{p_{\sigma_y}} \tag{8.11}$$

where $\sigma_{y,min}^0$ and $\sigma_{y,max}^0$ are the initial yield stresses for the two candidate materials, corresponding to $\rho = 0$ and $\rho = 1$ respectively. From a physical point of view, the penalization factor p_{σ_y} should be equal to p_E, but in many cases it is necessary to set $p_{\sigma_y} < p_E$ in order to avoid numerical difficulties arising when low density elements reach their yield limit. This is further discussed in Section 8.5.

In problem (III), the goal is to distribute two nonlinear materials, one of them represented by a von Mises model and the other by a Drucker-Prager model. This is achieved by using a Drucker-Prager model (8.4) with the interpolations (8.9) and (8.11) and adding the following interpolating function

$$\alpha(\rho_e) = \alpha_{max} - (\alpha_{max} - \alpha_{min})\rho_e^{p_\alpha}$$

For the choice $\alpha_{min} = 0$, the von Mises yield surface is obtained for the material corresponding to $\rho = 1$. For $\rho = 0$ we obtain the Drucker-Prager yield surface with the material parameter $\alpha = \alpha_{max}$.

8.3.3 Plastic strain minimization considering elasto-plasticity

For solving problem (II), the second stage involves the minimization of the equivalent plastic strains, subject to a volume constraint and a compliance constraint, and given a prescribed displacement and a reference distributed load. The objective function considered at this stage is

$$c(\boldsymbol{\rho}, {}^{N}\mathbf{v}) = \sum_{e=1}^{N_e} \sum_{k=1}^{4} {}^{N}\kappa_{e,k} \tag{8.12}$$

which is simply a sum over all values of the equivalent plastic strain measured at the Gauss points. Again, the nonlinear residuals ${}^{n}\mathbf{R}$ and ${}^{n}\mathbf{H}$ are defined in Section 8.2.2.1 according to the respective elasto-plastic model. The applied SIMP interpolation scheme is the same as above.

8.3.4 Sensitivity analysis for problems involving elasto-plasticity

Sensitivity analysis for topology optimization problems involving elasto-plasticity is fundamentally different than for geometric nonlinearities due to path-dependency of the nonlinear response. As mentioned earlier, the framework presented by Michaleris et al. (1994) is followed when deriving the backwards-incremental adjoint procedure for such problems. The general procedure, without reference to a particular objective or elasto-plastic model, is presented in Chapter 2.

For performing the backwards-incremental sensitivity analysis, the derivatives of the global and local residuals with respect to the analysis variables are required. These are given in this section for the two elasto-plastic models considered in the current study. In particular, we consider a plane stress situation, meaning the stresses and strains are collected in a vector with three entries: $\boldsymbol{\sigma} = [\sigma_{11}, \sigma_{22}, \sigma_{12}]^T$ and $\boldsymbol{\epsilon} = [\epsilon_{11}, \epsilon_{22}, \epsilon_{12}]^T$.

For J_2 flow theory, the required derivatives are as follows

$$\frac{\partial({}^{n}\mathbf{R})}{\partial({}^{n}\mathbf{v})} = \begin{bmatrix} \mathbf{0}_{(8\times3)} & \mathbf{0}_{(8\times1)} & -\mathbf{B}^T w J_{(8\times3)} & \mathbf{0}_{(8\times1)} \end{bmatrix}$$

$$\frac{\partial({}^{n}\mathbf{H})}{\partial({}^{n}\mathbf{u})} = \begin{bmatrix} \mathbf{0}_{(3\times8)} \\ \mathbf{0}_{(1\times8)} \\ \mathbf{D}\mathbf{B}_{(3\times8)} \\ \mathbf{0}_{(1\times8)} \end{bmatrix}$$

$$\frac{\partial({}^{n+1}\mathbf{H})}{\partial({}^{n}\mathbf{u})} = \begin{bmatrix} \mathbf{0}_{(3\times8)} \\ \mathbf{0}_{(1\times8)} \\ -\mathbf{D}\mathbf{B}_{(3\times8)} \\ \mathbf{0}_{(1\times8)} \end{bmatrix}$$

$$\frac{\partial({}^{n}\mathbf{H})}{\partial({}^{n}\mathbf{v})} = \begin{bmatrix} -\mathbf{I}_{(3\times3)} & 0_{(1\times1)} & \Delta^n\lambda\mathbf{P}_{(3\times3)} & \mathbf{P}^n\boldsymbol{\sigma}_{(3\times1)} \\ \mathbf{0}_{(1\times3)} & -1_{(1\times1)} & \Delta^n\lambda\sqrt{\frac{2}{3}}\frac{{}^{n}\boldsymbol{\sigma}^T\mathbf{P}}{\sqrt{{}^{n}\boldsymbol{\sigma}^T\mathbf{P}^n\boldsymbol{\sigma}}}_{(1\times3)} & \sqrt{\frac{2}{3}{}^{n}\boldsymbol{\sigma}^T\mathbf{P}^n\boldsymbol{\sigma}^T}_{(1\times1)} \\ -\mathbf{D}_{(3\times3)} & \mathbf{0}_{(3\times1)} & -\mathbf{I}_{(3\times3)} & \mathbf{0}_{(3\times1)} \\ \mathbf{0}_{(1\times3)} & -\frac{2}{3}HE(\sigma_y^0 + HE\kappa)_{(1\times1)} & {}^{n}\boldsymbol{\sigma}^T\mathbf{P}_{(1\times3)} & 0_{(1\times1)} \end{bmatrix}$$

$$\frac{\partial({}^{n+1}\mathbf{H})}{\partial({}^{n}\mathbf{v})} = \begin{bmatrix} \mathbf{I}_{(3\times3)} & 0_{(1\times1)} & \mathbf{0}_{(3\times3)} & -\mathbf{P}^{n+1}\boldsymbol{\sigma}_{(3\times1)} \\ \mathbf{0}_{(1\times3)} & 1_{(1\times1)} & \mathbf{0}_{(1\times3)} & -\sqrt{\frac{2}{3}{}^{n+1}\boldsymbol{\sigma}^T\mathbf{P}^{n+1}\boldsymbol{\sigma}}_{(1\times1)} \\ \mathbf{D}_{(3\times3)} & \mathbf{0}_{(3\times1)} & \mathbf{I}_{(3\times3)} & \mathbf{0}_{(3\times1)} \\ \mathbf{0}_{(1\times3)} & 0_{(1\times1)} & \mathbf{0}_{(1\times3)} & 0_{(1\times1)} \end{bmatrix}$$

where $\mathbf{B}$ is the standard strain-displacement matrix; w is the Gauss-point weight for numerical integration; J is the determinant of the Jacobian at the Gauss-point; $\mathbf{D}$ is the plane stress

constitutive tensor; and $\mathbf{P}$ and $\Delta^n\lambda$ are defined as follows

$$\begin{aligned}\mathbf{P} &= \begin{bmatrix} 2 & -1 & 0 \\ -1 & 2 & 0 \\ 0 & 0 & 6 \end{bmatrix} \\ \Delta^n\lambda &= {}^n\lambda - {}^{n-1}\lambda\end{aligned}$$

For the Drucker-Prager model, $\frac{\partial({}^n\mathbf{R})}{\partial({}^n\mathbf{v})}$ is the same since it does not depend on the particular elasto-plastic model employed. The derivatives of the local residual are

$$\begin{aligned}\frac{\partial({}^n\mathbf{H})}{\partial({}^n\mathbf{u})} &= \begin{bmatrix} \mathbf{B}_{(3\times 8)} \\ \mathbf{0}_{(1\times 8)} \end{bmatrix} \\ \frac{\partial({}^{n+1}\mathbf{H})}{\partial({}^n\mathbf{u})} &= \begin{bmatrix} -\mathbf{B}_{(3\times 8)} \\ \mathbf{0}_{(1\times 8)} \end{bmatrix} \\ \frac{\partial({}^n\mathbf{H})}{\partial({}^n\mathbf{v})} &= \begin{bmatrix} -\mathbf{D}^{-1} - \Delta^n\lambda\frac{\partial^2 f}{\partial^n\boldsymbol{\sigma}}_{(3\times 3)} & -\frac{\partial f}{\partial^n\boldsymbol{\sigma}}^T_{(3\times 1)} \\ \frac{\partial f}{\partial^n\boldsymbol{\sigma}}_{(1\times 3)} & -HE_{(1\times 1)} \end{bmatrix} \\ \frac{\partial({}^{n+1}\mathbf{H})}{\partial({}^n\mathbf{v})} &= \begin{bmatrix} \mathbf{D}^{-1}{}_{(3\times 3)} & \frac{\partial f}{\partial^{n+1}\boldsymbol{\sigma}}^T_{(3\times 1)} \\ \mathbf{0}_{(1\times 3)} & 0_{(1\times 1)} \end{bmatrix}\end{aligned}$$

where the derivative of the yield function with respect to the stress components is given by

$$\frac{\partial f}{\partial\boldsymbol{\sigma}} = \frac{1}{2\sqrt{3J_2}}\begin{bmatrix} 2\sigma_{11}-\sigma_{22} & 2\sigma_{22}-\sigma 11 & 6\sigma_{12} \end{bmatrix} + \alpha\begin{bmatrix} 1 & 1 & 0 \end{bmatrix}$$

As explained in Chapter 2, when implementing the adjoint procedure, the derivatives of the local residuals ${}^n\mathbf{H}$ and ${}^{n+1}\mathbf{H}$ should maintain consistency with respect to the analysis. This means that the actual loading/unloading situation encountered within a certain increment affects the computation of the derivatives of the respective residuals ${}^n\mathbf{H}$ and ${}^{n+1}\mathbf{H}$. Therefore the derivatives of the local residual are matrices of varying sizes, depending on the situation which is determined exclusively by the elastic trial state as described in Section 1.2.2.2.

The final component required for performing the sensitivity analysis is the derivative of the residual ${}^n\mathbf{H}$ with respect to the design variables, for each of the models considered. For the J_2 flow theory model we obtain

$$\frac{\partial({}^n\mathbf{H})}{\partial\rho_e} = \begin{bmatrix} \mathbf{0}_{(3\times 1)} \\ 0_{(1\times 1)} \\ \frac{\partial E}{\partial\rho_e}\mathbf{D}_0({}^n\boldsymbol{\epsilon}^{el} - {}^{n-1}\boldsymbol{\epsilon}^{el})_{(3\times 1)} \\ -\frac{2}{3}(\sigma_y^0 + HE\kappa)(\frac{\partial\sigma_y^0}{\partial\rho_e} + H\frac{\partial E}{\partial\rho_e}\kappa)_{(1\times 1)} \end{bmatrix}$$

where $\mathbf{D}_0$ is the elastic constitutive tensor for Young's modulus equal to 1 and $\boldsymbol{\epsilon}^{el}$ are the elastic strains. For the Drucker-Prager model we obtain

$$\frac{\partial({}^n\mathbf{H})}{\partial\rho_e} = \begin{bmatrix} -\frac{\partial(\mathbf{D}^{-1})}{\partial\rho_e}({}^n\boldsymbol{\sigma} - {}^{n-1}\boldsymbol{\sigma}) - \frac{\partial(\frac{\partial f}{\partial^n\boldsymbol{\sigma}})^T}{\partial\rho_e}\Delta^n\lambda_{(3\times 1)} \\ \frac{\partial\alpha}{\partial\rho_e}I_1 - \frac{\partial\sigma_y^0}{\partial\rho_e} - H\frac{\partial E}{\partial\rho_e}{}^n\lambda_{(1\times 1)} \end{bmatrix}$$

where

$$\begin{aligned}\frac{\partial(\mathbf{D}^{-1})}{\partial\rho_e} &= -\frac{1}{E}\frac{\partial E}{\partial\rho_e}\mathbf{D}^{-1} \\ \frac{\partial(\frac{\partial f}{\partial\boldsymbol{\sigma}_n})^T}{\partial\rho_e} &= \frac{\partial\alpha}{\partial\rho_e}\begin{bmatrix} 1 \\ 1 \\ 0 \end{bmatrix}\end{aligned}$$

8.4 Re-using information

The main idea behind re-using information is to take advantage of the fact that during the optimization process, we solve a sequence of nonlinear structural analysis problems. In some cases, the solution to two consecutive nonlinear analyses are similar since they correspond to similar structural layouts. Consequently, when performing the nonlinear analysis within a certain design cycle, it may be possible to use information gathered in the previous nonlinear analysis in order to facilitate a more efficient solution scheme. In the following, we describe three schemes that are based on re-using solutions (i.e. displacements vectors) and factorizations of tangent stiffnesses.

Re-using solutions This straightforward scheme is based on keeping the result of the nonlinear finite element analysis corresponding to a certain design cycle, and re-using it as a starting point for the analysis within the next design cycle. When the changes in the design between two consecutive cycles are not large, it is expected that also the corresponding displacements will be similar. Therefore the displacements in a certain design cycle can serve as a reasonable initial guess for the displacements corresponding to the next cycle. Consequently, it may be possible to reduce the number of Newton iterations performed for solving the analysis equations, since the starting point may be closer to the neighborhood of quadratic convergence.

In case the analysis is performed in increments, for example due to path-dependency, the information transferred between design cycles consists of a set of displacements vectors corresponding to the converged states at the end of all increments. As a consequence, the same incrementation must be applied when performing consecutive analyses. In case a coarser or a finer incrementation is desired, the analysis should be performed without using an initial solution.

Re-using displacements vectors goes hand-in-hand with displacement-controlled analysis. This is because the value of the prescribed displacement is likely to be fixed throughout the design process, meaning that at the prescribed degree of freedom the initial guess is accurate. This is demonstrated in Figure 8.1(a) on a force-displacement plot corresponding to the prescribed degree of freedom (DOF). The aim is to maximize the end-compliance for a certain prescribed displacement, meaning that the load level rises as the design is improved. At a certain design cycle k, the displacement vectors $\mathbf{u}_n$ $(n = 1, ..., N)$ corresponding to the solutions of the residuals ${}^n\mathbf{R} = \mathbf{0}$ are saved. Then, when performing the nonlinear analysis at the next design cycle $k + 1$, these vectors are used as initial estimates of the solutions. If the prescribed displacement remains unchanged, then these estimates are accurate at that particular DOF. If the prescribed displacement is modified or in case load control is employed, the estimates are approximate for all DOF. Nevertheless, convergence can still be achieved faster than with a standard procedure, especially if the design changes are small.

Re-using factorized tangent stiffnesses Two other schemes aiming at more significant savings are inspired by the Modified Newton-Raphson procedure (MNR), where the tangent stiffness matrix is factorized once in the beginning of each incremental step, see for example Bathe (1996). Then, only forward and backward substitutions are required at each iteration. This means that convergence of the Newton iterations is slower compared to the standard procedure but the overall cost may be reduced due to the fewer number of factorizations. When a sequence of nonlinear analyses is performed, it is suggested to re-use factorizations of tangent stiffness matrices corresponding to equilibrium at a certain design cycle, in a modified Newton-Raphson procedure at the next design cycle.

In the classical MNR procedure, the iterations within each increment are performed using the factorization corresponding to the last equilibrium configuration, meaning the load or prescribed displacement are one step smaller. In the proposed scheme, the iterations are performed

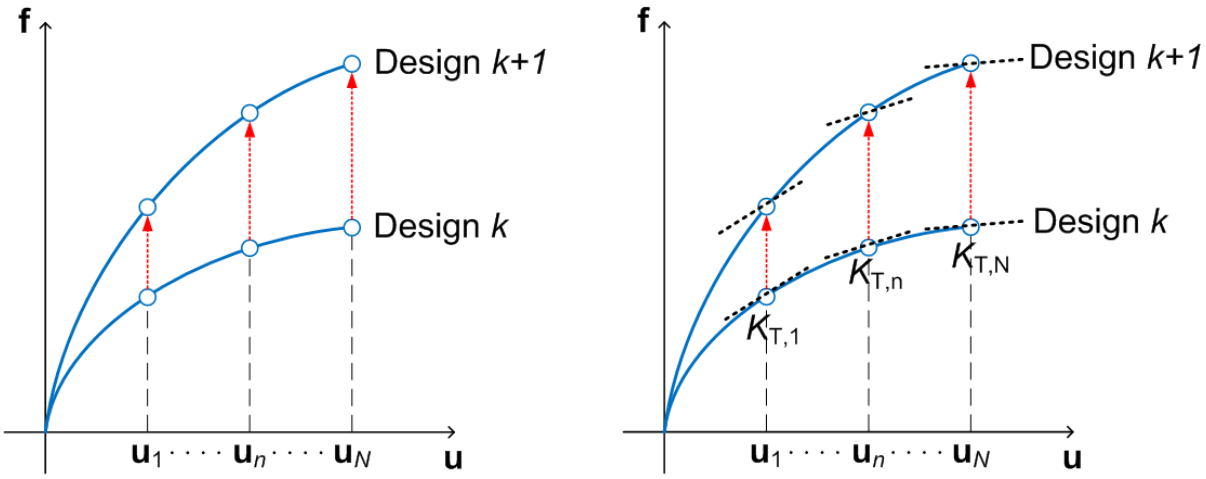

(a) Re-using displacements as initial estimates for the next design cycle.

(b) Re-using tangent stiffnesses as approximate stiffnesses for the next design cycle.

Figure 8.1: Re-using information between subsequent nonlinear analyses, demonstrated in a single degree of freedom space.

using the factorization corresponding to the equilibrium point with the same load or prescribed displacement, but at the previous design cycle. When design changes between subsequent design cycles are small, this approximate tangent stiffness can be very effective. In practice, the factorizations that are utilized are those that are performed for the purpose of sensitivity analysis, since they correspond to the converged equilibrium state and must be computed anyway after the analysis is complete. This scheme is demonstrated in Figure 8.1(b) on the same plot as for the first scheme. At a certain design cycle k, the factorized tangent stiffnesses $\mathbf{K}_T$ as well as the displacement vectors $\mathbf{u}$ corresponding to the solutions of the residuals ${}^n\mathbf{R} = \mathbf{0}$ $(n = 1, ..., N)$ are saved. Then, when performing the nonlinear analysis at the next design cycle $k+1$, a MNR procedure is performed with the available factorizations and the estimated displacements as initial guesses.

In our numerical experiments, the MNR procedure converged only when the design changes between consecutive design iterations were very small. Therefore we suggest a third scheme, which again is based on transferring the solutions and the tangent stiffnesses to the next design cycle. Then at each Newton iteration, an inexact Newton step is calculated using a reanalysis approach. The typical iterative Newton-Raphson equation system to be solved is

$$ {}^n\mathbf{K}^{i-1}\Delta\mathbf{u} = {}^n\mathbf{f}_{ext} - {}^n\mathbf{f}_{int}^{i-1} $$

where ${}^n\mathbf{K}^{i-1}$ is the tangent stiffness at iteration $i-1$ within increment n; $\Delta\mathbf{u}$ are the iterative displacements at iteration i; and ${}^n\mathbf{f}_{ext} - {}^n\mathbf{f}_{int}^{i-1}$ are the un-balanced forces. This can be rewritten as a reanalysis equation

$$ (\mathbf{K}_0 + \Delta\mathbf{K})\Delta\mathbf{u} = {}^n\mathbf{f}_{ext} - {}^n\mathbf{f}_{int}^{i-1} \tag{8.13} $$

Instead of factorizing the tangent stiffness matrix ${}^n\mathbf{K}^{i-1}$ every Newton iteration, the factorization of $\mathbf{K}_0$ is utilized in a reanalysis procedure. In the current context, $\mathbf{K}_0$ corresponds to the same increment but in the previous design cycle. An efficient solution of (8.13) is obtained using the Combined Approximations (CA) approach, see Kirsch (2008) for an overview of the method and Amir et al. (2008) for applications in nonlinear analysis.

In terms of accuracy and efficiency, this scheme is a compromise between the standard and the modified Newton-Raphson procedures. The iterative step is not as accurate as in a standard Newton procedure and not as cheap as a modified Newton iteration. Nevertheless, convergence is achieved in some cases in which MNR fails. Moreover, computational savings are expected

for medium- and large-scale problems when comparing to the standard Newton-Raphson procedure.

Monitoring design changes The effectiveness of the proposed schemes strongly depends on the magnitude of the design changes between subsequent designs. In some cases, these schemes are applied only once the design changes are small. For this purpose we monitor the cosine of the angle between subsequent design variable vectors

$$\cos(\beta) = \frac{\boldsymbol{\rho}_k^T \boldsymbol{\rho}_{k-1}}{\|\boldsymbol{\rho}_k\|_2 \left\|\boldsymbol{\rho}_{k-1}\right\|_2} \tag{8.14}$$

8.5 Examples

In this section, we examine the applicability of the proposed schemes by solving several test problems. Example 1 deals with maximizing the stiffness of a beam undergoing large deformations; Example 2 is concerned with finding a topology that combines high stiffness with minimum plastic straining, based on J_2 plasticity; and Example 3 deals with conceptual design of reinforced concrete using a Drucker-Prager material model. All test cases were solved using a 2D finite element mesh consisting of square, bi-linear plane stress elements. The optimization is performed by a nonlinear optimization program based on the Method of Moving Asymptotes (Svanberg, 1987). In order to obtain regularized designs and to avoid checkerboard patterns, a density filter is applied (Bourdin, 2001; Bruns and Tortorelli, 2001).

For each test case, we compare the performance of several schemes employed for solving the sequence of nonlinear structural analyses. The first scheme, denoted NR, is simply a standard Newton-Raphson procedure performed independently within every design cycle. In the second scheme, denoted FAST-NR, the same Newton-Raphson procedure is used but the solution of the previous nonlinear analysis (corresponding to the previous design cycle) is used as the starting point for the Newton iterations. The third scheme, denoted MNR, is only tested on Example 1 where the geometric nonlinear analysis is solved in one increment. In this scheme, the factorized tangent stiffness used for the adjoint equations in one design cycle is used in a modified Newton-Raphson procedure within the next design cycle. In the other examples involving elasto-plasticity, we apply the inexact Newton scheme where factorized tangent stiffnesses from all increments are re-used. Within each Newton iteration, an inexact step is obtained using the Combined Approximations (CA) reanalysis approach. This scheme is denoted MNR-CA.

8.5.1 Example 1: Large deformations of a clamped beam

In this example, the efficient schemes based on re-using information are tested on a topology optimization problem involving large deformations. The aim is to maximize the end-compliance of a clamped beam subject to a prescribed displacement at the middle of the upper fiber, see Figure 8.2(a). In order to avoid local buckling of loaded finite elements, the load is evenly distributed between 10 adjacent nodes. The displacement at the upper-center node is prescribed throughout all design iterations to the value $\delta = 0.1$. The model is discretized with a 200×40 FE mesh and the volume fraction is set to $V = 0.25$. Additional data regarding material properties and optimization parameters is given in Table 8.1.

The optimized design presented in Figure 8.2(b) is achieved after 100 design iterations. The convergence tolerance (1×10^{-2}) referring to the maximum change in an element density throughout the design domain was not reached. Nevertheless, the process was terminated after 100 cycles since the changes in objective value, as well as in the optimized layout, were practically negligible. The end-compliance corresponding to the optimized layout is 0.1661. Observing the optimized structure, the impact of incorporating large deformations is evident. If

Table 8.1: Solution parameters, GNL beam

Parameter	Value
E_{min}	1.0×10^{-3}
E_{max}	1.0×10^{3}
ν	0.3
SIMP penalty	3.0
Filter radius	0.075

only small deformations are considered, it is expected that the loaded region will be connected to the supports in the shortest path using compressed bars. These are unfavorable when large deformations are considered due to buckling. Therefore the layout consists of a combination of short bars in compression and longer bars in tension, meaning that buckling of internal members is avoided. Similar results were reported in various articles, for example by Buhl et al. (2000) and by Kemmler et al. (2005).

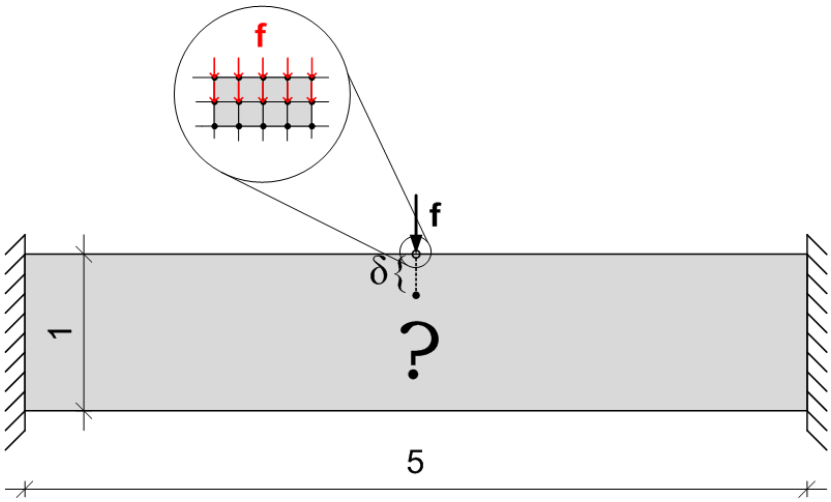

(a) Ground structure, boundary conditions and prescribed displacement.

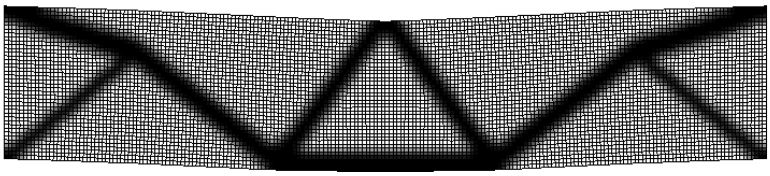

(b) Optimized layout after 100 design iterations.

Figure 8.2: Maximum end-compliance of a clamped beam subject to a prescribed displacement, considering large deformations.

For this test case, we compare the number of tangent stiffness factorizations performed using the three schemes: NR, FAST-NR and MNR. The FAST-NR scheme is employed throughout the whole optimization process, beginning from the second design cycle. Since the MNR scheme tends to diverge when significant changes in the design occur between subsequent design iterations, it is only used once the measure given in (8.14) exceeds 0.999. Until that stage, the FAST-NR scheme is used instead. The comparison is presented in Table 8.2 for 100 design iterations, where the factorizations performed for solving the adjoint systems are also taken into account. Observing Figure 8.3, it can be seen that the FAST-NR scheme is at least as fast as

the standard NR scheme, except for the second design cycle. Throughout 100 design iterations, re-using the solution as an initial point reduces the number of factorizations for nonlinear analysis by roughly 50%. As for the MNR scheme, it can be seen that once it is employed (after 22 design iterations), no extra factorizations are required for the analysis. This means that within each cycle, only one factorization is performed for solving the adjoint system. This factorization is then re-used in the solution of the analysis problem in the next design cycle. Concluding this example, we note that the objective values and obtained layouts are identical for all solution schemes.

Table 8.2: Computational performance, 100 design iterations, GNL beam

Solution scheme	Newton-Raphson iterations	Matrix factorizations (incl. adjoint)
NR	391	491
FAST-NR	201	301
MNR	363	158

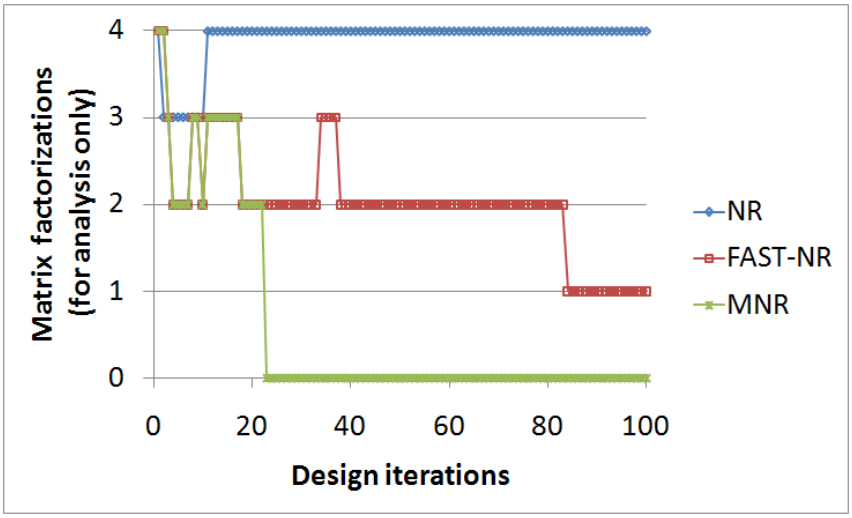

Figure 8.3: The number of matrix factorizations performed for nonlinear structural analysis, 100 design iterations.

8.5.2 Reducing stress concentrations in an L-bracket

In this example, the proposed schemes are utilized for topology optimization of an elasto-plastic structure. The aim is to find a conceptual design that avoids significant stress concentrations. As a representative case we optimize the L-bracket structure, see Figure 8.4 for the problem setting. This test case is often examined when considering stress constraints in topology optimization, see for example Le et al. (2010) for a recent report. The model is discretized with a FE mesh consisting of 6400 elements and the volume fraction is set to $V = 0.35$.

The overall procedure is as follows. We begin with maximizing the end-compliance for a prescribed displacement $\delta = 0.01$ which represents an acceptable deflection at the loaded point. This leads to a topology that is very similar to that obtained using linear material modeling, see Figure 8.5. In the particular case of the L-bracket, this means there is a significant stress concentration in the re-entrant corner. In the next stage, the objective is to minimize the plastic strains, subject to a compliance constraint. The target value for the constraint is set in accordance to

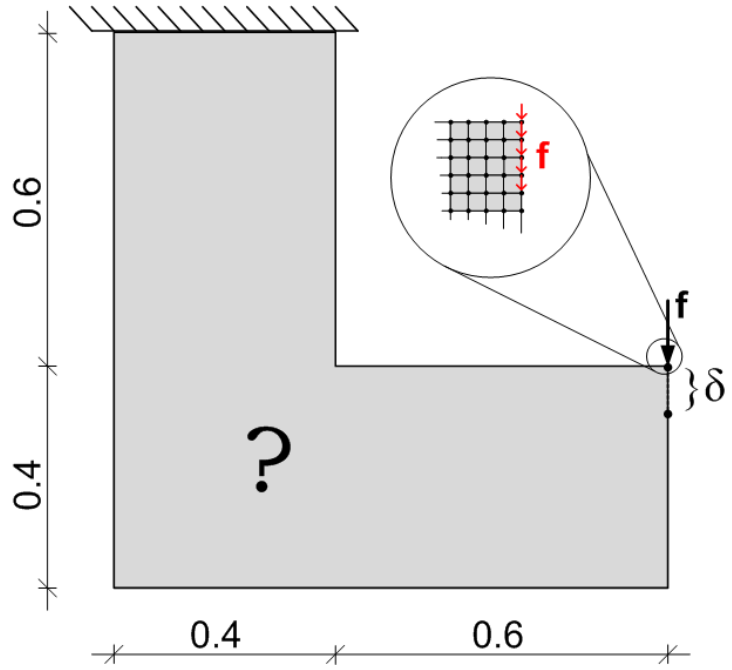

Figure 8.4: Ground structure, boundary conditions and prescribed displacement, the L-bracket problem.

the results of the first stage and with design considerations in mind - how much compromise can we accept in the compliance in order to achieve a design that has no plastic strains. The maximum end-compliance achieved at the first stage was 3.65×10^{-4}. The target compliance for the constraint was set to 3.0×10^{-4}, meaning a reduction of roughly 18% in the load-bearing capacity was assumed to be acceptable.

The minimization of plastic strains is performed in four gradual steps. Each step is terminated when the constraint is satisfied and the objective (8.12) is zero. In the final step, all material properties and penalty factors are identical to those used for the end-compliance objective so that the final designs are comparable. Details regarding these parameters are given in Tables 8.3 and 8.4. The evolution of the optimized design is presented in Figure 8.6. It can be seen that this procedure leads to an alternative design that avoids transferring the load through the re-entrant corner. However, this result requires further post-processing since plastic strains may re-appear when no penalization is applied. With the current penalization, the limit yield strain is artificially "delayed" in low-density elements in order to avoid numerical difficulties arising when they reach their yield limit. This means that in the final design, "gray" elements may actually yield if the true physical properties are considered. We believe that this can be resolved by either improving the filtering scheme or by simple post-processing.

For the maximum end-compliance objective, we compare the number of tangent stiffness factorizations required using the three schemes: NR, FAST-NR and MNR-CA. For the minimization of plastic strains, only the FAST-NR scheme is compared to the standard NR procedure. The FAST-NR and MNR-CA schemes are employed once the measure given in (8.14) exceeds 0.999. Until that stage, the NR scheme is used instead. If the FAST-NR scheme fails to solve the nonlinear analysis at a certain design cycle, then a standard solution is performed instead. If the MNR-CA fails, then the FAST-NR is utilized for both the current cycle and the following design cycle. The comparison of performances is presented in Tables 8.5 and 8.6.

It can be seen that the applicability of the efficient analysis schemes differs significantly between the two design objectives. For stiffness maximization, both the FAST-NR and the MNR-CA schemes offer some savings in terms of matrix factorizations. When evaluating the actual savings offered by the MNR-CA scheme it should be taken into account that every inexact Newton

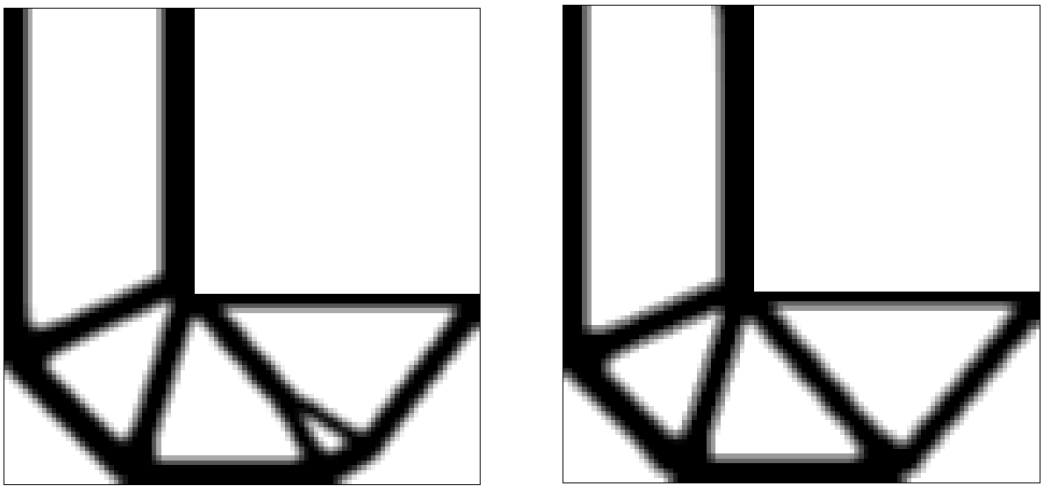

(a) Optimized layout for minimum compliance, linear modeling, 100 design iterations.

(b) Optimized layout for maximum end-compliance, nonlinear modeling with a prescribed displacement, 100 design iterations.

Figure 8.5: Stiffness maximization of an L-bracket.

Table 8.3: Solution parameters, maximum end-compliance of an L-bracket

Parameter	Value
E_{min}	1.0×10^{-3}
E_{max}	1.0×10^{3}
ν	0.3
H	0.01
p_E	3.0
p_{σ_y}	2.5
Filter radius	0.015

iteration costs roughly the same as 10 PCG iterations. For the minimization of plastic strains the FAST-NR scheme fails to reach a converged solution in many design cycles. In such cases a standard procedure is performed instead and the overall number of factorizations is higher due to "wasted" factorizations in the FAST-NR attempts.

There are two main reasons for the difficulties encountered in this test case. The first is related to the path-dependent nature of the solution. If the changes between subsequent designs lead to a different yielding sequence in the structure, it is expected that any of the efficient schemes will fail, because the re-used information is related to a different evolution of plasticity. The second obstacle is related to the optimization process. For stiffness maximization, the topology is roughly determined after 20-30 design iterations. Thereafter the design improves gradually, mostly by changing the densities of elements on the boundaries. Such design changes have little impact on the nonlinear response of the structure. However, when minimizing plastic strains subject to a compliance constraint, we observe significant design changes even in advanced stages of the optimization process. This may be related to the fact that the design is driven towards two conflicting targets.

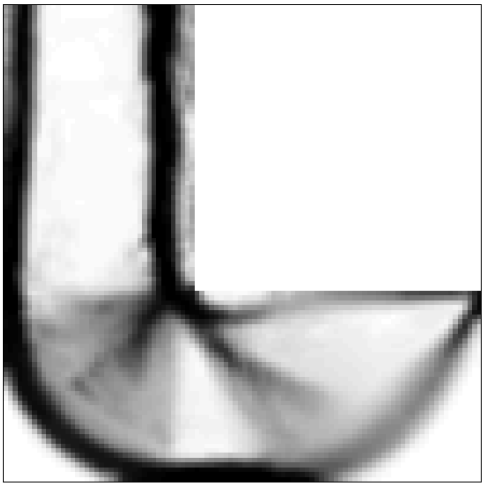

(a) Step 1: 36 design iterations with $p_E = 1.5$,$p_{\sigma_y} = 1.0$, filter radius $r = 0.015$ and hardening $H = 0.001$.

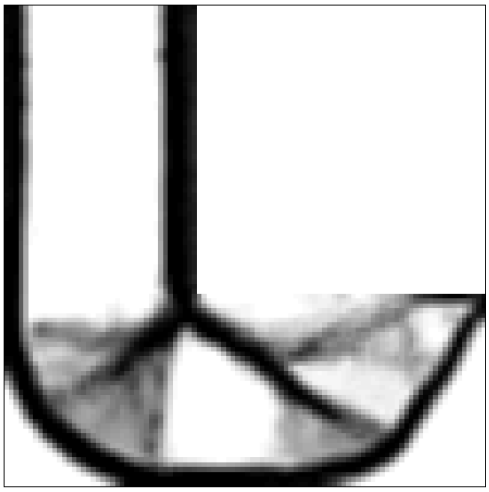

(b) Step 2: 35 further design iterations with $p_E = 2.0$,$p_{\sigma_y} = 1.5$, filter radius $r = 0.015$ and hardening $H = 0.001$.

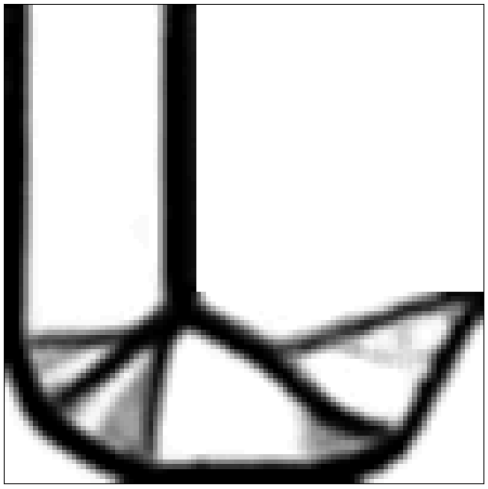

(c) Step 3: 51 further design iterations with $p_E = 2.5$,$p_{\sigma_y} = 2.0$, filter radius $r = 0.015$ and hardening $H = 0.001$.

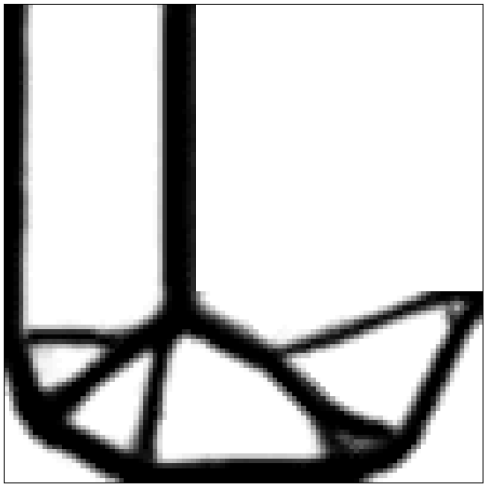

(d) Step 4: 35 further design iterations with $p_E = 3.0$,$p_{\sigma_y} = 2.5$, filter radius $r = 0.010$ and hardening $H = 0.01$.

Figure 8.6: Minimization of plastic strains in an L-bracket.

Table 8.4: Solution parameters, minimum plastic strains in an L-bracket

Parameter	Step 1	Step 2	Step 3	Step 4
E_{min}	1.0×10^{-3}	1.0×10^{-3}	1.0×10^{-3}	1.0×10^{-3}
E_{max}	1.0×10^{3}	1.0×10^{3}	1.0×10^{3}	1.0×10^{3}
ν	0.3	0.3	0.3	0.3
H	0.001	0.001	0.001	0.01
p_E	1.5	2.0	2.5	3.0
p_{σ_y}	1.0	1.5	2.0	2.5
Filter radius	0.015	0.015	0.015	0.010
Design iterations	36	35	51	35

Table 8.5: Computational performance, maximum end-compliance of an L-bracket, 100 design iterations

Solution scheme	Newton-Raphson iterations	Matrix factorizations (incl. adjoint)
NR	1045	1345
FAST-NR	624	924
MNR-CA	1223	610

8.5.3 Conceptual design of a reinforced concrete beam

In this example problem, we address the conceptual design of a reinforced concrete beam. The aim is to maximize the end-compliance subject to a constraint on the amount of available reinforcing steel. This example is identical to Example 2 in Chapter 7, so many of the details are omitted here and the discussion is limited to the application of efficient analysis procedures. The beam is subject to a distributed load and the analysis is controlled by a prescribed displacement at the middle of the top fiber, see Figure 8.7(a) for the problem setting. The model of the symmetric half is discretized with a 160×40 FE mesh; the volume fraction is set 0.1; and the magnitude of the prescribed displacement is $\delta = 0.005$. The load is modeled as 10 equally spaced point loads on one half of the beam. As in the previous example, gradual changes in penalization and filtering are necessary for obtaining the final design, see Table 7.3 for details. The optimized layout presented in Figure 8.7(b) is obtained after 150 design iterations.

Again we compare the number of tangent stiffness factorizations required using the three schemes: NR, FAST-NR and MNR-CA. The FAST-NR and MNR-CA schemes are employed once the measure given in (8.14) exceeds 0.999. Until that stage, the NR scheme is used instead. If the FAST-NR scheme fails to solve the nonlinear analysis at a certain design cycle, then a standard solution is performed instead. If the MNR-CA fails, then the FAST-NR is utilized for both the current cycle and the following design cycle. The comparison of performances is presented in Table 8.7. It can be seen that some savings are possible in terms of the number of matrix factorizations. However, the difficulty arising due to path-dependency of the solution leads to numerous failures of the efficient schemes. Consequently, the savings are not as promising as for path-independent problems.

Table 8.6: Computational performance, minimum plastic strains in an L-bracket, 157 design iterations

Solution scheme	Newton-Raphson iterations	Matrix factorizations (incl. adjoint)
NR	1979	2638
FAST-NR	2129	2788

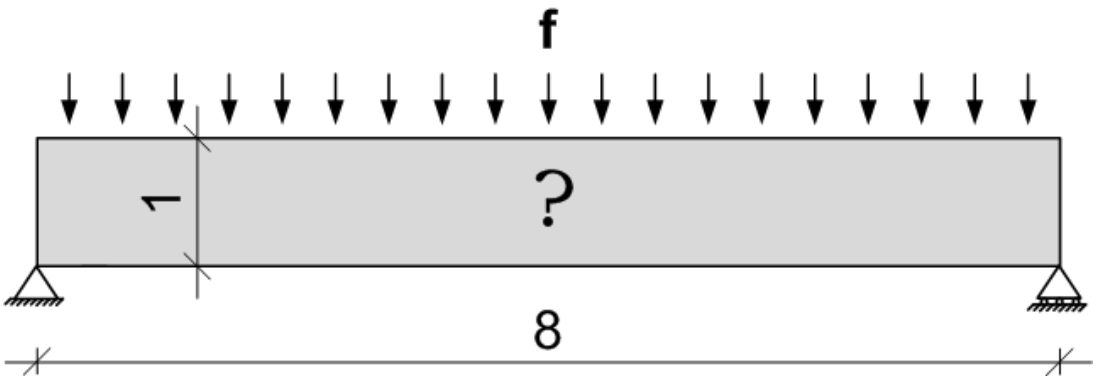

(a) Ground structure and boundary conditions.

(b) Optimized layout after 150 design iterations with gradual penalization and filtering.

Figure 8.7: Maximum end-compliance of a simply supported reinforced concrete beam subject to a distributed load. Black = steel, white = concrete. Steel consists of 10% of the total volume.

8.6 Summary and conclusions

Efficient schemes for nonlinear structural analysis in topology optimization were presented. The main idea is to transfer information between subsequent structural analyses, namely solutions and factorizations of tangent stiffnesses. It was shown that savings in computational effort can be achieved, essentially by reducing the number of matrix factorizations performed in the nonlinear structural analysis.

The suggested approach is most suitable for path-independent nonlinear response. For path-dependent problems such as elasto-plasticity, the efficient schemes are applicable only when the design changes between subsequent cycles are small. In future work, we hope to extend the approach for the case that a Newton-Krylov method is employed for the nonlinear analysis.

8.7 Acknowledgments

The authors wish to thank Krister Svanberg for allowing them to use the MMA code.

Table 8.7: Computational performance, 150 design iterations, reinforced concrete beam

Solution scheme	Newton-Raphson iterations	Matrix factorizations (incl. adjoint)
NR	2354	2814
FAST-NR	1935	2395
MNR-CA	2894	1671

References

N. Aage, T. H. Poulsen, A. Gersborg-Hansen, and O. Sigmund. Topology optimization of large scale stokes flow problems. *Structural and Multidisciplinary Optimization*, 35(2):175–180, 2008.

O. Amir and O. Sigmund. On reducing computational effort in topology optimization: how far can we go? *Structural and Multidisciplinary Optimization*, 2010. Published online.

O. Amir, U. Kirsch, and I. Sheinman. Efficient non-linear reanalysis of skeletal structures using combined approximations. *International Journal for Numerical Methods in Engineering*, 73: 1328–1346, 2008.

O. Amir, M. P. Bendsøe, and O. Sigmund. Approximate reanalysis in topology optimization. *International Journal for Numerical Methods in Engineering*, 78:1474–1491, 2009.

K.-J. Bathe. *Finite Element Procedures*. Prentice Hall, Upper Saddle River, New Jersey, 1996.

M. P. Bendsøe and N. Kikuchi. Generating optimal topologies in structural design using a homogenization method. *Computer Methods in Applied Mechanics and Engineering*, 71:197–224, 1988.

M. P. Bendsøe and O. Sigmund. *Topology Optimization - Theory, Methods and Applications*. Springer, Berlin, 2003.

B. Bourdin. Filters in topology optimization. *International Journal for Numerical Methods in Engineering*, 50:2143–2158, 2001.

T. E. Bruns and O. Sigmund. Toward the topology design of mechanisms that exhibit snap-through behavior. *Computer Methods in Applied Mechanics and Engineering*, 193:3973–4000, 2004.

T. E. Bruns and D. A. Tortorelli. Topology optimization of non-linear elastic structures and compliant mechanisms. *Computer Methods in Applied Mechanics and Engineering*, 190:3443–3459, 2001.

T. Buhl, C. Pedersen, and O. Sigmund. Stiffness design of geometrically nonlinear structures using topology optimization. *Structural and Multidisciplinary Optimization*, 19(2):93–104, 2000.

M. A. Crisfield. *Non-linear Finite Element Analysis of Solids and Structures*, volume 1. John Wiley & Sons, 1991.

D. C. Drucker and W. Prager. Soil mechanics and plastic analysis or limit design. *Quarterly of Applied Mathematics*, 10(2):157–165, 1952.

A. Evgrafov, C. J. Rupp, K. Maute, and M. L. Dunn. Large-scale parallel topology optimization using a dual-primal substructuring solver. *Structural and Multidisciplinary Optimization*, 36: 329–345, 2008.

R. Kemmler, A. Lipka, and E. Ramm. Large deformations and stability in topology optimization. *Structural and Multidisciplinary Optimization*, 30:459–476, 2005.

U. Kirsch. *Reanalysis of Structures*. Springer, Dordrecht, 2008.

C. Le, J. Norato, T. Bruns, C. Ha, and D. Tortorelli. Stress-based topology optimization for continua. *Structural and Multidisciplinary Optimization*, 41:605–620, 2010.

M. P. Bendsøe. Optimal shape design as a material distribution problem. *Structural Optimization*, 1:193–202, 1989.

K. Maute, S. Schwarz, and E. Ramm. Adaptive topology optimization of elastoplastic structures. *Structural Optimization*, 15(2):81–91, 1998.

P. Michaleris, D. A. Tortorelli, and C. A. Vidal. Tangent operators and design sensitivity formulations for transient non-linear coupled problems with applications to elastoplasticity. *International Journal for Numerical Methods in Engineering*, 37:2471–2499, 1994.

C. B. W. Pedersen, T. Buhl, and O. Sigmund. Topology synthesis of large-displacement compliant mechanisms. *International Journal for Numerical Methods in Engineering*, 50:2683–2705, 2001.

S. Schwarz, K. Maute, and E. Ramm. Topology and shape optimization for elastoplastic structural response. *Computer Methods in Applied Mechanics and Engineering*, 190:2135–2155, 2001.

J. Simo and T. Hughes. *Computational Inelasticity*. Springer, New York, 1998.

J. Simo and R. Taylor. A return mapping algorithm for plane stress elastoplasticity. *International Journal for Numerical Methods in Engineering*, 22:649–670, 1986.

K. Svanberg. The method of moving asymptotes - a new method for structural optimization. *International Journal for Numerical Methods in Engineering*, 24:359–373, 1987.

C. Swan and I. Kosaka. Voigt-Reuss topology optimization for structures with nonlinear material behaviors. *International Journal for Numerical Methods in Engineering*, 40(20):3785–3814, 1997.

R. von Mises. Mechanics of the ductile form changes of crystals. *Zeitschrift für Angewandte Mathematik und Mechanik*, 8:161–185, 1928.

S. Wang, E. de Sturler, and G. H. Paulino. Large-scale topology optimization using preconditioned Krylov subspace methods with recycling. *International Journal for Numerical Methods in Engineering*, 69:2441–2468, 2007.

G. H. Yoon and Y. Y. Kim. Topology optimization of material-nonlinear continuum structures by the element connectivity parameterization. *International Journal for Numerical Methods in Engineering*, 69:2196–2218, 2007.

K. Yuge and N. Kikuchi. Optimization of a frame structure subjected to a plastic deformation. *Structural Optimization*, 10:197–208, 1995.

O. C. Zienkiewicz and R. L. Taylor. *The Finite Element Method (5th edition) Volume 2 - Solid Mechanics*. Elsevier, 2000.